

# **Applications of Microstereolithography in Tissue Engineering**

Andrew A. Gill

September 2012

Thesis submitted to the University of Sheffield for the degree  
of Doctor of Philosophy

**Department of Materials Science and Engineering  
University of Sheffield**

# Abstract

---

Microstereolithography is a microfabrication technique based on the light induced cross-linking of a prepolymer according to a computer based design. The technology emerged in the 1980's as a rapid prototyping technique for the fabrication of small parts and devices. The technique has evolved into an important research tool with a diverse range of applications ranging from photonics to tissue engineering.

Two distinctly different branches of microstereolithography exist, differentiated by the fundamental mechanics involved. The first branch, based on the initiation of curing by the interaction of one photon of light with an initiator is a surface based technique. The photosensitised prepolymer or 'resin' is illuminated typically with ultraviolet light in order to cure the material within the first hundred micrometers of the surface and structures are constructed in a layer-by-layer fashion. The second, more recently developed 'branch' of microstereolithography was developed in the last decade of the twentieth century (although the underlying principles were predicted as early as the 1930's). Multiphoton polymerization is a technique similar to multiphoton microscopy, in which two or more photons interact with the photoinitiator within the lifetime of a virtual intermediate state, initiating curing. Due to the low probability of this occurrence curing is only initiated in areas of very high photon density, achieved by focusing a laser beam through a high numerical aperture objective into the resin. Photocuring then occurs in the central area of the focal point, within the volume of the resin.

The aim of this thesis was to investigate the applications of this technology (both one and two photon) in tissue engineering, for the fabrication of bespoke tissue scaffolds and other implantable devices. Photocurable oligomers based on bioresorbable materials already in clinical use were also explored and their suitability for tissue engineering applications investigated, with a focus on structuring and biocompatibility.

# Acknowledgements

---

Firstly I would like to thank my supervisor Dr Frederik Claeysens for his excellent supervision throughout this work, and for motivating me to continue with my research when progress seemed difficult. I would also like to thank all my colleagues at the University of Sheffield who have helped me with many aspects of this work. In particular I would like to thank Dr Louise E Smith for teaching me the basics of cell culture, having started this project as a complete beginner! I would also like to thank Dr Celia Murray-Dunning for her assistance in cell staining and confocal microscopy early in the project, and all my fellow PhD students who have provided many useful tips and tricks, as well as helpful conversations along the way. Also I would like to thank Dr Kiran Pawar for his advice and helpful discussions during our work together. Also at Sheffield I would like to thank members of the Haycock group including Dr Rossukon Kaewkhaw for supplying me with the necessary Schwann cells for this work.

I must also thank my collaborators at IESL-FORTH, especially Vasileia Melissinaki who assisted with many aspects of chapter five, especially the structuring. I would also like to thank Anastasia Koroleva and her colleagues at Laser Zentrum Hannover for her assistance with the structuring and Comet assay in chapter six.

I would like to thank my parents Adrienne and Lucian, my sisters Rachel and Michelle and the rest of my family (including Nana, Grandma and Shep, who are no longer with us) for their support, patience and understanding throughout my PhD, and for helping me to get where I am today.

Finally I would like to dedicate this thesis to my girlfriend Ílida, who I met through the work described in this thesis. Without your help in almost every aspect of the project as well as your support outside of the lab this work may never have been completed. When I submit this thesis, it will be three years to the day since we first went for a drink after the lab! Happy anniversary!

# Publications

---

## Journal Articles:

\*Melissinaki, V.; \*Gill, A. A.; Ortega, I.; Vamvakaki, M.; Ranella, A.; Fotakis, C.; Farsari, M.; and Claeysens, F., **Direct Laser Writing of 3D Scaffolds for Neural Tissue Engineering Applications** Biofabrication, 2011, 3 (4) (Authors marked \* contributed equally to this work)

\*Koroleva, A.; \*Gill, A. A.; Ortega, I.; Haycock, J. W.; Schlie, S.; Gittard, S. D.; Chichkov, B. N.; Claeysens, F., **Two-Photon Polymerization-Generated and Micromolding-Replicated 3-D Scaffolds for Peripheral Neural Tissue Engineering Applications** Biofabrication, 2012, 4 (2) (Authors marked \* contributed equally to this work).

Ortega, I.; Deshpande, P.; Gill, A. A.; MacNeil, S.; and Claeysens, F., **Development of a Microfabricated Artificial Limbus with Micropockets for Cell Delivery to the Cornea** (Submitted to Advanced Healthcare Materials, September 2012).

## Book Chapters:

Gill, A. A.; Claeysens, F., **3D Structuring of Biocompatible and Biodegradable Polymers Via Stereolithography** 3D Cell Culture, Methods in Molecular Biology, 2011; Vol. 695, pp 309-321.

Gill, A. A.; Claeysens, F., **Two Photon Polymerisation for Scaffold Fabrication** Optics in Regenerative Medicine (Awaiting Publication)

## Oral and Poster Presentations:

Gill, A. A.; Claeysens, F.; Pawar, K.; Ortega, I.; & Haycock, J., **Microstructuring of Photocurable Biomaterials with Applications in Neuronal Repair** Oral Presentation TCES 2011, Leeds

Gill, A. A.; Claeysens, F., **Laser Based Structuring of Biomaterials** Poster Presentation, TCES 2010, Manchester

Gill, A. A.; Pawar, K.; Claeysens, F., **Healing Nerves by Laser Direct Write** Poster Presentation, Royal Academy of Engineering, The 11<sup>th</sup> Annual Regional Public Lecture, 2011, Sheffield

Melissinaki, V.; Gill, A. A.; Ortega, I.; Vamvakaki, M.; Ranella, A.; Fotakis, C.; Farsari, M.; and Claeysens, F., **Direct Laser Writing of Poly(lactide) 3D Scaffolds for Neural Tissue Engineering Applications** Oral Presentation, ICMAT 2011, Suntec, Singapore

# Abbreviations

---

<b>2PP</b>	Two photon polymerization
<b>2/3D</b>	Two/ three dimensional
<b>CAD-CAM</b>	Computer-aided design and computer-aided manufacturing
<b>CCD</b>	Charge coupled device
<b>c/DMEM</b>	Completed Dulbecco's modified Eagle's medium
<b>CSM</b>	Contour scanning method
<b>CT</b>	Computed tomography
<b>DMD</b>	Digital micromirror device
<b>ECM</b>	Extracellular matrix
<b>fs</b>	Femtosecond
<b>GM</b>	Göppert-Mayer's
<b>H</b>	Hours
<b>IR</b>	Infra-red
<b>LDW</b>	Laser direct write
<b>ml</b>	Millilitre
<b>µl</b>	Microlitre
<b>mm</b>	Millimetre
<b>µm</b>	Micrometre
<b>MRI</b>	Magnetic resonance imaging
<b>MTT</b>	3-(4,5-Dimethylthiazol-2-yl)-2,5-diphenyltetrazolium bromide
<b>Nd:YAG</b>	Neodymium: Yttrium aluminium garnet
<b>nm</b>	Nanometre
<b>NA</b>	Numerical aperture
<b>NGC</b>	Nerve guidance conduit
<b>Ormocer</b>	Organically modified ceramic polymer
<b>PCL</b>	Polycaprolactone
<b>PDMS</b>	Polydimethylsiloxane
<b>PEG</b>	Polyethylene glycol
<b>PEGDA</b>	Polyethylene glycol diacrylate
<b>PGA</b>	Polyglycolic acid
<b>PLA</b>	Polylactic acid
<b>PSC</b>	Primary Schwann cell
<b>σ<sub>T</sub>TPA</b>	Two photon absorption cross-section
<b>s</b>	Seconds
<b>SFF</b>	Solid freeform fabrication
<b>SSM</b>	Single dimensional slicing method
<b>TEA</b>	Triethylamine
<b>Ti</b>	Titanium
<b>TMC</b>	Trimethylene carbonate
<b>TSM</b>	Two dimensional slicing method
<b>UV</b>	Ultraviolet

# Table of Contents

---

<b>Abstract</b> .....	<b>1</b>
<b>Acknowledgements</b> .....	<b>2</b>
<b>Publications</b> .....	<b>3</b>
<b>Abbreviations</b> .....	<b>4</b>
<b>Table of Contents</b> .....	<b>5</b>
<b>Chapter One: Applications of Microstereolithography in Tissue Engineering</b> .....	<b>11</b>
Abstract.....	11
1. Introduction.....	11
1.1 Microstereolithography.....	11
1.2 Microstereolithography in Comparison with Other Techniques .....	12
1.3 Features of Microstereolithography .....	13
1.4 Materials for Microstereolithography .....	14
1.5 Two Photon Polymerization .....	16
1.6 Two Photon Stereolithography .....	19
1.6.1 Initiation of Polymerization Processes.....	20
1.6.2 Experimental set-ups for Two Photon Polymerization.....	21
1.6.3 Improving the Efficiency and Cost of 2PP .....	22
1.7 Tissue Scaffolds and the Extracellular Matrix.....	23
1.8 Biomedical Applications of Microstereolithography.....	25
1.8.1 Implantable Medical Devices Created by 2PP.....	25
1.8.2 Prostheses.....	26
1.8.3 Microneedles.....	26
1.8.4 Valves .....	27
1.8.5 Bioresorbable Tissue Scaffolds.....	27
1.8.6 Cell Delivery Vehicles.....	28
1.8.7 Experimental Tissue Scaffolds .....	28
1.9 Conclusions.....	29
1.10 Thesis Aims and Objectives.....	30
<b>Chapter 2: Photocurable and Bioresorbable Polymers for Tissue Engineering</b> .....	<b>31</b>

Abstract.....	31
2.1 Introduction.....	31
2.2 Materials and Methods.....	34
2.2.1 Materials .....	34
2.2.2 Synthesis of Photocurable PLA .....	35
2.2.3 Synthesis of Photocurable PCL .....	36
2.2.4 Polymer Characterisation.....	37
2.2.5 Thin Film Preparation by Spin Coating .....	37
2.2.6 Swelling Analysis and Degradation of Photocurable PLA.....	38
2.2.7 Cell Culture.....	38
2.2.8 Human Dermal Fibroblast Culture.....	39
2.2.9 Human Dermal Fibroblast Medium .....	39
2.2.10 Cell Passaging.....	39
2.2.11 Cell Counting.....	40
2.2.12 MTT Assay .....	40
2.2.13 Statistical Analysis.....	41
2.2.14 Confocal Microscopy and Cell Staining .....	41
2.3 Results.....	41
2.3.1 Polymer Characterisation and Cell Culture .....	41
2.3.2 Polymer Characterisation.....	42
2.3.3 Swelling Analysis and Degradation.....	43
2.3.4 Human Dermal Fibroblast Culture on Polymeric Thin Films .....	45
2.4 Discussion .....	49
2.5 Conclusions.....	50
<b>Chapter 3: Dynamic Projection Microstereolithography for Tissue Engineering .....</b>	<b>51</b>
Abstract.....	51
3.1 Introduction.....	51
3.2 Materials and Methods.....	53
3.2.1 Design Study: Development of a Projection Microstereolithography Workstation .....	53
3.2.2 Photocurable Material Preparation .....	56
3.2.3 Sample development.....	57
3.2.4 Scanning Electron Microscopy .....	57
3.2.5 Cell Culture Methods.....	57

3.3 Results and Discussion .....	58
3.4.1 Applications: Microfabricated Stem Cell Niches for Corneal Repair .....	67
3.4.2 Applications: Nerve Guidance Conduits .....	73
3.5 Discussion .....	76
3.6 Conclusions.....	77
<b>Chapter 4: Development of a Two photon Laser Direct Write Workstation.....</b>	<b>78</b>
Abstract.....	78
4.1 Introduction.....	78
4.2 Materials and Methods.....	79
4.2.1 Design Study: Two Photon Laser Direct Write System .....	80
4.2.2 Laser Selection.....	80
4.2.3 Assembly of the System.....	82
4.2.4 Preparation of a Photosensitive Solution .....	83
4.2.5 Sample Preparation for Laser Direct Write .....	84
4.2.6 Focusing of the Beam .....	85
4.2.7 Writing of the Sample .....	87
4.2.8 Sample Development .....	88
4.2.9 Cell Culture Methods.....	88
4.2.10 Scanning Electron Microscopy .....	89
4.3 Results.....	89
4.3.1 Microstructuring of Photocurable PLA and Ormocer .....	89
4.3.2 Structuring of the Photocurable PLA.....	91
4.3.3 Improved Resolution using a Telescopic Lens Arrangement .....	93
4.3.4 Use of Solid State Lasers as a Compact Low Cost Light Source .....	95
4.3.5 Microfabrication of Lab on a Chip Arrays for the Analysis of Neuronal Cells .....	97
4.3.6 Porous Microstructures as Neural Cell Scaffolds or Niches.....	98
4.4 Discussion.....	101
4.5 Conclusions.....	102
<b>Chapter 5: Two Photon Laser Direct Write of Bioresorbable Resins for Neural Tissue Engineering Applications .....</b>	<b>103</b>
Abstract.....	103
5.1 Introduction.....	103
5.2 Materials and Methods.....	106
5.2.1 Synthesis of Photocurable PLA and PCL .....	106

5.2.2 Photocurable Polymer Characterization .....	106
5.2.3 Photosensitive Solution Preparation .....	107
5.2.4 Thin Film Preparation .....	107
5.2.5 Sample Preparation for Laser Direct Write .....	108
5.2.6 Laser Direct Write of 3D Structures .....	108
5.2.7 Characterisation of Thin Films .....	109
5.2.7.1 X-Ray Photoelectron Spectroscopy .....	109
5.2.7.2 Surface Wettability by Water Contact Angle Measurement.....	109
5.2.7.3 Scanning Electron Microscopy .....	109
5.2.8 Cell Culture and Biological Testing .....	109
5.2.8.1 General Cell Culture .....	109
5.2.8.2 Sample Fixation for SEM .....	110
5.2.8.3 MTT Assay .....	110
5.2.8.4 PicoGreen DNA Quantification Assay .....	111
5.2.8.5 Live-Dead Assay.....	111
5.2.8.6 Statistical Analysis and Significance .....	112
5.2.8.7 Phenotypic Analysis of NG108-15 Cells .....	112
5.2.8.8 Cell Visualization Using Confocal Microscopy .....	113
5.3 Results and Discussion .....	113
5.3.1 Polymer Characterisation.....	114
5.3.2 Surface Characterisation of Photocured Polylactic acid Thin Films .....	114
5.3.3 Structuring of the Photocurable PLA.....	118
5.3.4 Neuronal Cell Growth and Viability on Polymer Thin Films.....	118
5.3.5 MTT and Cell Proliferation Assay with NG108-15 Cell Line .....	119
5.3.6 DNA Quantification Assay .....	121
5.3.7 Live-Dead Staining with PC12 Cells.....	121
5.3.8 Cell Morphology on Photocurable PCL Thin Films.....	123
5.3.9 Cell Culture on Microfabricated Structures .....	124
5.3.10 Guided Cell Growth on Aligned Microstructures.....	125
5.3.11 Neuronal Cell Attachment and Growth on PLA Lines .....	126
5.3.12 Visualization of Neurites by Labelling for $\beta$ -III tubulin.....	127
5.3.13 NG108 Cell Growth on Suspended Fibre Model Structures .....	128
5.3.14 Self Assembled Scaffolds and Cell Delivery Vehicles.....	128

5.4 Conclusions.....	131
<b>Chapter 6: Replication of Two photon Laser Direct Write Produced Structures for Nerve Guidance Conduits with Functional Structure.....</b>	<b>132</b>
Abstract.....	132
6.1 Introduction.....	133
6.1.1 Soft Lithography using Poly(dimethylsiloxane).....	134
6.1.2 Synthetic Materials for Nerve Guidance Conduits.....	135
6.1.3 The Role of Schwann Cells in Nerve Regeneration.....	135
6.1.4 An Optimized Approach to Nerve Guidance Conduits.....	136
6.2 Materials and Methods.....	137
6.2.1 Photocurable Material Synthesis and Preparation.....	137
6.2.2 Four-armed PLA synthesis.....	137
6.2.3 Methacrylate Functionalization of the Four Armed PLA.....	138
6.2.4 Photosensitive Solution Preparation.....	138
6.2.5 Two Photon Laser Direct Write.....	138
6.2.6 PDMS Replication of Structures.....	139
6.2.7 Materials Characterization.....	139
6.2.8 Cell Culture and Analysis.....	139
6.2.8.1 Schwann Cell Isolation and Culture.....	139
6.2.8.2 Material Genotoxicity Analysis using Comet Assay.....	140
6.2.8.3 Schwann Cell Proliferation, Morphology and Purity on PLA Substrates.....	142
6.2.8.4 Cell Proliferation Assay.....	142
6.2.8.5 MTT Assay.....	142
6.2.8.6 Scanning Electron Microscopy.....	143
6.2.8.7 Confocal Imaging of Schwann Cells.....	143
6.2.8.8 Statistical Testing.....	144
6.2.8.9 Quantification of Schwann Cell Purity.....	144
6.3 Results.....	144
6.3.1 Structuring Resolution.....	145
6.3.2 Direct Write of Multi-Lumen Discs.....	145
6.3.3 Material Genotoxicity Analysis using Comet Assay.....	146
6.3.4 Schwann Cell Viability and Adhesion.....	147
6.3.5 Schwann cell Proliferation Assay.....	147
6.3.6 Analysis of Schwann Cell Morphology.....	149

6.3.7 Schwann Cell Culture on Stackable Multi-Lumen Discs .....	153
6.4 Discussion .....	155
6.5 Conclusions.....	157
<b>Chapter 7: Thesis Summary .....</b>	<b>159</b>
Abstract.....	159
7.1 Microfabrication of Designer Tissue Engineering Devices.....	159
7.2 Custom Polymers and Designer Biomaterials for Tissue Engineering.....	160
7.3 Device Fabrication using Microstereolithography.....	160
7.4 Future Work .....	161
<b>References.....</b>	<b>163</b>

# Chapter One: Applications of Microstereolithography in Tissue Engineering

---

*Adapted from the book chapter 'Two Photon Polymerisation for Tissue Engineering Scaffold Fabrication' by Andrew A. Gill and Frederik Claeyssens.*

## **Abstract**

The production of bespoke 3D microstructures from biocompatible and bioresorbable materials via free-form fabrication opens up a wide range of possibilities for the creation of structurally optimised and chemically functionalized tissue scaffolds, as well as other implantable medical devices such as microneedle arrays and patient specific prostheses. In this literature review the production of user-defined tissue engineering scaffolds and other implantable devices via microstereolithography is highlighted. This technique utilises photopolymerization processes (both 1- and 2-photon) to produce (sub)micrometer feature size 3D objects. Both the main fabrication processes used and relevant applications studied by researchers in this emerging field are discussed. Common fabrication systems will be examined as well as the expanding range of materials that may be used. The design of efficient photoinitiators facilitating the use of relatively inexpensive microlaser systems will be highlighted as well as future perspectives for the technology.

## **1. Introduction**

### **1.1 Microstereolithography**

Microstereolithography refers to a class of rapid prototyping technologies first explored in the 1980's (Narayan et al. 2010). The technique relies on the photo-crosslinking of a curable prepolymer or resin according to a predetermined design to create a solid polymerized object. Typically either a pattern of light is formed by a static or dynamic masking technique and projected into a thin layer of photosensitised prepolymer (Ha, Choi, and Lee 2008) (projection microstereolithography) or a focused laser beam is scanned over the photosensitised polymer according to a computer design, writing out the desired image

(scanning microstereolithography) (Gandhi and Deshmukh 2010). When the process is finished the remaining uncured prepolymer is washed out using a solvent (developer) leaving the resulting structure intact. To create three dimensional objects consecutive layers of prepolymer are added and cured, before the uncured prepolymer or resin is washed out to give a multi-layered structure.

## **1.2 Microstereolithography in Comparison with Other Techniques**

The use of microstereolithography for the fabrication of tissue scaffolds and other medical devices has evolved into a significant research area since its conception as a rapid prototyping technology in the 1980's. One of the main advantages of microstereolithography, as in other direct write techniques for scaffold fabrication is the ability to create scaffolds with a specific pore geometry and distribution simply by creating a 3D model in CAD-CAM software. Pre-existing technologies for the creation of bulk porous structures such as particulate leaching, gas foaming, freeze drying and phase separation are all capable of creating bulk structures with a high degree of porosity, but give little control over pore distribution, interconnectivity and pore geometry as well as the effect these features have on the bulk scaffold mechanical properties (Coutu, Yousefi, and Galipeau 2009).

Layer-by-layer solid free-form fabrication (SFF) techniques such as laser sintering, 3D printing or bioplotting using nozzle ejection systems provide a method of creating structures with designer features (Hollister 2005). The mechanical performance of scaffolds produced using SFF techniques is far superior to bulk processed ones. The maximum compressive modulus of scaffolds made by traditional processing techniques such as porogen leaching is around 0.4 MPa (Ma and Choi 2001), as porosity is inversely related to mechanical strength. The mechanical modulus of hard tissue (for example bone) is between 10-1500 MPa (Goulet et al. 1994; Hollister 2005) and clearly these scaffolds do not possess sufficient strength to match these properties. Fused deposition modelling of polycaprolactone (PCL) was used to produce scaffolds with a high porosity (48-77%) with compressive moduli ranging from 4-77 MPa and yield strength from 2.58 to 3.32 MPa (Hutmacher et al. 2001).

Computational models can be used to determine the optimum scaffold macro to nanostructure with respect to nutrient and metabolite diffusion, cell distribution and attachment and also scaffold mechanical strength (Chua et al. 2003a, 2003b). The benefit of a computer designed scaffold architecture that facilitates diffusion within a highly connected network of pores was

demonstrated by Melchels *et al.* (Melchels, Barradas, et al. 2010), who showed that cells within a microstereolithography produced scaffold were evenly distributed throughout the structure whereas cells in a scaffold produced by salt leaching with comparable overall porosity were limited to the very surface of the structure.

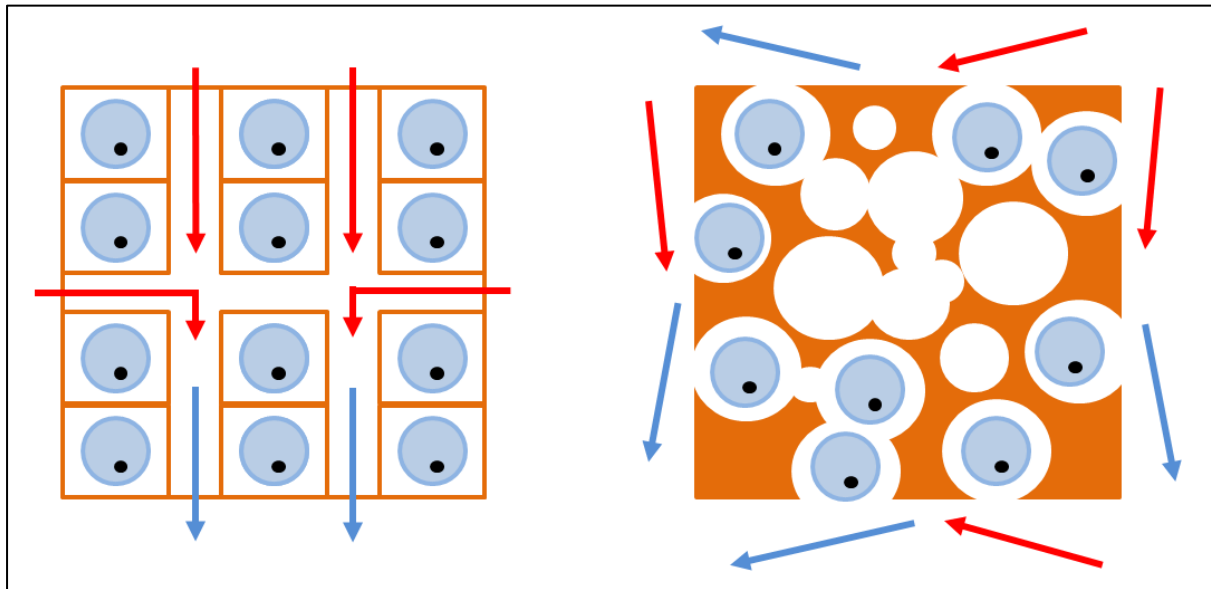


*Figure 1: Scaffolds prepared by microstereolithography (left) with uniform architecture allow even nutrient and cell distribution throughout the scaffold, whereas scaffolds prepared by foaming or porogen leaching (right) have limited cell and nutrient distribution and uneven mechanical properties.*

Another possibility with microstereolithography is the fabrication of patient specific scaffolds and other medical devices. In one example a scaled down model of a human kidney was produced using deconstructed medical CT data as a proof of concept (Choi, Wicker, Lee, et al. 2009). The fabrication of scaffolds with custom architecture allows the balancing of mass transport and mechanical support within the structure which allows an even distribution of cells to be achieved (Hollister 2005). Rapid prototyping can be viewed as an economic method of producing scaffolds with high reproducibility in terms of microstructure and mechanical properties (Hutmacher, Sittinger, and Risbud 2004).

### **1.3 Features of Microstereolithography**

Two photon polymerization trades fabrication speed for resolution. Whereas typical one photon scanning systems can have a write speed of up to  $500 \text{ mm s}^{-1}$ , 2PP is approximately a thousand-fold slower at around  $1 \text{ mm s}^{-1}$  (Stampfl et al. 2008). The benefit of this trade-off is

that resolutions of 200-300 nm can be achieved routinely (Serbin et al. 2003) and resolutions as low as 100 nm have been achieved, for example by using quenchers to prevent polymerization from spreading beyond the focal point (Takada, Sun, and Kawata 2005).

Due to its precise nature, the technique is ideally suited to the fabrication of small scale prototypes and high resolution microdevices with niche applications. Additionally, the true three-dimensional writing ability of 2PP makes it ideal for creating seamless microdevices with complex internal parts, such as microactuation valves (Schizas et al. 2010) and microphotonics (Ostendorf and Chichkov 2006).

As the field of scaffold fabrication by 2PP grows, the capabilities of the technique are increasing, due to advances in photoinitiators and lasers (Wang et al. 2002), computer model optimisation (Park et al. 2005), parallel processing (Kato et al. 2005), optics and instrument design (Hsieh et al. 2010) and materials development (Melchels, Feijen, and Grijpma 2009). The field is now nearing a point where it can grow from a small scale prototyping technique limited to a narrow range of materials to a state of the art technology which can be exploited for the fabrication of scaffolds with unparalleled resolution fabricated from a diverse range of polymers (Gill and Claeysens 2011), functionalized biological materials (Ovsianikov, Deiwick, et al. 2011) and hydrogels (Jhaveri et al. 2009).

Two photon polymerization presents a method for the production of patient specific devices with accurate resolution, and is ideal in situations where cells require contact guidance or a precise local environment in order to promote functional recovery. One example of this is in nerve entubulation devices or nerve guidance conduits (NGC's), where microstructure has been demonstrated to enhance functional recovery of transected nerves (Bunge 1994). Microstereolithography and 2PP may be used to optimise and produce nerve guidance conduits with performance superior to simple tubular devices (Melissinaki et al. 2011).

#### **1.4 Materials for Microstereolithography**

Early research into the use of 2PP in areas such as photonics (Ostendorf and Chichkov 2006) required materials that gave good structuring results without placing too many requirements on the specific chemical nature of the resulting structure beyond physical robustness. Well characterised photoresist materials used in conventional lithographic techniques, such as Ormocer (organically modified ceramic polymer) and SU8, fulfilled these demands and have been used in a wide range of applications. The demonstrated biocompatibility (Doraiswamy

et al. 2005) of Ormocer saw it used in a range of medical studies as discussed in following sections. Additionally, these materials exhibit low shrinkage (Winfield and O'Brien 2011), a problem often encountered with small molecule resins (Farsari et al. 2006) which can reduce final structure quality. The drawback with these materials for the creation of tissue scaffolds is that they are not bioresorbable (biodegradable) and once implanted into the body will remain there permanently or until removed, requiring follow up surgery.

Bioresorbable photocurable polymers based on well characterised polymeric biomaterials such as polylactic acid (PLA), polycaprolactone (PCL), polyglycolic acid (PGA), trimethylene carbonate (TMC) amongst others have been developed (Kwon and Matsuda 2005; Mizutani and Matsuda 2002a, 2002b; Matsuda, Kwon, and Kidoaki 2004; Bat et al. 2011; Melchels, Barradas, et al. 2010; Melchels, Feijen, and Grijpma 2009; Melchels et al. 2011; Pego et al. 2003; Seck et al. 2010; Claeysens et al. 2009). The common feature of these polymers is the inclusion of hydrolysable ester bonds between monomers which allow them to degrade following implantation. Typically a low molecular weight oligomer is prepared from a multi-armed initiator which serves as the core for ring opening polymerization with the selected monomer using stannous octoate catalyst (Gill and Claeysens 2011). Photo-crosslinkable end groups such as methacrylates or coumarins are then added to make the oligomers photocurable. Microwave assisted synthesis has recently been employed in the preparation of polyethylene glycol based resorbable hydrogels incorporating polylactic acid segments and methacrylate end groups, presenting a rapid and easily accessible method of preparing photocurable materials with a diverse range of monomers (Seck et al. 2010). Structuring of photocurable gelatin was also recently reported using methacrylate functionalization (Ovsianikov, Deiwick, et al. 2011).

Another important class of materials commonly used for tissue engineering purposes are hydrogels (Lee and Mooney 2001; Mahoney et al. 2005). These soft polymers are attractive scaffold materials due to their biocompatibility and tuneable cell adhesiveness as well as high moisture content (Halstenberg et al. 2002; Luo and Shoichet 2004). Photocurable hydrogel materials such as polyethylene glycol diacrylate (PEGDA) are amenable to direct structuring in aqueous media (Jhaveri et al. 2009) or photo-crosslinking via one photon curing to create a cross-linked network followed by three-dimensional patterning of photolabile chemical cues which influence the behaviour of cells contained within the gel (Luo and Shoichet 2004).

A range of techniques have been investigated for patterning of hydrogels, such as one photon lithography (Yu and Ober 2003), microfluidic patterning (Tan and Desai 2003) and 3D-printing (Mironov et al. 2003) amongst other additive layer technologies (Mironov et al. 2008). These layer-by-layer processing techniques give the desired control over features of individual layers, however in the vertical or 'z' plane the coherence between individual layers is poor (Luo and Shoichet 2004). In this respect, there is an apparent advantage of 'in-volume' two photon direct write over these competing technologies.

Hydrogels allow the encapsulation of live cells into scaffolds. For example in the study by Lee *et al.* (Lee, Moon, and West 2008) a photocurable and degradable acrylate-PEG-(peptide-PEG)<sub>n</sub>-acrylate hydrogel was prepared and used to encapsulate human dermal fibroblasts, by cross-linking via one photon curing. The encapsulated cells were then soaked with a solution containing acrylate conjugated PEG-RGDSK (Arg-Gly-Asp-Ser-Lys, a cell adhesive ligand), and two photon laser scanning technique was used to selectively conjugate the cell adhesive ligand throughout the matrix according to a pre-determined design. This technique was demonstrated to guide cell migration throughout the hydrogel. Similar techniques have been applied in order to pattern growth factors and other proteins within hydrogel constructs (Schneider et al. 2001; Melchels, Bertoldi, et al. 2010) and influence stem cell differentiation.

### **1.5 Two Photon Polymerization**

Microstereolithography systems based on one photon processes rely on the linear absorption of light by a photoinitiator within the volume of the prepolymer, as described by the Beer-Lambert law. Drawbacks with these systems include overpenetration of light within the photosensitive resin leading to overcuring of layers, light scattering within the resin reducing resolution and the accumulation of partially cured oligomers within the internal features of the fabricated structures (Choi, Wicker, Lee, et al. 2009). Furthermore, the need to fabricate structures in a layer-by-layer process can lead to 'stepping effects' resulting in small ridges on the external features of the structure. Oxygen quenching of radicals on the surface can further complicate the curing process, requiring materials to be purged with nitrogen or argon prior to curing and nitrogen blanketing during the cure step.

To overcome these drawbacks careful calibration of the cure depth, exposure time and light intensity is required. Light absorbing dyes have been used to successfully improve resolution

by reducing penetration and scattering (Choi, Wicker, Cho, et al. 2009), however when preparing implantable devices for regenerative medicine the effects of these additives on the biocompatibility of the fabricated structures requires further investigation. Cure times are also increased due to the absorption of light by the dye, which reduces the curing rate. Purging individual layers between exposures with an inert liquid such as perfluorohexane has also been shown to improve feature resolution by washing away partially cured oligomers (Han et al. 2008), improving internal feature definition but further complicating the fabrication process.

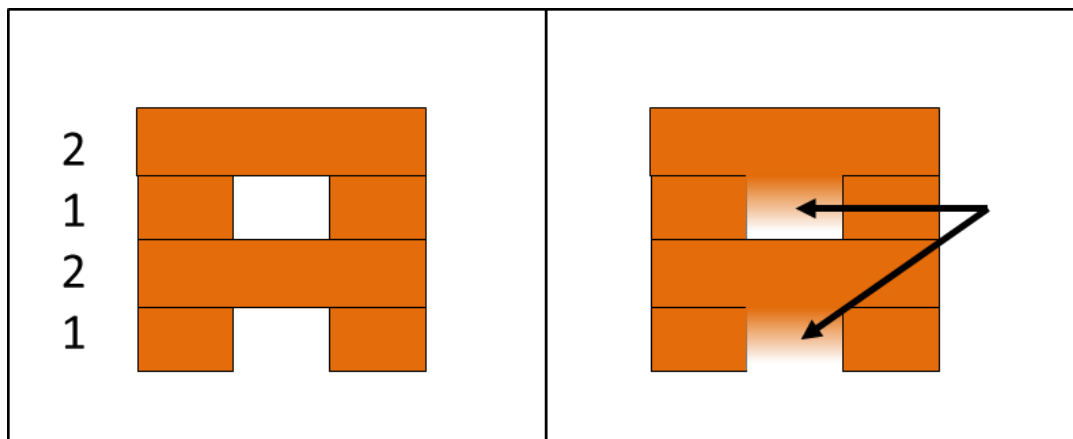


*Figure 2: Image illustrates a structure consisting of two layers (1 and 2) cured consecutively to create overhanging features. Structure on right displays overcuring of layer 2 (indicated by arrows) leading to loss of spaces between layers. For an example see Choi et al. (Choi, Wicker, Cho, et al. 2009).*

First applied to lithography in 1992 by Wu *et al.* (Wu et al. 1992) with the aim of improving the resolution of UV lithography for microelectronics applications, non-linear optical processes have been utilised to overcome the problems of typical one photon lithography methods. These multiphoton processes were first predicted by Maria Göppert-Mayer (Göppert-Mayer 1931) in 1931 and demonstrated by Kaiser and Garrett in 1961 (Kaiser and Garrett 1961).

Similar to multiphoton microscopy, two photon polymerization (2PP) relies on the non-linear absorption of two photons of light simultaneously by a photoinitiator to initiate curing processes. Due to the short lifetimes of the intermediate states involved (around  $10^{-15}$ s for true three dimensional two photon polymerization (Lee et al. 2006)) initiation only occurs at very high photon density, as predicted by the theory in 1931.

Polymerization is usually achieved by focusing femtosecond pulsed radiation from a Titanium: sapphire laser through a high numerical aperture lens, with initiation occurring at the focal point of the objective (see figure 3). Since polymerization is only initiated at the focal point of the objective, by scanning the focal point within the volume of a photosensitive resin, three dimensional structures can be written out according to a computer model in a CAD-CAM fashion (Serbin and Chichkov 2003; Stute et al. 2004).

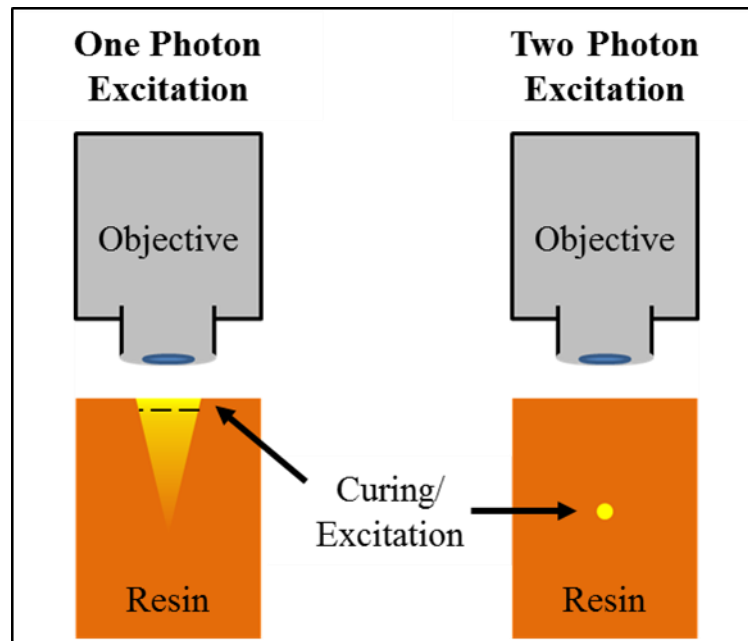


*Figure 3: In one photon polymerization light is absorbed and initiates curing in a linear fashion with curing limited to the first few hundred micrometres of resin below the surface (left). In two photon polymerization curing occurs only at the focal point of the beam where photon density is high enough to initiate two photon processes (right).*

The majority of materials used for 2PP are the same as those used in UV photolithography, due to their commercial availability. Organically modified ceramic resists (ORMOCERS) for example give excellent structuring results in both UV curing and 2PP (Lee et al. 2006). Initially explored for more typical microfabrication applications such as photonics and micro-optics (Ha, Choi, and Lee 2008; Gandhi and Deshmukh 2010; Choi, Wicker, Cho, et al. 2009), research using these materials has attracted the attention of tissue engineers. The high resolution of 2PP allows the creation of designer tissue scaffolds with defined pore size (Claeysens et al. 2009), microneedles with reduced penetration cross section (Doraiswamy

et al. 2006), microvalves with defined internal structure (Schizas et al. 2010) and a wide range of other potential applications.

The choice of photoinitiators has also until recently relied on commercially available initiators typically used for one photon processes such as Michler's ketone (4,4'-bis(*N,N*-dimethylamino)benzophenone). Efforts are now under way to create more suitable photoinitiators with an improved two photon absorption cross-section (Lemercier et al. 2006). Although the majority of published work relies on femtosecond pulsed Ti: sapphire lasers emitting at around 800 nm, comparable results have also been achieved with less powerful laser systems. Q-switched Nd<sup>3+</sup>:YAG microlasers emitting at 1064nm and 532nm with peak powers between 0.1 and 1kW, sub-nano/ picosecond pulse durations and repetition rates on the kHz scale have also been shown to be capable of initiating 2PP (Wang et al. 2002).

The efficiency with which 2PP can be initiated is determined not only by the two photon absorption cross section of the photoinitiator (a measure of the ability of the initiator to absorb two photons simultaneously) but also the ability of the initiator to generate radicals in the excited state. A good initiator will require a low power to efficiently generate polymerization. Additionally the energy gap between the initiation threshold and the power threshold at which material damage occurs should be as high as possible for reproducible structuring. The design of efficient photoinitiators is highlighted later in this chapter.

## **1.6 Two Photon Stereolithography**

Two photon polymerization can achieve higher resolution three dimensional structuring than any commercially competing technology (however experimental techniques such as two colour lithography can demonstrate better resolution (Scott et al. 2009)). According to Abbe's diffraction limit, the resolution of a focussed laser is limited by the wavelength of light used and the numerical aperture (NA) of the focusing objective, preventing one photon based stereolithography techniques achieving a sub micrometer resolution (Fischer and Wegener 2011). Other high resolution techniques such as e-beam lithography are limited to surface effects, unlike two photon polymerization which is an in-volume technique. (Farsari, Vamvakaki, and Chichkov 2010). Although there are exceptions such as carbon vapour deposition (van Dorp and Hagen 2008), these techniques are not well suited to scaffold fabrication due to limitations for example on the materials that can be used. Sub 100 nm three dimensional structuring with 2PP has been achieved (Haske et al. 2007).

### 1.6.1 Initiation of Polymerization Processes

Two photon absorption occurs by two mechanisms, sequential and simultaneous absorption of two photons of light. In sequential absorption, one photon of light is absorbed by the excited species promoting the absorber to a real intermediate excited state. A second photon is then absorbed within the lifetime of this excited species ( $10^{-4}$  to  $10^{-9}$  seconds) (Lee et al. 2006). The presence of the real intermediate state would require the material to absorb at this wavelength and hence absorption would be governed by the Beer-Lambert law (Farsari, Vamvakaki, and Chichkov 2010). The process which drives 2PP involves the simultaneous absorption of two photons of light by the photoinitiator. As there is no real intermediate state the material is transparent to light of the wavelength of the exciting radiation and two photons must arrive within the lifetime of the virtual excited state ( $10^{-15}$ s) to initiate polymerization. The short lifetime of the virtual state means that high intensities of light are required. This is typically achieved with a femtosecond pulsed Ti: sapphire laser. Ti: sapphire lasers are favoured because of their short pulse length which limits thermal damage or burning of the sample, and because these lasers typically emit light at around 800 nm, which is appropriate for the two photon excitation of a wide range of UV sensitive photoinitiators, as the energy gap corresponds to approximately twice the energy of a photon at this wavelength. Many UV initiators and curable materials are also transparent at this wavelength allowing light to be focussed within the volume of the material and interact only with the desired initiator via two photon mechanisms.

The two photon absorption cross section ( $\sigma_{TPA}$ ) of an initiator determines the suitability of an initiator for two photon polymerization, and describes the ability of the initiator to absorb two photons of light simultaneously. This is typically expressed in units of GM (Göppert-Mayer's, after Maria Göppert-Mayer, with 1 GM being equivalent to  $1 \times 10^{-50} \text{ cm}^4 \text{ s photon}^{-1}$  (Wu, Serbin, and Gu 2006)). Molecular engineering of photoinitiators seeks to maximise the two photon absorption cross section by conjugating electron donating (D) or electron accepting (A) groups to a  $\pi$  charge transfer system in a symmetric sequence (D- $\pi$ -A- $\pi$ -D) allowing stabilization of the intermediate state by charge delocalization. Unsymmetrical 'push-pull' molecules, for example a D- $\pi$ -A systems also enhance the two photon susceptibility of the molecule increasing the two photon absorption cross section (Baldeck, Stephan, and Andraud 2010; Gan et al. 2009). The development of better photoinitiators is an important step in making 2PP systems more available and reducing the dependence on expensive femtosecond-pulsed laser systems.

Another important factor for efficient photoinitiators is their ability to generate radicals in the excited state. Initiator-coinitiator systems which facilitate radical transfer from initiator to polymer have been explored (Belfield et al. 2000) as well as molecules which (a) have improved absorption cross sections and (b) contain amine groups which facilitate radical generation (Kuebler, S. M. et al. 2001). Two photon sensitive initiators for Ti: sapphire lasers emitting at around 800 nm have seen extensive optimisation (Lemercier et al. 2006). Additionally, initiators tuned to the operating wavelengths of Q-switched Nd:YAG microlasers (532 nm, 1064 nm) have been synthesised to facilitate efficient structuring with lasers of much lower specification and cost, and these lasers are expected to become a routine alternative to powerful femtosecond Ti: sapphire systems (Baldeck, Stephan, and Andraud 2010).

### **1.6.2 Experimental set-ups for Two Photon Polymerization**

The CAD-CAM nature of two photon polymerization makes it an attractive technique for tissue scaffold fabrication, allowing a diverse range of scaffold architectures to be explored simply by changing the computer model. Typical setups combine a femtosecond pulsed Ti: sapphire laser emitting in the region of 800 nm with a Galvano-scanner controlled by CAD-CAM software which moves the focus of the beam within the horizontal plane of a high NA objective. Vertical stepping is most commonly achieved using a piezo-electric stage. On-line monitoring may be achieved by focusing a CCD camera through the focusing system using a dichroic mirror to image the curing process within the volume of the resin. Since most materials undergo a change of refractive index upon curing, the polymerization process can be visualised by the appearance of the structure within the polymer.

A three dimensional computer model of the desired structure is generated with modelling software. This model is then sliced into a series of horizontal slices which are written out in a layer-by-layer fashion by scanning the beam within the volume of the resin, with the height of the substrate being adjusted by a high precision piezo-electric stage. Either the entire volume of the structure is cured in the writing step (raster scanning) or only the outline is cured in the writing step (contour scanning) (Lee et al. 2006) and the inner volume of the structure cured in a post-processing step using one-photon curing (Sun and Kawata 2003).

### 1.6.3 Improving the Efficiency and Cost of 2PP

Barriers to the more mainstream adoption of 2PP as a routine research technique include the costs involved, mainly resulting from the high power laser systems required and additionally the small scale of the structures that can be fabricated due to the limited write area or ‘footprint’ of most systems currently in use.

Many 2PP systems use oil immersion lenses due to their high numerical aperture and precise focusing. Moving from oil lenses to air lenses overcomes the height limitations imposed by the need to dip the lens within a small drop of oil, as demonstrated in the study by Hsieh et al. (Hsieh et al. 2010). Structures fabricated with oil lenses are limited to a height of about 1mm (the focal length of the objective, which cannot be lifted from the oil droplet) however using an air lens the authors claim a scan height of 30 mm. A scan speed of 30 mms<sup>-1</sup> is also reported along with a resolution of around 100 nm. Finally the authors produced a cubic porous scaffold applied to hepatocyte culture with dimensions of 2.5 mm<sup>3</sup> representing a step forwards from micrometer scale to millimetre scale scaffolds.

A range of optical components and techniques have also been investigated for improving the processing time required for 2PP. Parallel processing using refractive and diffractive optics to split the beam into an array of smaller beams has been demonstrated (Kato et al. 2005; Winfield et al. 2007a) and up to 227 structures have been fabricated simultaneously in one fabrication cycle (Bhuiyan et al. 2007). Axicon lenses have also been explored as a way of generating three dimensional shapes in a single exposure (Winfield et al. 2007b; Bhuiyan et al. 2007).

A common method for creating structures from a 3D computer model via 2PP is the single dimensional scanning method (SSM) (Park et al. 2005). A 3D digital model of the object to be fabricated is converted to a polyhedral one and then sliced into a series of parallel layers along a plane defined by the user. These layers are then converted into a scanning path for the laser. The slowest fabrication method is to write out the entire volume of the structure using this map (raster scanning). A more efficient way is to only write out the solid outer shell or ‘contours’ of the structure (contour scanning method, CSM), also known as vector scanning (Sun and Kawata 2003), solidifying the internal volume of the structure post-development by exposure for example to UV light. This method reduces the number of individual voxels (volume pixels) which make up the structure. As demonstrated by Sun and Kawata (Sun and Kawata 2003), a ‘microbull’ structure composed of 2x10<sup>6</sup> voxels was fabricated by raster

scanning in a time of 3 h. The outer shell of the bull could be recreated accurately using only 5% of these voxels, and using the contour scanning method the bull was recreated in only 13 minutes.

Contour scanning has been further improved to compensate for difficulties in creating near flat surfaces within polymerized objects. If an object created by contour scanning is not sealed sufficiently before development the outer shell can tear and release the inner uncured resin leading to collapse of the structure. As the fabricated surface approaches horizontal, careful stepping of the layers is required to create sufficient overlap, preventing breakage. This requires a large number of voxels and leads to very long fabrication times. A two dimensional slicing method (TSM) has been developed to simplify the scan paths of structures with near flat surfaces (Liao et al. 2007). In one example, a polyhedral model of a microdragon sliced by SSM consisting of 871414 polygons was reduced using TSM to 16620 polygons. Using TSM the fabrication took nineteen minutes, it is estimated that using SSM it would have taken 12.66 h. The fabricated dragon is shown in figure 4.

### **1.7 Tissue Scaffolds and the Extracellular Matrix**

A particular challenge that two photon polymerization is suited to address is that of tissue scaffold fabrication (Hsieh et al. 2010). Tissue scaffolds generally provide an artificial extracellular matrix (ECM) in which cells can proliferate and grow, forming an engineered tissue (Langer and Vacanti 1993). Additionally these scaffolds may be made from a biodegradable material which breaks down as the cells form their own extracellular matrix, eventually disappearing completely (Atala et al. 2006). The purpose of the scaffold is to provide mechanical protection for the growing tissue, as well as providing a general structure for cell attachment (Bellucci et al. 2011). The three-dimensional micro environment of the tissue scaffold has also been demonstrated to affect the behaviour and proliferation of the cells within, with cells cultured in a 2D monolayer fashion not behaving as closely to those in normal living tissue compared to their 3D scaffold cultured counterparts (Abbott 2003).

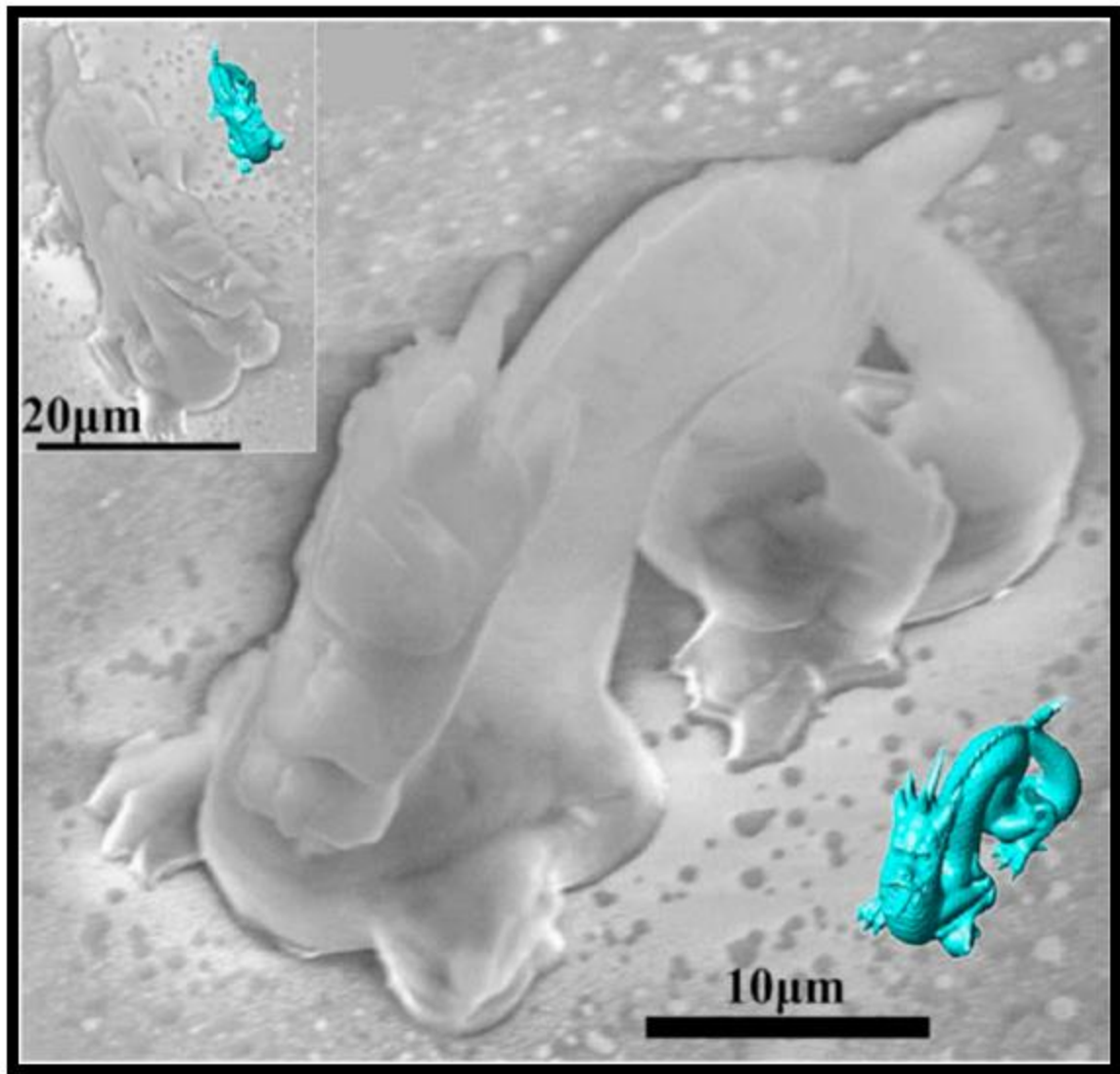


*Figure 4: Microdragon fabricated using two dimensional slicing method (TSM) technique, showing 3d model. Reprinted with permission from (Liao et al. 2007). Copyright 2007, American Institute of Physics.*

It has been demonstrated that different cell types perform better in different internal pore geometries, and so in creating custom scaffolds the pore shape may be tailored to the desired tissue type. Furthermore, different cell types have different optimum pore sizes, for example bone cells (osteoblasts) function optimally in scaffolds with a pore size of around 350  $\mu\text{m}$ , liver cells (hepatocytes) prefer smaller pores of around 20  $\mu\text{m}$  and fibroblasts 5-15  $\mu\text{m}$  (Whang et al. 1999).

Typical bulk scaffold fabrication methods consist of techniques such as particulate leaching or gas blowing to create porous foams. Scaffolds fabricated in this way tend to perform

poorly, with cell ingrowth being confined to the first 200  $\mu\text{m}$  of the scaffold below the surface (Awwad et al. 1986; Colton 1995). Additionally, these scaffolds typically do not give sufficient mechanical strength for load bearing applications such as bone scaffolds, or even soft tissues (Hollister 2005). Mass transport is also poor due to low pore interconnectivity (Melchels, Barradas, et al. 2010).

Stereolithography (including two photon polymerization) is an ideal technique for addressing these issues. Pore geometry and the overall scaffold porosity can be changed simply by changing the computer model, and furthermore medical imaging data such as computerized tomography (CT) and magnetic resonance imaging (MRI) may be converted directly to CAD models in order to produce patient and injury specific scaffolds (Schlosshauer et al. 2006).

### **1.8 Biomedical Applications of Microstereolithography**

As discussed in earlier sections, microstereolithography is well suited to the production of tissue scaffolds with optimum pore geometry with respect to nutrient and metabolite diffusion. User defined scaffold structuring via 2PP allows the investigation and production of scaffolds which can be tailored to the ideal pore size and geometry of a given tissue simply by adjusting the 3D model in a CAD-CAM software suite. It has been demonstrated that microscale features can have a profound effect on cell behaviour (Chen et al. 1997; Dike et al. 1999), as well as cell migration and scaffold mechanical properties. Additionally features such as vasculature for nutrient/ metabolite transport and features that can give mechanical strength to the structure can be written directly into the scaffold.

Beyond the development of tissue scaffolds, the technique is finding applications in patient specific prostheses and geometrically optimised implantable devices such as microneedles and cell delivery vehicles, which will be discussed below.

#### **1.8.1 Implantable Medical Devices Created by 2PP**

Initial work into the fabrication of permanent scaffolds from off the shelf materials such as Ormocers and SU8 assessed the biocompatibility of these materials (Schlie et al. 2007; Ovsianikov, Schlie, et al. 2007) and demonstrated cell growth on small scale scaffold like structures. The suitability of these and similar materials for two photon based microstructuring and their demonstrated biocompatibility and cell adhesiveness led to a number of publications regarding their use in small scale medical devices (Schizas et al.

2010) (Doraiswamy et al. 2006; Ovsianikov, Ostendorf, and Chichkov 2007; Ovsianikov, Chichkov, Mente, et al. 2007).

### **1.8.2 Prostheses**

Ovsianikov *et al.* (Ovsianikov, Chichkov, Adunka, et al. 2007) used two photon polymerization ofOrmocer for the fabrication of ossicular replacement prostheses, implantable devices which are intended to improve hearing by reconstructing ossicles, structures located within the inner ear which may be damaged by disease (Albu, Babighian, and Trabalzini 1998). This application requires structures which exhibit good stability and mechanical properties, retaining their structure throughout the lifetime of the implant. The material must be non-toxic, cell adhesive and the device must have good acoustic transmission. Pre-existing surgical options include reshaping of autologous inner ear bone tissue (Colletti and Fiorino 1999), which is not always available due to the extent of the damage, or cadaveric donor tissue, now disfavoured due to the risk of infection (Glasscock, Jackson, and Knox 1988) or degradation of stiffness. Mass produced artificial implants do not take into account the variability of individual patient anatomy. The authors demonstrated that 2PP may be used to generate easily implanted devices which can easily be tailored to the needs of a particular patient.

### **1.8.3 Microneedles**

ORMOCER® Microneedle arrays fabricated by 2PP have been explored for applications such as transdermal drug delivery (Ovsianikov, Chichkov, Mente, et al. 2007). The CAD-CAM nature of 2PP processing allows for total control over features such as surface area, penetration cross section, mechanical strength and diffusion within the needles simply by changing the computer model (Doraiswamy et al. 2006; Ovsianikov, Ostendorf, and Chichkov 2007; Ovsianikov, Chichkov, Mente, et al. 2007). Comparable micro-cone arrays fabricated using one photon based layer-by-layer microstereolithography fabricated by Kwon and Matsuda (Kwon and Matsuda 2005) show visible ridges due to the curing of individual layers consecutively, an effect that the high resolution of two photon direct write eliminates.

Microneedle arrays fabricated by 2PP have also been used for the delivery of fluorescent quantum dots to porcine skin facilitating imaging by multiphoton microscopy (Gittard et al. 2011). Material biocompatibility was assessed by the proliferation of neonatal human

epidermal keratinocytes and human dermal fibroblasts. The authors indicate that 2PP microneedle fabrication allows the delivery of theranostic agents (agents which can indicate the correct therapeutic process for individual patients) to epidermal, dermal or subdermal tissues depending on the computer design in a patient specific manner.

One concern with implantable microneedle arrays is the risk of infection. Microneedle arrays prepared by 2PP and replicated by PDMS stamping were prepared from a mixture of polyethylene glycol diacrylate and 2mg/mL of the antimicrobial agent gentamicin sulphate. The efficacy of this agent in inhibiting the growth of the pathogen *Staphylococcus aureus* on the resulting structures was demonstrated by agar plating assay (Gittard et al. 2010).

#### **1.8.4 Valves**

Prototype valves optimised for the flow conditions encountered in small human veins were fabricated by Schizas *et al.* (Schizas et al. 2010) from a zirconium sol-gel based material. Consecutive layers were cured by 2PP to create a 360  $\mu\text{m}$  long by 120  $\mu\text{m}$  wide microvalve. The stair step effect created by layer-by-layer fabrication was eliminated by a combination of feature design to include mainly vertical features and also the optimisation of laser fluence to give the best possible material resolution. This study demonstrates how an optimised computer designed model can be converted directly into a prototype by two photon polymerization.

#### **1.8.5 Bioresorbable Tissue Scaffolds**

Despite the success of ormocers and similar materials for the fabrication of devices such as microneedle arrays and valves these materials are limited to the production of permanent devices as they are not bioresorbable. Claeysens *et al.* (Claeysens et al. 2009) reported the successful fabrication of scaffold like structures from a bioresorbable polymer based on poly( $\epsilon$ -caprolactone-co-trimethylenecarbonate)-b-poly(ethylene glycol)-b-poly( $\epsilon$ -caprolactone-co-trimethylenecarbonate). This polymer was reported to degrade at a rate close to that of tissue formation (Mizutani and Matsuda 2002a, 2002b) and was demonstrated to have no negative effect on cell viability.

### **1.8.6 Cell Delivery Vehicles**

The injection of stem cells into damaged brain tissue has been suggested as a method for treating brain injury, for example following a stroke. The use of degradable microparticles which can be injected with the cells and provide a support structure has been demonstrated has been shown to facilitate tissue regrowth (Bible et al. 2009a). Two photon polymerization of photocurable polylactic acid (PLA) has been used to create degradable cell delivery vehicles, which can be loaded with cells prior to injection with the possibility of optimising the shape and size of the cell delivery vehicles to give maximum protection to the cells during injection, and giving maximum cell loading of the microparticles (Melissinaki et al. 2011).

### **1.8.7 Experimental Tissue Scaffolds**

As well as implantable devices, the resolution and reproducibility of 2PP scaffold fabrication allows the production of experimental tissue scaffolds which may be used to investigate the effect of factors such as three-dimensional culture, pore size and geometry on the behaviour of cells within.

In work by Tayalia *et al.* (Tayalia et al. 2008) 2PP fabricated constructs were used to study the effect of scaffold architecture on cell adhesion and migration. Woodpile based structures with different pore sizes were seeded with cells and the movement of the cells within was monitored over time to investigate cell migration. It was found that cells reached higher speeds of migration in the three dimensional constructs compared to a flat substrate. Furthermore it was found that smaller pore sizes inhibited the movement of the cells leading to a less uniform distribution whereas cells moved faster and distributed more evenly in the scaffolds with the largest pores. The ratio of the different oligomers within the curing mixture was varied allowing control over the mechanical properties of the scaffold, making it possible to investigate the effect of scaffold elasticity on cell behaviour in structurally identical scaffolds.

Cell migration studies involving natural matrix materials such as matrigel and ECM proteins derived from tissue have been extensively performed (Friedl and Wolf 2003; Grinnell et al. 2006), as have studies involving traditional porous scaffold fabrication techniques such as gas foaming, particulate leaching and phase inversion (Panseri et al. 2008). Drawbacks with these studies include the variability of pore size within fabricated scaffolds and the highly cell adhesive nature of natural matrix materials, limiting cell migration. 2PP constructs allow

greater control over the material properties of the scaffold and the ability to define pore size and shape.

As discussed earlier, Hsieh *et al.* (Hsieh *et al.* 2010) used two photon polymerization to produce three dimensional scaffolds from a commercially available non-degradable polymer for hepatocyte culture and demonstrated liver specific cell functions (urea synthesis and urea secretion) were retained for longer in cells cultured in the scaffold compared to cells cultured on spin coated substrates of the same polymer. This demonstrates the effect of culturing cells in three dimensional constructs instead of a flat monolayer fashion.

Although non-bioresorbable, polyethylene glycol (PEG) has been used extensively in internal medical applications such as constipation aids (Tack 2011). Polyethylene glycol diacrylate (PEGDA) was investigated as a suitable material for the creation of 2PP structured scaffolds (Ovsianikov, Malinauskas, Schlie, Chichkov, Gittard, Narayan, Lobler, *et al.* 2011). A resolution of 200 nm was achieved, and the authors suggest that the technique may be used to explore the effect of surface topography on cell-scaffold interaction. Furthermore a thorough investigation of scaffold material/ photoinitiator toxicity was carried out and it was determined that freshly prepared scaffolds release photoinitiator and monomer material which is toxic to fibroblasts, however ageing of the samples in distilled water for 6 days led to much improved biocompatibility and negligible cytotoxicity. The swelling of the scaffold materials in water also suggests that although the devices may deviate slightly from their original shape the ensuing increase in porosity will allow greater nutrient transport within the scaffold and the scaffolds could be loaded with biological agents such as growth factors, as shown in previous studies highlighted by the authors (Gittard *et al.* 2010).

## **1.9 Conclusions**

Two photon polymerization is becoming an established technology for the creation of designer tissue scaffolds. Scaffolds with appropriate dimensions for the engineering of tissues and organs which can be fabricated on a reasonable timescale have been produced (Hsieh *et al.* 2010). Smaller scale devices for niche applications have been fabricated demonstrating the potential of this technology for direct clinical applications (Ovsianikov, Chichkov, Adunka, *et al.* 2007).

More efficient photoinitiators (Lemercier *et al.* 2006) and new materials for microstereolithography (Melchels, Feijen, and Grijpma 2009) combined with new slicing

techniques for 3D scan path optimisation (Liao et al. 2007), voxel elongation (Li, Winfield, O'Brien, and Crean 2009) and parallel processing (Bhuiyan et al. 2007) are being developed to reduce the reliance of the technique on high-end laser systems whilst reducing processing times and limitations on the size of scaffold that can be achieved. Demonstrated advantages of custom scaffold features (Melchels et al. 2011) over first generation scaffolds made by simple bulk processing methods make microstereolithography, particularly 2PP an attractive technique for the creation of a new generation of functional tissue scaffolds.

### **1.10 Thesis Aims and Objectives**

As can be seen throughout the literature review, the fundamental mechanisms of microstereolithography and its application to tissue engineering are well understood. Despite this the technique has not yet found routine clinical application. To address this, the aims of this thesis were to:

1. Establish simple microstereolithography systems for device and microstructure fabrication.
2. Prepare resins for microstereolithography based on materials in current clinical use, and assess their toxicity and ability to act as a substrate for cell growth.
3. Use the developed microstereolithography systems with both the prepared resins and commercially available photocurable resins to create structures and explore cell-structure interactions.
4. Assess potential clinical applications of the technique as a proof of concept, preparing biocompatible microstructures with potential clinical applications.

# Chapter 2: Photocurable and Bioresorbable Polymers for Tissue Engineering

---

## **Abstract**

A key limitation in the use of microstereolithography for tissue engineering applications is a lack of suitable materials. Excellent structuring results have been obtained with commonly used commercially available resins used for photolithography and rapid prototyping, however these materials are limited in their use due to their poor biocompatibility and limited cell adhesion. Most commonly used UV curable resins are also non-bioresorbable, which is a requirement for many tissue engineering devices. In this chapter the production of photocurable oligomers based on bioresorbable polymers such as polylactic acid (PLA) and poly(caprolactone) (PCL) which are already in routine clinical use is described. The materials were assessed for their biocompatibility and degradability and were found to be both degradable and biocompatible.

## **2.1 Introduction**

In order to produce bioresorbable tissue scaffolds by microstereolithography, a versatile protocol for the synthesis of photocurable polymers with hydrolytically cleavable ester linkages was developed (Gill and Claeysens 2011). Commercially available photocurable polymers such as polyethylene glycol di(meth)acrylate (PEGDA) have been explored for tissue engineering applications such as cell encapsulation (Durst et al. 2011), nerve guidance conduits (Arcaute et al. 2005) and the creation of experimental tissue scaffolds (Ovsianikov, Malinauskas, Schlie, Chichkov, Gittard, Narayan, Lobler, et al. 2011), however unmodified PEGDA is not degradable and unless removed will remain intact indefinitely. Other commercially available materials for microstereolithography such as organically modified ceramic polymers (Ormocers) (Doraiswamy et al. 2005) share this limitation.

Biodegradable polymers such as polylactic acid (PLA) (Kulkarni et al. 1971), poly(caprolactone) (PCL) (Porter, Henson, and Popat 2009), poly(glycolic acid) (PGA) (Ashammakhi et al. 2000), poly(trimethylene carbonate) (PTMC) (Hou, Grijpma, and Feijen 2009) and poly(hydroxybutyrate-co-valerate) (PHBV) (Martin and Williams 2003) and their

mixtures and copolymers are popular materials for tissue engineering purposes due to their bioresorbability and history of clinical use. Bioresorbable polyesters were first adopted in the 1970's for the production of sutures and devices for bone fixation (Kulkarni et al. 1971). Polymers based on lactide, glycolide and caprolactone monomers are now in common clinical usage (Griffith 2000). Other degradable polymers such as poly(3-hydroxybutyrate) (PHB) (Amass, Amass, and Tighe 1998) and PTMC (Pego et al. 2003) are still under development and have the potential to expand the range of tissue engineering applications for polymeric materials.

These polymers are typically produced commercially by the ring opening polymerization of cyclic dimers or monomers. Polylactic acid for example is produced from lactic acid by the catalytic depolymerization of lactic acid oligomers into cyclic lactide dimers followed by the ring opening polymerization of the resulting dimers to produce high molecular weight PLA (Lim, Auras, and Rubino 2008).

By using a multifunctional alcohol as an initiator, branched oligomers based on bioresorbable materials such as PCL, PTMC and PLA can be prepared (Matsuda, Mizutani, and Arnold 2000). The produced oligomers have hydroxyl terminated chains which can then be functionalized with photo-crosslinkable groups such as coumarins (Matsuda, Mizutani, and Arnold 2000) and methacrylates (Melchels, Feijen, and Grijpma 2009). By increasing the degree of branching, oligomers with a greater functionality can be prepared resulting in increased photocuring rates and shorter microstereolithography fabrication times (Matsuda, Mizutani, and Arnold 2000). It is important to note that despite cross linking of the oligomers their degradability by hydrolysis is retained (Mizutani and Matsuda 2002b).

Following a review of the literature a protocol for the production of a diverse range of photocurable bioresorbable resins was proposed. In step 1, the appropriate monomer and multifunctional alcohol initiator are selected and refluxed together in the presence of stannous octoate catalyst to produce multi-armed hydroxyl terminated oligomers. In step 2, the oligomers are functionalized with cross-linkable acrylate or methacrylate groups to yield a photocurable polymer. Finally, in step 3 the photocurable polymers are mixed with an appropriate photoinitiator and cured to yield a cross linked degradable network. This process is shown in figure 5.

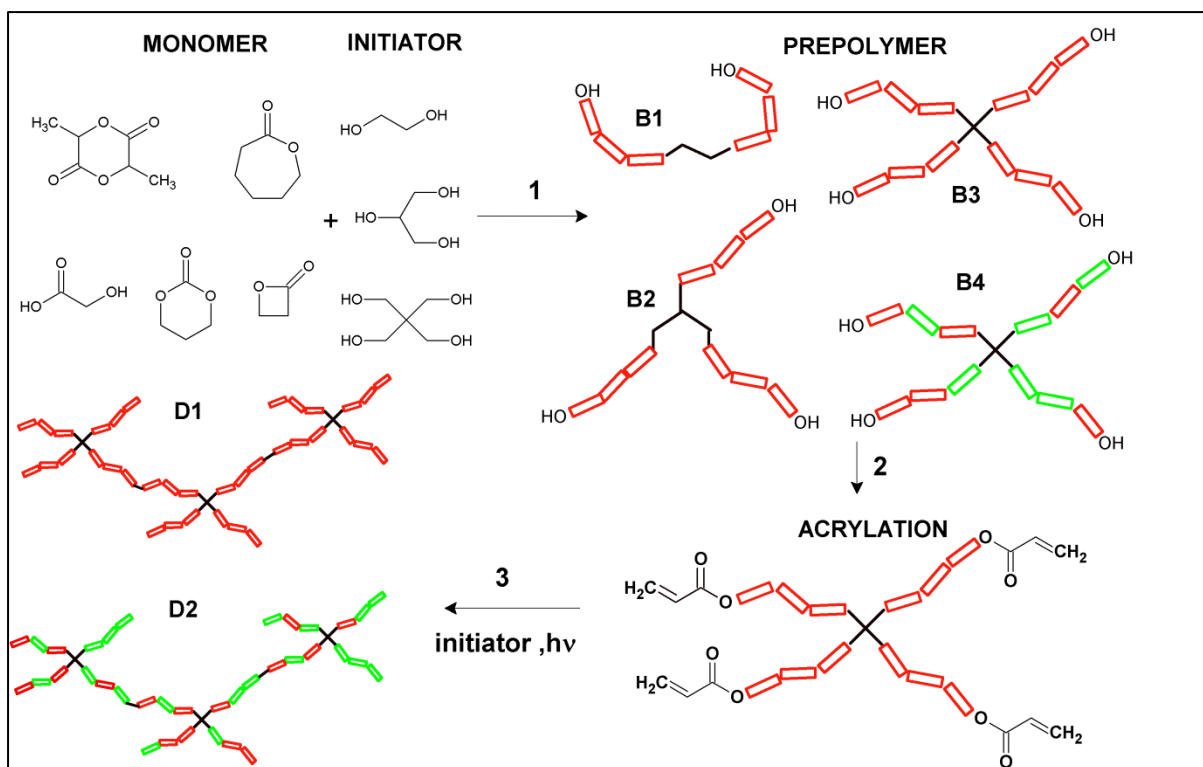


Figure 5: The selected monomer and initiator are polymerized together to yield an oligomer of the desired functionality (step 1). The prepolymer or oligomer is then functionalized with a cross-linkable functional group such as an acrylate (step 2). Finally the curable oligomers are cross-linked by irradiation in the presence of a suitable initiator to form a cured network (step 3). Adapted from Gill and Claeysens (Gill and Claeysens 2011) with permissions.

Functionalization of the oligomers with acrylate or methacrylate groups was chosen over functionalization with coumarin derivatives, as used for example by Mizutani and Matsuda (Mizutani and Matsuda 2002b) due to the commercially available nature of the necessary reagents. The synthesis of acyl chloride functionalized coumarin which can react with the free hydroxyl end groups of the oligomer requires several synthetic steps making this procedure less readily accessible.

The suggested protocol allows the preparation of a wide range of copolymers, and the molecular characteristics and final mechanical properties can be controlled to a degree by the ratio of monomer to initiator. For the purposes of this project four armed oligomers based on PLA and PCL were prepared and their biocompatibility assessed. Initially the oligomers were functionalized using acryloyl chloride and triethylamine (TEA), as demonstrated by other authors (Claeysens et al. 2009). Although this process yielded photocurable oligomers large quantities of salt were generated which required filtration to remove, after which the yield of

the final product was low despite repeated washing. The procedure also yielded highly chromophoric impurities which proved difficult to separate, resulting in a deep red coloration of the oligomer. Additionally, acrylate groups tend to be unstable under storage and the products had a tendency to cure prematurely.

Another procedure for the methacrylate functionalization of hydroxyl terminated oligomers and proteins is the reaction of methacrylic anhydride in the presence of a base. This procedure was recently used by Ovsianikov *et al.* for the production of photocurable gelatin (Ovsianikov, Deiwick, et al. 2011), and by Seck *et al.* for the production of photocurable PLA-PEG-PLA triblock oligomers (Seck et al. 2010). This procedure was found to be the most accessible route for the production of photocurable oligomers. The products can be isolated by rotary evaporation followed by precipitation in cold isopropanol with little colouration due to impurities.

## **2.2 Materials and Methods**

Two methacrylate functionalized resins were initially prepared, one based on PLA and the other on PCL. Initial characterization was performed using  $^1\text{H}$  NMR and IR spectroscopy, and the general biocompatibility was verified using techniques including MTT assay and fluorescence imaging of cells. The polymers were successfully cured under UV illumination and gave excellent structuring results. The resins were used in the following chapters to produce a range of structures by both one and two photon polymerization.

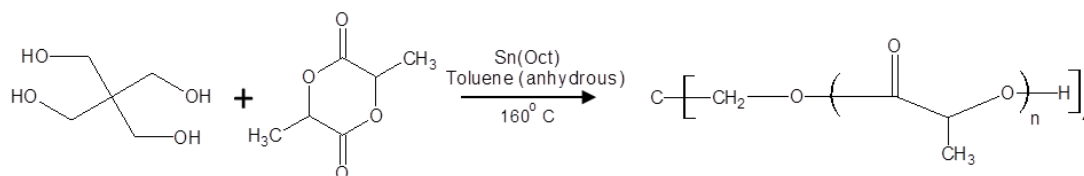
### **2.2.1 Materials**

The photocurable PLA and PCL were prepared via the ring opening polymerization of (3S)-cis-3,6-dimethyl-1,4-dioxane-2,5-dione (Sigma-Aldrich, 98%) or  $\epsilon$ -Caprolactone (Sigma-Aldrich, 97%), using pentaerythritol (Sigma-Aldrich, >98%) as the multifunctional alcohol initiator and tin 2-ethylhexanoate (Sigma-Aldrich, 95%) as a catalyst with toluene (Sigma-Aldrich, anhydrous, 99.8%) as solvent. The methacrylate functionalization was performed using triethylamine (Sigma-Aldrich, >99%) and methacrylic anhydride (Sigma-Aldrich, 94%) with dichloromethane (Sigma-Aldrich, anhydrous, >99.8%, 50 ppm amylene stabilizer) as a solvent. Isopropanol (Sigma-Aldrich, anhydrous, 99.5%) was used for precipitation of the methacrylate functionalized oligomer.

### 2.2.2 Synthesis of Photocurable PLA

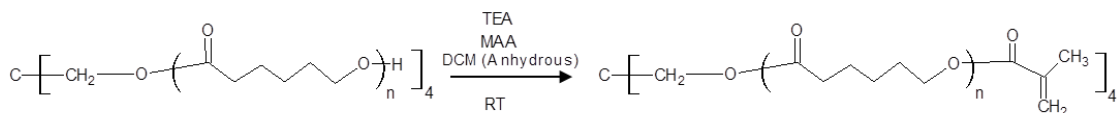
A photocurable PLA oligomer with a targeted molecular weight of  $\sim 1200 \text{ g mol}^{-1}$  was prepared and methacrylate functionalized as described below. All glassware was dried at  $120^\circ\text{C}$  overnight and flushed with nitrogen prior to use. Reactions were performed under a nitrogen atmosphere.

The hydroxyl terminated oligomer was prepared by refluxing of (3S)-cis-3,6-dimethyl-1,4-dioxane-2,5-dione (25.5 g, 0.177 moles, 8 molar equivalents) and pentaerythritol (3g, 0.022 moles, 1 molar equivalent) at  $160^\circ\text{C}$  in 50 mL of toluene in the presence of 1 drop of stannous octoate catalyst. After 8 hours the reaction was allowed to cool to room temperature, and the product formed as a viscous bottom layer. The toluene solvent was decanted and the oligomer dried by vacuum distillation to yield the product as a clear highly viscous resin.



*Scheme 1: Synthesis of four armed polylactic acid (PLA). The cyclic lactide dimer undergoes a ring opening polymerisation reaction in the presence of a multifunctional alcohol initiator (pentaerythritol) in the presence of stannous octoate catalyst at  $160^\circ\text{C}$  for 8 hours using toluene as a solvent.*

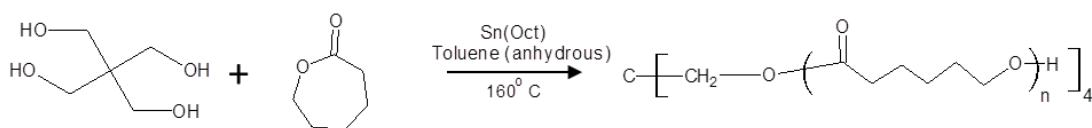
The methacrylate functionalization was performed in a minimum quantity of dichloromethane as solvent. The hydroxyl terminated PLA oligomer (12.5 g,  $\sim 0.01$  moles, 1 molar equivalent) was carefully dissolved in the solvent in a round bottom flask under a nitrogen atmosphere. The solution was cooled to  $0^\circ\text{C}$  in an ice bath and triethylamine (22.30 ml, 0.16 moles, 16 molar equivalents) was added. Methacrylic anhydride (11.92 ml, 0.08 moles, 8 molar equivalents) was then added dropwise using an addition funnel and the reaction was brought up to room temperature. The mixture was stirred for a further 24 h before the product was isolated by vacuum distillation followed by precipitation in isopropanol at  $-20^\circ\text{C}$ . The precipitated product was collected by decanting the isopropanol and dried under vacuum at room temperature for 24 h to yield a clear viscous resin.



*Scheme 2: The terminal OH groups on the four-armed PLA are methacrylate functionalised by reaction with methacrylic anhydride (MAA) in the presence of triethylamine (TEA) and dichloromethane (DCM) as solvent.*

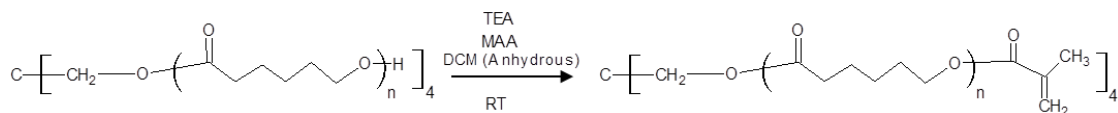
### 2.2.3 Synthesis of Photocurable PCL

$\epsilon$ -Caprolactone (Sigma-Aldrich, 97%), (0.1 mol, 11.2 g, 10.87 ml, 8 mol eq.) was added to a mixture of pentaerythritol (0.0125 mol, 1.70 g, 1 mol eq.) in 100 ml of toluene under a nitrogen atmosphere with magnetic stirring. The reaction mixture was then brought up to 160°C and 1 drop of stannous octoate was added. The reaction mixture was then left for 8h and then cooled at room temperature allowing the precipitation of the product as a lower viscous layer which was separated by decanting the toluene, and the remaining solvent removed by rotary evaporation.



*Scheme 3: Synthesis of four armed polycaprolactone (PCL). The cyclic monomer  $\epsilon$ -caprolactone undergoes a ring opening polymerisation reaction in the presence of a multifunctional alcohol initiator (pentaerythritol) in the presence of stannous octoate catalyst at 160 °C for 8 hours using toluene as a solvent.*

The methacrylate functionalized oligomer was prepared by dissolving the hydroxyl terminated PCL (3.50 g, 0.003 mol, 1 molar equivalent) in 50 ml of dry dichloromethane and triethylamine (2.03 g, 2.79 ml, 0.02 mol, 8 mol eq.). Methacrylic anhydride (3.13 g, 2.98 ml, 0.02 mol, 8 mol eq) was added dropwise using an addition funnel. Following addition of the methacrylic anhydride the reaction mixture was brought up to room temperature and left to react for 24 h. The solvent and TEA were then removed under reduced pressure and the product purified in isopropanol at -20 °C.



*Scheme 4: The terminal OH groups on the four-armed PCL are methacrylate functionalised by reaction with methacrylic anhydride (MAA) in the presence of triethylamine (TEA) and dichloromethane (DCM) as solvent.*

## 2.2.4 Polymer Characterisation

The PLA and PCL based oligomers were analysed before and after methacrylate functionalization by <sup>1</sup>H NMR spectroscopy. Samples were prepared by dissolving 20 mg of the sample in deuterated chloroform (Sigma-Aldrich, 100%, 99.96% atom D) and filtering into a standard NMR tube. Spectra were recorded at 400 MHz using a Bruker AV1-400 spectrometer. IR Spectra of the photocurable PLA were obtained on a Perkin-Elmer SPECTRUM 2000 IR spectrometer, by sandwiching a small droplet of the resin between two KBr disks to create a thin film.

Further characterisation of the products, for example by gel permeation chromatography was not performed. The focus of this thesis is in the structuring and biocompatibility of the polymers and their applications in microstereolithography. Extensive characterisation has been performed by other authors on this class of materials by other authors (Claeysens et al. 2009; Matsuda, Mizutani, and Arnold 2000; Seck et al. 2010; Meier and Schubert 2005).

## 2.2.5 Thin Film Preparation by Spin Coating

In order to create thin films for cell culture and surface characterisation, photosensitive solutions of the methacrylate functionalized PLA and PCL oligomers were prepared. In an amber glass vial 250 µl of 4-methyl-2-pentanone (Sigma-Aldrich, ≥98.5%) was added to 1 g of the photocurable oligomer and 20 mg of 4,4'-bis(diethylamino)benzophenone (Sigma-Aldrich, ≥99%) and the mixture was stirred for 15 minutes using a magnetic stirrer bar. Prior to use the mixture was taken up in a syringe and passed through a polycarbonate filter of 0.45 µm pore size.

The photocurable solution was then spin coated onto glass coverslips functionalized with 3-methacryloxypropyltrimethoxysilane (MAPTMS) (Polysciences Inc.). MAPTMS functionalization was performed by soaking standard borosilicate glass coverslips in a 40 mM

solution of MAPTMS in chloroform (Sigma-Aldrich, amylene stabilized,  $\geq 99\%$ .) for a minimum of three hours. The silane functionalization provides methacrylate groups on the surface of the glass which allow the polymer to bind to the surface upon curing. Without this functionalization the films had a tendency to detach from the surface and float off during cell culture. Spin coating was performed by depositing 1 drop of the photosensitive material onto the glass substrate and spinning for 60 s at 4000 rpm followed by drying under vacuum to remove the solvent. Similar conditions were used for the spin coating of polycaprolactone by other authors (Marletta et al. 2005). The films were then cured using a UV lamp (EXFO Omnicure S1000 100W) for 300 s at  $30 \text{ mW cm}^{-2}$ .

### **2.2.6 Swelling Analysis and Degradation of Photocurable PLA**

In order to investigate the swelling behaviour of the photocurable PLA, the polymer was mixed with 2% w/w photoinitiator in 4-methyl-2-pentanone as described above and pipetted into a PDMS mould measuring 1 cm x 1 cm x 0.2 cm. The solvent was removed under vacuum until the sample reached a constant weight. The material was then cured by direct exposure to the UV lamp to produce cured squares of the material. Following curing the samples were developed by soaking in 4-methyl-2-pentanone for one hour and dried again under vacuum. For comparison, samples of linear PLA (NatureWorks Ingeo 7000D) with the same dimensions were cut from tensile testing samples prepared using a Haake MiniJet II injection moulding device at a temperature of  $215 \text{ }^\circ\text{C}$ , a nozzle pressure of 600 bar and a mould temperature of  $40 \text{ }^\circ\text{C}$ .

The samples were all dried to a constant weight and the mass of each sample recorded before immersion in distilled water. The samples were removed from the water, wiped dry and the mass recorded before replacing in the water at each time point. For the degradation analysis the samples were immersed in 0.5 M aqueous sodium hydroxide solution, and the solution changed every day to maintain a constant concentration.

### **2.2.7 Cell Culture**

The biocompatibility of the photocurable oligomers was initially verified using human dermal fibroblasts by MTT assay and confocal microscopy. MTT Assay gives an indication of the number of living cells on a sample by colorimetric methods, and can be used to

compare between material samples and a control. Confocal microscopy is used to examine cell morphology by staining cells with a fluorescent dye and imaging the fluorescence.

### **2.2.8 Human Dermal Fibroblast Culture**

Human dermal fibroblasts were harvested from split thickness skin grafts (STSGs) obtained from specimens following routine abdominoplasties and breast reductions, with the informed consent of all patients for the skin to be used for research through a protocol approved by the Ethical Committee of the Northern General Hospital Trust, Sheffield, UK. Cell isolation and culture were as published previously (Smith, Rimmer and Macneil 2006). Cells were isolated by members of the Biomaterials and Tissue Engineering Group (University of Sheffield) and were received at P7 and used up until P12. Cells are grown in an incubator at 37°C gassed with 5% CO<sub>2</sub> and cultured in completed Dulbecco's modified Eagles media (cDMEM).

### **2.2.9 Human Dermal Fibroblast Medium**

61.25 ml of DMEM (Dulbecco's modified Eagle's medium) are removed from a 500 ml flask. To the flask, Foetal Calf Serum (FCS) (50 ml), L-Glutamine (100×) (5 ml), penicillin-streptomycin (10,000 µg/ml, 10,000 µg/ml) (5 ml) and amphotericin (Fungizone<sup>TM</sup>) (1.25 ml) were added to make 500 ml cDMEM. Sterility was checked by transferring 3 ml to an incubator and storing for 72 h, before examining under an optical microscope. The was stored for at 4°C and was replaced every 4-6 weeks.

### **2.2.10 Cell Passaging**

To passage cells the medium was removed, followed by washing twice with phosphate buffered saline (PBS) (removal of media containing proteins was essential to prevent inhibition of the trypsin). Following this, 1.5 ml of trypsin was then added and the flask incubated for 5 minutes at 37°C. The flask was then tapped to detach the cells (detachment checked under microscope) and 10 ml of cDMEM added to quench the Trypsin. The resulting cell suspension was centrifuged for 5 minutes at 1000 rpm, the supernatant removed and the cell pellet resuspended in a known volume (1 ml) of medium. A cell count was then performed and 250,000 cells can be added to a T75 flask containing 15 ml of cDMEM. Cells should be used before 80% confluence. Optical microscopy images of typical human dermal fibroblasts approaching confluence are shown in figure 6.

### 2.2.11 Cell Counting

To perform a cell count, 9  $\mu\text{l}$  of cell suspension was pipetted into the chamber of a haemocytometer. The number of cells within the volume of the chamber was then counted, and multiplied by  $10^4$  to give the number of cells in 1 ml of the suspension. To account for cells along the edges of the counting area, those touching the top and left side of the grid were counted, those touching the bottom and right were not.

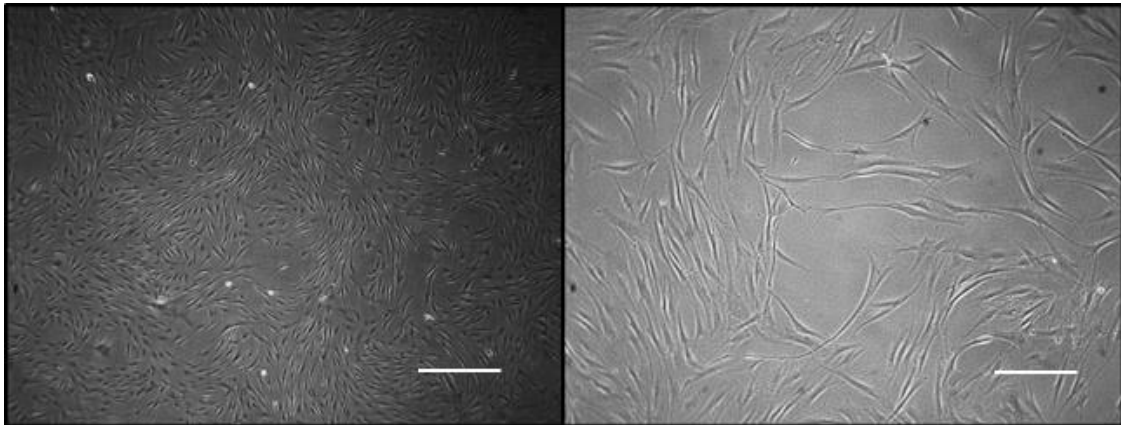


*Figure 6: Human dermal fibroblasts cultured in a T75 flask in cDMEM. Cells are approaching 80% confluence and the typical human dermal fibroblast morphology can be observed. Scale bars: Left 100  $\mu\text{m}$ , right 25  $\mu\text{m}$*

### 2.2.12 MTT Assay

MTT Assay measures cell metabolic activity by the conversion of an artificial hydrogen acceptor substrate by dehydrogenase enzymes within the cells (Macneil et al. 1993; Ealey et al. 1988). The artificial substrate is reduced within the cells to form a coloured product which can be eluted and quantified by spectrometry. This can be used to give an indication of cell number as enzyme activity usually relates to cell number. In a typical procedure, cells are cultured overnight in a well plate. The medium is removed and the cells carefully washed once or twice with PBS (1 ml per well). 1 ml of MTT solution (0.5 mg/ml MTT powder in PBS) is added to each well and the plate left at 37°C in an incubator for 40 minutes. The MTT is then removed and 300  $\mu\text{l}$  acidified isopropanol (25  $\mu\text{l}$  concentrated HCl in 20 ml isopropanol) is added to each well. Two 150  $\mu\text{l}$  samples are then transferred to a 96 well plate and the optical density measured in a plate reader at 540 nm and referenced at 630 nm.

### **2.2.13 Statistical Analysis**

Statistical analysis (two tailed Student's *t*-test) was performed using the program GraphPad Prism 6 (GraphPad Software Inc.) to indicate statistical significance.

### **2.2.14 Confocal Microscopy and Cell Staining**

In order to visualise the cells using fluorescence microscopy, cells were stained with TRITC-phalloidin (for actin) and 4',6-diamidino-2-phenylindole (DAPI) (for the nuclei). Human dermal fibroblasts were seeded in 1 ml of media at a density of 50,000 cells per ml and cultured on the samples for ten days. Following culture for the required amount of time, the cells were removed from the incubator and carefully washed with PBS. The samples were then left to soak in PBS at room temperature for 30 minutes, permeabilized by soaking in Triton X-100 in PBS for 5 minutes and then rinsed again three times with clean PBS. The PBS was then removed from the samples and enough staining solution (1:1000 parts phalloidin-TRITC and DAPI) to cover the samples was added. The solutions were left in contact with the samples at room temperature for 30 minutes before rinsing again three times with PBS. The samples were then mounted using fluorescent mounting medium for imaging using a using a Carl Zeiss LSM510-META confocal microscope. TRITC-phalloidin images (actin) were taken at  $\lambda_{ex} = 545 \text{ nm}$ / $\lambda_{em} = 573 \text{ nm}$ , DAPI images (nuclei) were taken at  $\lambda_{ex} = 358 \text{ nm}$ / $\lambda_{em} = 461 \text{ nm}$ .

## **2.3 Results**

### **2.3.1 Polymer Characterisation and Cell Culture**

Photocurable resins based on PLA and PCL were synthesised as described in the methods section. The photocurable polymers were characterised using spectroscopic techniques (NMR, IR) prior to curing. The photocurable polymers were spin coated and cured to produce thin films on the surface of glass coverslips. A range of cell culture and imaging techniques were then used to determine the biocompatibility of the polymers post-curing. The films were further characterised using X-ray photoelectron spectroscopy, water contact angle analysis and SEM, as described in chapter 5.

### 2.3.2 Polymer Characterisation

The polymer resins were characterised using  $^1\text{H}$  NMR spectroscopy. NMR Characterisation was used to determine the ratio of the initiator to monomer in the final resin, as demonstrated in (Claeyssens et al. 2009). Resins with a targeted molar ratio of a) 1 molar equivalent of initiator (pentaerythritol) to 8 molar equivalents of  $\epsilon$ -caprolactone (monomer) and b) 1 molar equivalent of initiator (pentaerythritol) to 8 molar equivalents of lactide (a cyclic dimer of two lactic acid monomers) were prepared and the overall ratio of monomer to initiator was found to be in general agreement with the results of the NMR integration. The effect of side reactions and dimerization was not explored. The appearance of vinyl peaks in the 5.5-6.5 ppm region of the  $^1\text{H}$  NMR spectra were used to verify the methacrylate functionalization. It is apparent from multiple peaks in the vinyl region that some methacrylic acid may remain in the sample as a side product, and that further purification (for example using an aqueous work up) would be needed to remove this.

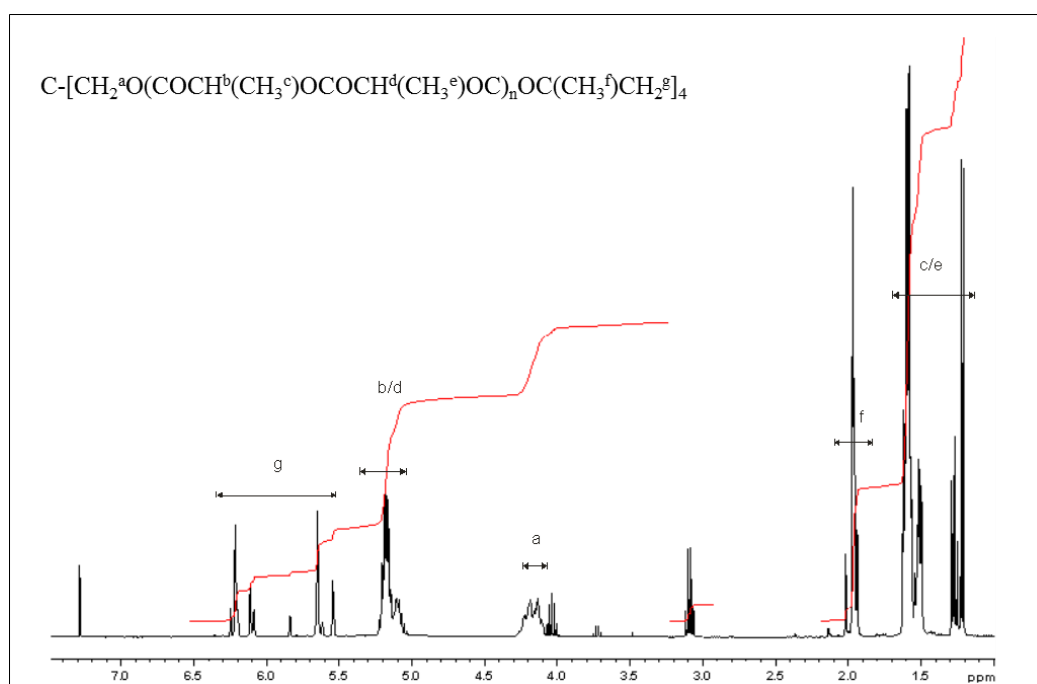


Figure 7:  $^1\text{H}$  NMR Spectrum of methacrylate functionalized PLA based oligomer prepared from a pentaerythritol initiator. Ratio of pentaerythritol methylene groups ( $\text{CH}_2$ , 'a') to CH group in lactide monomer (b/d) approximately 1:2, in agreement with theoretical ratio of pentaerythritol to lactide in reaction (1:8). Vinyl peaks (5.5-6.5 ppm) indicate methacrylate functionalization of oligomer.

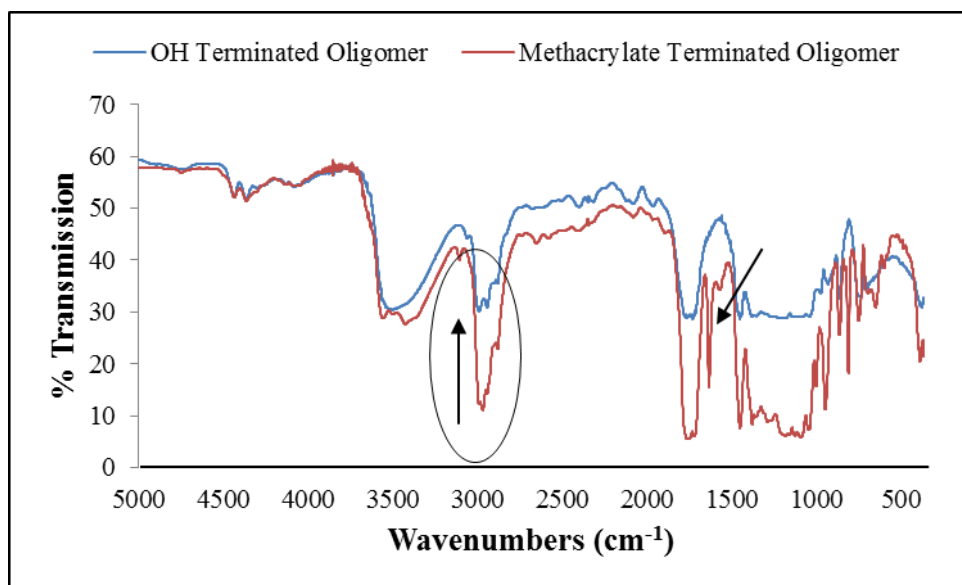
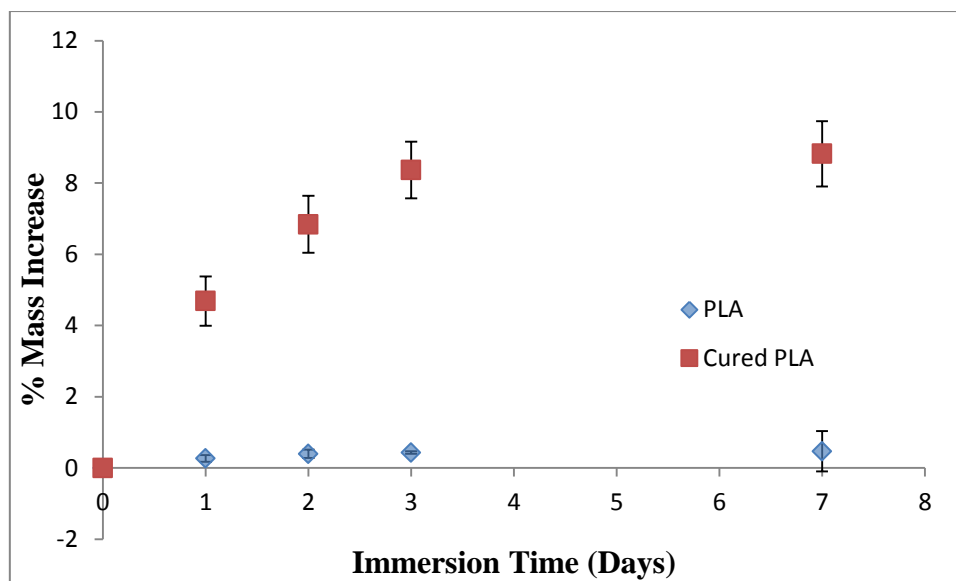


Figure 8: IR Spectrum of methacrylate functionalized PLA oligomer indicating reduced intensity of  $-OH$  signal ( $\sim 3000\text{ cm}^{-1}$ ) relative to  $OH$  signal at  $3500\text{ cm}^{-1}$  and appearance of methacrylate signal ( $1650\text{ cm}^{-1}$ ).

FT-IR spectroscopy was also used to confirm methacrylate functionalization of the oligomers, by the appearance of peaks characteristic of carbon-carbon double bonds at  $1600\text{ cm}^{-1}$ . Example spectra of the PLA based oligomer described in the methods section are provided above in figures 7 and 8.

### 2.3.3 Swelling Analysis and Degradation

The mass increase of the polymer samples was expressed as the percentage mass increase from the dry sample. The data reported is the average of three repeats. The photocured PLA samples were found to undergo rapid uptake of water upon immersion at room temperature, absorbing 9% of their dry mass in water and reaching maximum absorption after around three days. The linear injection moulded PLA samples on the other hand exhibited far more typical swelling behaviour, comparable to swelling values reported by other authors (Balakrishnan et al. 2011) (see figure 9). The high water uptake of the cured PLA sample indicates inefficient packing of the polymer chains as a result of the branched nature of the oligomers. Water is therefore able to penetrate into free space within the structure. The ability of the cured PLA to absorb more water may make this material less hydrophobic and allow greater cell attachment than linear PLA.



*Figure 9: Swelling of linear and photocured PLA samples in distilled water expressed as percentage mass increase against time. Data is shown as mean  $\pm$  standard deviation ( $n=3$ ).*

*The photocured PLA can be seen to increase in mass to around 9% higher than original value whereas the commercially available PLA gains less than 1% in mass.*

The degradation profile of cured PLA was compared to that of linear PLA by immersion in 0.5 M aqueous sodium hydroxide solution (pH: 13.7). It became impossible to measure the mass loss (or increase due to swelling) of the cured PLA samples due to the rapid change in sample structure. After 24 h immersion in the solution the cured PLA samples had begun to swell and turned opaque. After 48 h immersion the samples had swollen to several times their original size indicating rapid breakdown of the structure due to ester hydrolysis and subsequent water uptake. After seven days in the solution the structure has broken down completely leaving swollen fragments of the material in solution. The linear PLA control samples on the other hand had retained their original structure and appearance, losing around 0.15% of their original mass after 7 days (data not shown).

Although the photocurable PLA samples did undergo breakdown in aqueous sodium hydroxide solution, further work is needed to verify that the photocured material will undergo hydrolysis at physiological pH. The data presented here indicates that the material forms a branched network upon curing facilitating rapid uptake of water and swelling of the material. The material was also shown to degrade in basic conditions and is susceptible to ester hydrolysis.



*Figure 10: Swelling and fragmentation of cured PLA samples. The PLA samples rapidly increased in mass, turning opaque and finally undergoing fragmentation. Images taken after 0, 1, 2 and 7 days (left to right).*

The increased swelling and rapid degradation of the structure compared to linear PLA may also result from decreased crystallinity due to the high degree of cross-linking and branching in the cured polymer. Crystallinity reduces the overall permeability of PLA by reducing the amorphous fraction in which diffusion of penetrants may occur by molecular ‘hopping’ between voids created by random thermal motion of the polymer chains (Drieskens et al. 2009).

### **2.3.4 Human Dermal Fibroblast Culture on Polymeric Thin Films**

In order to investigate the biocompatibility of the photocured PLA and PCL based polymers an MTT assay was performed. Using the protocol described in the methods section human dermal fibroblast proliferation on thin films of the cured PLA and PCL was compared to proliferation on a glass coverslip control. Using 50,000 cells per sample in 1 ml of medium the samples were cultured for 1, 3 and 7 days in a 24 well plate. Medium was changed every three days or as necessary. Six repeats per sample were performed.

The results of the MTT assay indicate that the photocured PLA and PCL have no negative effect on fibroblast proliferation, as would be expected for polymers based on these materials. In fact, the MTT assay indicates that cell proliferation is significantly better on the photocured PLA after three and seven days and better on the photocured PCL after seven days ( $p < 0.05$ ). The growth curve on the glass, PLA and PCL substrates are similar showing the same general trend. The higher cell count on the polymeric substrates as inferred by higher absorption at 540 nm may imply better cell adhesion on the cured polymers than on the glass. As a result of the improved adhesion the cells may proliferate more rapidly or be

more difficult to dislodge when removing media or PBS prior to the MTT assay. The better adhesion may be a result of the high water absorption of the polymers.

To verify that the higher MTT absorbance values were not the result of a chemical reaction between the polymers and the MTT substrate, MTT solution was applied to cured PLA and PCL films directly and incubated for 40 minutes, however no colour change resulted indicating that the MTT was not reduced by the polymers (or impurities such as remaining photoinitiator contained within the film).

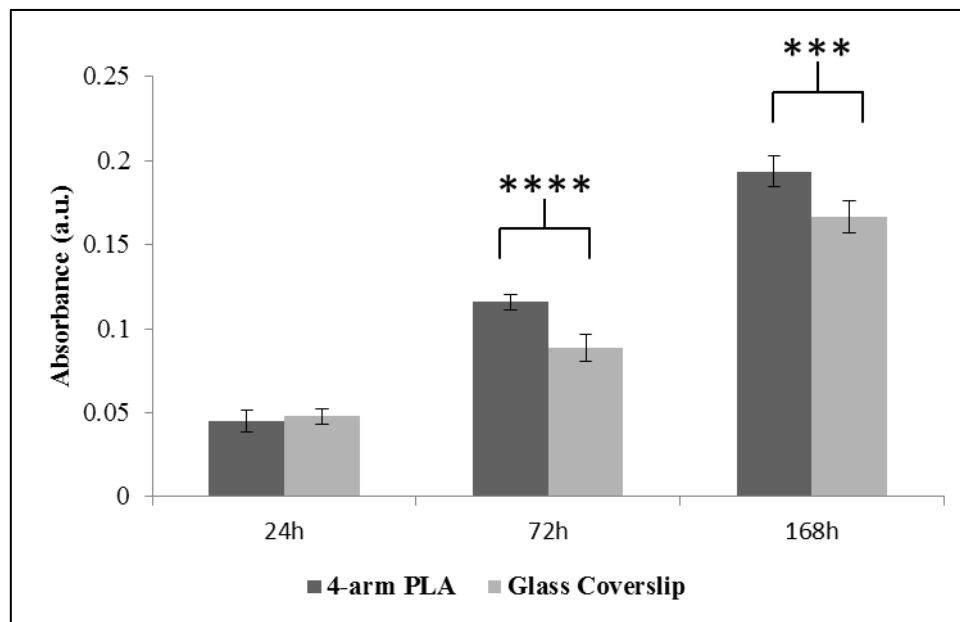


*Figure 11: MTT Comparing proliferation of human dermal fibroblasts on spin coated PLA and glass coverslip control. Data reported as mean  $\pm$  standard deviation (n=6). Data were analysed using two-tailed Student's *t*-test; \*\*\*\* $p < 0.0001$ , \*\*\* $p < 0.0003$ . The result indicates cell proliferation was significantly higher on the photocured PLA after 3 and 7 days.*

The adhesion of human dermal fibroblasts on the photocurable PCL material was further compared to glass coverslips and a tissue culture plastic control using MTT assay. Photocured PCL films, glass coverslips and empty tissue culture plastic (TCP wells) were seeded with 50,000 cells in 1 ml of media for 24h. The glass coverslips and PCL films were then transferred to an empty well plate and MTT assay performed both in the wells the samples were removed from, and on the films in the new well plate to determine the proportion of cells growing on the material compared to the number growing in the well. The proportion of cells growing on the PCL film was determined to be 95%, whereas the proportion growing on the glass coverslips was found to be 75% (see figure 13).

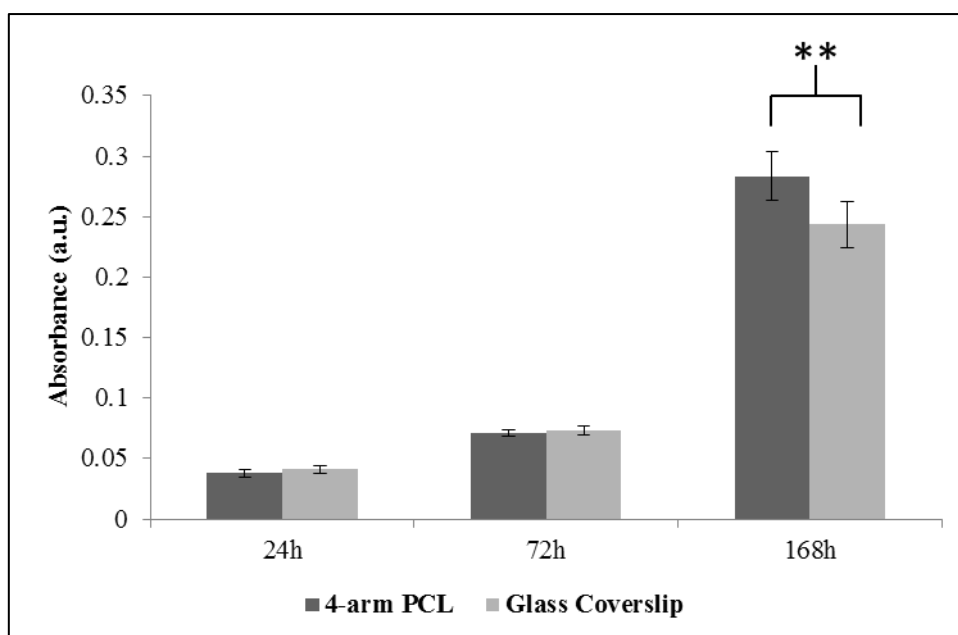


*Figure 12: MTT Comparing proliferation of human dermal fibroblasts on spin coated PCL and glass coverslip control. Data reported as mean  $\pm$  standard deviation (n=6). Data were analysed using two-tailed Student's t-test;  $**p < 0.005$ . The results indicate that proliferation was higher on the photocurable PCL after 7 days.*

To assess the morphology of human dermal fibroblasts cultured on the photocurable polymers, cells were seeded at a density of 50,000 cells per well in 1 ml of medium and cultured for ten days. The cells were then fixed and stained with DAPI (to visualize the nuclei) and TRITC-phalloidin to visualize the actin filaments. The cells had reached confluence and were observed to exhibit a typical fibroblast morphology, spreading over the surface and appearing elongated with long actin fibres.

Cells cultured on a material which either has a degree of toxicity or which they cannot attach to typically appear very rounded and ball like, and proliferation is retarded. The confocal images obtained at ten days indicate that cells are capable of attaching to and proliferating on this material as well as exhibiting typical fibroblast morphology. The proliferation assay results also indicate the materials are biocompatible and cells exhibit some degree of attachment.

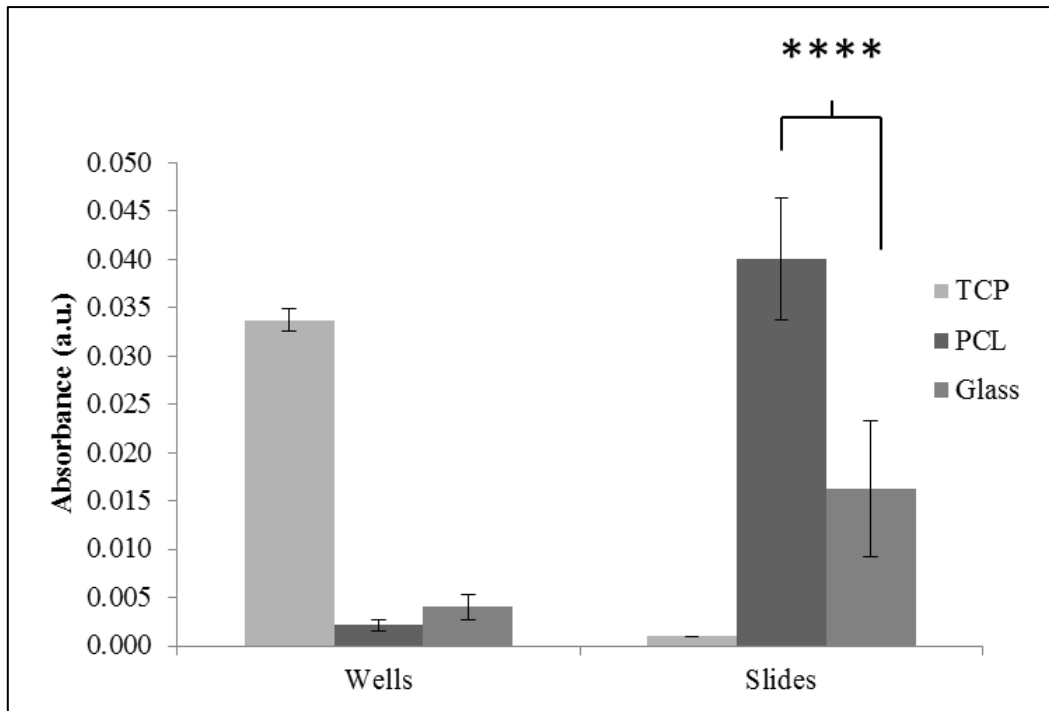


*Figure 13: MTT of human dermal fibroblasts cultured on TCP control, photocured PCL and Glass coverslips. Cells were cultured on slides for 24h before the slides were moved to new wells for the MTT assay. MTT assay was then performed on both the relocated slides and the original wells, to determine the proportion of cells attached to the coverslipas compared to those left in the original well. Data reported as mean  $\pm$  standard deviation (n=6). Data were analysed using two-tailed Student's t-test; \*\*\*\*p<0.0001.*

The preliminary results of both the MTT assay and confocal microscopy indicate that the photocurable polymers are both biocompatible and cell adhesive once cured as a thin film. Human dermal fibroblasts have been shown to proliferate normally at one three and seven days in culture, and exhibit typical fibroblast like morphology after ten days in culture. The adhesion of neuronal type cells on the photocurable polymers will be examined in greater detail in chapters 5 and 6, along with further techniques such as DNA quantification assay and live dead staining. Advanced techniques such as Comet assay are demonstrated in chapter 6.

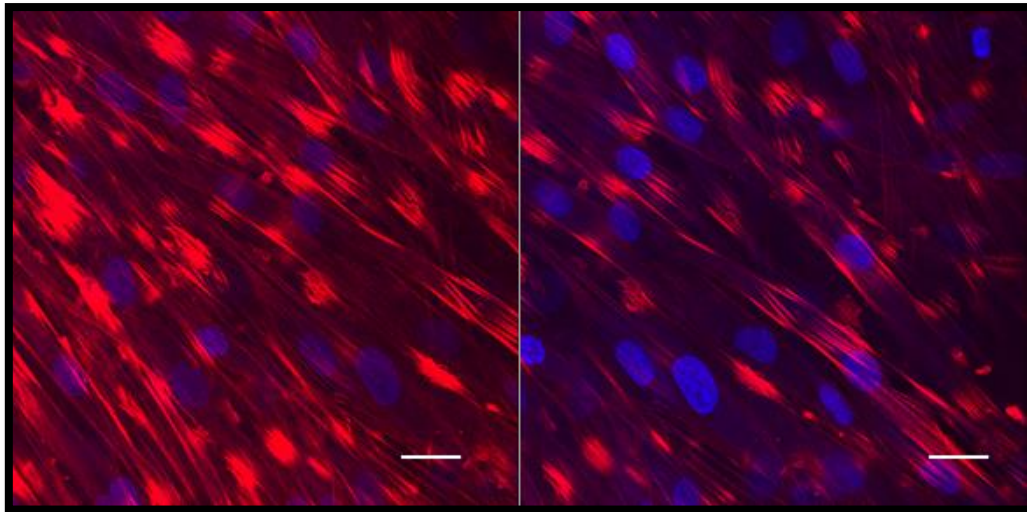


*Figure 14: Human dermal fibroblasts cultured on photocurable PLA for ten days and visualized by confocal microscopy. Nuclei are indicated by blue stain (DAPI) whereas actin filaments throughout cell body appear red (TRITC-phalloidin). Cells appear confluent exhibiting a typical fibroblastic morphology. Scale bars 5  $\mu\text{m}$ .*

## **2.4 Discussion**

The preparation of photocurable oligomers based on polylactic acid and polycaprolactone was performed using commonly used synthetic techniques. The use of these materials in microstereolithography is attracting an increasing number of publications (Melchels, Feijen, and Grijpma 2009; Mizutani and Matsuda 2002b; Claeysens et al. 2009) expanding the range of applications for microstereolithography in tissue engineering.

The characterisation of the materials produced in this chapter indicates that the oligomers were successfully methacrylate functionalized, and cured films and blocks of the material were produced. The photocurable PLA based material was shown to absorb significantly more water than the thermoplastic linear analogue. The photocured PLA material was also shown to degrade more rapidly in sodium hydroxide solution than thermoplastic PLA. This would indicate a network of cross-linked oligomers with loose packing of the polymer chains.

Cell viability of the materials was investigated using both fluorescent microscopy (to assess cell morphology) and MTT assay (to assess cell metabolic activity, which is indicative of cell number). The data collected suggest that these materials are suitable for cell culture, with cell proliferation and adhesion on the photocurable materials being significantly better than on the glass coverslip controls.

Further work is needed in order to characterise better the molecular weight and distribution of the synthesised polymers, as well as the mechanical properties and full degradation profile in physiological conditions. The focus of this thesis is the structuring and biocompatibility of these materials, and this is investigated thoroughly in the following chapters. The synthesis of these oligomers has shown that photocurable analogues of common bioresorbable polymers may be produced.

Copolymer production and control of molecular weight allows control over characteristics such as degradation rate (Choi and Park 2002), modulus (Cohn and Salomon 2005), elongation at break (Zhang et al. 2012) and hydrophobicity (Kim et al. 2003). The combination of polymers with customised properties and user defined structuring by microstereolithography will allow the creation of tissue engineering devices with designer mechanical performance and structure, allowing scaffolds to match the wide range of tissue environments encountered within the human body.

## **2.5 Conclusions**

A protocol for the production of a range of photocurable biomaterials with a range of properties was described. Two example resins based on polycaprolactone and polylactic acid were prepared and characterised, and their biocompatibility was assessed using MTT assay and cell imaging techniques and primary human cell lines. As described in chapter one, material properties can influence the behaviour of cells, for example by influencing stem cell specification. In the following chapters the structuring of these materials will be detailed, in order to combine designer biomaterials with bespoke microstructure fabrication in order to create next generation tissue scaffolds.

# Chapter 3: Dynamic Projection Microstereolithography for Tissue Engineering

---

## **Abstract**

In this chapter the design and construction of a projection microstereolithography workstation based on a digital multimirror device (DMD) allowing user defined patterning of photocurable materials is described. Using a cure depth control approach the system was also used to create three-dimensional porous constructs from both commercially available resins and in-house prepared photocurable resins. Cell culture was performed on the structures to demonstrate potential applications of this technology, and applications in tissue scaffold fabrication, corneal cell delivery devices and nerve guidance conduits were explored. A horizontal resolution of 10  $\mu\text{m}$  was achieved, and structures on the centimetre scale were produced.

## **3.1 Introduction**

Microstereolithography was first developed in the 1980's as a rapid prototyping technology for the fabrication of small parts or 'prototypes' using a focussed beam of light to selectively polymerize or cure patterns into a photosensitive resin according to a three-dimensional computer model (Narayan et al. 2010). To create three-dimensional structures a layer-by-layer methodology is used in which the three dimensional computer model is converted into horizontal slices which are sequentially written out with stepping in the z-direction. The material to be cured is commonly a liquid pre-polymer, but may also take the form of a powder or whole sheets of material.

The ability of microstereolithography to rapidly create small parts with a high amount of detail has attracted the attention of tissue engineers due its suitability for the creation of tissue scaffolds with optimised pore geometry for cell and nutrient diffusion (Melchels, Barradas, et al. 2010; Melchels et al. 2011), nerve repair devices with unique architecture allowing greater cell loading (Arcaute et al. 2005), patterned networks of encapsulated cells (Liu and Bhatia 2002), patient or structure specific scaffolds created from reconstructed microtomography data (Solaro et al. 2008), potential vascular networks or grafts (Baudis et al. 2009) microwell

arrays loaded with cells and other devices for studying cell-structure interactions such as grooved surfaces and a wide range of geometrically optimised structures (Chua et al. 2003a, 2003b).

Microstereolithography first evolved around more commonly observed one photon based curing processes, however two photon based techniques are growing in their application to microfabrication for tissue engineering (Maruo and Fourkas 2008). In this chapter, one photon microstereolithography will be explored with a focus on dynamic mask projection. In following chapters two photon microstereolithography will be explored in more detail.

One photon microstereolithography, in which curing is initiated by the absorption of one photon by a photoinitiator is accomplished by two distinctly different approaches. In projection microstereolithography, an image is projected into the curable polymer resulting in curing according to the projected pattern (Han et al. 2008). In scanning microstereolithography, the focal point of a laser is scanned across the surface of the resin in order to write out the desired pattern in a point to point fashion (Kwon and Matsuda 2005). A further advancement in the field of projection microstereolithography is the use of dynamic masking technology (Choi, Wicker, Cho, et al. 2009), which eliminates the need for the creation of individual masks prior to structuring.

In this study the construction and operation of a dual light source projection microstereolithography workstation is described. The system may be used with either an ultraviolet (UV) light source with a peak emission at 365 nm or a blue laser operating at 473 nm, allowing curing with different photoinitiators at two different wavelengths. Patterned light is generated using a digital micromirror device (DMD) and the resulting image is projected into a photosensitive resin supported in a sample holder. Vertical stepping to generate three dimensional structures was accomplished using a three axis translation stage. The system was used for the production of experimental tissue scaffolds, nerve guidance conduits and polymeric rings containing micropockets which may be used as stem cell delivery vehicles with further development. The produced structures represent valid potential clinical applications for this technology. Further development of the described innovative applications in corneal regeneration and nerve repair is ongoing.

### 3.2 Materials and Methods

The initial development and construction of the system is detailed in the following design study. The system was used to produce a range of patterns and single layer structures before layer-by-layer stepping and direct z translation were used to create three-dimensional devices, which were imaged using optical microscopy and scanning electron microscopy. Cell culture was used to demonstrate potential applications of this technology for the production of tissue scaffolds and tissue engineering devices.

#### 3.2.1 Design Study: Development of a Projection Microstereolithography Workstation

A projection microstereolithography workstation based on a DMD dynamic projection system was designed and built. The system incorporates interchangeable light sources, beam forming optics, a DMD for image formation, image focusing optics and a sample support mounted on an  $(x,y,z)$  translation stage in order to position the sample in the horizontal plane and provide vertical stepping. The system was constructed on an optical breadboard to allow precise positioning of optical components. A simplified schematic of the projection system is shown in figure 15.

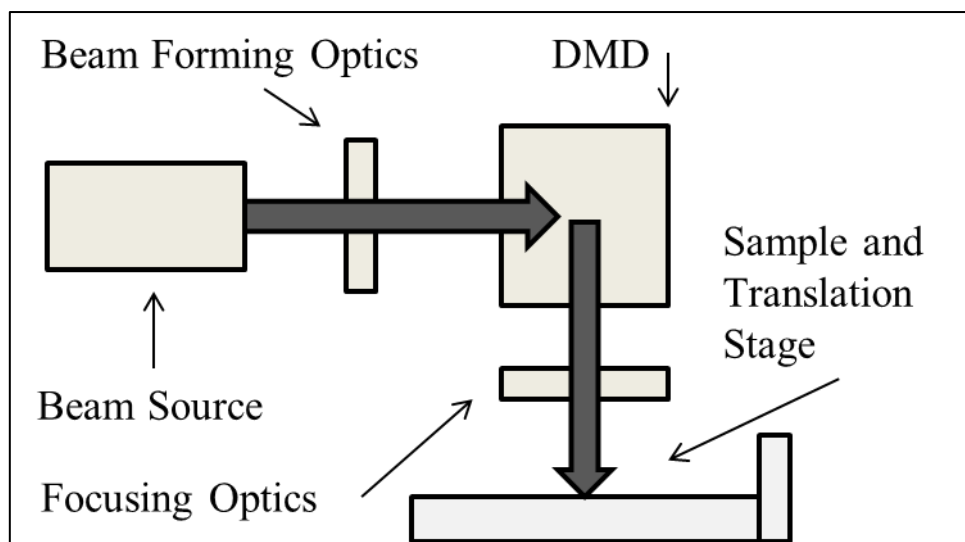


*Figure 15: Schematic of projection stereolithography system. Radiation is emitted and passes through an optical arrangement in order to form a suitable beam. The beam is reflected by a digital micromirror device which generates images according to a computer model. The image then passes through a lens where it is focussed into a photosensitive solution where curing occurs. Vertical stepping is accomplished using a translation stage.*

The projection microstereolithography device was built on an anodised aluminium optical breadboard (Thorlabs). The selected breadboard has a matte black finish preventing unwanted reflections which present a potential hazard when working with lasers. The breadboard allows exact positioning and interchanging of optical components. The system was enclosed within a metal framed cage (Thorlabs) covered with black cardboard panels to contain the radiation during curing. Furthermore, when using the laser device the system was interlocked to prevent accidental exposure to radiation. All lenses, lens mounts and optical posts were supplied by Thorlabs unless otherwise specified.

Two different light sources were selected for illumination. The system was first assembled with a UV lamp (EXFO Omnicure S1000 100 W) as the light source. The lamp generates UV light over a range of wavelengths with a peak emission at 365 nm. Since the lamp produces a divergent beam, the light requires collimation to maintain a uniform diameter and intensity along the beam path. To collimate the beam, the radiation is passed through a lens with a focal length of 2.5 cm. At the focal length of this lens (2.5 cm) a pinhole lens is used to block any scattered radiation, and a lens with a focal length of 5 cm is placed 5cm from the pinhole (7.5 cm from the 2.5 cm lens). This results in a collimated beam. To achieve light of only one wavelength, a filter can also be placed in the beam, this avoids chromatic aberration. Figures 16 and 17 demonstrate the process of collimating the beam.

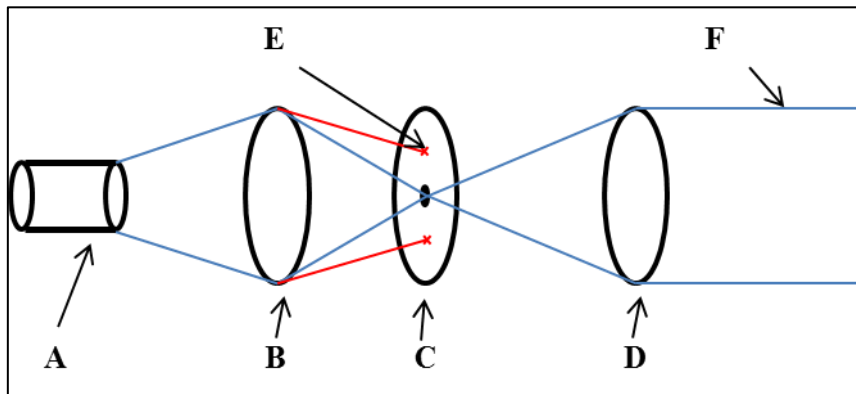


*Figure 16: Collimation of the UV Lamp. The beam is emitted (A) and passes through a 2.5 cm lens (B). Scattered light (E) is blocked by a pinhole lens (C) and the beam is directed towards the DMD using a 5 cm lens (D) resulting in a collimated beam (F).*

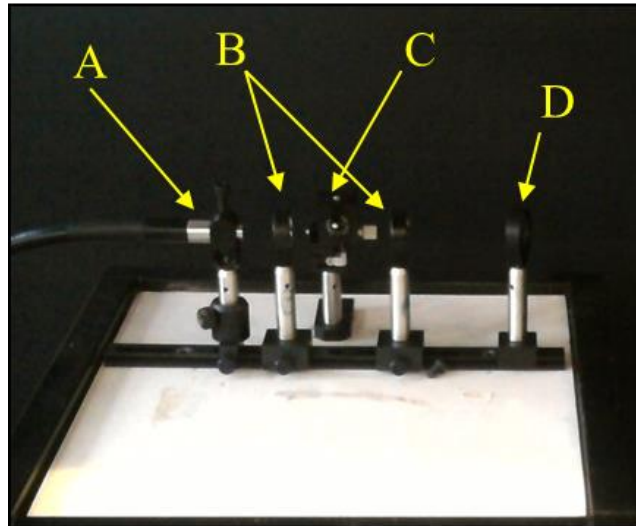


*Figure 17: Formation of a collimated UV beam. Light from the UV lamp is emitted through an optical cable (A) and passes through a telescopic lens set (B) with a pinhole lens in the centre to block stray radiation. The collimated beam passes through a monochromatic filter (D) allowing only light of a specific wavelength (365 nm) to pass through.*

As an alternative light source to the UV lamp a blue laser (CNI Laser, MBL-473, 473 nm~150 mW) was used. The benefit of using a laser is that the beam does not require collimation, and only light of a single wavelength is generated. Furthermore, the beam is not divergent preventing distortion or blurring of the image. Since the beam diameter emitted by the laser is not large enough to cover the whole of the DMD surface, the beam was again expanded using a telescopic lens arrangement. The beam passes through a lens with a focal length of 2.5 cm followed by a 15 cm lens placed 17.5 cm ( $2.5 + 15$  cm) later. This results in a  $6 \times$  expansion of the beam diameter allowing larger structures to be produced.

In order to form the desired image a digital micromirror device (DMD) (Texas Instruments) was used. The DMD consists of an array of micromirrors (768 rows of 1024 mirrors each) which can be turned on or off according to a bitmap. By creating a bitmap of the desired image the user can control directly the pattern that is reflected by the DMD. Each micromirror on the DMD is on a hinge which can be rotated to either plus or minus  $12^\circ$ . The on and off positions correspond to either plus or minus  $12^\circ$  as determined by the user. When the DMD is illuminated the mirrors which are 'on' will reflect the light in the direction of the focusing lenses, and those that are 'off' will reflect the negative of the desired image in a dummy direction where it is absorbed by a beam stop. The use of a DMD has been

demonstrated for example by several authors (Choi, MacDonald, and Wicker; Han et al. 2008).

Once the desired image has been formed the image focussed into the photocurable resin using a lens, typically with a magnification of 5-10 times. The size of the image and also the resolution can be controlled by the power of the final focusing lens. A more powerful lens can create a smaller structure with a better resolution, whereas a lens of lower power can create a larger image with a larger minimum feature size.

In order to create structures in three dimensions a three axis linear translation stage (PT3 Translation Stage, Thorlabs) was used. By curing onto a surface which could be lowered into the photocurable resin three dimensional objects could be created, either by lowering the sample continuously into the resin or by curing the sample in a layer-by-layer fashion and lowering the sample holder to maintain a fixed distance between the surface of the resin and the focusing lens. The most rapid method of producing simple structures such as hollow tubes was to lower the structure continuously into the resin whilst curing. This technique was explored for the production of nerve guidance conduits, as described later in this chapter.

Han *et al.* demonstrate the fabrication of tissue engineering scaffolds using a layer-by-layer method (Han et al. 2008). This method allows the creation of structures with well resolved internal geometry. Between the curing of consecutive layers the structure being created is lowered into an inert liquid which has a higher density than the photosensitive resin and forms a lower layer. As the structure is lowered into the inert liquid partially cured oligomers which can build up between the internal features are washed away, resulting in improved resolution. The drawback of this method is that cure times are increased. This technique may be explored in future studies with the microstereolithography work station.

### **3.2.2 Photocurable Material Preparation**

For initial curing trials with the microstereolithography system using the ultraviolet lamp a commercially available UV curable adhesive known as NOA 81 was used (Norland Optical Adhesive 81, Norland Products). This clear and transparent viscous liquid material cures rapidly in the presence of UV radiation and is used directly from the bottle without the need to add a photoinitiator.

Structures were also created using low molecular weight polyethylene glycol (PEGDA) diacrylate ( $M_w$  258 g/mol, 100 ppm MEHQ inhibitor, Sigma-Aldrich). To prepare this polymer for photocuring, the material was first passed through an inhibitor remover column (Aldrich) to remove the inhibitor.

For the ultraviolet light source, 4,4'-bis(diethylamino)benzophenone was added to the solution to the concentration stated in the individual experiments (typically 1-2%) and sonicated thoroughly for 10 minutes in a sonic bath at room temperature. To prepare the material for curing with the blue laser light source camphorquinone (97%, Sigma-Aldrich) was used as a photoinitiator, and prepared by sonication in order to mix the powder with the resin. Photocurable polylactic acid resin was prepared as described in chapter 2. The analysis of cell viability and adhesion on this material and the interaction of cells with devices created from this material is examined in detail in chapters 4, 5 and 6.

### **3.2.3 Sample development**

Samples prepared from NOA81 were developed by immersion in toluene for ten minutes in order to remove uncured material. Polyethylene glycol diacrylate structures were developed by soaking in isopropanol overnight unless stated otherwise. Photocurable PLA structures were developed by immersion in 4-methyl-2-pentanone and rinsing with isopropanol as described in following chapters.

### **3.2.4 Scanning Electron Microscopy**

Samples were imaged using an Inspect F scanning electron microscope (SEM) using an accelerating voltage of 10 kV and a spot size of 3, after the application of a thin gold coating to the samples using an Emscope SC500 sputter coater. Samples containing cells from cell culture were dehydrated using increasing concentrations of ethanol in distilled water, followed by pure ethanol, ethanol mixed with hexamethyldisilazane (HMDS,  $\geq 97\%$ , Sigma-Aldrich) and finally pure HMDS according to the protocol presented in chapter 5.

### **3.2.5 Cell Culture Methods**

Human dermal fibroblasts were extracted from human skin under a tissuebank licence. Rabbit limbal fibroblasts were kindly supplied by Dr Í. Ortega (University of Sheffield). In brief, the cells were extracted from waste rabbit eyes from a pet food company (Woldsway Foods Ltd,

Spilsby, UK). The cells were cultured in completed Dulbecco's modified Eagles medium (cDMEM) containing foetal calf serum, Fungizone<sup>TM</sup> (amphotericin B), L-Glutamine and penicillin/ streptomycin.

To visualise the cells by MTT staining, cells were cultured according to the individual experiment before washing twice with phosphate buffered saline (PBS) before incubation at 37 °C for 40 minutes in a prepared by adding 0.5 mg MTT in 20 mL of PBS. After the required time the solution was removed before imaging of the cells.

### **3.3 Results and Discussion**

The microstereolithography system was first used to create patterned arrays from photocurable materials in order to investigate the ability of the system to recreate the input bitmap. Three dimensional structuring was then demonstrated and structures were selected in order to represent potential applications of this technology in tissue engineering.

The development of a dynamic mask projection based microstereolithography device as discussed in the previous section allows the production of a wide variety of surface patterns which can be modified simply by changing the computer design. In order to create the desired surface morphology a bitmap is created and loaded into the control software, forming the desired pattern on the surface of the DMD, which is then projected into the photosensitive resin by exposure to the curing radiation. The dynamic masking capability provides advantages over established photomask based lithography techniques, eliminating time consuming and costly photomask production techniques such as electron beam etching, step by step production or laser printing (Chen et al. 1998).

The generation of structures directly from a bitmap was demonstrated by exposure of a photocurable material to UV light. A readily available photocurable material (Norland Optical Adhesive 81, Norland Products) was used to test the image reproduction of the system developed in the previous section. A bitmap was created using CorelDraw, and loaded into the DMD control software. A 13 mm glass coverslip spin-coated with a thin layer of optical adhesive was positioned in the sample support and exposed to ultraviolet radiation (365 nm) from the UV lamp at an intensity of 10 mWcm<sup>-2</sup> for 30 s. The resulting structure was developed by immersion in toluene and the resulting structure imaged using a light microscope.

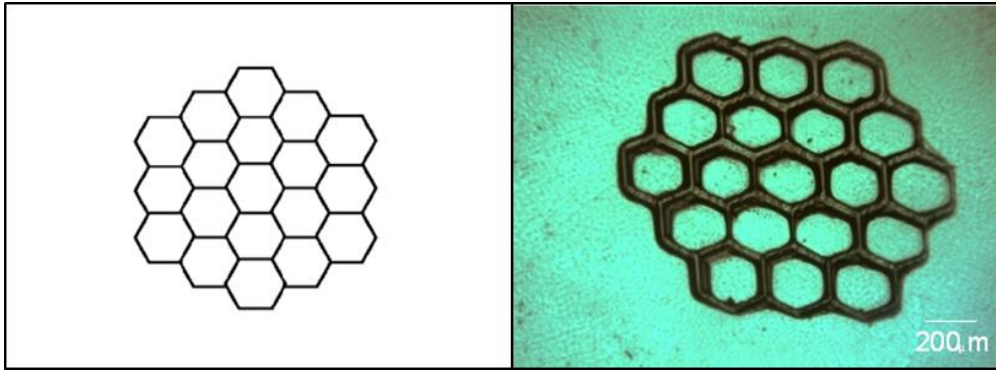


*Figure 18: Input bitmap loaded into DMD device (left) and resulting structure formed curing of the material (right, scale bar 200  $\mu\text{m}$ ). The bitmap was recreated accurately in the material indicating that the system is well aligned.*

As shown in figure 18 the structure accurately reproduces the projected bitmap, resulting in a well-defined structure. Slight ‘blurring’ of the features towards the bottom right of the structure as displayed in figure 18 has occurred, most likely due to variations in intensity across the diameter of the beam, however this may be alleviated by careful control of curing conditions such as exposure time and layer thickness. Close examination of the structure of the pattern indicates a feature resolution of around 25  $\mu\text{m}$  and a clear boundary between the cured material and glass substrate.

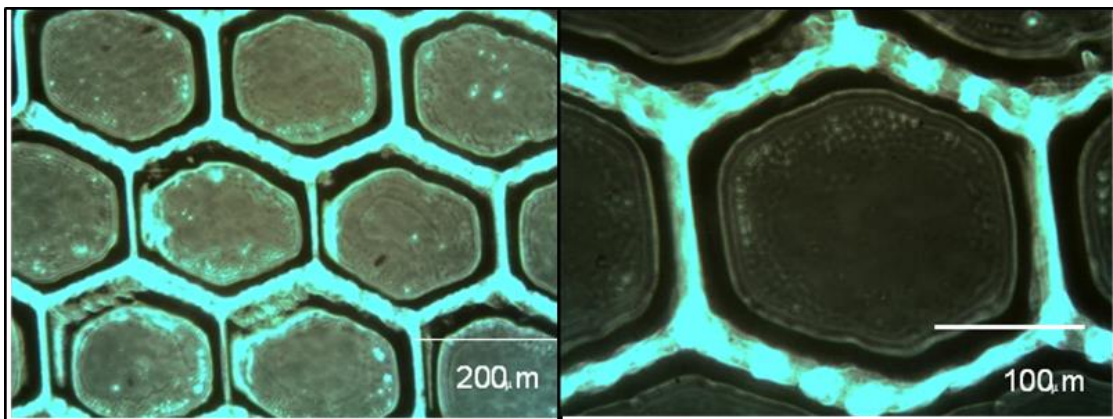


*Figure 19: Honeycomb patterned layer created using photocurable material NOA81 cross-linked by exposure to patterned ultraviolet (UV) light using the developed microstereolithography device, demonstrating the machines ability to produce surfaces of varied morphology.*

The structure displayed in figures 18 and 19 also demonstrates further the potential applications of the projection lithography technique, as comparisons may be drawn with the

structures produced by Engelmayr *et al.* produced for cardiac tissue engineering where the unique scaffold structure allowed the anisotropic properties of the native tissue to be recreated (Engelmayr et al. 2008).

The resolution of the device was further verified by creating a structure using polyethylene glycol diacrylate (PEGDA). A solution of PEGDA containing 2% w/w of the photoinitiator 4,4'-bis(diethylamino)benzophenone was prepared, and a thin film of the resin was deposited onto a 13 mm coverslip in a 12 well plate supported in the sample holder. Using the UV light source and an intensity of  $30 \text{ mWcm}^{-2}$  and an exposure time of 60 s, a circular image consisting of lines with a thickness of 1 pixel was loaded into the DMD control software and cured into the resin. The thick circular structure was used to act as a support and protect the fine lines in the developing process. Using lines of 1 pixel in thickness the minimum resolution of the machine could be determined.

The structure was developed by soaking thoroughly in isopropanol as described in the methods section and then left under vacuum to dry overnight. A 10-20 nm thick coating of gold was then applied to the structure, which was then visualised using scanning electron microscopy. The thickness of the lines was again determined to be approximately  $25 \mu\text{m}$  (see figure 20), representing the resolution of the machine.

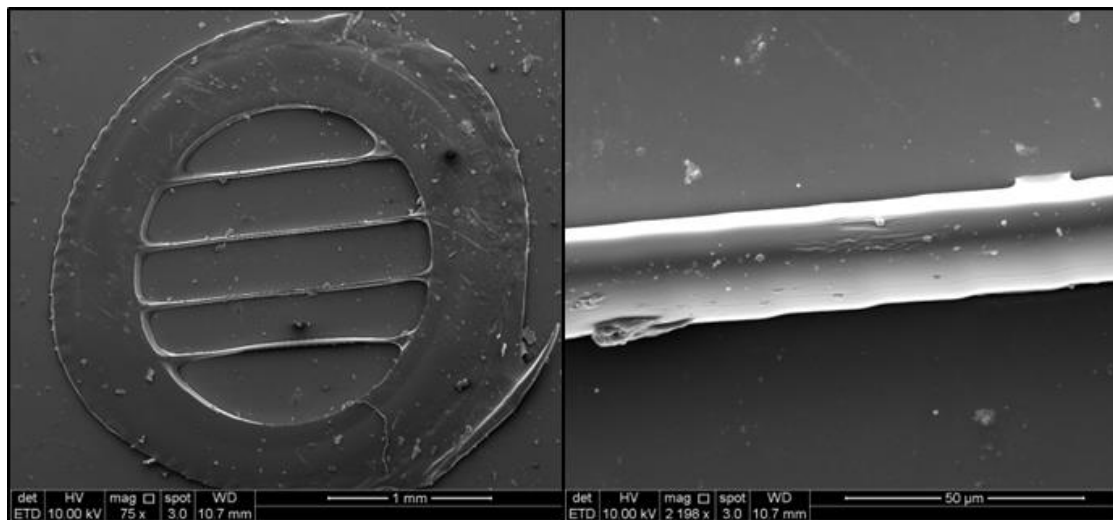


*Figure 20: PEGDA Structure produced by projection microstereolithography, demonstrating a resolution of  $25 \mu\text{m}$ .*

The ability of the device to produce larger grooved devices was demonstrated by projecting images into optical adhesive. Grooves of different thicknesses were created using optical

adhesive as shown in figure 21. Groove widths of 100 and 200  $\mu\text{m}$ , and single and parallel geometries were explored. Microblocks of photocurable poly(lactic acid) were also produced using spin coated films of photocurable PLA from a photosensitized solution as described in chapter 2. Using an exposure time of 60 s and an intensity of  $30 \text{ mWcm}^{-2}$  blocks of PLA with dimensions of 50  $\mu\text{m}$  by 50  $\mu\text{m}$  were prepared as shown in figure 21.

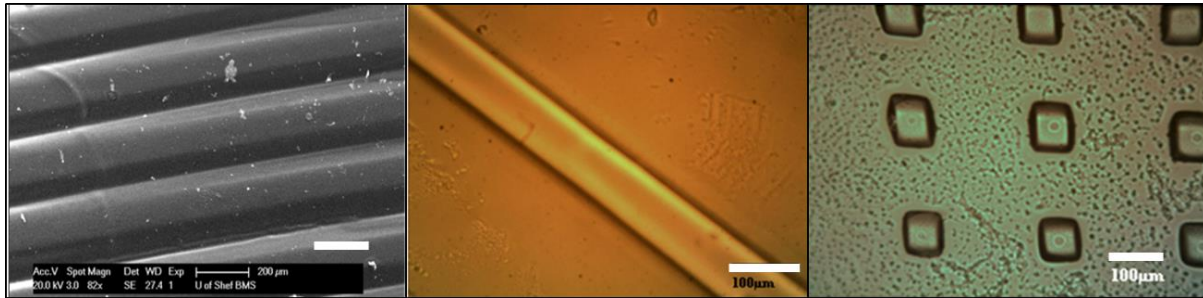


*Figure 21: Microgrooves produced from optical adhesive (left, centre) and microblocks of photocured PLA (right) using the developed projection microstereolithography device. Scale bars: left 200  $\mu\text{m}$ , centre and right 100  $\mu\text{m}$ .*

Surface structure and topography is an important factor affecting the behaviour of cells in culture, and can influence the cellular response to an implant surface *in vivo* (Scheideler et al. 2003). Chen *et al.* were able to demonstrate the relationship between cell shape and cell function using a microcontact printing technique to create cell adhesive islands of fibronectin on a non cell adhesive substrate (Chen et al. 1998). By restricting cell attachment to the fibronectin coated areas cell shape could be controlled by changing the shape of the fibronectin deposits. Reducing the size of cell adhesive areas was demonstrated to switch the behaviour of cells from growth to apoptosis. Cell shape was demonstrated to determine cell fate, regardless of the type of protein or integrin mediating adhesion (Chen et al. 1997).

The effect of surface structure on cell alignment is also of interest in neural tissue engineering, and is an important step towards creating nerve repair devices or ‘conduits’ with in-built structural cues which can enhance functional recovery (Lietz et al. 2006). Hsu *et al.* demonstrated that nerve guidance conduits for peripheral nerve repair prepared by a combined phase transition/ microprinting technique performed better when a grooved surface was created on the conduit rather than a smooth one, as evidenced by improved myelination and a greater number of regenerated vessels following animal implantation. Furthermore, functional recovery was shown to be greater in the grooved conduits (as opposed to smooth ones) implanted into rats with transected sciatic nerve injury, demonstrated by walking track

analysis (Hsu and Ni 2009). The effect of microchannels on the 10-100  $\mu\text{m}$  scale has been shown to influence neurite extension and alignment (Mahoney et al. 2005). Micro-grooved substrates created from NOA 81 are shown in figure 22.

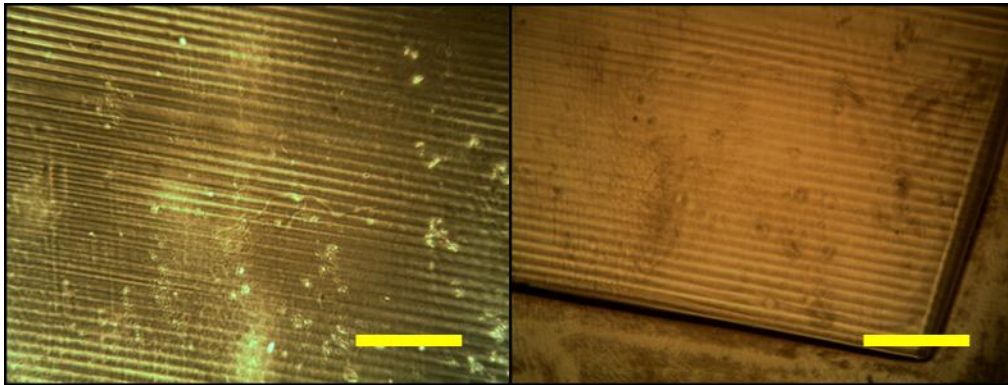


*Figure 22: Microgrooved surfaces produced in Norland Optical Adhesive (NOA) 81 using in-house projection microstereolithography device. Scale bars indicate 500  $\mu\text{m}$  (left) and 250  $\mu\text{m}$  (right).*

In order to take the applications of projection microstereolithography beyond surface patterning, structuring must be achieved in all three dimensions. Microstereolithography is well suited to the creation of small scale devices with complex geometries, having been developed originally as a rapid prototyping technique (Yan and Gu 1996).

In order to create true three dimensional structures, a layer-by-layer methodology was used. Curing of multiple layers can present problems due to overcuring and over-penetration of radiation, and a balance must be between cure time, intensity and the extent of curing. If insufficient cure time or exposure is used, then the structure may not cure completely and will become brittle, however excessive curing will lead to loss of resolution. Choi *et al.* demonstrated that by using a small percentage of a light absorbing die, the penetration depth of the curing radiation can be reduced, which allows multilayer structures to be built without loss of features in the vertical plane (Choi, Wicker, Cho, et al. 2009).

A test structure was created to assess the cure depth of the radiation using the 473 nm blue laser. The structure consisted of alternating layers of square ‘posts’ acting as spacers and a hollow square structure to act as a cross-beam between the posts (see figure 23). This design was intended to demonstrate the effect of overcuring on vertical resolution. As can be seen from the figure, no gaps were observed between the individual layers, as a result of curing beyond the desired depth.

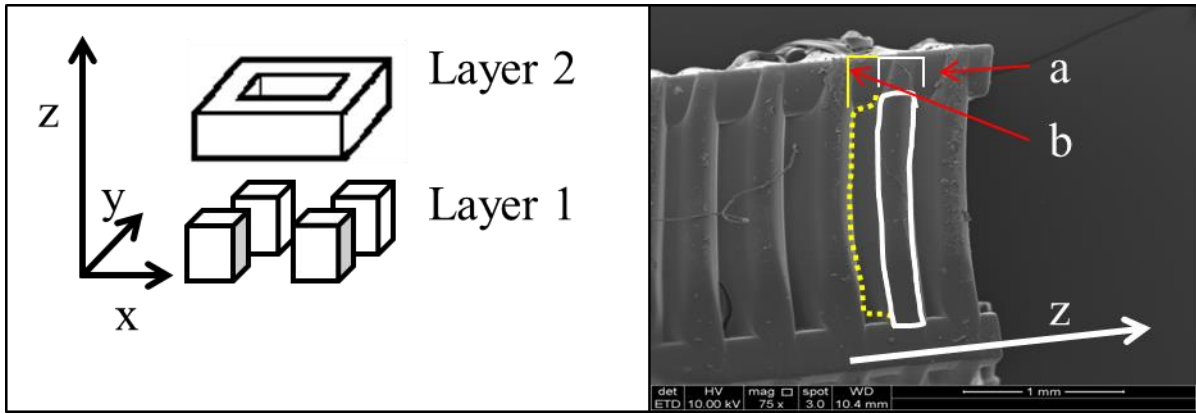


Figure 23: Design for multilayer structure (left) and illustration of overcuring (right). Right image shows desired layer thickness (a) and extent of overcure (b). Overcuring between layers is a common problem encountered with microstereolithography systems and prevention requires careful adjustment of cure time and exposure intensity.

Structures based on the design in figure 23 were created, however instead of using alternating layers a table like structure was created. By the addition of a small quantity of the dye Eosin-Y, the cure depth of the laser system was successfully reduced, allowing the creation of well-defined three dimensional structures with good vertical resolution. The table created using a light absorber in the photosensitive mixture showed far better vertical resolution than the structure created without the dye (see figure 24). This was due to absorption of the curing radiation leading to reduced penetration depth.

A variation of this method was also demonstrated by Choi *et al.* where samples were exposed to radiation for different time points. Following exposure the depth of cure was determined by measuring the thickness of the upper layer and the results were used to plot a calibration graph. By selecting the desired cure depth the correct exposure time may be selected (Choi, Wicker, Cho, et al. 2009). This was demonstrated in this study using NOA81, by determining the cure depth for different time points as shown in figure 25.

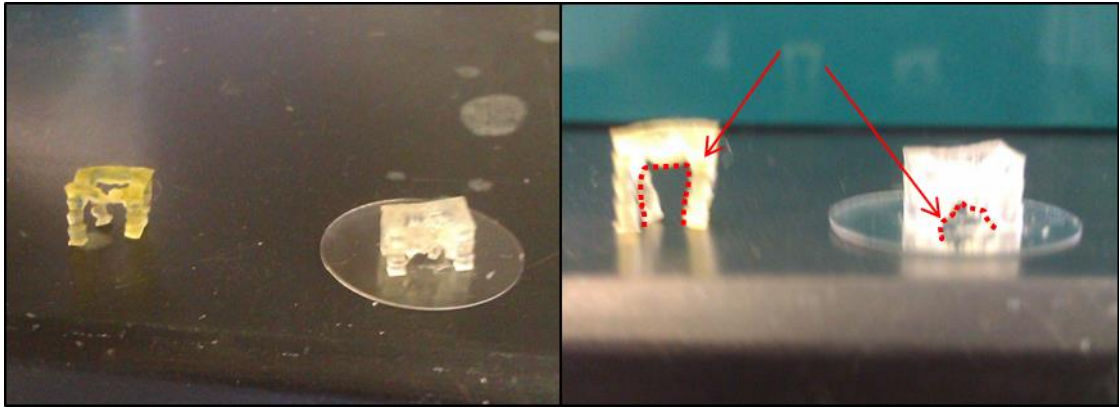


Figure 24: Reduction of cure depth using light absorbing dye. Left hand structure in both images was created from solution containing light absorbing dye, whilst right hand structure was not. Warping of structures caused by contraction of low molecular weight PEGDA upon drying.

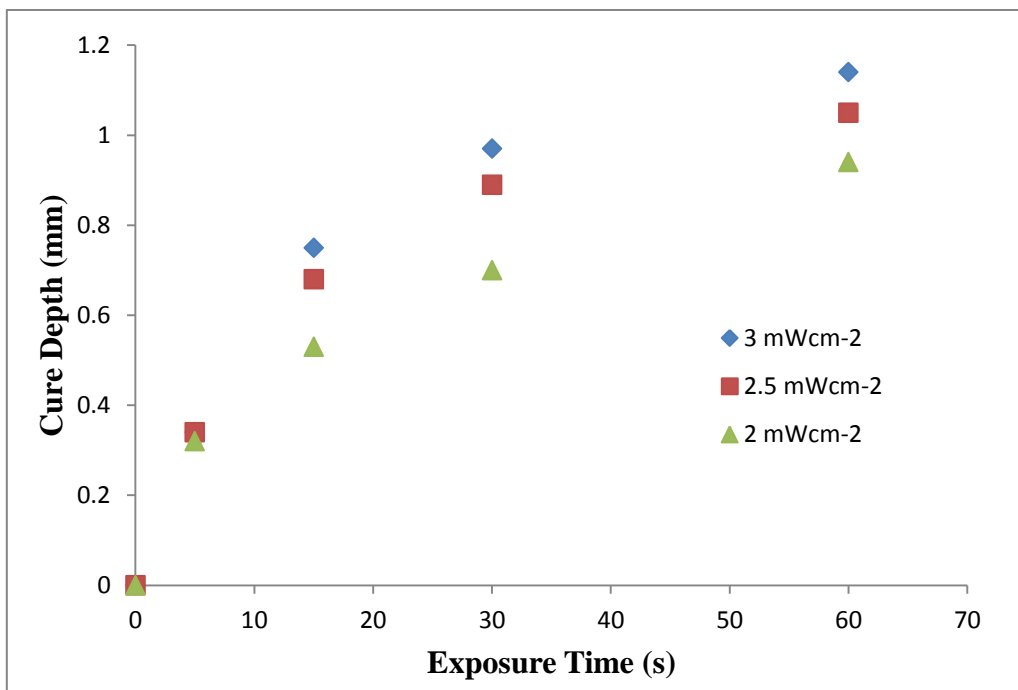
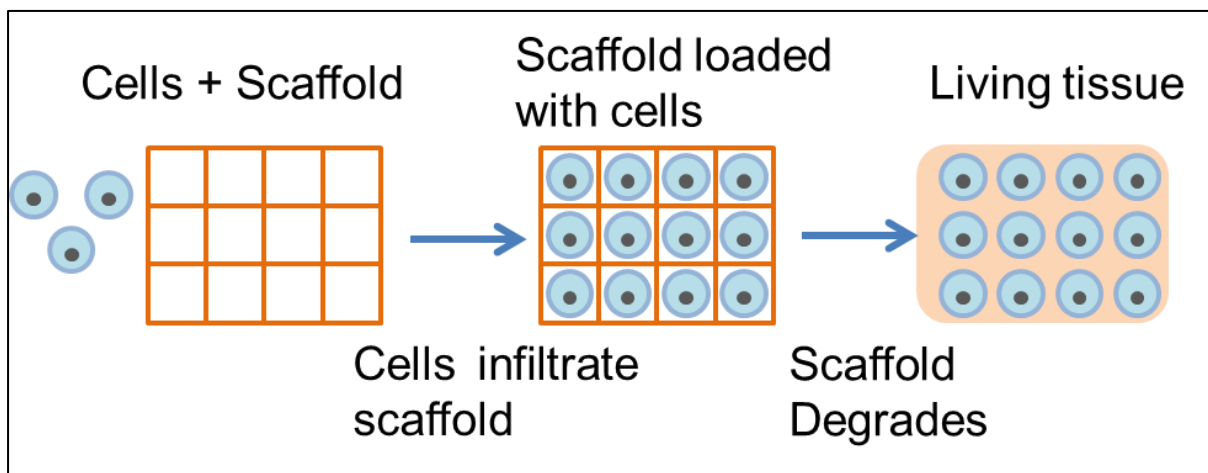


Figure 25: Cure depth control plot for NOA81. Increased exposure time leads to greater cure depth, as does increased intensity. The cure depth appears to reach a limiting value determined by the intensity, as described by the Beer-Lambert law.

Tissue engineering seeks to create replacements for damaged or diseased tissues through the use of tissue scaffolds. As discussed in the introduction tissue scaffolds form a porous support structure for cells as they build up a new tissue. Scaffolds produced from resorbable materials protect cells as they build up a new extracellular matrix within the pores of the scaffold. As the tissue forms the scaffold will degrade at an appropriate rate so that it will be replaced by the tissue, eventually resulting in an engineered tissue. Scaffolds may be explored for a wide range of applications, for example creating new bone, skin or nervous tissue. Therefore a wide range of geometries and also materials must be explored to provide scaffolds with the correct properties for the selected applications. The process of scaffold based tissue engineering is demonstrated in figure 26.



*Figure 26: Simplified process diagram of tissue engineering using tissue scaffolds. A degradable porous scaffold is loaded with cells which create new extracellular matrix (ECM) as the scaffold degrades.*

Using a layer-by-layer approach experimental tissue scaffolds were created using layer-by-layer microstereolithography. The scaffolds were created from a 50/50 mixture of photocurable PLA and PEGDA, which was used to adjust the viscosity. Camphorquinone initiator was also used at 2% w/w and Eosin Y was used to reduce the cure depth of the laser. The scaffolds were designed with a three dimensional open geometry to maximise nutrient diffusion and cell dispersion. The scaffolds were soaked in de-ionised water for seven days before seeding with human dermal fibroblasts and culturing in an incubator at 37 °C for 7 days. The cell culture media was then removed and the cells stained for 40 minutes with MTT solution. The resulting blue staining indicated the location of living cells. As can be

observed from the staining, the cells have successfully attached to and proliferated on the scaffolds (see figures 27 and 28).

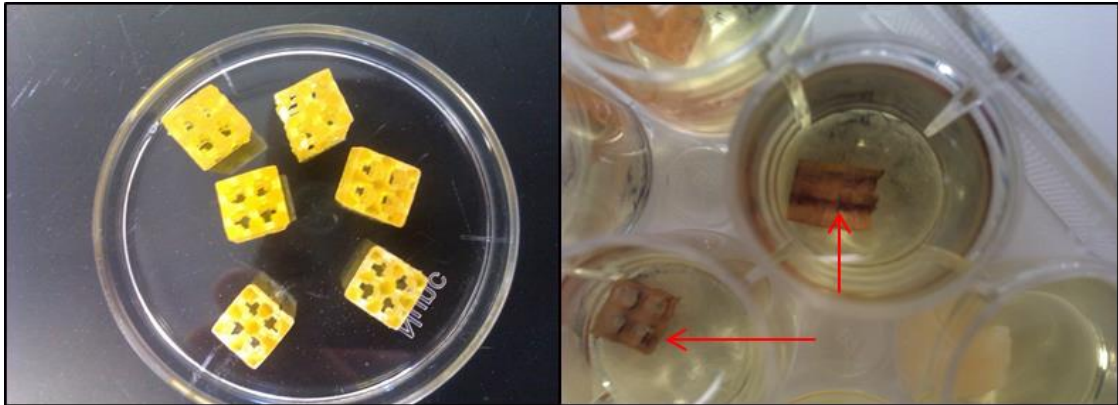


*Figure 27: PLA/ PEGDA Scaffolds created by layer-by-layer microstereolithography. Human dermal fibroblasts located on the scaffolds stained blue using MTT solution.*

The preparation of scaffolds with user defined architecture has been demonstrated for example by Grijpma *et al.* in the creation of tissue scaffolds with optimised geometries for cell and nutrient dispersion and the maintenance of cell viability (Melchels, Bertoldi, et al. 2010; Melchels et al. 2011). Another advantage of user defined structuring is the control over scaffold mechanical properties, which can be poor when porous foams and other high porosity structures are used (Hutmacher et al. 2001; Hollister 2005).

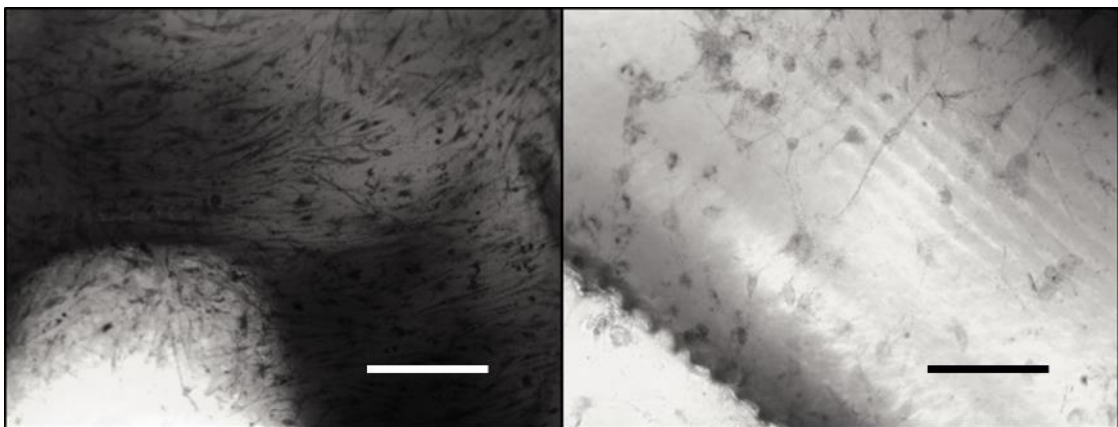


*Figure 28: Human dermal fibroblasts cultured on scaffolds produced by layer-by-layer projection microstereolithography. Scale bars: left 200  $\mu\text{m}$ , right 100  $\mu\text{m}$ .*

### **3.4.1 Applications: Microfabricated Stem Cell Niches for Corneal Repair**

Stem cells are vital in the regrowth, renewal and maintenance of healthy tissue. They possess the ability to self-renew and differentiate towards a certain cell type depending on specific metabolic and environmental signals (R. Lanza 2006). Stem cell niches, as observed by Fuchs *et al.* (Fuchs, Tumber, and Guasch 2004) are specific microenvironments in which stem cells reside. The niches present certain structural and biochemical cues which regulate the cell behaviour and ensure the survival of a constant population of healthy stem cells which support tissue renewal. Examples of anatomically defined niches include the crypts of the intestinal villus, and the bulge section of hair follicles (Tumber et al. 2004).

Corneal stem cells, located in the limbus (the region between the cornea and sclera) (Schermer, Galvin, and Sun 1986) are vital for the constant renewal of the cornea. Cells migrate from the limbus across the surface of the cornea maintaining a healthy and transparent tissue (Cotsarelis et al. 1989; Ebato, Friend, and Thoft 1987). The niches within the limbus are referred to as the palisades of Vogt. Destruction of the limbus, occurring when the cornea is injured results in loss of the stem cell population, and migration of cells from the neighbouring conjunctiva results in scar tissue formation leading to corneal blindness (Huang and Tseng 1991).

Corneal blindness is mainly treated by corneal or stem cell transplantation from a donor cornea (allografting) (Coster, Aggarwal, and Williams 1995). One obvious drawback of this procedure is the requirement for a donor cornea. The success rate one year after transplantation is 93 %, falling to 72 % after 5 years (Henderson, Coster, and Williams 2001). If a donor cornea is not available then one alternative treatment is stem cell delivery, this is typically achieved by delivering cultured stem cells on a donor amniotic membrane, which possesses suitable transparency and anti-inflammatory properties (Tseng et al. 1998). This technique is again limited by donor availability with respect to the membrane, and also the possibility of viral and bacterial transmission. The success rate of this technique is around 85 % after one year, although this is reduced to 45 % after three years.

Limitations of existing therapies present a clear need for synthetic or more readily available alternatives to existing donor tissue based stem cell transplantation. Alternative carriers under development include modified (cross-linked) human collagen (Dravida et al. 2008), polyethylene glycol based hydrogels (Sitalakshmi et al. 2008) and also electrospun membranes based on poly(lactide-co-glycolide) (Deshpande et al. 2010).

A further possibility is the microfabrication of custom stem cell delivery devices by microstereolithography, as will be discussed in this chapter. This application presents many possibilities for which the technique of microstereolithography is ideal. The technique allows the creation of patient specific devices, incorporating important structural cues which will provide a suitable microenvironment for stem cells. Custom polymers would allow tuning of the mechanical cues experienced by the cells, and further functionalization may provide chemical and biological cues.

The initial aim of this work was to develop a transplantable polyethylene glycol diacrylate ring containing stem cell niches for cell delivery. The ring was designed to match the approximate dimensions of the limbus of the human eye, with an approximate outer diameter of 1.2 cm. The niches, based on the dimensions of the palisades of Vogt, are located around the centre or inner diameter ring with approximate dimensions of 150  $\mu\text{m}$  in width and 30  $\mu\text{m}$  in depth. The basic process conditions were optimized and niches of two distinctly different morphologies were produced. Preliminary cell culture was performed using rabbit limbal fibroblasts. Morphology and location of the cells was examined using scanning electron microscopy (SEM). Further development work into the use of biodegradable materials, surface functionalization of the niches for stem cell adhesion and also the combination of microstereolithography with other techniques is ongoing, with a view to taking this technology to the clinic in next few years.

The projection microstereolithography workstation developed as discussed earlier in this chapter was used to fabricate rings containing micropockets or potential 'niches'. As a starting material for fabrication, polyethylene glycol diacrylate was chosen due to its history of clinical use. Low molecular weight PEGDA was used due to its low viscosity, facilitating easy delivery into the curing system.

Polyethylene glycol diacrylate was passed through an inhibitor removal column (Aldrich) to remove the inhibitor prior to use, to facilitate curing of the resin. To prepare a photosensitive mixture 0.1 g of camphorquinone as initiator (97%, Aldrich) was added to an amber glass vial and made up to 10 g with PEGDA, resulting in a 1 % w/w solution. The mixture was then stirred for 10 minute using a magnetic stirrer bar. Camphorquinone is approved for medical use, and is sensitive at the emission wavelength of the blue laser.

Initial optimisation of the photocuring mixture was performed using higher concentrations of camphorquinone, and also ethyl 4-(dimethylamino)benzoate (EDAB) as a co-initiator. Curing

was also attempted without the use of the inhibitor removal column. Without the use of the column curing results showed a greater degree of variability, possibly due to a higher threshold power required for curing making the curing process more sensitive to slight variations in the power of the beam or oxygen quenching. The use of EDAB as a co-initiator greatly increased the rate of curing, but also affected the viability of cells cultured on the resulting structures (data not shown), in agreement with other studies (Nie and Bowman 2002). Optimization of the curing times was therefore performed based on a 1 % w/w solution of camphorquinone in PEGDA.

The projection microfabrication workstation was used as described earlier in this chapter, using the blue laser (MBL-III 473 nm) as a light source. The laser power before beam expansion and focusing was measured to be 150 mW. A simple two layer approach was used for fabrication of the rings containing micropockets, as demonstrated in figure 29. A base layer was created consisting of a flat ring, and an upper layer containing the pockets was subsequently cured on top. Curing was performed on top of a thin Teflon sheet in a 12 well plate, the Teflon sheet facilitating detachment of the final structure. The photocurable solution was added by pipette, again in a layer-by-layer fashion to build up the final structure. The ideal fabrication conditions were determined by experiment to be a two layer projection of 60 s for each layer.

The simple two layer nature of the rings allows optimisation of the cure conditions manually without the need to calibrate the cure depth of the resin. As the height of the ring increases the distance from the focusing lens changes leading to blurring of the image, however the rings are sufficiently thin to not require height adjustment using the translation stage.

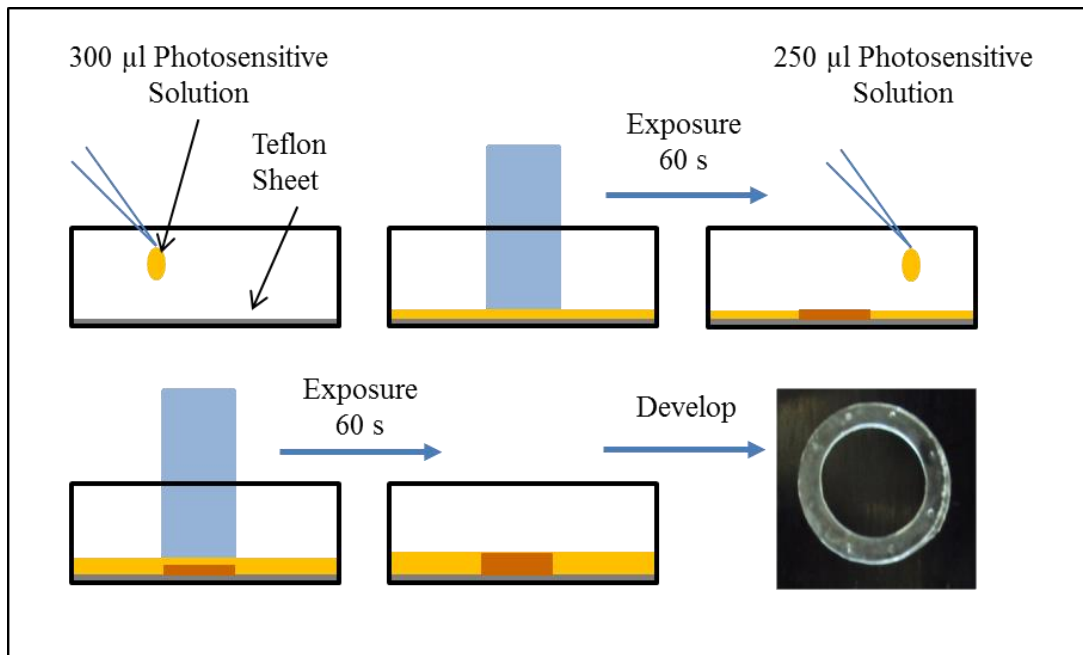


*Figure 29: Curing process for production of microfabricated rings. A drop of the photocurable solution is deposited onto a Teflon sheet in a 12 well plate and allowed to spread evenly over the surface. The first layer of the structure is then cured by exposure to the projected image (indicated in the figure by a blue rectangle). A further drop is then deposited and the second layer of the structure is created by exposure to the new image. The structure is then developed by washing to remove any uncured resin leaving the final structure which may be detached from the Teflon.*

In figure 30 the effects of overcuring are demonstrated, and overcuring of the polymer can be clearly observed as excess material around ring and poorly defined niches. A close up image of a niche on a ring produced using the optimized conditions is also shown.

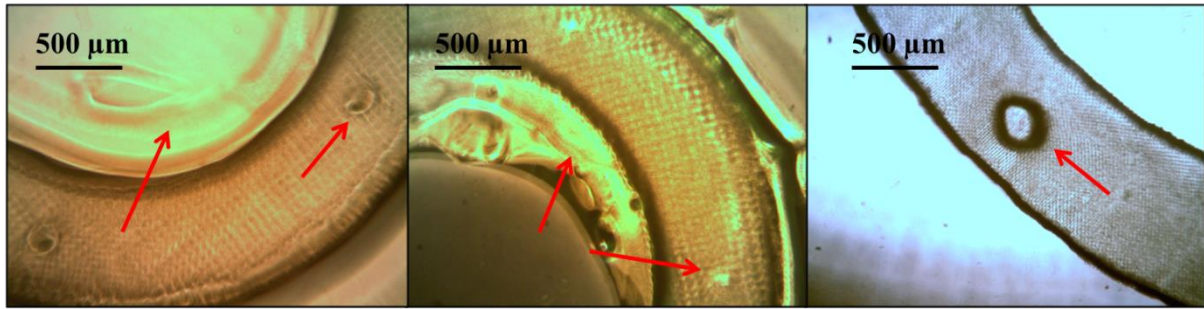


*Figure 30: Overcured rings (left and middle) and optimized ring/niche (right) produced by microstereolithography. Overcuring is characterised by spreading of features beyond their intended position and blurring of the final features.*

Niches of different geometries were created using the optimized curing conditions. The rings were developed by soaking in isopropanol overnight followed by soaking in phosphate buffered saline for 7 days to remove any impurities such as remaining photoinitiator.

Rings of the desired diameter of 1.2 cm were successfully created in a reproducible manner by layer-by-layer microstereolithography. Furthermore different micropocket geometries were also explored, as shown in figure 31. By changing the input design on the DMD micropockets with both open rectangular morphology and also circular morphology were produced.

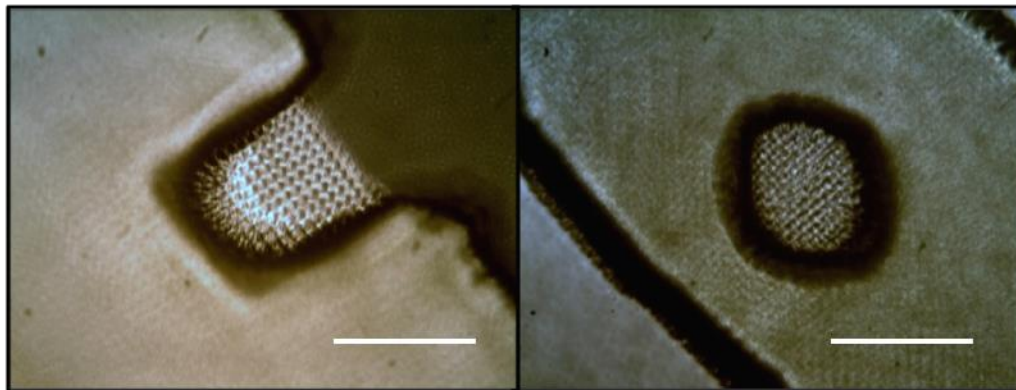


*Figure 31: Micropockets with open rectangular morphology (left) and circular morphology (right). Scale bars 300 μm.*

The morphology of rabbit limbal fibroblasts located within the micropockets was assessed using scanning electron microscopy (SEM). The cells were seeded onto the micropockets using an Eppendorf Micropipette, by taking 1 μl of a concentrated cell solution (175,000 cells

ml<sup>-1</sup>) and dispensing directly onto the micropockets. To aid in visualization of the micropocket and facilitate accurate dispensing a dissection microscope (Wild Heerbrugg M 3Z) was used. Medium was then added (1 ml) and the cells cultured on the construct for 7 days before fixing with HDMS and visualizing under SEM. Soaking of the constructs in PBS for sufficient time prior to cell seeding was found to be crucial in order for cells to attach. If the samples were not soaked for 7 days prior to cell culture cells appeared ball like and did not exhibit a typical fibroblast morphology. However, samples that were soaked for 7 days in PBS proved suitable for cell attachment, and fibroblasts exhibited a greater degree of spreading on the surfaces. This can be observed in figure 32, where cells cultured on a non-washed ring appear markedly different compared to those cultured on a washed ring.

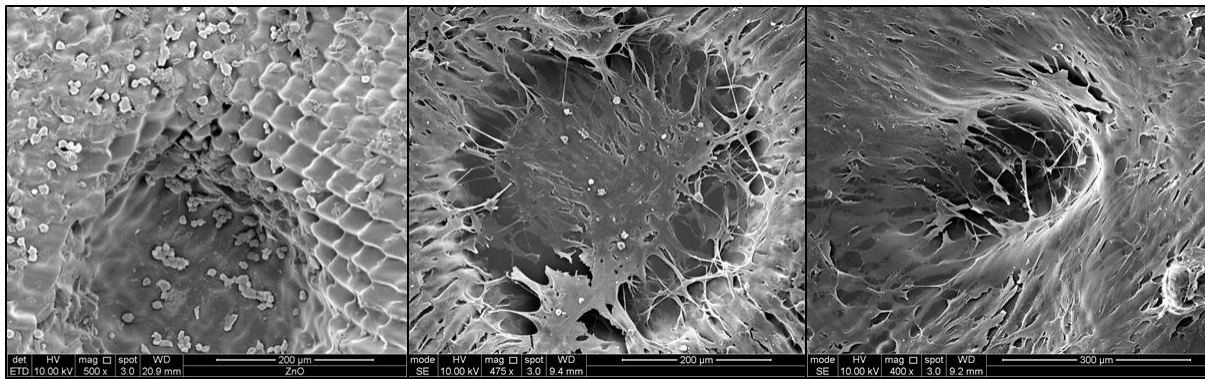


*Figure 32: Fibroblasts cultured on a non-washed ring (left) appear ball like and fail to proliferate whereas cells cultured in circular and open micropockets (center and left) on rings soaked for 7 days in PBS appear normal.*

Preliminary work towards the development of a transplantable ring containing micropockets as potential stem cell niches was presented. Cell proliferation within the niches was verified by SEM, and the necessity of soaking of the samples in PBS for at least 7 days following production in order to remove photocuring process related impurities was demonstrated, in agreement with other published studies on microstereolithography (Narayan et al. 2010). The optimum process conditions for two layer microstereolithography were determined and rings with micropockets of differing geometry were produced.

Rings containing micropockets capable of mimicking the stem cell niche are now being developed in order to bring this technology to the clinic. The remaining challenges include creating a true stem cell ‘niche,’ by surface functionalization and material optimization.

### 3.4.2 Applications: Nerve Guidance Conduits

The peripheral nervous system is an attractive target for tissue engineering due to its unique ability to regenerate, in contrast for example with the central nervous system in which inhibitory factors prevent regeneration following injury (Bell and Haycock 2012). In order to utilize the regenerative potential of the peripheral nervous system, various clinical techniques have been developed for the treatment of peripheral nerve injury. Established techniques include autografts, allografts and more recently nerve guidance conduits. Autografting is commonly considered as the ‘gold standard’ treatment for transected nerves, however this requires a second surgical site to harvest the donor nerve and also results in donor site morbidity (Millesi and Schmidhammer 2007). Donor availability and also the requirement for immune suppression presents problems with allografts, however results comparable to autografting are achieved (Mackinnon et al. 2001).

A promising alternative to transplantation is the use of artificial nerve guidance conduits (Jiang et al. 2010). These devices work primarily by entubulation of the severed nerve and the incorporation of biological, mechanical and structural cues in order to guide functional recovery of the nerve. Nerve guidance conduits and their structure and function are described in more detail in chapter 6.

Simple tubular conduits were initially produced using low molecular weight polyethylene glycol diacrylate (PEGDA, a low viscosity resin) due to its commercial availability and low viscosity, which made it possible to make structures by lowering the sample support into the resin at a constant rate. The first tubes to be produced were created using the UV light source, but later devices were produced using the blue laser due to the formation of surface grooves by extension of the pixels in the  $z$ -plane as will be discussed.

The projection microstereolithography workstation was used as described in the design study. In brief light from the blue laser (MBL-III 473 nm, 150 mW) was expanded to cover the face of the digital micromirror device (DMD), which formed the desired image according to a user created bitmap. The reflected image was focussed using a mirror for beam direction onto a sample support through a final focusing lens. In this case the sample support was a thin anodized aluminium strip of approximately 1 cm in width and 5 cm in length, with the final 1 cm end section folded at 90 ° to make an ‘L’ shape. This sample support was attached to the  $z$ -stage (Thorlabs) using carbon sticky tape as used to hold samples in place for scanning electron microscopy (SEM). This allowed the sample support to be lowered at a uniform

speed into the photocurable solution contained in the well of a 24 well tissue culture plate, giving translation in the  $z$ -plane. This process is demonstrated in figure 33.

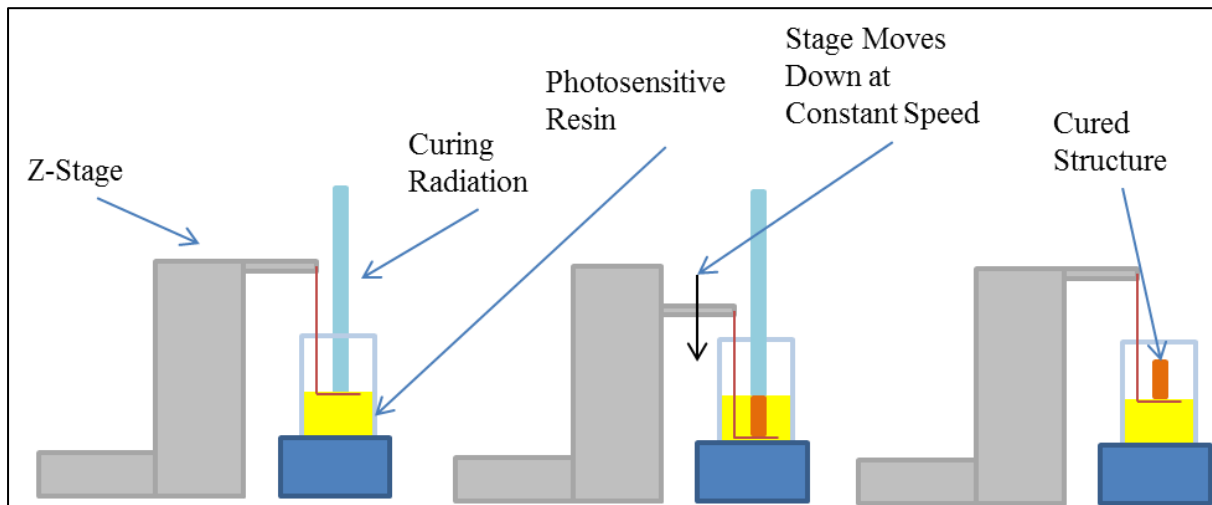


*Figure 33: Experimental set-up for making the NGC tubes. Vertical translation of sample support was achieved by attachment to a single axis Thorlabs translation stage, which allowed the structure under production to be gradually lowered into the resin. Following the curing process the structure was lifted out of the resin, detached and developed.*

An important factor in the accurate fabrication of the conduits was the speed at which the  $z$ -stage lowered the sample into the resin. Lowering the sample too rapidly caused poorly formed or no samples due to insufficient cure time, and lowering the samples too slowly caused overcuring of the features. The samples were cured in the well of a 24 well plate, and the maximum conduit length was limited by the depth of the well.

Initially a simple open tubular structure was created using the UV lamp (and 4,4'-bis(diethylamino)benzophenone at 2% by weight as photoinitiator). By experiment an optimum write speed of  $50 \mu\text{m s}^{-1}$  was determined. An open tubular conduit was produced by projecting a circular image with the DMD and lowering the sample support into the photocurable PEGDA solution. With a write speed of  $50 \mu\text{m s}^{-1}$  the production step lasted three minutes ( $9 \text{ mm} / 0.05 \text{ mm s}^{-1}$ ). The resulting structure and an example design are shown in figure 34.

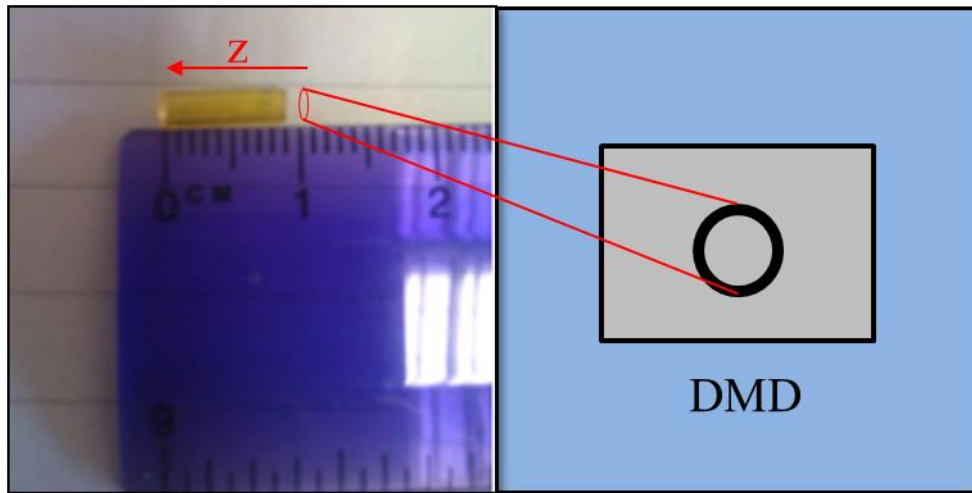


*Figure 34: A hollow PEGDA tube produced by projection microstereolithography shown with example image for DMD projection.*

The unintended pixelation effect encountered when combining the blue laser with the DMD was found to be of benefit when producing potential conduits with the projection microstereolithography device. Extension of the pixels in the vertical plane created a grooved effect which was observed on the resulting conduits, creating a potential guidance mechanism for axonal regeneration. The grooved effect can be observed in figure 35.

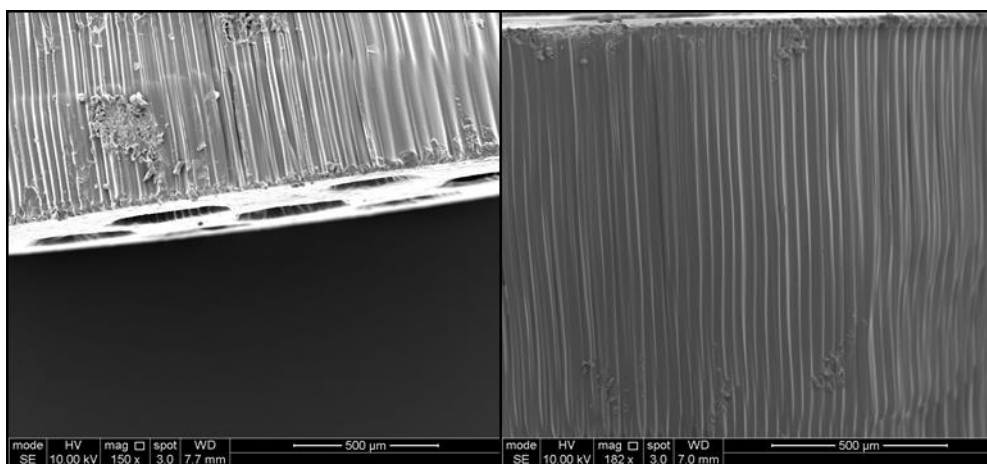


*Figure 35: Side-on view of nerve guidance conduit produced by microstereolithography. Grooves caused by pixelation of image and translation in z-direction are visible, creating contact guidance mechanism for cell alignment.*

The incorporation of multiple inner lumens into nerve guidance conduits allows a greater surface area for Schwann cell attachment. Schwann cells have been shown to be beneficial when incorporated into nerve guidance conduits, and play a key role in regeneration of peripheral nerve. The multi-lumen structure also matches more closely the structure of peripheral nerves, as demonstrated in figure 36. This topic is explored in greater detail in chapter 6.

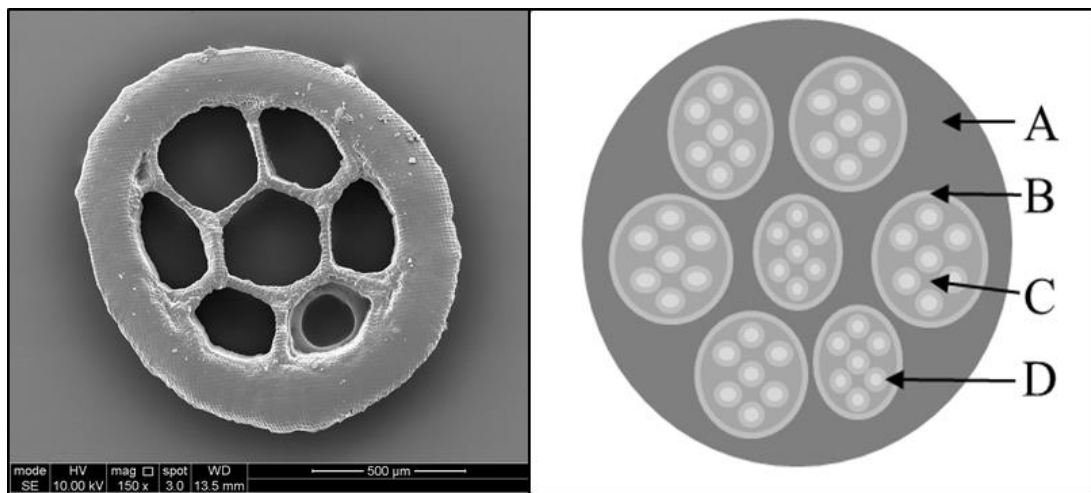


*Figure 36 Cross section of multi-lumen nerve guidance conduit prepared by microstereolithography (left) designed to mimic structure of peripheral nerve epineurium represented in diagram (right) showing epineurium (A), perineurium (B), endoneurium (C) and basal lamina (D) consisting of axons encircled by Schwann cells. Diagram adapted from Schmidt and Leach (Schmidt and Leach 2003).*

### **3.5 Discussion**

To date microstereolithography has been mainly applied to experimental studies aimed at demonstrating factors such as the relationship between diffusion, pore size, cell viability and scaffold mechanical performance (Melchels et al. 2011). Less attention has been focussed on the actual clinical applications of microstereolithography. This is due to various factors including the limited size of the structures which may be produced, a lack of materials suitable for internal medical use (as discussed in chapter 2) and also concerns regarding the biocompatibility of the initiators required (Ovsianikov, Malinauskas, Schlie, Chichkov, Gittard, Narayan, Lobler, et al. 2011).

In this chapter the design and operation of a simple projection microstereolithography system was demonstrated and potential applications in the production of tissue scaffolds, the fabrication of stem cell delivery devices for corneal regeneration and also the production of nerve guidance conduits was demonstrated. These represent potential real world applications in which the structuring ability and resolution of microstereolithography offers advantages over existing technology.

### **3.6 Conclusions**

In this chapter the construction of a dynamic projection microstereolithography workstation has been detailed. The microstereolithography system was used to generate patterned surfaces and 3D structures of interest in tissue engineering and biology. The use of photocurable biomaterials was combined with bespoke microfabrication techniques in order to produce experimental tissue scaffolds and nerve guidance conduits. Production of constructs for further clinical applications such as stem cell transplantation for corneal blindness was also explored.

# Chapter 4: Development of a Two photon Laser Direct Write Workstation

---

## Abstract

In this chapter the design, construction and operation of a laser direct write system capable of high resolution microstructuring via two photon polymerization is described. The system was constructed using a titanium-sapphire laser as a power source, a high numerical aperture objective fixed on an aluminium support to focus the beam and a high precision translation stage in order to write structures directly into a photocurable resin. The structuring of a photocurable polylactic acid oligomer synthesised as described in chapter 2 on a single micrometre scale was demonstrated, and further modifications to the structuring system including the use of low cost micro-lasers were explored. Cell interactions with the microstructures were also explored with potential applications as cell niches.

## 4.1 Introduction

Microstereolithography was developed as a rapid prototyping technology in the 1980's (Narayan et al. 2010). Early systems were based on curing via one photon absorption, using photomasks or scanning of the beam in a point to point fashion. Limitations of the technique include over-penetration of the curing radiation leading to overcuring between layers, scattering of radiation within the resin and the resulting accumulation of partially cured oligomers within the internal parts of structures with increasing cure time (Han et al. 2008).

Two photon polymerization emerged as a technique for microfabrication was first reported by Maruo, Nakamura and Kawata in 1997 (Maruo, Nakamura, and Kawata 1997; Sun and Kawata 2004). Originally described theoretically by Maria Goeppert-Mayer in 1931, multiphoton excitation was first demonstrated in the early 1960's by Kaiser and Garrett (Kaiser and Garrett 1961). In their work  $\text{CaF}_2:\text{Eu}^{2+}$  crystals were excited with a ruby laser (694 nm) to emit fluorescent blue light (425 nm). Multiphoton excitation occurs when two or more photons interact with the same molecule in a single quantum event to excite a molecule by a single quantum of energy. The frequency with which this process occurs is very low, requiring very high photon flux in order for the necessary photons to interact within the

lifetime of the event. In the context of microstereolithography, two photon excitation is initiated by the subsequent absorption of two photons of light by a photoinitiator, leading to the generation of radicals and initiation of the curing process (Lee et al. 2006).

Two mechanisms of two photon absorption exist. The first mechanism is sequential excitation, in which one photon is absorbed by the initiator which is promoted to a 'real' intermediate excited state with a lifetime of  $10^{-4}$  to  $10^{-9}$  s. A second photon is absorbed within this lifetime leading to initiation. The second mechanism proceeds via a virtual excited state caused following the interaction of the initiator with one photon. The virtual excited state has a much shorter lifetime of just  $10^{-15}$  seconds, during which the second photon must be absorbed (Lee et al. 2006). The second mechanism requires very high photon density or flux in order to proceed, typically requiring a femtosecond laser. Both processes proceed by the promotion of an electron by the absorption of two photons, each possessing half the total energy of the transition. Ti: sapphire lasers are therefore favoured for this process since their central wavelength of 800 nm is approximately half the wavelength or energy required for the excitation most ultraviolet photoinitiators. They also have a suitable energy profile for two photon absorption, as multiphoton absorption requires high pulse intensity but the average power is low due to the short pulse duration which is typically five or six times shorter than the repetition rate of the laser (LaFratta et al. 2007).

Originally explored for applications in physics and optics, two photon polymerization is increasingly being explored for medical applications, partly because of the emergence of new photocurable materials which are more appropriate for tissue engineering. In this chapter a basic 2PP system is constructed and used for the structuring of photocurable polylactic acid, prepared as described in chapter 2. The precise structuring of this material is demonstrated and initial cell culture work performed, demonstrating a proof of concept study on the structuring of biopolymers via high resolution microstereolithography.

## **4.2 Materials and Methods**

The photocurable PLA based material was synthesised as described in chapter 2, based on a molar ratio of 1 molar equivalent of pentaerythritol to 8 molar equivalents of lactide dimer. The oligomer was methacrylate functionalized and the ratio of monomer to initiator as well as the presence of methacrylate functional groups was checked using NMR and IR spectroscopy, as described in chapter 2. In this section the construction and operation of the

developed laser direct write system will be outlined, as well as the preparation and development of resin samples and the creation of basic programs which direct the fabrication process.

#### **4.2.1 Design Study: Two Photon Laser Direct Write System**

The two photon fabrication process is commonly achieved by one of two different mechanisms for translation of the focal spot. Either the beam is focussed to a fixed spot and the sample itself is moved using a high precision translation stage, or the sample is fixed in place and a set of translation mirrors known as a Galvano scanner is placed before the objective in order to manipulate the horizontal position of the focal spot, and vertical stepping is achieved using a  $z$ -stage. In this study the former technique is used, reducing the cost of the system by eliminating the need for a Galvano-scanner. Claeysens *et al.* demonstrate a combination of the two systems in which the Galvano scanner is used to write the structure and a piezo-electric stage shifts the sample so that the same structure can be repeated and overlapped, allowing larger structures to be created in a step and repeat methodology (Claeysens et al. 2009).

The in-house laser direct write system developed in the study presented here was based on a femtosecond pulsed laser focussed through a high numerical aperture microscope objective. Translation of the focal spot was achieved by moving the sample using a high precision ( $x,y,z$ ) stage controlled by a computer. Power was controlled using a mounted reflective variable neutral density filter (Thorlabs), and beam delivery controlled using a beam shutter (response time  $<1.5$  ms, Thorlabs) linked to a shutter controller (SC10, Thorlabs). The system was constructed on an optical breadboard, supported on an optical table to reduce the effect of vibrations. The system is outlined in figure 37.

#### **4.2.2 Laser Selection**

Two photon polymerization is initiated by the subsequent absorption of two photons of light within a finite lifetime determined by the half-life of the intermediate state of the initiator. The absorption rate depends on the square of the laser intensity, and is affected by the penetration depth of the radiation as well as the tight confinement of the light using a high numerical aperture (NA) lens. One limitation on the process is the poor sensitivity of commonly used commercially available ultraviolet sensitive photoinitiators to two photon

excitation (Wang et al. 2002). The poor sensitivity of commercial photoinitiators necessitates the use of lasers with high peak powers, fast repetition rates and ultrashort pulse widths in order to generate the high intensities required. As a result of this Ti: sapphire lasers are commonly employed in two photon stereolithography. Although capable of producing excellent structuring results, the high intensities used risk damage to the material being cured and present a narrow processing power window within which to operate. Research into more efficient photoinitiators for two photon initiated polymerization is expanding the range of wavelengths and laser systems which can be used for the technique (Lemerancier et al. 2006).

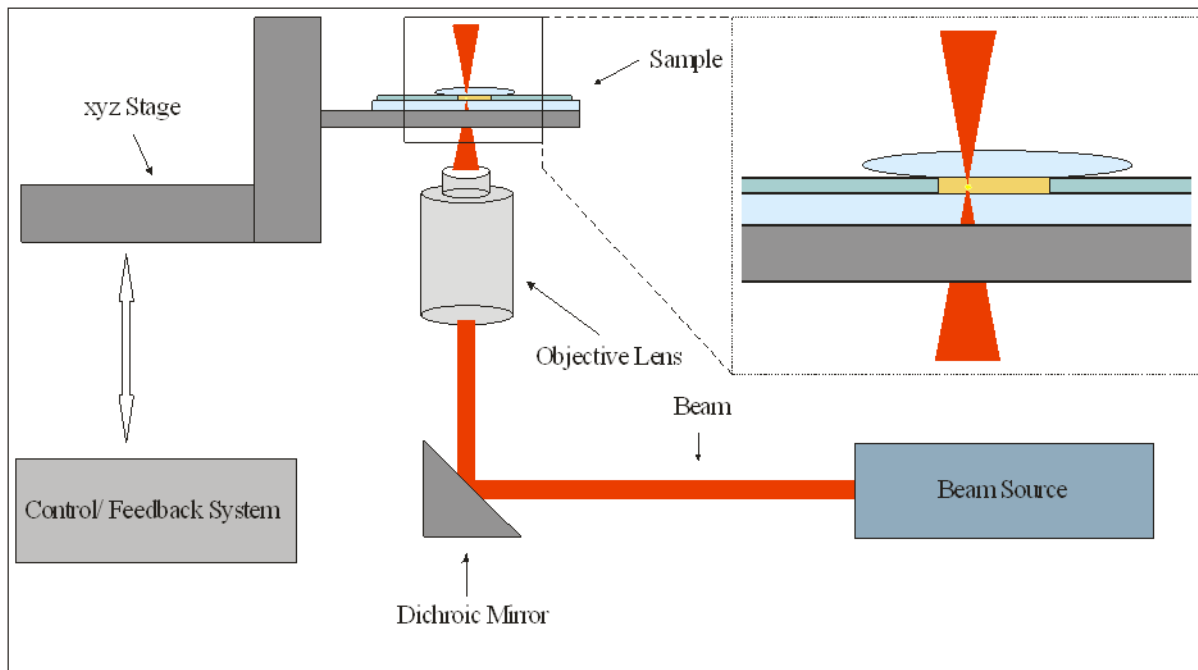


*Figure 37: Schematic of in-house laser direct write system. The laser beam is focussed within the volume of the resin using a high NA objective lens, where polymerization occurs. The structure is written out by translation of the sample by the translation stage, and beam delivery and power controlled by a shutter and neutral density filter respectively.*

The in-house 2PP system was constructed around a Ti: sapphire laser (Coherent Mira-900 810 nm, repetition rate 76MHz, pulse width 200fs) supplied by the laser loan pool. This laser model has been used in many studies and allows structuring by two photon induced polymerization initiated using Michler's ketone (4,4'-bis(diethylamino)benzophenone), the same photoinitiator as used in previous sections. A diode pumped Q switched Nd:Yag laser (PULSELAS-P-1064-300-FC, Alphas, 532 nm, repetition rate 15 kHz, duration 800 ps) was also used as an alternative light source as described later.

### 4.2.3 Assembly of the System

Due to the space and carefully controlled environment required by the system, a dedicated laser room was required. To prepare the room for this, all windows and points of exit for the laser beam were covered in black cladding. This was necessary in order to prevent stray radiation exiting the room, which prevents a risk to safety. An interlock system was installed in order to remove power from the laser should the door be opened unexpectedly. Where possible, the beam path was shielded from view to prevent accidental exposure.

To prevent vibrations interfering with the accuracy of the write process, the laser system was situated on an aluminium breadboard (Thorlabs). The optical components were also supported on a separate damped matte black breadboard. The overall layout of the system is shown in figure 38.

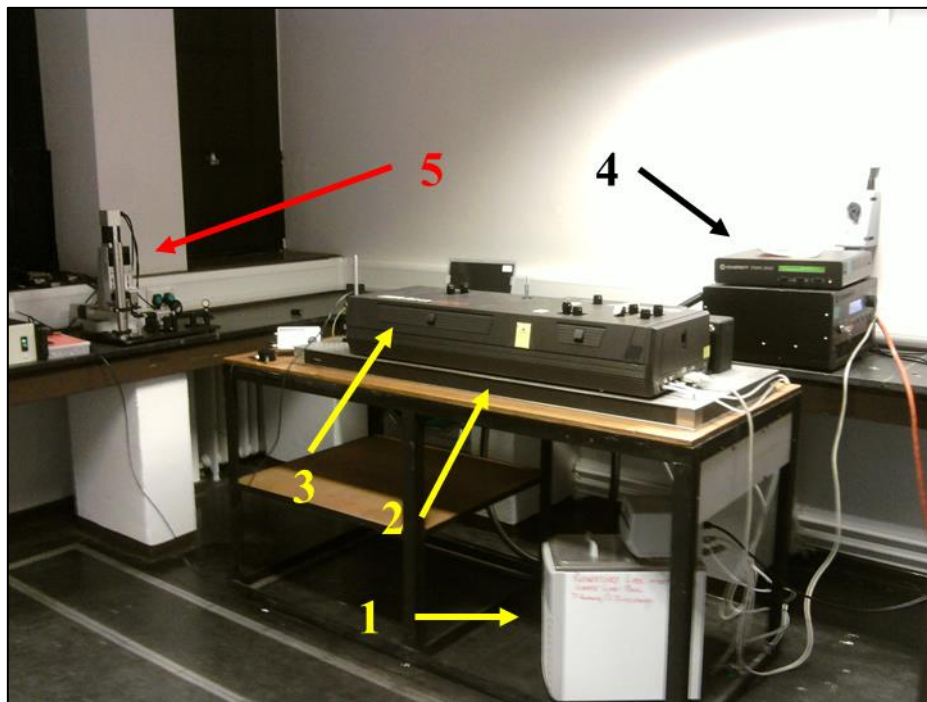


*Figure 38: Overview of Laser direct write System showing cooling unit (1), breadboard (2), Ti: sapphire laser (3) laser power pack (4) and optical assembly (5). The optical assembly is shown in more detail in figure 39.*

The arrangement of the optical assembly is shown in figure 39. The assembly consisted of a mirror to direct the radiation from the laser, a neutral density filter in order to reduce the power of the beam, an analogue power meter (to measure beam power) and a telescopic lens set to expand the beam diameter before the final mirror guides the radiation into the

objective. The objective was supported on a solid aluminium post secured on the breadboard. In figure 39, only the supports for the telescopic lens set and power meter are shown.

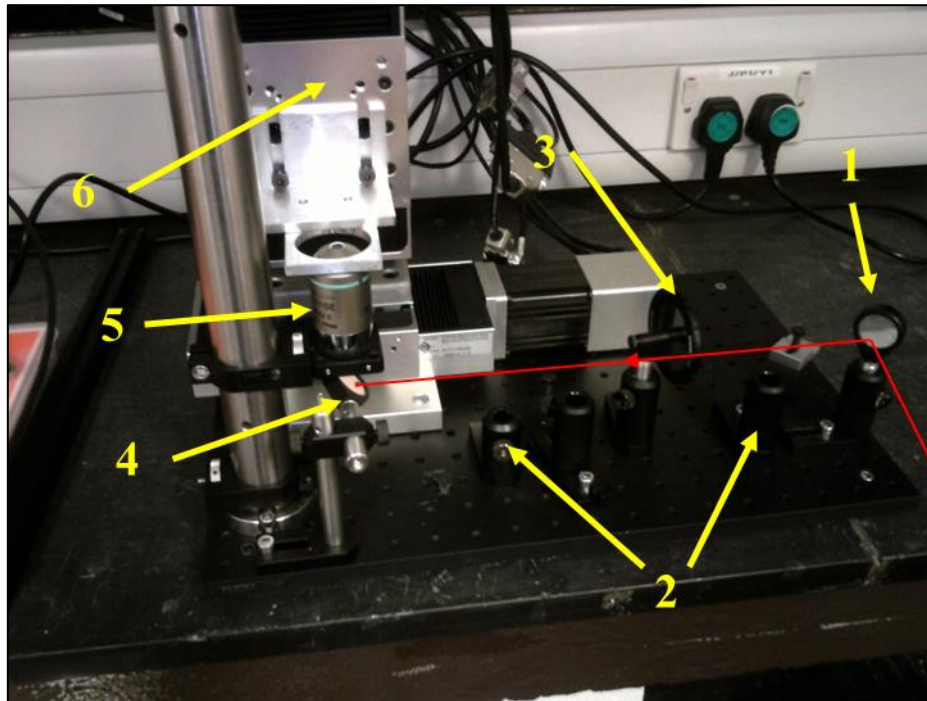


*Figure 39: Optical components in laser direct write system. The laser beam (path indicated by red line) is directed by the mirrors (1 & 4) through the neutral density filter (3) which controls the power. The beam power may be measured using a power meter fixed after the neutral density filter, and expanded by placing a telescopic lens arrangement in the included posts (2). The final mirror directs the beam into the objective (5), which focusses the beam to within the volume of the resin supported in place on the high precision translation stage (6).*

In order to produce structures, the sample is prepared on a glass coverslip which is fixed in place on an aluminium ring over the objective lens. The beam is focussed to a point within the resin and the movement of the stage writes the sample directly into the photocurable polymer. A close up image of the objective lens, and structures fabricated using this system are shown in figure 40.

#### **4.2.4 Preparation of a Photosensitive Solution**

In a first approach we used ORMOCERs (ORganically MODified CERamics). The Ormocer material (Ormocomp US-S4 hybrid polymer) was used as supplied, as it already contained the necessary photoinitiator. To prepare a photosensitive solution of the photocurable PLA,

2% w/w of the photoinitiator 4,4'-bis(diethylamino)benzophenone ( $\geq 98\%$ , Aldrich) was added to 0.5 g of the photocurable PLA dissolved in 250  $\mu\text{l}$  of 4-methyl-2-pentanone and the

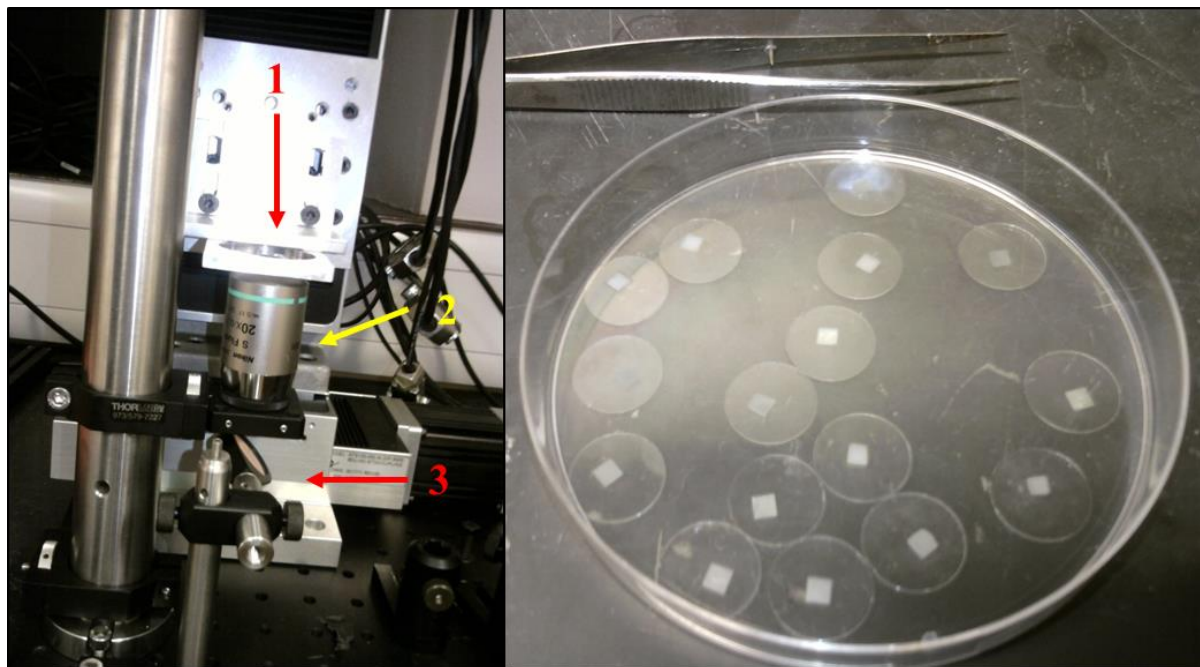


*Figure 40: Close up of objective lens (2) supported on aluminium post. Light is directed into the central area of the objective by a mirror (3) and focussed into the volume of a photocurable resin supported on the aluminium ring (1). The right hand image shows various structures produced by the system following development, as described later in the methods section.*

solution was stirred for 15 minutes using a magnetic stirrer bar. The solution was then passed through a 0.45  $\mu\text{m}$  pore size polycarbonate filter to remove any particulate matter.

In order to structure the photocurable PLA and polyethylene glycol diacrylate with the Nd:YAG microlaser., the polymers were mixed directly with 3% by weight of the UV sensitive photoinitiator of Irgacure 127, in order to structure with the laser emission at 532 nm.

#### **4.2.5 Sample Preparation for Laser Direct Write**

Samples were prepared for structuring by sandwiching a drop of photosensitive solution between a silanized coverslip and a glass microscopy slide. In the case of the photocurable

PLA, this was accomplished by depositing one drop of the material in the centre of a glass coverslip and vacuum drying overnight to remove the solvent. Strips of adhesive tape were applied between the coverslip and slide in order to act as spacers. This ‘sample sandwich’ format has been demonstrated previously by other authors (Claeyssens et al. 2009). Alternative spacers such as fine polydimethylsiloxane (PDMS) rings have also been demonstrated. Silane treatment of the glass coverslips allows the fabricated structures to bind covalently to the surface, preventing detachment of the structures during the development process.

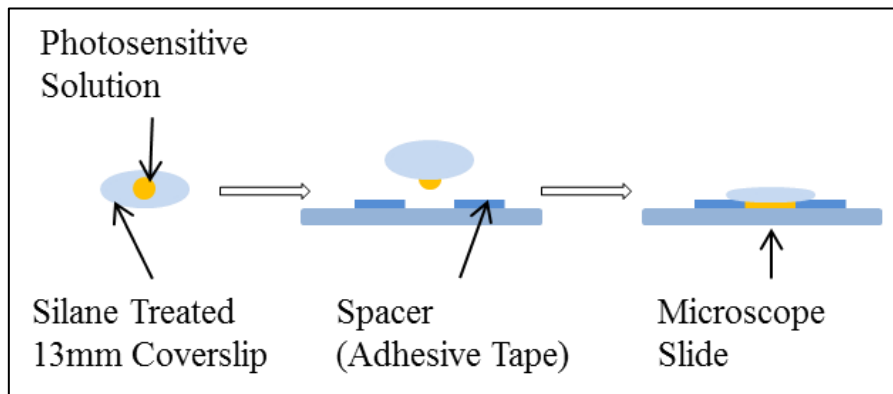


*Figure 41: Sample sandwich format. The photosensitive resin is deposited on a coverslip and any solvent removed under vacuum. The resin is then sandwiched between the coverslip and a microscope slide using adhesive tape as a spacer.*

#### **4.2.6 Focusing of the Beam**

In order to constrain the initiating radiation to a point of intensity where two photon initiated curing was possible, the beam was focussed using a high numerical aperture lens (20×, 0.75 NA, Nikon). The area in which is cured during exposure is known as a voxel (volume-pixel). The volume of the voxel is determined by the laser intensity, the numerical aperture of the lens, exposure time and also the curing efficiency of the material.

In common two photon polymerization systems, the 3D CAD model is sliced into a series of layers in the (x,y) plane, so that the structure to be created is sliced into a stacked series of (x,y) sections. In order to write out the individual layers the control software will create a path along which the voxel will be scanned to create the layers. The spacing of the lines which will create the (x,y) sections is determined by the horizontal cross section is determined by the diameter of the voxel, and the vertical spacing of the layers is determined by its height.

Galvano scanners have been used by many authors in order to facilitate translation of the voxel. Using a set of mirrors the central area of the beam is scanned in the  $(x,y)$  plane and a translation stage provides stepping in the  $z$ -direction.

The photocurable sample was prepared in the sample sandwich format as previously described, and fixed in place on a sample holder attached to the translation stage. The system was configured so that the objective remains stationary and the photosensitive resin sample is moved using the stage to provide translation of the focal point within the resin.

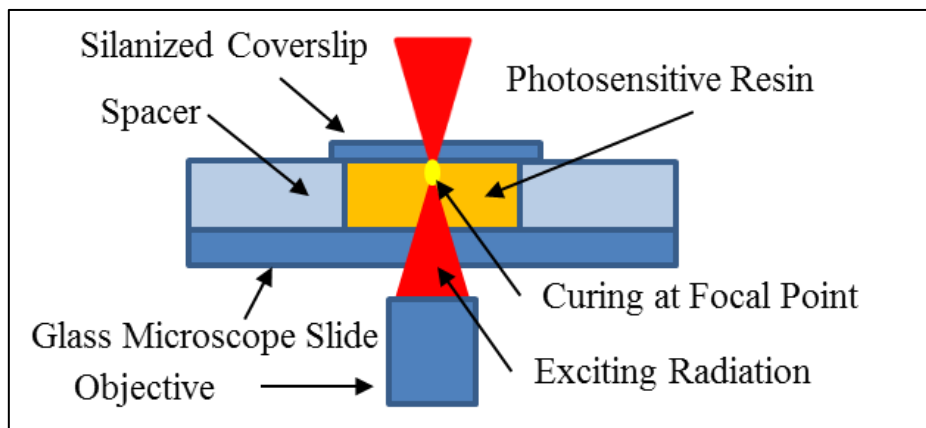


*Figure 42: Radiation focussed within volume of the resin. The resin is cured selectively only at the focal point of the beam within the resin. Translation of the sample by a motorised stage allows direct writing of structures.*

In order to locate the surface of the sample, a series of lines were written at  $10\ \mu\text{m}$  increments in the  $z$ -plane starting above the height of the resin. The onset of curing (see figure 42), which was indicated by bright fluorescence of the resin, indicated the boundary of the upper surface of the resin and the coverslip, and thus the first layer of the structure. Two photon polymerization systems commonly direct the exciting radiation into the Galvano scanner using a dichroic mirror. By positioning a CCD camera behind the dichroic mirror the curing process can be visualized by a change in the refractive index of the resin. This allows the surface of the coverslip to be located with ease, by creating a series of single exposures until the voxel is located at the boundary of the resin and the coverslip. This provides a more reliable way of locating the surface.

The incorporation of a dichroic mirror and CCD camera and dichroic mirror into the system was explored, however problems were encountered in focusing of the camera, the transparency of the mirror and also insufficient illumination in order to visualize the curing of

the resin online through the CCD. The stereolithography systems described in the coming chapters use an LED lamp in order to illuminate the sample, and incorporation of an illumination source into the system would be an objective for future work.

#### **4.2.7 Writing of the Sample**

The use of a high precision translation stage allowed structures to be created without the need for a Galvano scanner. Instead, structures were created by fixing the objective lens in place, and moving the photosensitive sample using the translation stage. The system performed structuring at a high speed partly due to the large voxel dimensions achieved. In order to create the  $\sim 10\ \mu\text{m}$  thick walls of the structures described in the results section, only a single pass was required to create the entire wall. In a Galvano system a much smaller voxel size (e.g. diameter 250 nm) would be used and the wall would be written by overlapping parallel scans in order to write the entire wall. For a  $10\ \mu\text{m}$  thick object, this would require at least 40 250 nm thick scans in order to write one  $10\ \mu\text{m}$  object. A reduced voxel size was also achieved using telescopic lenses as described above, if required for higher resolution structures.

The translation stage (Aerotech) was controlled using the supplied nView software. Commands were supplied to the stage as a series of linear instructions. The user interface allowed individual instructions to be given to the stage, by specifying the direction, axis and velocity. To create structures in an automated fashion a simple program can also be created as a sequence of commands which specify speed (denoted 'F' in the program, in mm per second), direction (+/-  $x$ ,  $y$  or  $z$ ) and distance, and the number of repeats. As an example, to write a series of ten parallel  $0.5\ \text{mm}$  lines in the  $x$  direction, with a speed of  $5\ \text{mm s}^{-1}$  and a spacing of  $50\ \mu\text{m}$  the following series of commands would be entered:

<b>F= 5</b>	: <i>Sets the speed as 5 mm s<sup>-1</sup></i>
<b>Repeat 5</b>	: <i>Sets the number of repeats to 5</i>
<b>X+ 0.5</b>	: <i>Translation of 0.5 mm in +X direction</i>
<b>Y+ 0.05</b>	: <i>Translation of 0.05 mm in +Y direction</i>
<b>X- 0.5</b>	: <i>Translation of 0.5 mm in -X direction</i>
<b>Y+0.05</b>	: <i>Translation of 0.05 mm in +Y direction</i>
<b>End Repeat</b>	: <i>Specifies end of block to be repeated</i>

Figure 43: Example of code used by nView program. Instructions are given in bold and correspond to actions to be performed by the translation stage. Descriptions of each instruction are entered in italics to assist the user.

Other commands include steps in the  $z$  direction, entered in the same way as the  $x$  and  $y$  commands, and potentially commands to send a signal that opens or closes a shutter device. This was not implemented during this study but would improve the capabilities of the system. In order to write structures, without control of the shutter by the program the shutter open command must be pressed manually by hand before the writing process, and at the end of the program the shutter close button must be pressed quickly, to prevent the sample burning due to prolonged exposure of a single point to the laser radiation.

#### 4.2.8 Sample Development

The PLA based samples were developed by soaking in 4-methyl-2-pentanone for 30 minutes before rinsing with isopropanol and drying under vacuum. The samples produced from ormocer were developed using toluene as a solvent and the PEGDA samples were washed with methanol followed by soaking in water.

#### 4.2.9 Cell Culture Methods

NG108-15 neuronal cells were used as a readily available cell line to investigate basic cell-structure interactions. The cells were supplied by the American Type Culture Collection (ATCC). This cell line is a hybrid of mouse neuroblastoma and rat glioma cells displaying a neuronal morphology serving as a neuronal type cell line.

Cells were cultured in completed 10% high glucose DMEM (Dulbecco's Modified Eagles Medium (DMEM)). To prepare the completed solution one vial of penicillin/ streptomycin (5 ml), one vial of glutamine (5 ml), 1 vial of Fungizone<sup>TM</sup> (1.25 ml) and 1 vial of foetal calf serum (50 ml) were added to a 500 ml flask of 10% high glucose DMEM with 61.25 ml of the media removed giving a final volume of 500 ml.

To detach the cells for subculture, trypsin is not necessary. Instead the flask may be tapped sharply and pipetted back and forth a few times to obtain an even cell suspension. To subculture, 0.5 ml of cell suspension is seeded into a T75 flask containing to 9.5 ml of medium. The cells are ready for subsequent sub-culturing after 3-5 days.

#### **4.2.10 Scanning Electron Microscopy**

Images were obtained on an Inspect F field emission gun SEM, using a spot size of 3 and an accelerating voltage of 10 kV. Samples were coated in a fine layer of gold using an Emscope SC 500 sputter coater prior to imaging. To prepare cell culture samples for imaging, samples were fixed using hexamethyldisilazane (HMDS) procedure (Bray, Bagu, and Koegler 1993).

### **4.3 Results**

The structuring ability of the laser direct write system was first assessed using a commercially available UV curable ormocer resin in order to demonstrate the structuring ability of the system. Following successful structuring of theOrmocomp material, large microstructures on the millimetre scale were quickly fabricated from a photocurable polylactic acid analogue synthesised as described in chapter 2. The voxel size of the system was then reduced using a telescopic lens set in order to demonstrate the resolution achievable with this structuring system and resin. Structuring with a low cost Nd:Yag microlaser and polydimethylsiloxane (PDMS) replication were also explored in order to demonstrate the possibility of reduced cost and cycle times for simple microstructure replication. Basic cell-microstructure interactions were also investigated with potential applications as tissue scaffolds and stem cell niches.

#### **4.3.1 Microstructuring of Photocurable PLA and Ormocer**

The laser direct write system was first assessed using a commercially available Ormocer (organically modified ceramic polymer) (Ormocomp US-S4 hybrid polymer). This hybrid

material, also referred to by the trade name Ormocomp is an ultraviolet sensitive material containing the photoinitiator Irgacure 369. Although non-bioresorbable, these materials have been shown to be non-cytotoxic and suitable for cell attachment as well as giving excellent structuring results (Doraiswamy et al. 2006; Doraiswamy et al. 2005; Ovsianikov, Chichkov, Adunka, et al. 2007). Using a power of 50 mW and a write speed of 50 mm s<sup>-1</sup> a test structure was manually created by giving the translation stage a series of linear translations using the control software. The laser trace and the resulting structure are shown in figure 44.

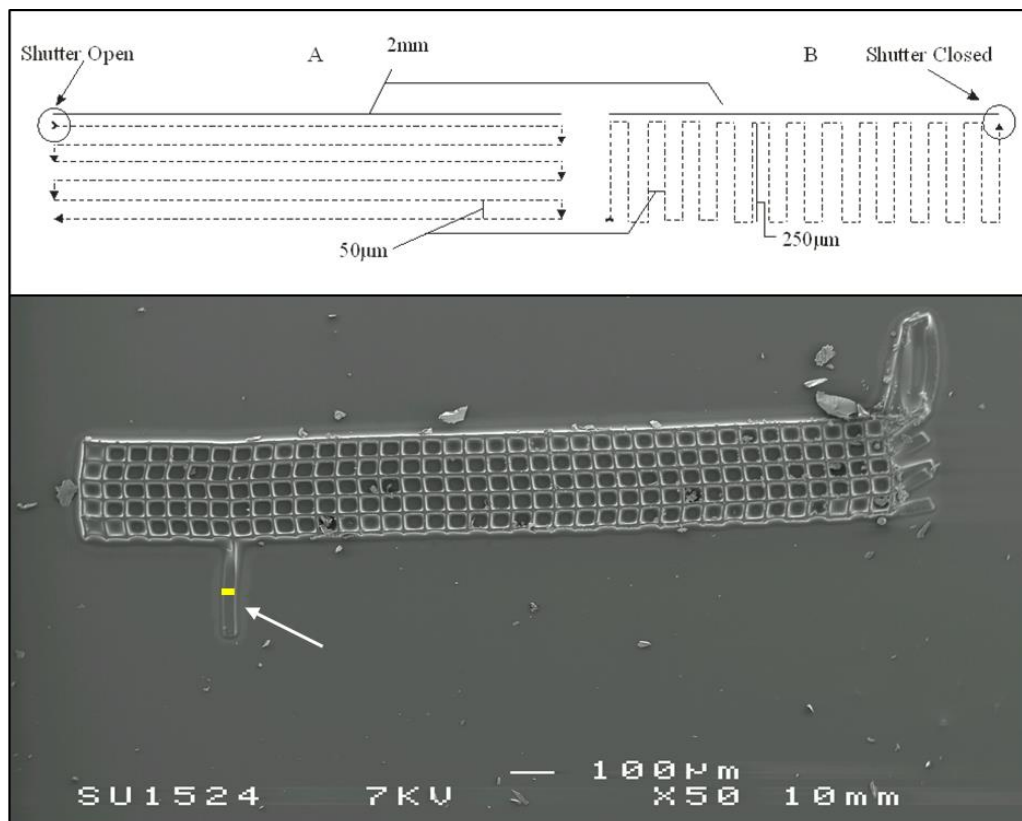


*Figure 44: Path followed by laser trace and resulting structure made from ormocer. The translation stage performs the instructions given in the nView code (represented by the trace in the top part of the figure) writing out the resulting structure (bottom).*

It can be observed in figure 44 that the width of the lines in the horizontal (x,y) plane is around 10 µm. At one point in the fabrication process a command was incorrectly repeated resulting in an additional line extending from the structure, as indicated by the arrow in figure 44. Following development of the structure (in toluene solvent to remove uncured Ormocer) this arm rotated and was observed lying flat. This allowed the height of the voxel in the z

direction to be determined as 20  $\mu\text{m}$ . The conditions employed therefore resulted in a typical elongated voxel with a diameter of 10  $\mu\text{m}$  and a height of 20  $\mu\text{m}$  for this material. Accurate structuring of the Ormocer material was successfully achieved using the laser direct write system.

#### **4.3.2 Structuring of the Photocurable PLA**

Accurate microstructuring of the Ormocer substrate was demonstrated using conditions similar to those used in other studies with this material. In order to explore applications of this technology in tissue engineering, and in particular for the creation of bioresorbable medical devices such as tissue scaffolds, a wider range of materials for stereolithography must be developed. Polymers such as polylactic acid (PLA) and polycaprolactone (PCL) may be functionalized in order to make them photocurable (Gill and Claeysens 2011; Elomaa et al. 2011; Melchels, Feijen, and Grijpma 2009). A photocurable analogue of PLA was prepared according to the protocol described in chapter 2, and the material was investigated for microstructuring using the in-house two photon polymerization system.

To determine the optimum conditions for structure fabrication a test program was created which wrote a sequence of parallel lines in the resin with increasing speed, resulting in the array of lines presented in figure 45. A power of 1W was used, giving rapid curing of the material requiring short exposure times. The material proved to be generally stable during the write process even at powers exceeding this level, indicating a high polymerization threshold for this material. Typical powers used in two photon polymerization are on the scale of 30-50 mW and exceeding these powers may lead to burning of the sample. The material was found to give good structuring with a write speed of 5 mm s<sup>-1</sup>. A cross hatched structure was then created using this power and write speed, as shown in the figure below.

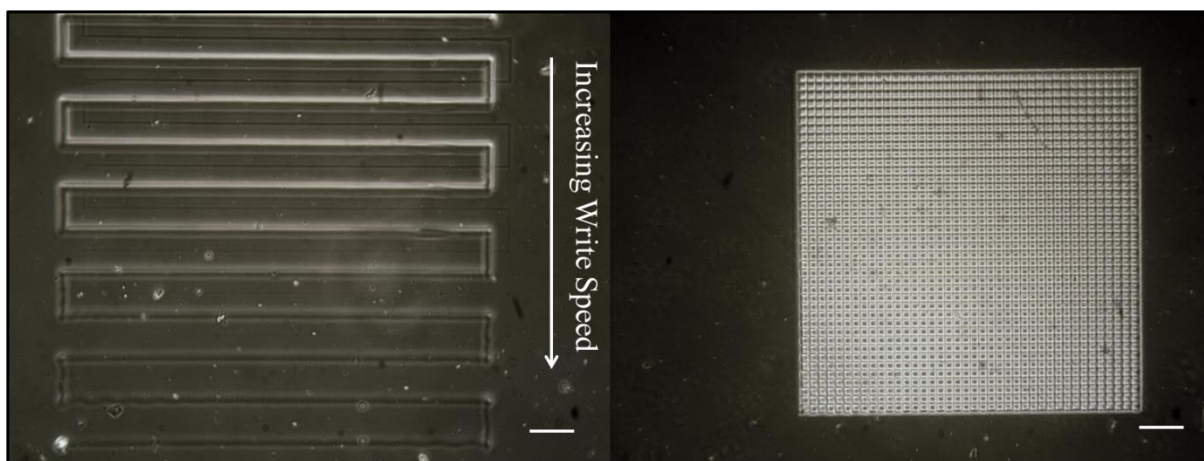


*Figure 45: Lines fabricated in the photocurable PLA based resin at 1W and different write speeds (left, scale bar 100  $\mu\text{m}$ ) and 2mm x 2mm cross-hatched structure fabricated at  $1\text{mm s}^{-1}$  (right, scale bar 250  $\mu\text{m}$ ).*

The voxel dimensions are dependent on exposure time, power, the refractive index of the material and the numerical aperture of the objective (Lee et al. 2006). Exposure time is also related to the write speed, as the amount of time any selected point in the write path is exposed reduces with increasing write speed. This can be clearly observed in figure 45 as a thinning of the lines as the speed increases. By varying the power the voxel aspect ratio may be controlled, this is an important aspect for accurate microstructuring.

In order to create basic structures for cell culture, a series of 3mm x 3mm cross hatched structures were created using the microstereolithography device. The structures were written onto methacrylate functionalized glass coverslips in a layer-by-layer fashion in order to create a series of microwells into which cells could migrate. The line centre to line centre spacing in the (x,y) plane was 50  $\mu\text{m}$  and the line thickness was around 10  $\mu\text{m}$ . The structures consisted of two layers, fabricated with the first layer suspended in the resin second and the second layer on the surface of the coverslip, holding the structure on the surface.

The structures were written by first creating the horizontal lines in the x direction, then writing the lines in the y direction before stepping up 10  $\mu\text{m}$  in the z direction and writing the next identical layer on top. One of the cross-hatched structures created by this process is shown in figure 46. The total write time for this structure was below ten minutes. With a write speed of 5  $\text{mm s}^{-1}$  a 3 mm by 3 mm dimensions consisting of two layers, each consisting of two sets of 60 parallel 3 mm lines can be accomplished in less than 3 minutes. The system was therefore capable of producing 3  $\text{mm}^2$  structures very quickly by two photon

microstereolithography. A collection of these structures is shown in figure 40. A scanning electron microscope image of a cross hatched structure produced by this method is shown in figure 46.

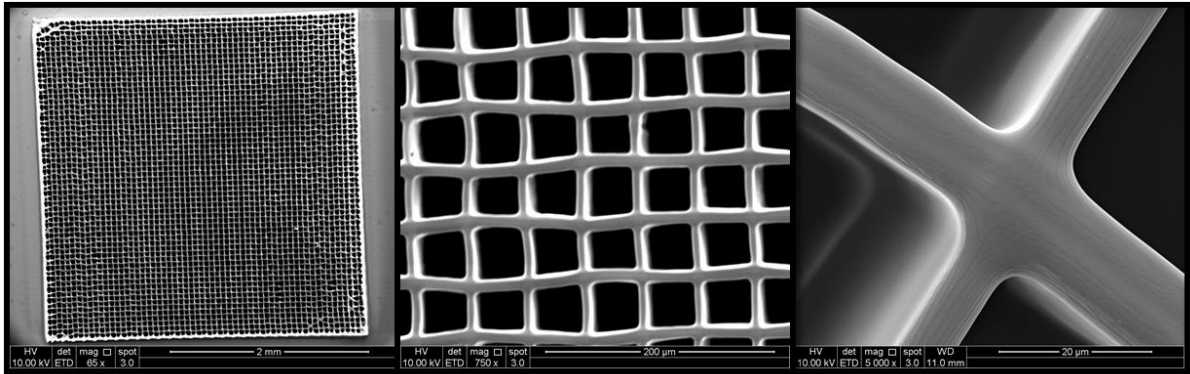


*Figure 46: Cross hatched structures produced from photocurable PLA using the in house laser direct write system, with a nominal resolution of  $10\ \mu\text{m}$ . Magnification: left  $65\times$  (scale bar  $2\ \text{mm}$ ), middle  $750\times$  (scale bar  $200\ \mu\text{m}$ ) and right  $5000\times$  (scale bar  $20\ \mu\text{m}$ ).*

#### **4.3.3 Improved Resolution using a Telescopic Lens Arrangement**

Using a telescopic arrangement of lenses, the beam may be expanded before entering the objective, resulting in better resolution. A lens with a focal length of 5 cm was placed before the attenuator, and a 15 cm lens placed 20 cm from the 5 cm lens in order to expand the beam approximately three times. By expanding the beam a resolution of approximately  $1\ \mu\text{m}$  in the (x,y)-direction and  $2\ \mu\text{m}$  in the z plane indicating a typical ovoid voxel with a high aspect ratio was achieved.

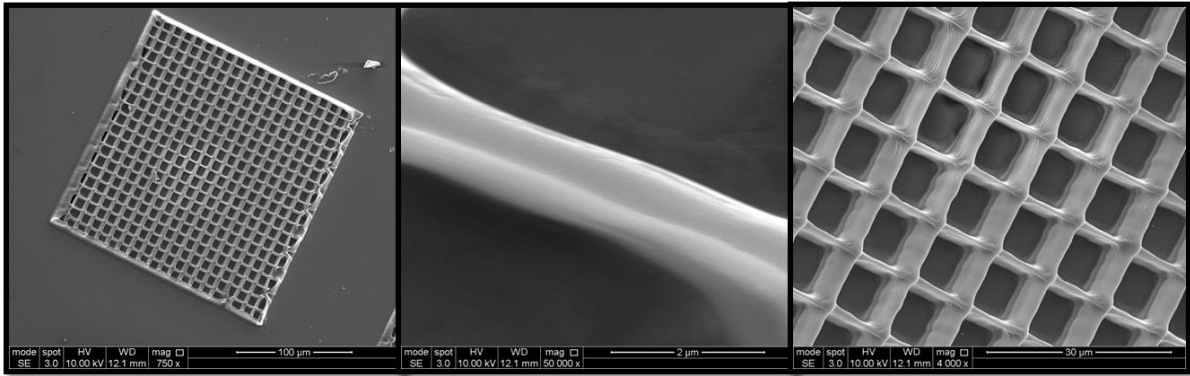


*Figure 47: PLA Structures made using in house direct write system with a resolution of around 1  $\mu\text{m}$ . Magnification: 750 $\times$  (left, scale bar 100  $\mu\text{m}$ ), 50,000 $\times$  (middle, scale bar 2  $\mu\text{m}$ ) and 4000 $\times$  (right, scale bar 30  $\mu\text{m}$ ).*

Three dimensional porous structures were also produced at this resolution, and by translation in the  $z$ -plane and offsetting alternate cross hatched layers in order to produce experimental scaffolds with defined pores on the single micrometre scale. Individual pores in the structure with an approximate diameter of 2.5  $\mu\text{m}$  were visible under SEM, although some narrowing and filling of the gaps within the pore spaces was apparent due to curing spreading around the focal point of the laser.

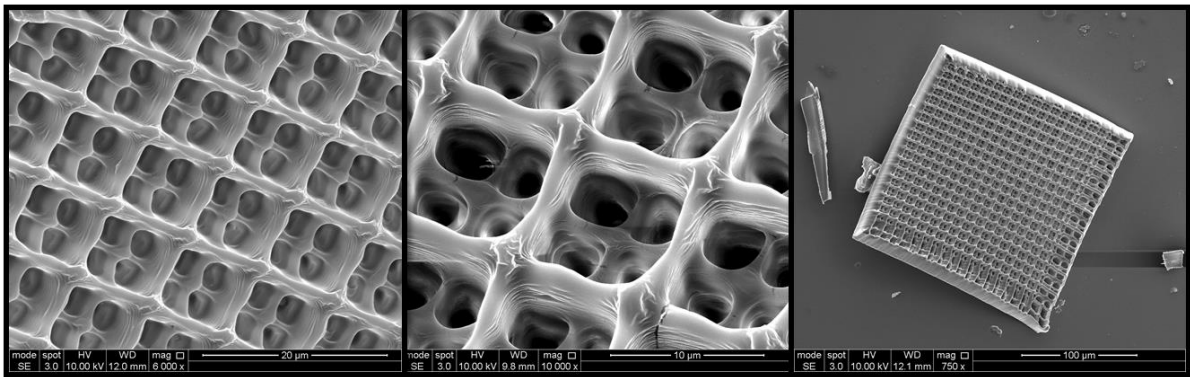


*Figure 48: Three-dimensional structures with  $\sim 1 \mu\text{m}$  line resolution fabricated in the photocurable PLA material by writing out layers in the  $(x,y)$  plane and stepping in the  $z$ -direction. Magnification: 6000 $\times$  (left, scale bar 20  $\mu\text{m}$ ), 10,000 $\times$  (middle, scale bar 10  $\mu\text{m}$ ) and 750 $\times$  (scale bar 100  $\mu\text{m}$ ).*

The combination of bioresorbable PLA based photoresins with a high accuracy microstructuring technique in order to produce truly three dimensional user defined scaffolds,

demonstrating the potential application of microstereolithography for tissue engineering applications.

#### 4.3.4 Use of Solid State Lasers as a Compact Low Cost Light Source

The use of low cost solid state lasers offers considerable savings in cost and space when employed as a light source for two photon polymerization (Wang et al. 2002). The in-house laser direct write system was adapted to use a Nd:YAG microchip laser (specifics), and structuring using the emission at 532 nm was attempted with photocurable PEGDA and photocurable PLA. Photocurable solutions were prepared by mixing the photocurable material with 3% by weight with the initiator Irgacure 127. An initial experiment was performed in order to optimise the write speed and power. Using a write speed of  $0.5 \text{ mms}^{-1}$  a series of test structures were created using PEGDA, beginning with maximum laser output and incrementally decreasing the laser power. Decreasing the power led to poor structuring results, resulting in the structure breaking up as shown in figure 49.

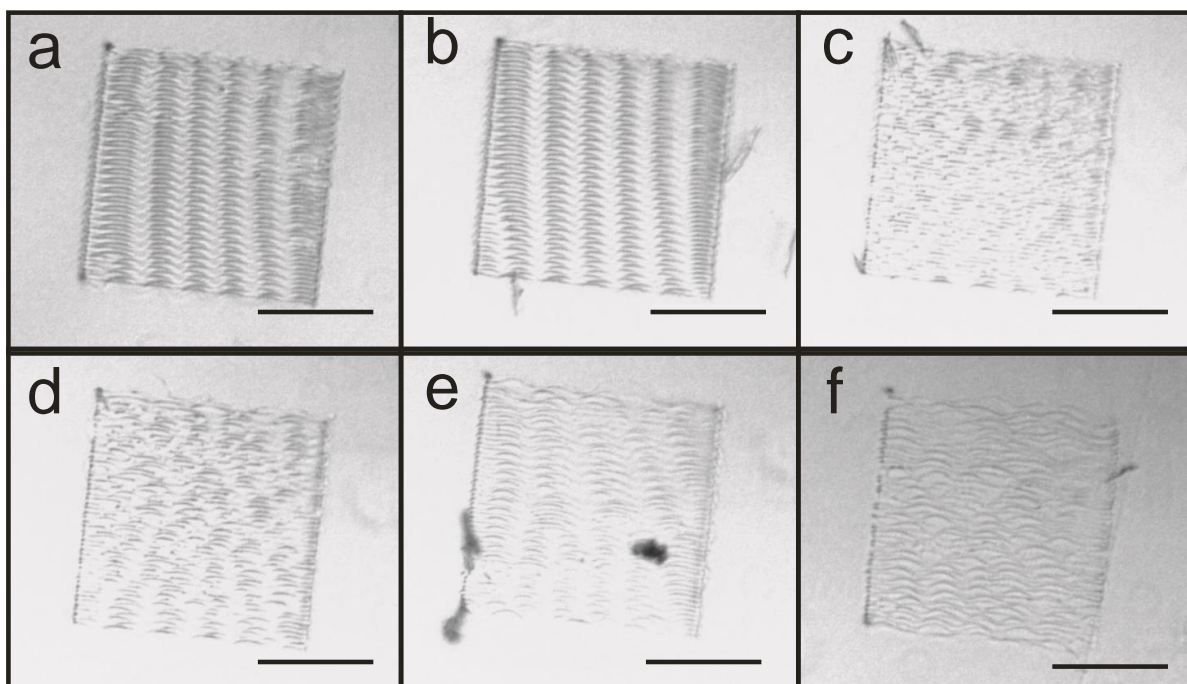


*Figure 49: PEGDA Structures Fabricated at  $0.5 \text{ mms}^{-1}$  with LD Current of 2.7 (a) to 2.2 (f) at 0.1 Intervals. Scale Bars are 0.25mm*

The small voxel size of the microchip laser necessitated careful focusing of the beam in order to give good structuring results. If the focal point was located within the glass, the surface would be etched, leading to cracking. If the focus was not close enough to the surface, the structure would not attach, as indicated in figure 50.

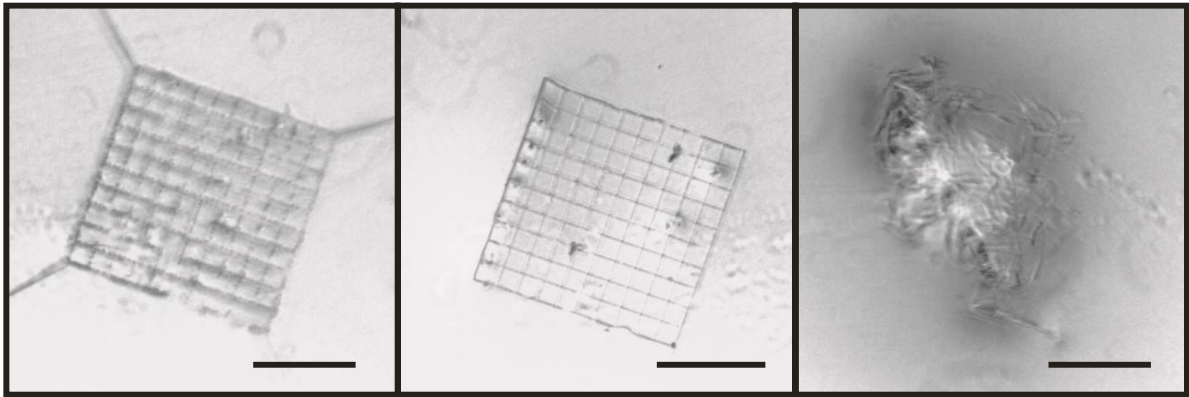


*Figure 50: PEGDA test structure made with focus within glass leading to etching (left), on surface giving good structuring (middle) and above surface leading to detachment of structure (right).*

The microlaser system was found to give good structuring results with PLA. The PEGDA structures produced showed visible ‘rippling’ of the lines. The photocurable PLA on the other hand was well defined with straight edges, as can be seen in figure 51.

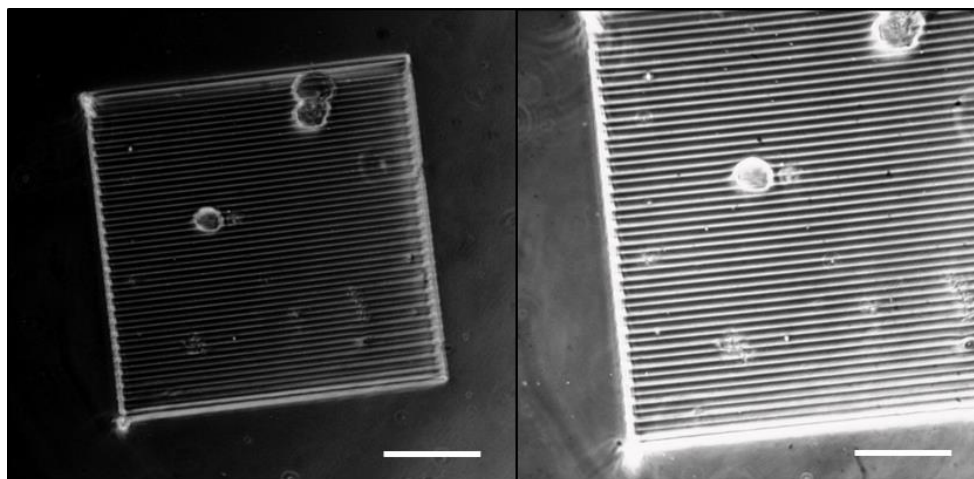


*Figure 51: PLA structure Fabricated with microlaser, imaged under an optical microscope prior to development. Voids created by ‘dust’ or impurities in the resin are visible. Scale bar 250  $\mu\text{m}$*

It is clear that the write speed of the low cost microlaser system is much lower than the femtosecond laser based system, but allowing savings in both space and equipment costs to be made. The reduced space requirements may allow the production process to be sped up by creating multiple parallel systems in the same room, as the entire system only requires the equivalent space of around half an optical breadboard as opposed to a whole room for the larger system. The synthesis of more efficient photoinitiators will facilitate rapid microstructure fabrication allowing this technology to achieve credible structuring speeds for microdevice fabrication.

#### **4.3.5 Microfabrication of Lab on a Chip Arrays for the Analysis of Neuronal Cells**

Typical applications for microstereolithography include the fabrication of porous cell scaffolds (Hsieh et al. 2010), cell encapsulating scaffolds (Lee, Rhie, and Cho 2008), medical prototyping (Narayan et al. 2010) and micro-medical devices (Gittard et al. 2011; Schizas et al. 2010). Further potential applications include cell container arrays as geometrically defined cell microenvironments (Truckenmuller et al. 2012) and niches (Lutolf and Blau 2009) which regulate stem cell proliferation and differentiation as well as protecting the cells from external environmental stresses (Underhill and Bhatia 2007).

Microfabrication of microwell arrays, allowing individual cells to be isolated and tracked is of particular interest in stem cell biology (Underhill and Bhatia 2007). The ability to fabricate and reproduce microwell arrays with user defined geometry allows for greater miniaturization of established cell culture techniques, and is much more efficient than the use of multiple well and plate assays.. Chin *et al.* (Chin et al. 2004) used microfabrication to create a 10,000 well microwell array on a single glass chip that allowed the study of individual stem cell proliferation and differentiation. The typical well dimensions were between 10-500  $\mu\text{m}$  in height and 20 to 500  $\mu\text{m}$  in diameter.

In this study, microwell devices were fabricated from the photocurable PLA and reproduced using PDMS stamping (which is examined in more detail in chapter 6). Two photon polymerization allows the rapid fabrication of microwell arrays of a user defined geometry in a short amount of time with excellent resolution and eliminates the use of complex static photomasks as used in other studies. A photocurable PLA based microwell structure and its PDMS replicated replica is shown in figure 52.

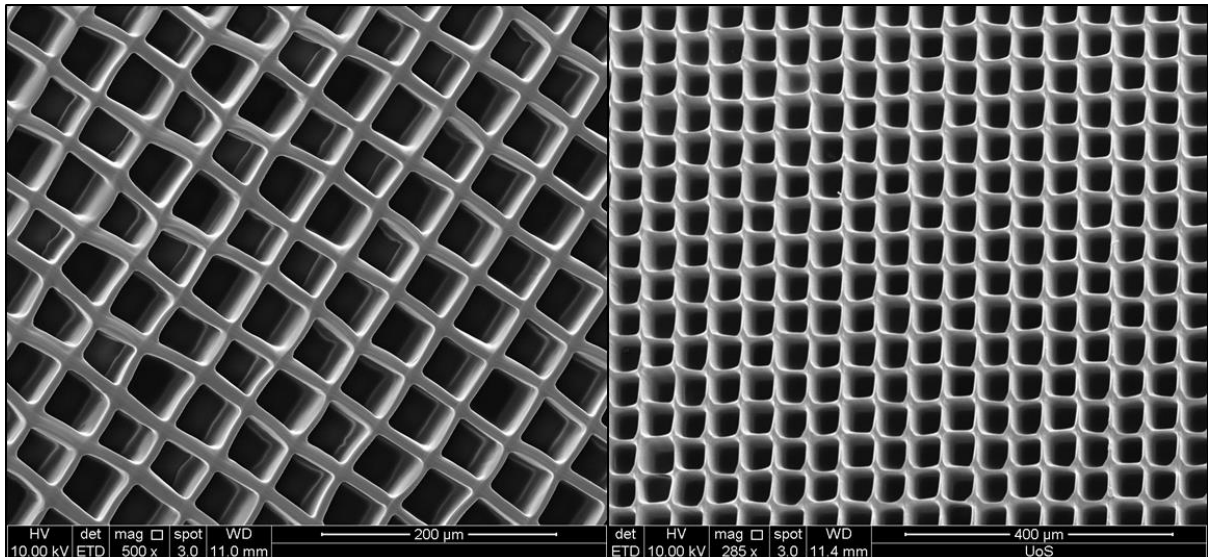


*Figure 52: PLA structure created by laser direct write (left) and PDMS stamping (right). Line widths of replica structure remain within 10% of original thickness, although some differences in the definition of the lines is observable.*

#### **4.3.6 Porous Microstructures as Neural Cell Scaffolds or Niches**

The interaction of NG108-15 neuronal cells with the photocurable PLA based microstructures was examined using scanning electron microscopy. An analysis of the material biocompatibility was performed in chapter 2, and the adhesion and viability of this cell line cultured on photocured PLA is examined in detail in chapter 5. Primary Schwann cell viability, adhesion and morphology are examined in chapter 6. In this experiment we examine the migration of cells into the scaffolds and also the cellular extensions between the wells.

PLA scaffolds were produced by both microstereolithography and PDMS replication before soaking in phosphate buffered saline (PBS) overnight and then seeded with NG108-15 neuronal cells at a density of 5,000 cells per well in 2 mL of media per sample. The cells were fixed for SEM between 2 and 7 days and imaged by SEM. The samples were seeded in triplicate and representative images are shown in figure 53.

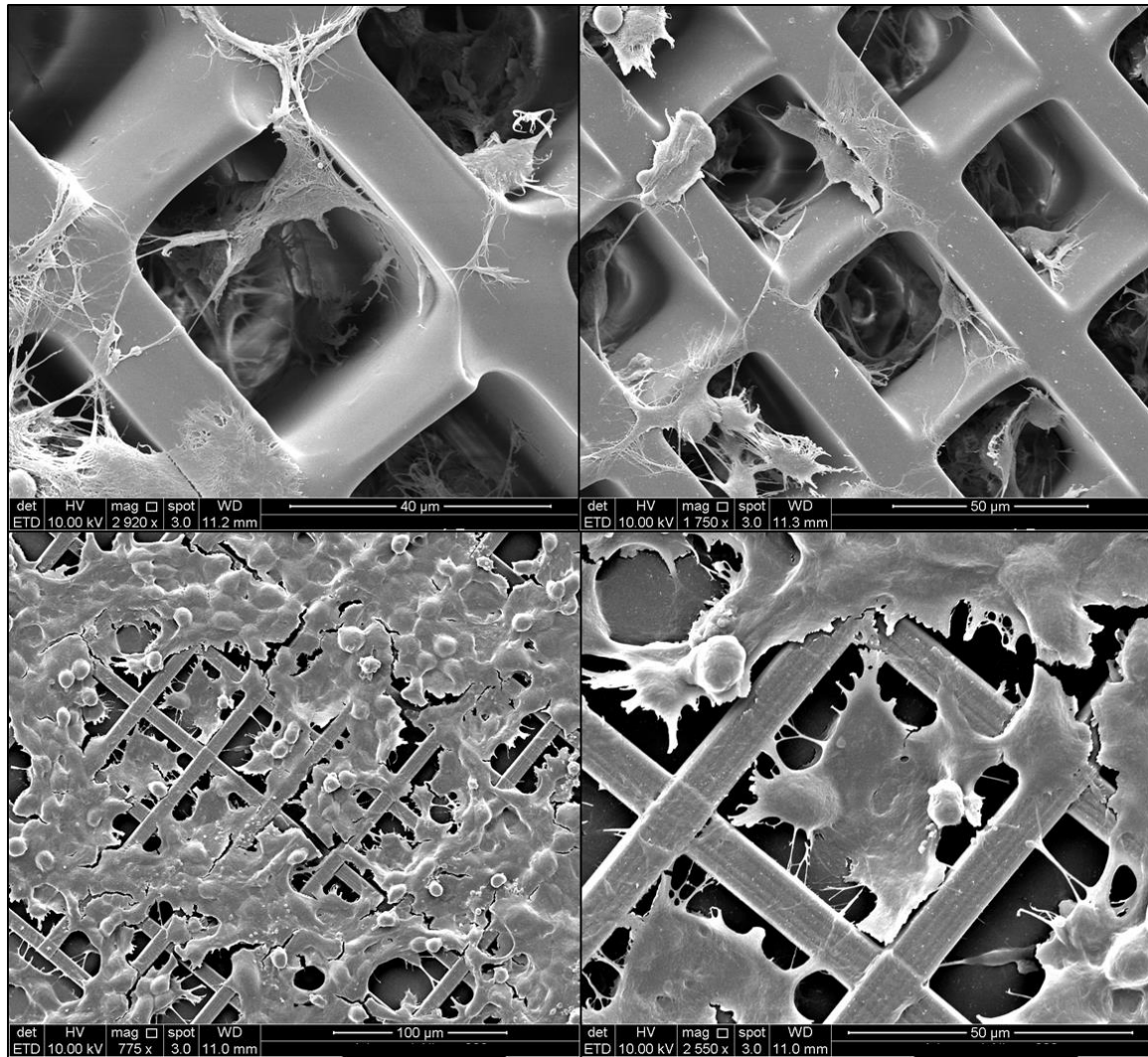


*Figure 53: NG108-15 neuronal cells cultured on microfabricated photocurable PLA scaffolds for two days (top row) and seven days (bottom row).*

The cells were observed to have proliferated on the PLA material and had filled the majority of micropockets. The images taken after two days show multiple individual cells in each micropocket, expressing cellular projections or neurites typical of neuronal cells. After seven days in culture the cells had formed a monolayer over the structure, making it difficult to distinguish individual cells. This indicates that the cells have continued to proliferate beyond two days and been able to form a confluent layer of cells on the microstereolithography produced and PDMS replicated scaffolds created from photocurable PLA.

After two days in culture, the extent to which cells had filled the micropockets or ‘niches’ was quantified by cell counting using SEM images. Three areas were selected at random and imaged at a magnification of 750×. Niches at the edge of the image with part of the pocket outside the image were not counted. The average number of niches per image was  $34.7 \pm 0.6$ .

The distribution of the cells within the pockets is shown in figure 54, showing the number of cells per well by percentage of the total number of cells for each image. Cells sitting between the pockets were not counted.

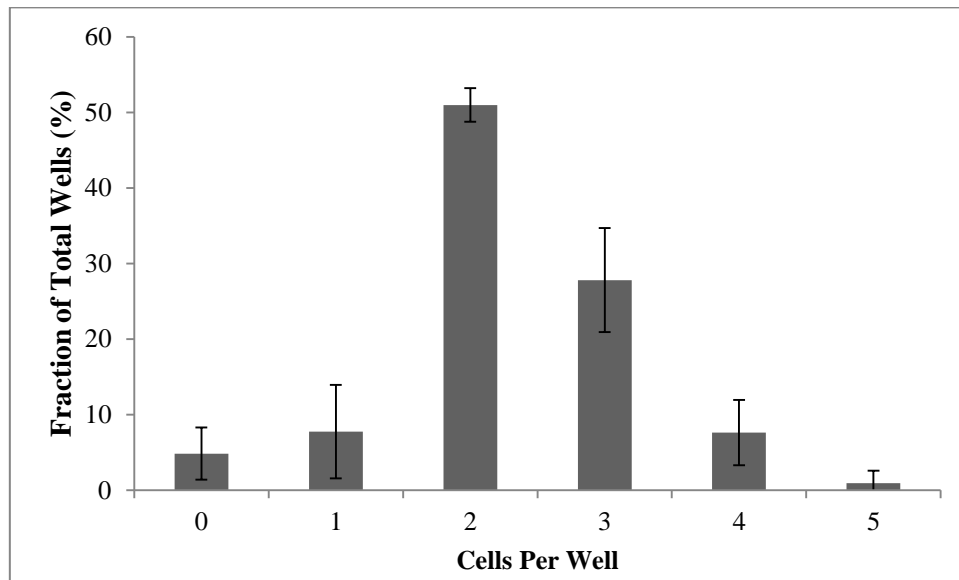


*Figure 54: Average cell count based on SEM study of PLA microwell structures. More than 95% of the wells contained cells after 48h in culture. Values reported are average of three repeats ( $n=3$ )  $\pm$  the standard deviation.*

It can be seen from figure 54 that the cells have migrated successfully into the pockets. Around 50% of the wells contain two cells, and less than 5% of the wells contain no cells at all. Further studies, for example by live dead staining could be used to verify the viability of the cells located within the pockets although this has not been performed at this stage. Staining of the nuclei with DAPI would also allow more accurate cell counting, as the fibrous morphology displayed in these images makes it difficult to image individual cells. Long cellular projections between individual cells (demonstrated to be neurites, as verified by DAB staining of  $\beta$ -III tubulin in chapter 5) were also observed (see figure 70).

The rapid microstructuring of microwell arrays from photocurable PLA by two photon polymerization has been demonstrated, and the technique allows the creation of pockets with user defined geometry according to a computer model. This technique may find applications in quantitative stem cell studies and the fabrication of potential stem cell niches long extensions between cells are present and extend over the surface of the structure.

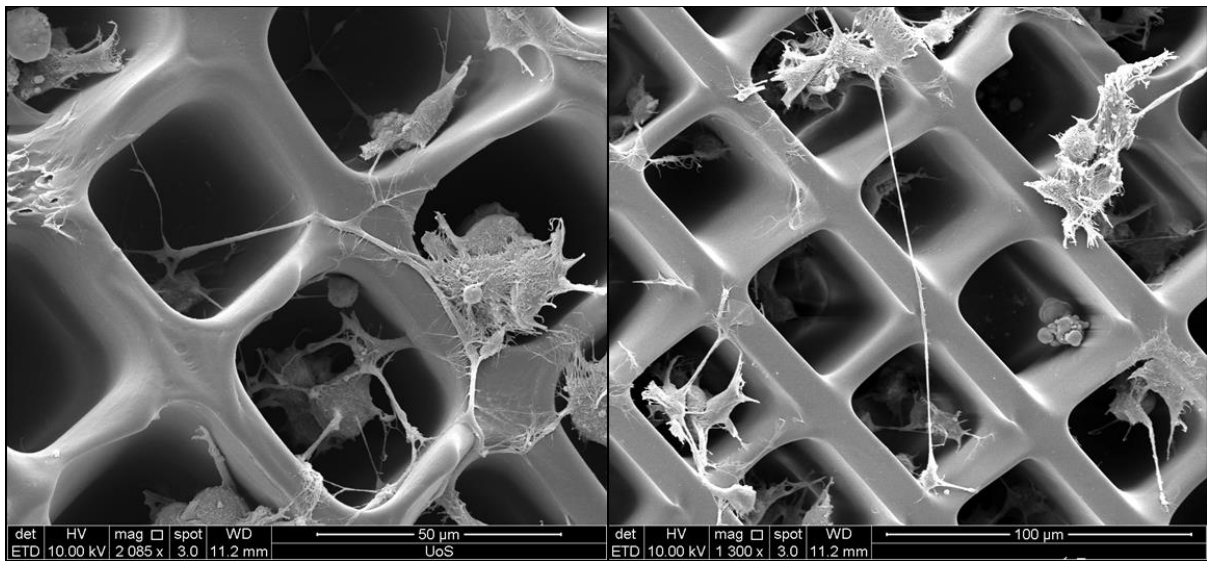


*Figure 55: NG108 neuronal cells cultured in PLA microwells after two days in culture. Neurites expressed by the cells are present on the structure indicating that the cells are highly adherent.*

#### **4.4 Discussion**

In this study the development of a laser direct write system capable of high resolution (1-2  $\mu\text{m}$ ) and fast microstructuring with a polylactic acid (PLA) based photocurable oligomer was demonstrated. The incorporation of a low cost microlaser was also demonstrated however much optimisation work still needs to be performed. Cell-structure interactions were investigated with microwell arrays fabricated from the photocurable PLA and potential applications in the creation of stem cell niches were explored.

The use of low cost microlasers is attracting growing attention and the subsequent reductions in cost this will achieve will ensure that this technology is available to a wider range of researchers. The development of efficient photoinitiators will help drive this technology and rapid high resolution microstructuring will become a reality. In this study a commercially available polymer and initiator were combined with promising results. The photocurable PLA was also cured successfully with this system.

Migration of neuronal type cells into PLA micropockets was successfully demonstrated and further work will focus on the relationship between dimensions, geometry and cell ingrowth into the micropockets, potentially allowing arrays of single cells to be created and studied. In

chapters 5 and 6 the use of a Galvano scanner will be explored for more complex structuring of this material allowing the creation of cell loaded devices as neural cell delivery vehicles or Schwann cell loaded implants which may be incorporated into nerve guidance conduits leading to improved recovery of damaged nerves.

#### **4.5 Conclusions**

In this chapter a custom made two photon laser direct write system was constructed, and used for the accurate microstructuring of a photocurable PLA based material. The system was able to rapidly fabricate large microstructures with good (10  $\mu\text{m}$ ) resolution in just a few minutes. A maximum resolution of around 1  $\mu\text{m}$  was achieved by expanding the beam using a telescopic lens arrangement. The speed and resolution achieved with the system was comparable to commercially available microstereolithography systems, and the PLA based resin gave excellent structuring results. Further to this, the accurate structuring of both commercially available polyethyleneglycol diacrylate and also the photocurable PLA was demonstrated using a low cost micro-laser, making this technology more accessible in terms of cost. The results achieved demonstrate how this technology may one day be able to create bioresorbable devices for tissue engineering.

# Chapter 5: Two Photon Laser Direct Write of Bioresorbable Resins for Neural Tissue Engineering Applications

---

*Aspects of this chapter published in (Melissinaki et al. 2011) with significant modification.*

*The author would like to thank V. Melissinaki (IESL-FORTH) for assistance with microstructure fabrication and imaging, PC12 cell culture and live-dead staining. The author was responsible for resin synthesis and characterisation, thin film preparation and analysis, NG108 neuronal cell culture and analysis and aspects of the microstructure design and fabrication.*

## **Abstract**

In this chapter, the use of photocurable analogues of polylactic acid (PLA) and also polycaprolactone (PCL) for neural applications is investigated. Neuronal cell type (NG108-15 and PC-12) and also NIH-3T3 fibroblast viability, proliferation and adhesion on thin films of the photocurable materials were evaluated. Accurate two photon microstructuring of the photocurable PLA with a Galvano scanner was investigated and the material was shown to give excellent structuring results. Potential applications for microfabricated structures were investigated including cell delivery vehicles and devices for studying cell alignment, an important factor for nerve repair devices.

## **5.1 Introduction**

It has been demonstrated that cells are directly influenced by the three-dimensional environment in which they are cultured, and cells grown in a monolayer fashion respond differently to biochemical stimuli compared to those cultured in a three-dimensional matrix (Abbott 2003). The relationship between surface chemistry, mechanical properties, microstructure and nanotopography and the effect these factors have on cellular behaviour within a tissue scaffold are an important aspect of tissue engineering (Haycock 2011). Three-dimensional cell culture seeks to recreate accurately the physiology of living tissue. Beyond cell-scaffold interactions, tissue scaffold structure and the degree of porosity also have an

effect on the mechanical performance of the device (Hutmacher et al. 2001; Hutmacher, Sittinger, and Risbud 2004).

Tuning of surface morphology and wettability can influence cell adhesion (Falconnet et al. 2006; Ranella et al. 2010), and features such as ideal pore size can vary depending on cell or tissue type. Pore size is a critical factor in tissue scaffold design (Whang et al. 1999). It has been demonstrated for example that a pore size of 5  $\mu\text{m}$  has been reported to be optimal for neovascularization in bone tissue (Brauker et al. 1995), pores of 5-15  $\mu\text{m}$  in size facilitate the ingrowth of fibroblasts whereas pores of 40-100  $\mu\text{m}$  facilitate osteoid (bone) cell ingrowth (Klawitter and Hulbert 1971) and that mammalian skin regeneration requires pore sizes of 20-125  $\mu\text{m}$  (Gogolewski and Pennings 1983). It was originally determined that the optimal pore size for bone regeneration was between 200–350  $\mu\text{m}$  (Klawitter and Hulbert 1971), large enough to facilitate the process of ‘osteosynthesis’ in which microvasculature and osteal progenitor cells migrate from the surrounding bone into the pores of the scaffold and develop into bone tissue, a process known as ‘creeping substitution’ (Stoeltinga and Cawood 2011). This was later revised by Whang *et al.* using poly(lactide-*co*-glycolide) scaffolds prepared using freeze drying technique (Whang et al. 1999), as the limited technology of the time did not allow accurate determination of pore size in the earlier studies. It was found that bone regeneration could occur in scaffolds with median pore sizes of 16  $\mu\text{m}$ , by the infiltration of osteoprogenitor cells via capillary action. Capillary action as a result of surface wettability and pore size was found to be a crucial factor in bone regeneration. Furthermore, if a scaffold does not allow sufficient nutrient diffusion then cells will only exist on the outer surfaces (around 200  $\mu\text{m}$ ) of the structure, as cells isolated from a supply of nutrients such as oxygen will die (Laschke et al. 2006).

Bulk methods for porous scaffold fabrication including gas foaming (Sheridan et al. 2000), phase separation and particulate leaching (Cai et al. 2002) may allow some degree of control over pore size, but pore interconnectivity can be poor preventing cell infiltration into the scaffold. Cell dispersion within scaffolds fabricated by microstereolithography with a gyroid architecture designed to enhance cell and nutrient distribution was compared to scaffolds of a similar porosity and pore size (determined by microcomputed tomography ( $\mu\text{-CT}$ )) prepared by particulate leaching by Melchels *et al.* (Melchels, Barradas, et al. 2010). After five days in static culture, cells were found to be evenly dispersed throughout the microfabricated gyroid scaffold however on the scaffold prepared by particulate leaching cells were limited to the outer surface of the scaffold, as visualised by methylene blue

staining. Interestingly, the further importance of nutrient diffusion and waste metabolite dispersion was demonstrated by the lack of living cells within the gyroid scaffold after 20 days in static culture. This was rationalized to limitations on how long scaffolds can be cultured in static conditions. The use of microstereolithography to create larger interconnecting ‘vascular’ channels was suggested as a solution.

The use of laser direct write (LDW) by two photon polymerization (2PP) allows far higher resolution than one photon techniques and has been demonstrated for a range of experimental tissue engineering and biomedical applications, as well as medical prototyping (Narayan et al. 2010). In this study the use of a Galvano-scanner for the accurate microstructuring of a photocurable PLA based polymer was demonstrated. Galvano-scanners consist of a set of mirrors controlled using a computer in order to translate the focus of a laser beam within the focal plane of a microscope objective, allowing accurate microstructuring according to a computer model. Vertical stepping was achieved with a high precision translation stage. A schematic of the key features of the structuring system is shown in figure 56.

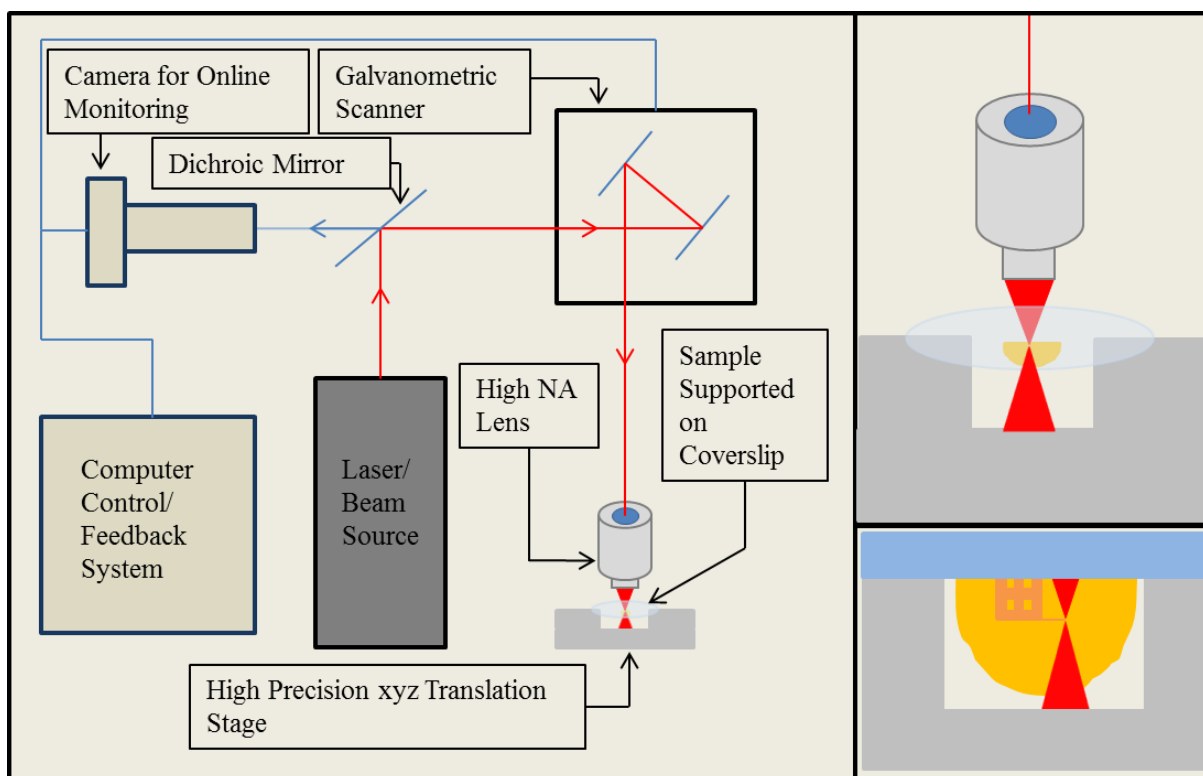


*Figure 56: Two photon microstereolithography system with Galvano-scanner.*

This system has been previously demonstrated for the microstructuring of a biodegradable triblock copolymer based on polyethylene glycol, polycaprolactone and polylactic acid

segments (Claeyssens et al. 2009). In this study a low molecular weight photocurable PLA based oligomer with a higher degree of methacrylate was demonstrated, and potential neural tissue engineering applications of this technology were explored. A PCL based photocurable oligomer was also prepared and evaluated alongside the photocurable PLA to further investigate neuronal cell adhesion on these photocurable oligomers. Microstructuring was however focussed on the PLA based material.

## **5.2 Materials and Methods**

### **5.2.1 Synthesis of Photocurable PLA and PCL**

The synthesis of the photocurable polymers was described in detail in chapter 2. In brief, a photocurable PLA based oligomer with four arms and four lactic acid monomers per arm, and a four armed PCL oligomer with two caprolactone monomers per arm was targeted. This was achieved using pentaerythritol (pentaerythritol (Sigma-Aldrich, >98%) as a multi-armed initiator and either  $\epsilon$ -caprolactone (Aldrich, 97%) or (3S)-cis-3,6-dimethyl-1,4-dioxane-2,5-dione (Sigma-Aldrich, 98%) in a molar ratio of 1:8 (pentaerythritol: cyclic monomer (caprolactone) or dimer (lactide)) with stannous octoate (Aldrich, 98%) as catalyst. The reaction was performed using an appropriate quantity of toluene (anhydrous, Sigma-Aldrich, 99.8%), as solvent for 8h in dry glassware before cooling, precipitation of the product and vacuum drying to remove solvent. The products were methacrylate functionalized in dichloromethane solvent (anhydrous,  $\geq 99.8\%$ ) using a 16 molar excess of triethylamine (TEA) (Sigma-Aldrich, >99%) and methacrylic anhydride (MAA) (Sigma-Aldrich, 94%) based on the predicted molar mass of the oligomer and allowed to react for 24 h at room temperature. The products were isolated by vacuum distillation to remove the unreacted TEA and MAA and the products precipitated in isopropanol at -20 °C.

### **5.2.2 Photocurable Polymer Characterization**

The photocurable polymers were characterized as described in chapter 2. Briefly, the polymers were characterized by FT-IR spectrometry using a Perkin-Elmer SPECTRUM 2000 spectrometer, by deposition of a thin film of the hydroxyl terminated and methacrylate functionalized oligomer between two KBr Discs.  $^1\text{H}$  NMR Spectra were taken by preparing 20-40 mg of the oligomer in deuterated chloroform (100%, 99.6 atom%, Aldrich) and

filtering into a standard NMR tube. Spectra were recorded on a Bruker AV1-400 spectrometer operating at 400 MHz.

### 5.2.3 Photosensitive Solution Preparation

To prepare a photosensitive solution, one gram of the photocurable polymer was mixed with 20 mg of 4,4'-bis(diethylamino)benzophenone ( $\geq 98\%$ , Aldrich) and 250  $\mu\text{l}$  of 4-methyl-2-pentanone ( $\geq 98.5\%$ , Sigma-Aldrich). The solution was stirred for 15 minutes using a magnetic stirrer bar and taken up in a syringe and filtered through a polycarbonate filter (pore size 0.45  $\mu\text{m}$ ) into an amber glass vial. Filtering of the sample is essential to remove any particulate matter present in the sample, such as agglomerates of photoinitiator. Samples containing particulates had a tendency to ignite or 'bubble' when the sample was irradiated due to the highly focussed radiation. The photocurable material itself is largely transparent to the radiation, however particulate debris is quickly ignited destroying the surrounding structure. This was observed as the sudden appearance of large bubbles on the CCD display used to monitor the fabrication process.

### 5.2.4 Thin Film Preparation

The photocurable solution was spin coated onto glass coverslips functionalized with 3-methacryloxypropyltrimethoxysilane (MAPTMS) (Polysciences Inc.). MAPTMS functionalization was performed by soaking standard borosilicate glass coverslips in a 40 mM solution of MAPTMS in chloroform (Sigma-Aldrich, amylene stabilized,  $\geq 99\%$ ) for a minimum of three hours. The silane functionalization provides methacrylate groups on the surface of the glass which allow the polymer to bind to the surface covalently. Without this functionalization the films had a tendency to detach from the surface and float off during cell culture. Spin coating was performed by depositing 1 drop of the photosensitive material onto the glass substrate and spinning for 60 s at 4000 rpm followed by drying under vacuum to remove the solvent. The films were then UV cured using either a UV lamp (EXFO Omnicure S1000 100W) for 300 s at 30  $\text{mW cm}^{-2}$  or an excimer laser (Lambda-Physic, LPX 210, 248 nm, 34 ns) using 20 shots at 58  $\text{mJ cm}^{-2}$ . The cured films were developed by immersion in 4-methyl-2-pentanone for 5 minutes before drying in a vacuum oven for 24 h.

In order to prepare commercially available linear PLA and PCL films for comparison, the polymers were each dissolved in dichloromethane (DCM) to make a 4% w/w solution of PLA

or PCL in DCM. The solutions were spin coated onto glass coverslips and dried under vacuum to remove the solvent.

### **5.2.5 Sample Preparation for Laser Direct Write**

To prepare samples for laser direct write (LDW), one drop of the photocurable solution was deposited onto the methacrylate functionalized coverslips and dried under vacuum overnight to remove the solvent. The presence of solvent in the photocurable solution was also found to lead to bubbling or burning of the samples during the direct write process. The glass coverslip was placed on the sample support in the LDW system with the polymer ‘droplet’ facing up and laser illumination occurring from below the sample.

### **5.2.6 Laser Direct Write of 3D Structures**

Laser direct write was performed as described extensively by other authors (Klein et al.; Farsari and Chichkov 2009). In this study a Ti: sapphire laser (Femtolasers Fusion) emitting at 800 nm with a repetition rate of 75 MHz and sub 20 fs pulse duration was used to supply the exciting radiation. This laser has a maximum output power of 450 mW and a beam diameter of approximately 2 mm. The beam was expanded 5x using a telescopic lens set in order to fully illuminate the back aperture and achieve the best possible resolution. The expanded beam was focussed within the volume of the resin using a high numerical aperture lens (40x, 0.95 NA, Zeiss, Plan Apochromat). Resin samples were prepared by depositing a drop of the photosensitized solution (prepared as described in section 2.3) onto a MAPTMS coverslip and removing the solvent under vacuum for 24 h. Scanning of the laser beam was achieved using an ( $x,y$ ) scanner (Scanlabs Hurriscan II computer-controlled by SCAPS SAMLight software). Translation in the  $z$  plane and large ( $x,y$ ) translations were accomplished using a high precision ( $x,y,z$ ) translation stage (PI). Beam delivery was controlled using a mechanical shutter (Uniblitz) and beam power was tuned using a motorized attenuator (Altechna). Overall control of the system was controlled using 3DPoli software ([3DPoli@gmail.com](mailto:3DPoli@gmail.com)). Visualization of the direct write process and location of the substrate surface was achieved using a CCD camera mounted behind a dichroic mirror. Structures were fabricated layer-by-layer with fine stepping in the  $z$ -plane. The final layer of each structure was located on the MAPTMS functionalized coverslip in order to covalently bind the structure to the surface and avoid detachment. Structures were developed post curing by immersion in 4-methyl-2-pentanone for one hour.

## **5.2.7 Characterisation of Thin Films**

### **5.2.7.1 X-Ray Photoelectron Spectroscopy**

Thin films of the photocurable PLA were prepared by spin coating as described above and analysed by X-ray photoelectron spectroscopy (XPS) using an Axis Ultra DLD spectrometer (Kratos Analytical, UK). Scan spectra were obtained from the surface at 160 eV pass energy, 1 eV step size, from 1200 eV to -5 eV and processed using Casa XPS.

### **5.2.7.2 Surface Wettability by Water Contact Angle Measurement**

Water contact angle measurements were conducted using a Rame-Hart Contact Angle Goniometer by the deposition of a drop of deionised water on the surface of the sample and measuring the angle between the droplet edge at the contact point of the surface and the surface itself.

### **5.2.7.3 Scanning Electron Microscopy**

SEM was used to determine film thickness by scratching the surface with a metal tip before applying a thin (~10 nm) gold coating. Images were taken on an Inspect F field emission gun scanning electron microscope (FEG-SEM) using an accelerating voltage of 10 kV and a spot size of 3. By taking the images from an oblique angle the depth of the scratch could be used to determine the film thickness and smoothness.

## **5.2.8 Cell Culture and Biological Testing**

### **5.2.8.1 General Cell Culture**

In order to investigate the suitability of the photocured PLA resin for biological applications, particularly with respect to neuronal applications two neuronal cell lines were used for cell culture. NG108-15 and PC-12 cells were obtained from the American Type Culture Collection (ATCC). Cell counting with a 1:1 0.4 % Trypan blue stain was performed using a Neubauer chamber and cells were seeded as required by the individual experiment. The NG108-15 cell line was cultured in T-75 flasks using 10% high glucose DMEM containing Foetal Bovine Serum (FBS, 10 %), glutamine (1 %), penicillin-streptomycin (1 %) and fungizone (0.25 %). PC12 Cells were cultured using DMEM containing 10 % horse serum, 5

% FBS and 1% antibiotic solution (GIBCO, Karlsruhe, Germany). Cells were incubated at 37 °C in a humidified atmosphere with 5 % CO<sub>2</sub> according to standard procedure. Cells were grown to within 80 % of confluence before being shaken vigorously to detach the cells and seeded according to the specified density for the individual experiment.

#### **5.2.8.2 Sample Fixation for SEM**

In order to prepare samples with cells for scanning electron microscopy, the cells were dehydrated using hexamethyldisilazane (HMDS) (Bray, Bagu, and Kogler 1993). Following cell culture the cells were washed twice with phosphate buffered PBS for 2 minutes each time, in order to remove the media. The PBS was removed and the samples rinsed with glutaraldehyde solution (2.5% in PBS for one hour). The samples were washed again with PBS three times, leaving for 15 minutes each time. The samples were then rinsed with distilled water and dehydrated using a series of ethanol dilutions, leaving each solution for 15 minutes at a time. The solutions used were 35% ethanol in water, followed by 60% ethanol, 80%, 90% and then 100% in ethanol followed by soaking in a 1:1 solution of hexamethyldisilazane (HMDS) and ethanol for one hour followed by soaking twice in pure HDMS for five minutes at a time. Following removal of the HDMS the samples were left to dry in a desiccator or other dry environment before sputter coating with a thin coating of gold or Palladium for SEM microscopy.

#### **5.2.8.3 MTT Assay**

The MTT assay measures cell metabolic activity by the conversion of an artificial hydrogen acceptor substrate (MTT, 3-(4,5-Dimethylthiazol-2-yl)-2,5-diphenyltetrazolium bromide) by dehydrogenase enzymes within the cell. The artificial substrate is reduced within the cells to form a purple formazan product which can be eluted using acidified isopropanol and quantified by spectrophotometry. This can be used to give an indication of cell number as dehydrogenase enzyme activity usually relates to cell number.

Following cell seeding according to the particular experiment, the medium was removed and the cells carefully washed once or twice with PBS (1 ml per well). 1 ml of MTT solution (0.5 mg/ml MTT powder in PBS) was added to each well and the plate left at 37°C in an incubator for 40 minutes. The MTT was then removed and 300 µl acidified isopropanol (25 µl concentrated HCl in 20 ml isopropanol) was added to each well. Two 150 µl samples were

then transferred to a 96 well plate and the optical density measured in a BIO-TEK ELx plate reader set to 540 nm and referenced at 630 nm.

#### **5.2.8.4 PicoGreen DNA Quantification Assay**

The DNA quantification assay works by extracting genetic material from cells by repeated freeze thawing, followed by binding a fluorescent marker to the extracted DNA allowing the total DNA to be determined by measuring the fluorescence. The assay allows total cell number between samples to be compared, with a higher fluorescence indicating a greater amount of DNA and therefore a greater number of cells. By seeding known cell numbers and performing the assay a calibration curve may be prepared to estimate the actual number of cells, however in this case the values were only used comparatively. Following cell culture the samples were treated with Triton X-100 solution (500  $\mu$ M) in 1% carbonate buffer and freeze thawed three times from  $-80^{\circ}\text{C}$  to  $37^{\circ}\text{C}$ . A standard PicoGreen DNA protocol was followed (500  $\mu$ l trypsin-EDTA 1:20 in  $\text{H}_2\text{O}$  with 500  $\mu$ l PicoGreen 5:1000 in trypsin-EDTA solution. Reagent bound DNA fluorescence was measured at 520 nm with an excitation wavelength of 480 nm using a BIO-TEK ELx 80 plate reader.

#### **5.2.8.5 Live-Dead Assay**

The ratio of living to dead cells (PC12 cell line) was examined on the photocured PLA films using live-dead assay. Following cell culture a live-dead cell staining kit (BioVision) was used to differentiate between live and dead cells. Only living cells are stained by the live only cell permeable dye (Syto-9, excitation 488 nm, emission 518 nm) and fluoresce green whereas dead cells are stained by the non cell-permeable propidium iodide (ex: 488 nm, em: 615) and fluoresce yellow/ red. Cell viability can be inferred by counting the number of red and green cells in randomly selected areas.

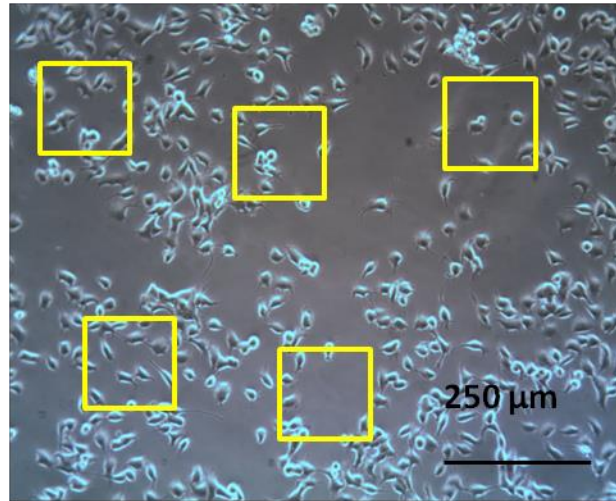


*Figure 57: Optical micrograph of NG108 cells showing randomly selected areas for cell counting using ImageJ program.*

#### **5.2.8.6 Statistical Analysis and Significance**

Cell viability assays were performed in triplicate, and unpaired Student's *t*-test was used to compare significance levels between test and control values where appropriate.

#### **5.2.8.7 Phenotypic Analysis of NG108-15 Cells**

In order to verify the phenotypic purity of the NG108-15 cells and to facilitate imaging of the neurites without fluorescent microscopy techniques 3,3'-diaminobenzidine (DAB) staining was used. NG108-15 Cells were seeded on 10 μm diameter lines of the photocured PLA created by laser direct write on a silane functionalized coverslip at a density of 10,000 cells per ml in 1 ml of media per sample and cultured for 72 h. The cells were then fixed and permeabilized before immunostaining with monoclonal mouse anti-β-tubulin III antibody (1:2000, Promega, UK) overnight. The following day the samples were washed with PBS and incubated with horseradish peroxidase (HRP) conjugated anti-mouse secondary antibody (1:250) before rinsing with PBS and addition of the DAB staining solution (Vector Laboratories) at room temperature for approximately 5 minutes until appropriate staining developed. The stained samples were carefully mounted and imaged on a MOTIC digital phase contrast microscope. This strategy for specific staining of β-III-tubulin was adapted from that used by Kaewkhaw *et al.* for the verification of NG108-15 cell purity (Kaewkhaw, Scutt, and Haycock 2011).

#### **5.2.8.8 Cell Visualization Using Confocal Microscopy**

NG108-15 neuronal cells were cultured as above on the linear PLA structures and stained for confocal microscopy. Actin filaments were stained using TRITC-phalloidin, and nuclei stained using DAPI. Samples were imaged using a Confocal Microscope (Carl-Zeiss LSM510-META). TRITC-phalloidin images (actin) were collected at  $\lambda_{ex} = 545 \text{ nm}$ / $\lambda_{em} = 573 \text{ nm}$ , DAPI images (nuclei) were collected at  $\lambda_{ex} = 358 \text{ nm}$ / $\lambda_{em} = 461 \text{ nm}$ .

### **5.3 Results and Discussion**

The photocurable polylactic acid (PLA) and polycaprolactone (PCL) oligomers described in chapter 2 were prepared as described in the methods. The surface properties of the PLA based material were examined in detail using x-ray photoelectron spectroscopy (XPS) and contact angle analysis. A more detailed study of cell proliferation and adhesion on both materials was performed using NG108-15 neuronal type cells and the results compared with the results of the surface characterization studies. A combined study of the material surface properties and the effect on cell adhesion demonstrates the suitability of this type of materials for neural tissue engineering applications.

Due to the ability of neural cells to attach to and proliferate on this material, a range of microdevices which contained open pores of different geometries were created using two photon polymerization (2PP), as potential cell delivery vehicles which can be injected into the site of a brain injury, for example following a stroke where a section of brain tissue has died. The increased area for cell attachment and the mechanical protection this provides would offer benefits over simple spherical microparticles of degradable poly(lactide-*co*-glycolide) (PLGA) which have been investigated for this purpose (Bible et al. 2009b).

Furthermore, cell alignment and attachment on structures fabricated from this material by 2PP was investigated using a combination of fluorescence microscopy, immunostaining and scanning electron microscopy (SEM). Three dimensional structures consisting of 'guidewires' or posts suspended between two solid blocks were created, with posts of different diameter and structures with guidewires at different heights and spacing were created as a proof of principle model for studying optimum fibre diameter and spacing for cell attachment and fibre myelination in nerve guidance conduits (Ahmed and Brown 1999).

### 5.3.1 Polymer Characterisation

The polymer resins were characterised using  $^1\text{H}$  NMR spectroscopy. NMR characterisation was used to determine the ratio of the initiator to monomer in the final resin, as demonstrated in Claeysens *et al.* (Claeysens et al. 2009). Furthermore, the appearance of vinyl peaks in the 5.5-6.5 ppm region were used to verify the methacrylate functionalization. FT-IR spectroscopy was also used to confirm the methacrylation of the oligomers, by the appearance of peaks characteristic of carbon- carbon double bonds at  $1600\text{ cm}^{-1}$ .

### 5.3.2 Surface Characterisation of Photocured Poly(lactic acid) Thin Films

Thin films of the photocurable PLA were cured onto the surface of glass coverslips functionalized with MAPTMS as described in chapter 2. If MAPTMS functionalization was not performed the films detached when submerged in cell culture media during incubation. The films were gold coated and examined under SEM in order to determine the surface roughness and thickness. By scratching the film using a fine steel tip the thickness of the film could be visualised. The films were found to be smooth on the micrometer scale, with a thickness of around  $1\ \mu\text{m}$ . The thickness of the films is expected to be sufficient for investigation of cell adhesion, which is influenced by the chemical functionality of the top 0.4 nm of a surface (Zelzer et al. 2008). A scratched film of the photocured PLA is shown in figure 58.

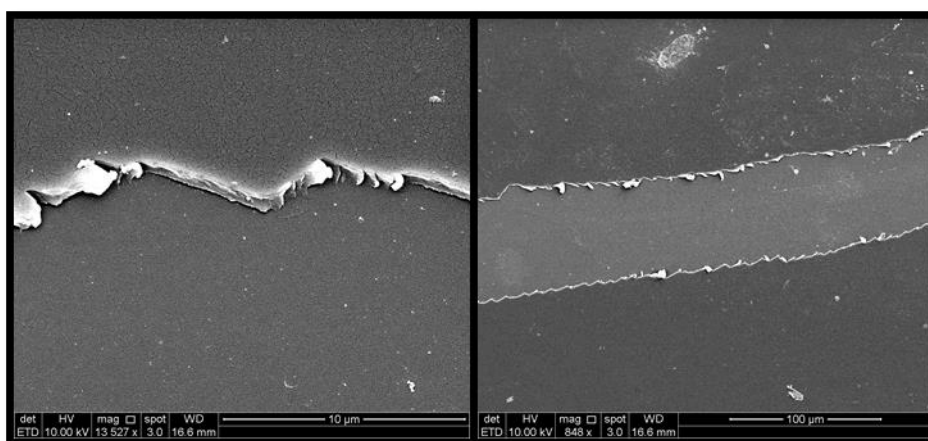


*Figure 58: SEM images of photocured PLA thin films scratched using a metal tip, allowing thickness of the film to be determined.*

Surface topography or ‘roughness’ has been demonstrated to influence cell response on chemically identical materials (Kaiser, Reinmann, and Bruinink 2006; Jain and von Recum

2004). From the SEM images it can be seen that the polymer thin films are smooth on the sub-micrometer scale.

In order to characterise the surface of the photocured material, x-ray photoelectron spectroscopy (XPS) and water contact angle measurements were used on the photocured PLA films. Developed by Kai Siegbahn in the 1960's (Hagstrom, Nordling, and Siegbahn 1964), XPS is one of the most commonly used surface characterization techniques (McArthur 2006). The sample surface (in this case the photocured PLA film) is irradiated with an X-ray source resulting in the ejection of photoelectrons within the top 10 nm of the sample. The energy of the ejected electrons may be assigned to particular elements in order to identify the elemental composition of the surface. The chemical state of the surface elements may also be identified, as the binding energy of an electron emitted from a carbon atom in an aliphatic hydrocarbon will be lower than that of an electron emitted from a carbon belonging to a carbonyl group. This allows polymer structures to be verified by a comparison of the stoichiometry of different carbon environments. This technique has been applied for example to polylactic acid, where the polymer stoichiometry was verified by comparing the C1s core level (Barry et al. 2006).

In the case of the photocured PLA, the survey scan reveals a carbon to oxygen ratio of 1.83 (C/O), close to the figure indicated by the NMR spectrum and the theoretical value of 1.73. The high resolution C1s scan indicates 38.5% C-C bonding, 24.5% O-C=O bonding, 25.5% C-O bonding and 11.5% C-COOH bonding, indicating the presence of some carboxyl groups, which could be created by oxidation and chain scission during UV curing. The XPS spectrum is shown in figure 59.

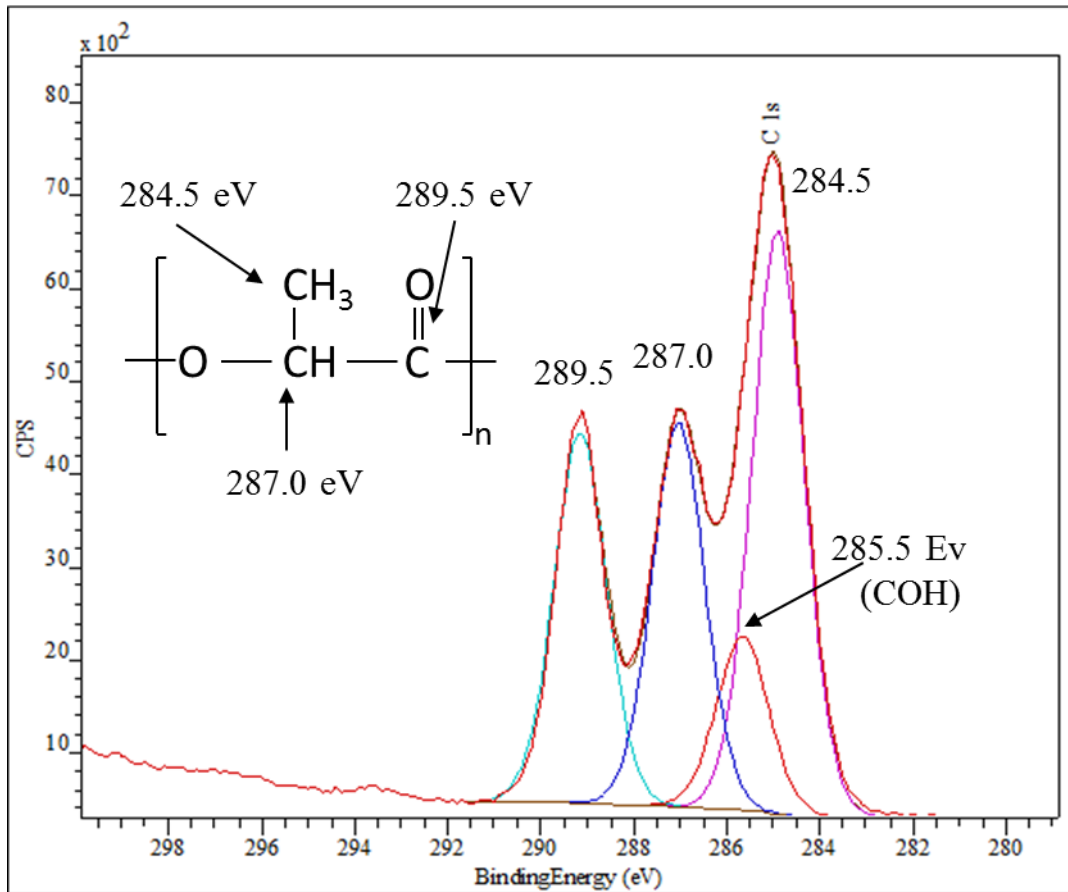


Figure 59: XPS spectrum of PLA cured films

The photocured PLA thin films were compared to commercially available linear PLA thin films using contact angle analysis. Surface chemistry, and in particular surface energy has a strong effect on cell attachment (Roach et al. 2010; Zelzer et al. 2008). Surface wettability, as determined by surface contact angle measurement is one of the most commonly examined surface properties due to the simplicity with which a reading can be taken. Although the technique does not give any indication as to the identity or concentration of the surface groups, it is very fast and surface sensitive (the depth of sensitivity is within 0.33 to 1 nm of the surface) (Bain and Whitesides 1988).

The contact angle is measured as the tangent of the droplet surface at the point at which it meets the sample (in this case the PLA and cured PLA films). The resulting figure is the result of a balance of three interfacial forces, the solid: liquid interface, the liquid: vapour interface and the solid: vapour interface. As a result of the balance between these forces the droplet may spread over the sample surface or remain as a droplet. A high water contact angle indicates a hydrophobic surface, whereas a low angle indicates a hydrophilic one.

The dominant factor in cell-surface adhesion in serum-containing media is protein adsorption (Koenig, Gambillara, and Grainger 2003). Cell-surface interactions are often discussed in terms of surface energetics, with water contact angle being the most commonly reported parameter (Sigal, Mrksich, and Whitesides 1998). Increased cell density is often correlated with lower water contact angle and therefore lower hydrophobicity, as demonstrated in several studies (Koenig, Gambillara, and Grainger 2003; Keselowsky, Collard, and Garcia 2003, 2004).

To compare the surface wettability of the photocured and linear PLA, the pH of the droplet was varied from pH 7 to pH 2 in order to investigate the effect of UV exposure on surface oxidation, which generates acidic groups (Koo and Jang 2008), in addition to those already present in linear PLA. The contact angle of the commercially available PLA remains at 69° over the pH range. The photocured PLA film has a contact angle of 67° at pH 7 but below pH 4 rises to 69°. The irradiated commercially available PLA reduces to 65° at pH 7 but returns to 69° at pH 2.2 due to protonation of the surface acid groups. The reduction in contact angle at pH 7 is less pronounced in the photocurable PLA compared to the commercially available PLA, and the effect of surface oxidation on cell attachment is expected to have little effect on the attachment of cells on UV cured films compared to those cured using infra-red radiation during the two photon polymerization process.

Water Contact Angle	Commercially available PLA	Commercially available PLA: 9 W/cm <sup>2</sup> UV light	Photocured PLA: 9 W/cm <sup>2</sup> UV light
pH 7.0	69.4 ° ± 0.9°	65.4° ± 0.5°	67.2° ± 1.3°
pH 2.2	69.0 ° ± 0.9 °	69.0° ± 1.2°	69.4° ± 2.3°

*Table 1: Effect of UV irradiation on surface oxidation of PLA films on surface hydrophobicity, determined by exposure of films to radiation and measurement of contact angle at different pH values. Repeat measurements were taken five times (n=5) and values are reported as mean ± standard deviation.*

### 5.3.3 Structuring of the Photocurable PLA

After some optimization the PLA based photocurable oligomer was found to give accurate structuring with a laser power of 30 mW and a write speed of  $50 \mu\text{m s}^{-1}$ . These figures are comparable with data reported by Claeysens *et al.* (Claeysens et al. 2009) who reported on the structuring of polycaprolactone (PCL) based photocurable polymers using the same system. The photocurable PLA material was shown to produce excellent structuring results, with little shrinkage or swelling/ cracking occurring post-development. A minimum resolution of 800 nm was demonstrated in this study. Structures showing the minimum resolution and excellent structuring results are shown in figure 60.

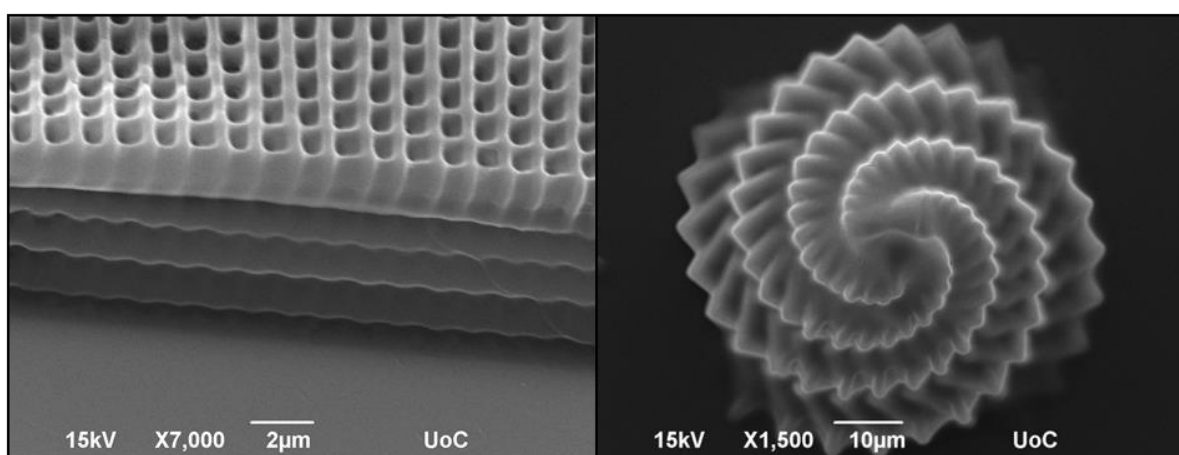


*Figure 60: Cross-hatched structure showing ~800 nm resolution (left) and 'sea-shell' structure showing accuracy of the 2PP technique (right).*

### 5.3.4 Neuronal Cell Growth and Viability on Polymer Thin Films

The ratio of live to dead cells (PC12 and NG108-15 cell lines) was examined on thin films of the photocured polymers using live-dead staining (PC12 cells at 1, 3 and 5 days) and in more detail using the more adherent NG108-15 cell line at 24, 48 and 72 h (proliferation assay), 72 h (DNA quantification assay) and 24, 72 and 120 h (MTT assay). Neuronal type cells were selected to reflect potential applications of microstereolithography in neural tissue engineering, where aligned cell growth induced by scaffold microstructure and architecture is an important area of research (Ribeiro-Resende et al. 2009).

### 5.3.5 MTT and Cell Proliferation Assay with NG108-15 Cell Line

MTT assay provides an indication of cell number by colorimetric methods and was discussed in detail in chapter 2. In this study NG108 proliferation on thin films of the photocured PLA was compared to a proliferation on a glass coverslip control at 24, 72 and 120 h. Additional controls included tissue culture plastic, the methacrylate functionalized glass coverslips and spin coated thin films of linear PLA for comparison (all examined at 24 h and 72 h). This extensive set of controls shows no significant difference for the TCP or methacrylate functionalized glass from the standard glass coverslips, indicating that the glass coverslips are a valid control and also that the silane treatment of the coverslips does not cause a cytotoxic effect. After 120 h the cell metabolic activity is significantly higher ( $p < 0.05$ , Student's *t*-test) on the photocured PLA film, indicating a higher cell count. This potentially indicates better cell adhesion on this material, however further in depth analysis would be required to verify that the cells on the glass coverslip control have not become over-confluent more rapidly than on the PLA substrate.

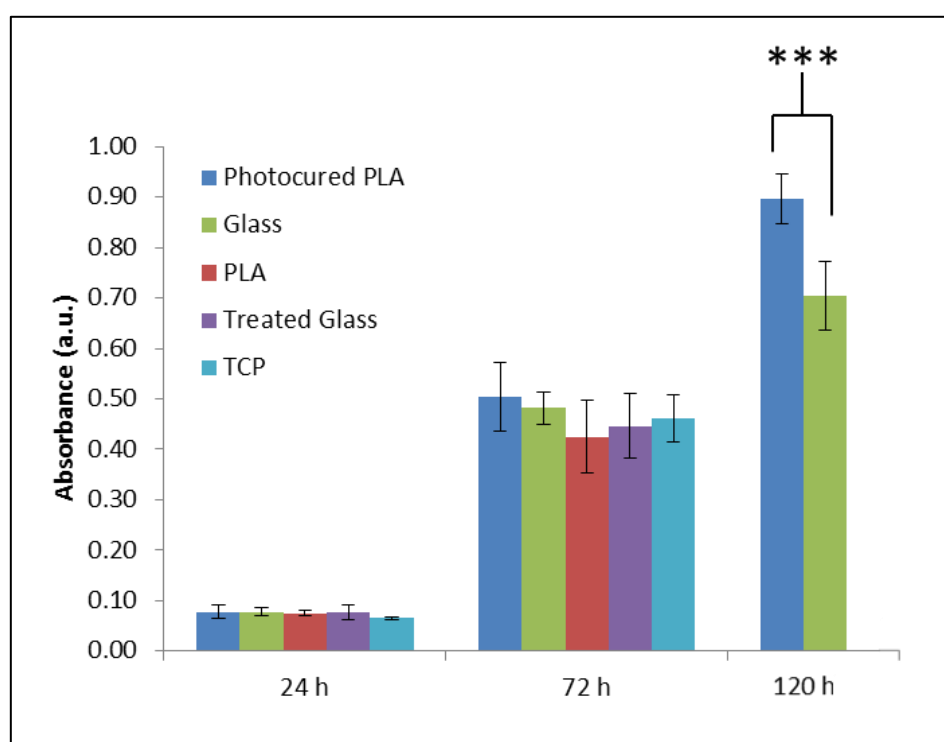
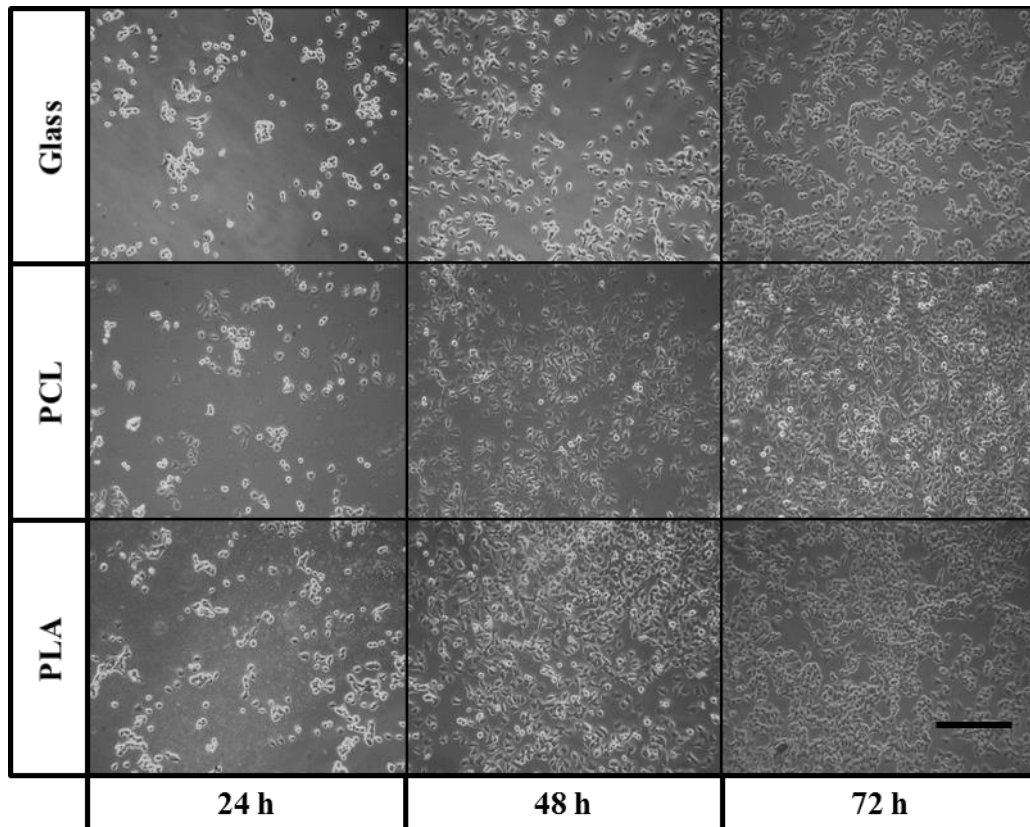


Figure 61: MTT Assay of Photocurable PLA and controls, comparing NG108 neuronal cell number (as indicated by metabolic activity) on the photocurable PLA and glass, linear PLA, MAPTMS treated glass and tissue culture plastic controls. Values reported are mean of six repeats ( $n=6$ )  $\pm$  standard deviation. Significance determined by two-tailed Student's *t*-test;

\*\*\* $p < 0.0003$ .

In order to visually examine the confluence of the NG108 cells and corroborate the results of the MTT assay, cell proliferation was also compared using cell counting. Cells were seeded on thin films of the photocurable PLA and also photocurable PCL material for comparison, and again compared to a glass coverslip control at 24, 48 and 72 h. Cell numbers were counted from randomly selected areas as discussed in the methods section. The proliferation rate increased in a similar fashion on all three substrates over the duration of the test, in agreement with the results of the MTT assay.



*Figure 62: Phase contrast micrographs of NG108 cells cultured on photocurable PLA, PCL and glass coverslip controls at 24, 48 and 72 h in culture. Scale bar 200  $\mu$ m.*

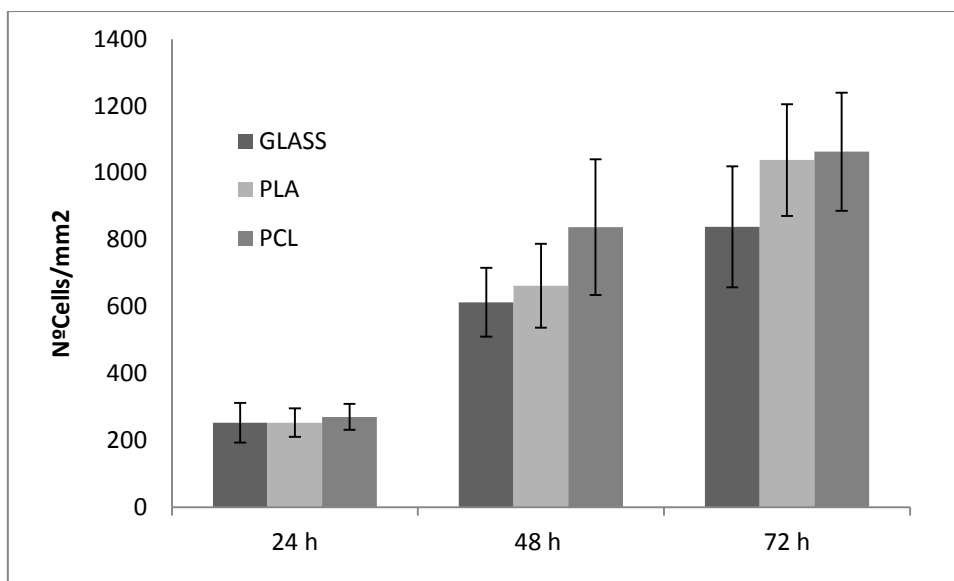


*Figure 63: NG108 neuronal cell density at 24, 48 and 72h as determined by cell counting using optical microscopy. Samples are reported as mean of 15 repeats (n=15)  $\pm$  standard deviation.*

### 5.3.6 DNA Quantification Assay

DNA Quantification assay quantifies the relative number of cells present in a sample by the lysis and fluorescent labelling/ measured fluorescence of cell genetic material. Using a calibration curve the actual number of cells in a sample can be determined. The technique is also suitable for giving comparative values between samples, and was used to compare between the number of cells present on photocured PLA and PCL thin films and a glass coverslip at 72 h. The results were in agreement with the MTT and proliferation assay, and verify that the photocurable thin films have no effect on cell proliferation rates compared to a glass coverslip control. The DNA quantification assay selectively labels double stranded DNA (dsDNA), and does not distinguish between living and dead cells. In combination with the other techniques the effect of the photocurable polymers on cell proliferation was thoroughly examined using this technique.

### 5.3.7 Live-Dead Staining with PC12 Cells

The live-dead assay is a fluorescent staining technique which allows the quantification of living and dead cells in a sample population. Living cells are selectively stained green

whereas dead cells are stained red. PC12 cells cultured on the photocurable PLA were compared to a glass control at 25, 72 and 120 h on the material.

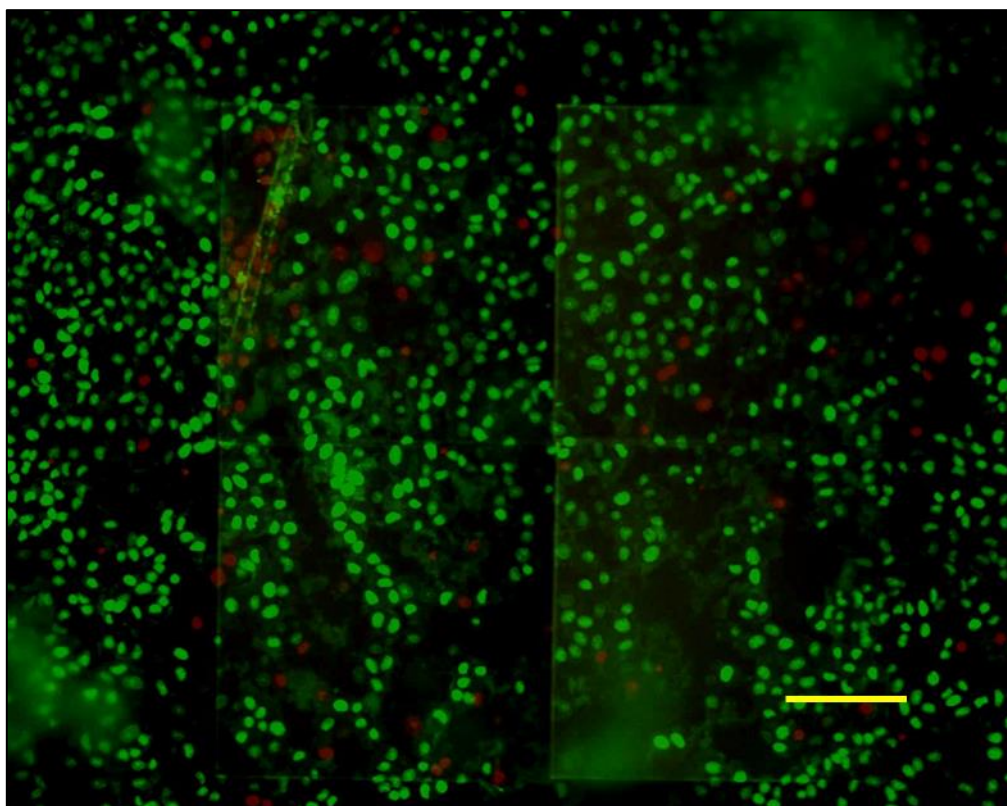


*Figure 64: Typical Live-Dead Stain of PC12 cells cultured on photocured PLA squares. Live cells are labelled green, whereas dead cells are red. Scale bar 50  $\mu\text{m}$ .*

The overall viability of the PC12 days after 5 days in culture was 91%, with 9% of the cells being dead. This high value is comparable to the glass control. Overall the live cell density on the photocured PLA thin films increased more rapidly than on the glass controls, as shown in figure 65. The results of the live dead stain are in agreement with the MTT assay, proliferation assay and DNA quantification assay indicating that the photocurable PLA is capable of supporting neuronal cell growth and attachment.

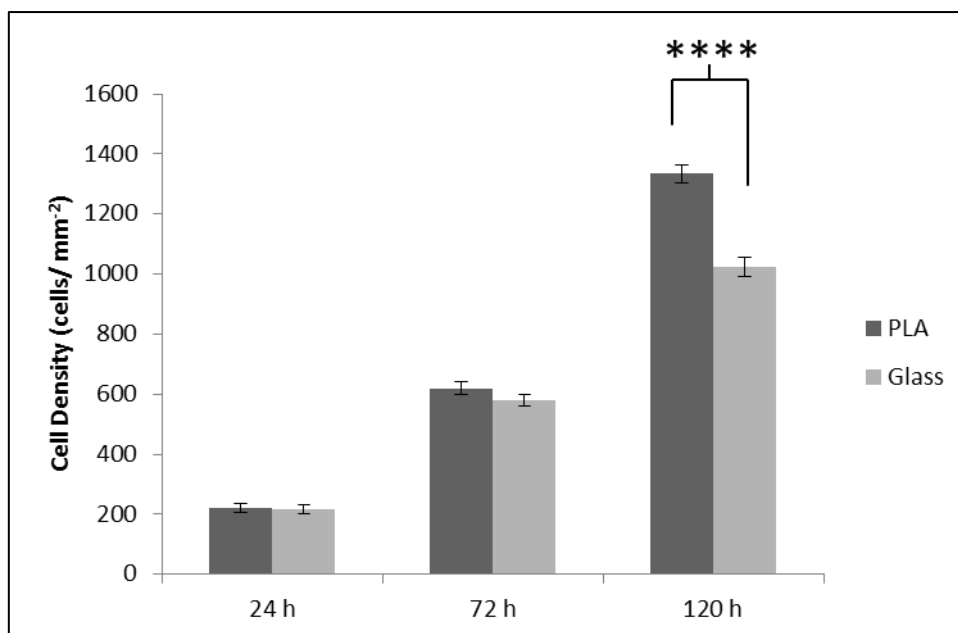
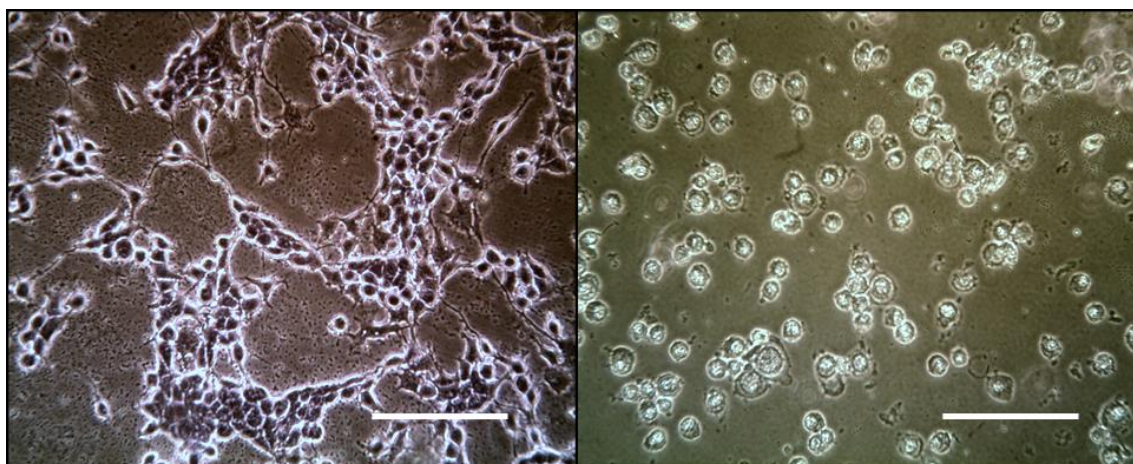


Figure 65: Quantification of cell (PC12) density at 24, 72 and 120 h on spin coated thin films of the photocurable PLA compared to a glass control. Sample reported as average of four repeats ( $n=4$ )  $\pm$  standard deviation. Cell density is significantly higher on the photocured PLA compared to the glass control after 5 days (\*\*\*\* $p<0.0001$ ).

### 5.3.8 Cell Morphology on Photocurable PCL Thin Films

An important indicator of cell adhesion on a surface is cell morphology. If cells are poorly attached to a surface, or experiencing a cytotoxic effect they will appear rounded or ‘ball like’ and detach easily, whereas cells cultured on a surface on which they have a high degree of attachment will exhibit a high degree of spreading and display a flattened morphology, with projections such as neurites or filopodia extending from the cell body. NG108 cells were cultured on thin films of the photocurable PCL and their morphology compared to that of those cells cultured on thin films of linear PCL. The cells cultured on the photocured PCL exhibited a higher degree of spreading on the cured PCL surface, whereas those on the linear PCL were rounded. The high hydrophobicity of PCL is often cited as the reason for its poor cell adhesion, however the photocurable PCL appears to be a better cell substrate than its linear analogue.



*Figure 66: NG108 cells cultured on photocured PCL (left) and linear PCL (right). Scale bars 125  $\mu$ m. Cells cultured on photocured PCL exhibit a greater degree of spreading with more visible neurites (not quantified) whereas cells cultured on commercially available linear PCL appear ball like and ready to detach.*

### **5.3.9 Cell Culture on Microfabricated Structures**

The high resolution and three dimensional structuring capabilities two photon polymerization (2PP) allow the production of highly detailed bespoke structures according to a user generated model. The combination of 2PP with photocurable materials based on polymers approved for internal medical use makes possible the production of advanced medical devices. The structures created in this study were chosen to reflect potential applications for this technology, for example where the internal features of the scaffold may be used to influence cell behaviour and lead to improved recovery from injury. Applications where precise or designed microstructure and topography have been demonstrated to be beneficial include regenerative therapies in the peripheral and central nervous system (Huang and Huang 2006) and scaffolds requiring complex responses to environmental forces such as stretching, as demonstrated by Engelmayr *et al.* (Engelmayr et al. 2008).

The fabrication of cell delivery vehicles or self-assembled scaffolds was also explored. The use of degradable microspheres as a supporting matrix for neural stem cells has been suggested as a treatment for brain injuries or strokes (Bible et al. 2009a). The fabrication of micro-scale porous blocks or ‘scaffolds’ was explored and cell migration into the microcarriers demonstrated using neuronal type cells. Cell attachment to three dimensional structures created from the photocurable PLA material was demonstrated using PC12 cells

(figure 67). The cells successfully attached to the structures and grew in a three dimensional fashion, with cells connecting between adjacent structures as observed in figure 67.

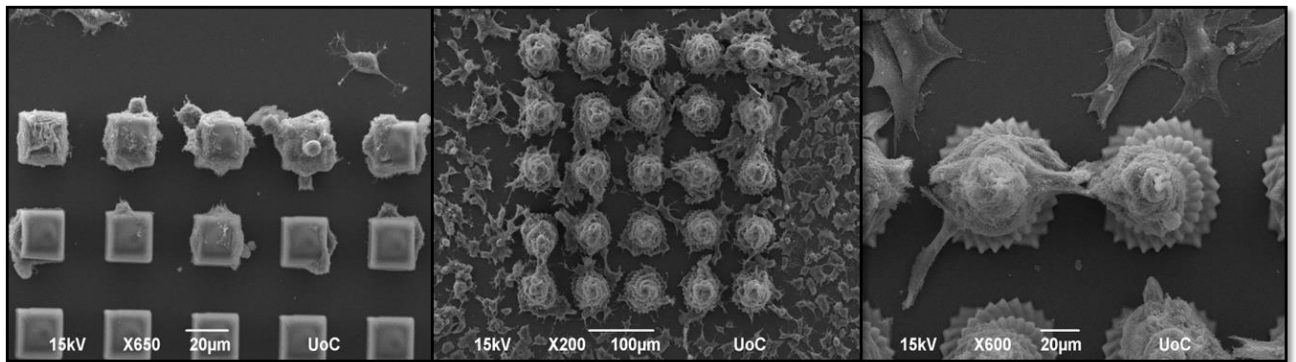


*Figure 67: Scanning electron micrographs of PC12 cells cultured on PLA microstructures. Cells can be observed adhering to the microstructures and interacting with cells situated on neighbouring structures.*

### **5.3.10 Guided Cell Growth on Aligned Microstructures**

In peripheral nervous system injury, a key strategy towards improved functional recovery is the enhancement of axon regeneration through the use of nerve guidance conduits containing advanced structural features. By the inclusion of guidance channels or microfibres into nerve entubulation devices, functional recovery is enhanced by guided cell migration (Huang and Huang 2006). Aligned cell growth is often demonstrated in two and a half dimensions using grooved structures produced by photomask based lithography (Mahoney et al. 2005), ion etching on silicon chips (Lietz et al. 2006) or surface patterning techniques (Schneider et al. 2001). In three dimensions, a common technique for fibre production is electrospinning (Daud et al. 2012). Two photon polymerization (2PP) presents an ideal method for the production of aligned microfibres with user defined geometry, spacing and length, in order to optimise these features with simple lab scale studies. Using suspended fibres may present the possibility of studying Schwann cell myelination of fibres, which is not possible on flat ‘tracks’ or lines, as the cells cannot completely encircle the structure (Ahmed and Brown 1999).

To demonstrate potential applications of 2PP, a series of fibres were fabricated onto glass coverslips and the growth and alignment of NG108 cells was investigated using different imaging techniques. Furthermore, to demonstrate the true three dimensional nature of 2PP and its suitability for this application a series of suspended horizontal posts of varying

spacing and diameter were fabricated, and preliminary cell culture with neuronal type (NG108) cells was performed.

### 5.3.11 Neuronal Cell Attachment and Growth on PLA Lines

In a first experiment, 7  $\mu\text{m}$  thick lines of the photocured PLA with a spacing of 50  $\mu\text{m}$  were fabricated on silane treated glass coverslips. NG108 cells were seeded on the structures at a density of 5000 cells  $\text{ml}^{-1}$  and cultured for 48 h. The cells were then fluorescently labelled with TRITC-phalloidin (for actin) and DAPI (for the nuclei). The samples were cultured in triplicate and representative images are shown.

The PLA material was found to be auto-fluorescent throughout the range of wavelengths achievable with the microscope, making it difficult to visualize cell projections on the lines. It was however possible to image the cell bodies, which were shown to be in contact with the lines and exhibiting some degree of attachment. The lines were also visible due to autofluorescence (see figure 68).

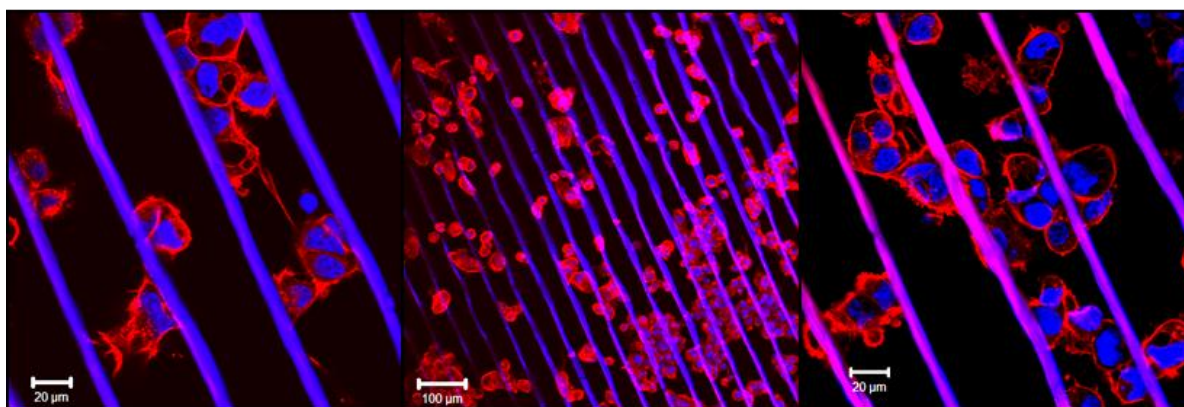


*Figure 68: Confocal Images of NG108-15 cells cultured on PLA filaments fabricated by two photon laser direct write. With a thickness of around 10  $\mu\text{m}$ . Scale bars: left 20  $\mu\text{m}$ , centre 100  $\mu\text{m}$  and right 20  $\mu\text{m}$ .*

In order to visualize more closely the presence of neurites extending from the cells, scanning electron microscopy was used. Cells were cultured as for the confocal experiment, and again cells were observed to be attached to the PLA lines, with some degree of orientation (see figure 69). The results shown in both figure 68 and 69 are representative of a minimum of three repeats.

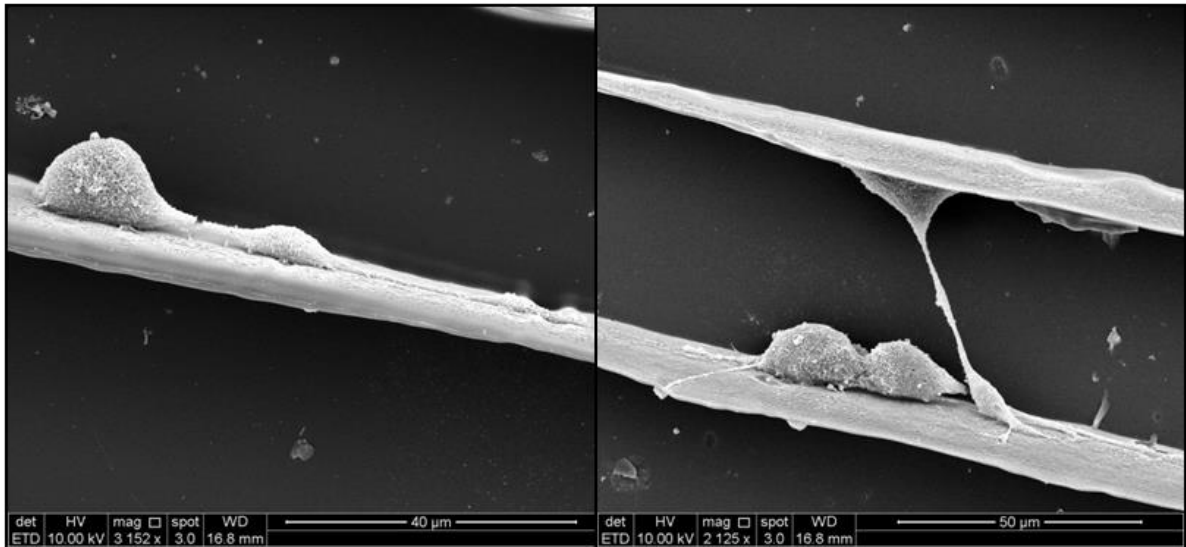


*Figure 69: SEM Images of NG108-15 cells extending along PLA filaments. Scale bars: left 40  $\mu\text{m}$  and right 50  $\mu\text{m}$ .*

### 5.3.12 Visualization of Neurites by Labelling for $\beta$ -III tubulin

To verify the presence of neurites extending along the polymer ‘tracks’, 3,3’ diaminobenzidine (DAB) staining was used. This technique also allowed the observation of NG108 cells using optical microscopy without the problem of polymer autofluorescence, and also verified the phenotypic purity of the cell line. The DAB staining kit allowed the specific staining of HRP labelled  $\beta$ -III tubulin. NG108-15 cells were observed to exhibit a degree of alignment on the photocured tracks of PLA.

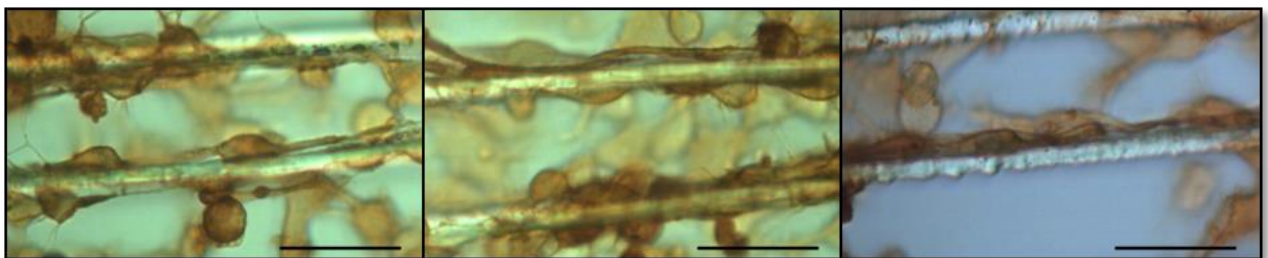


*Figure 70: Aligned NG108-15 cells cultured on photocured PLA tracks with a thickness of around 10  $\mu\text{m}$ , fabricated by two photon laser direct write. The cells were visualised by first labelling  $\beta$ -III tubulin with horseradish peroxidase (HRP). By applying DAB solution the HRP labelled  $\beta$ -III tubulin was stained brown allowing the cells to be observed using optical microscopy.*

### 5.3.13 NG108 Cell Growth on Suspended Fibre Model Structures

Further studies were performed using PC-12 and NG108-15 cells on fully three dimensional suspended fibres. Fibres of varying diameter and spacing were fabricated and cells cultured on the created structures, in order to study cellular alignment in three dimensions. Cells were observed growing on the suspended wires, as demonstrated in figure 71.

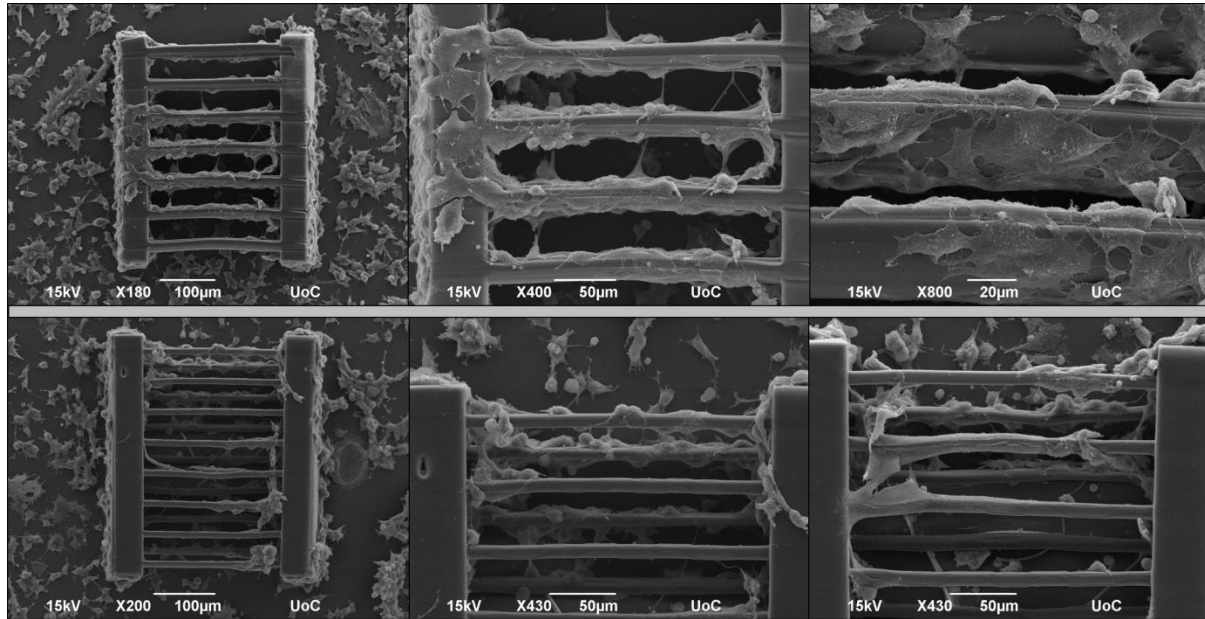


*Figure 71: PC12 cells cultured on suspended post structures and imaged using SEM. Cells appear to have attached more to thicker posts (top row) as opposed to thinner posts (bottom row). Cells cultured on thinner posts exhibit a more flattened morphology.*

From a qualitative examination of the images shown it appears that a critical diameter is reached between 10 and 50 micrometers, beyond which the cells can no longer entirely encircle the fibres (as seen in figure 72) and instead attach and migrate along the wire.

### 5.3.14 Self Assembled Scaffolds and Cell Delivery Vehicles

The write area or ‘footprint’ of the Galvano scanner is limited to the focal area of the objective used. The large fabrication times required also prevented the production of larger structures (medical devices or tissue scaffolds). The narrow footprint of the technique may be overcome by combining the scanning method with a high precision translation stage, using a ‘step and repeat’ methodology as demonstrated by Claeysens *et al.* (Claeysens *et al.* 2009) in which the structure size is increased by creating the scaffold as a series of overlapping identical structures. Write times are also improving with the creation of more efficient

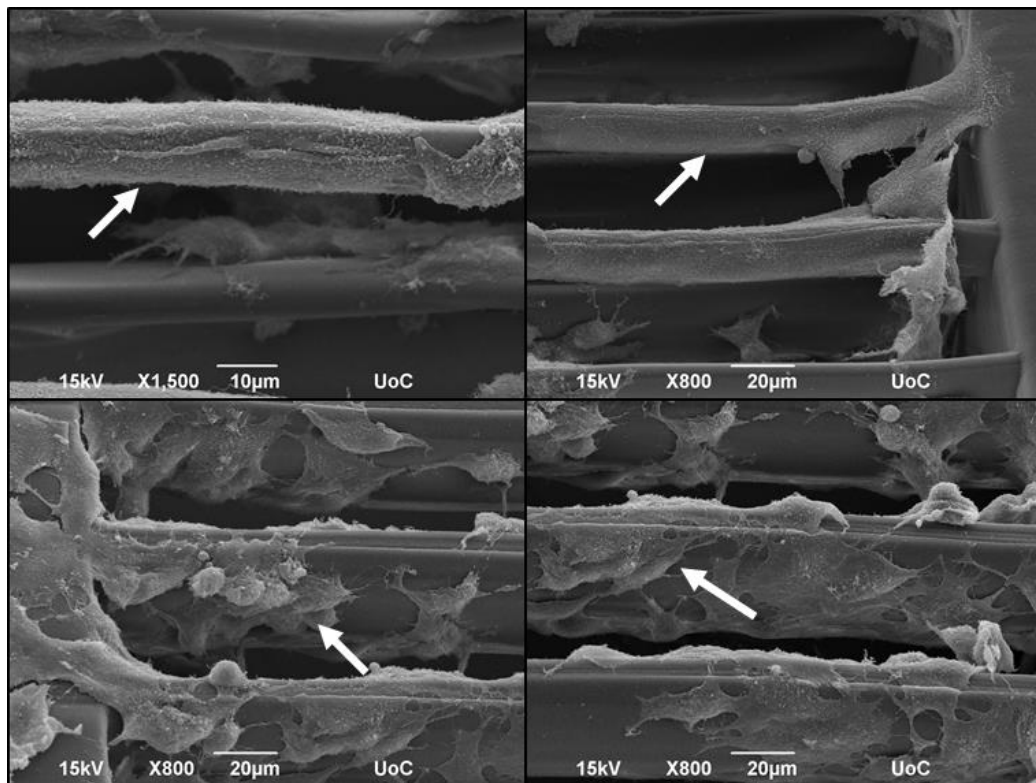


*Figure 72: PC12 cells cultured on suspended posts of different diameters. Cells cultured on thinner posts spread along and encircle the posts (highlighted by arrows in top row) whereas on thicker posts multiple cell bodies may be observed (indicated by arrows on bottom row).*

photoinitiators, materials and scanning systems. Hsieh *et al.* for example reported on the fabrication of a porous scaffold by 2PP with dimensions of 2.5 mm<sup>3</sup> (Hsieh *et al.* 2010). Compared to other fabrication techniques such as robocasting however the technique is still too slow for the creation of large scale implants.

One solution to this is the creation of self-assembled scaffolds or cell carriers. In this modular approach the scaffold is created as a series of individual porous blocks which are loaded with cells and then injected into the site of injury, where the cells will create the matrix which binds the blocks together. Chemical functionalization may be used to guide the self-association of the blocks into structures, for example to sequentially assemble vascular tubes from hydrogel encapsulated cells (Du *et al.* 2011). The 2PP based fabrication of arrays of identical structures such as micro-needles has been demonstrated in numerous studies (Gittard *et al.* 2011; Gittard *et al.* 2010; Ovsianikov, Chichkov, Adunka, *et al.* 2007), and the production process may be sped up by the use of advanced optical techniques such as voxel elongation (Li, Winfield, O'Brien, and Chen 2009; Li, Winfield, O'Brien, and Crean 2009),

patterned beam delivery (Bhuan et al. 2007) and multiple spot fabrication with microlens arrays (Kato et al. 2005).

The use of polymeric microspheres as injectable cell delivery has been investigated as a treatment for brain injuries such as strokes (Bible et al. 2009a). Chen *et al.* demonstrated the use of porcine gelatin based micro-carriers for the modular assembly of adult bone tissue from adult mesenchymal stem cells (MSCs) (Chen et al. 2011), overcoming the diffusion limit associated with monolithic scaffold structures. In our work the rapid microfabrication of micro-scale cell carriers with different pore sizes and morphologies from photocurable PLA was demonstrated. After 5 days in culture the scaffolds were completely filled with cells, as shown in figure 73.

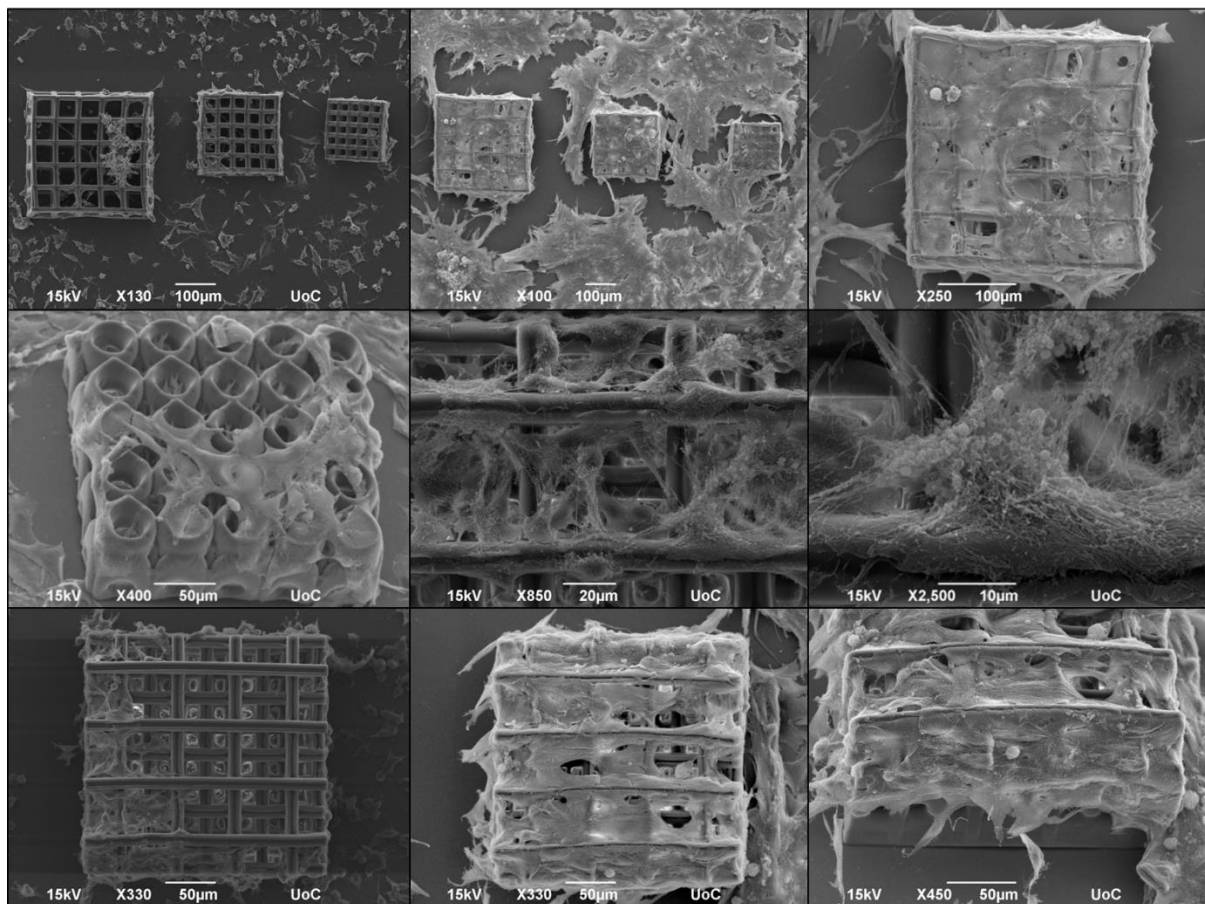


*Figure 73: Scanning electron microscopy images of cell delivery vehicles fabricated from photocurable PLA after culture with NIH-3T3 cell line. Cell ingrowth into structures demonstrates potential application as cell delivery vehicles, as discussed in section 5.3.14.*

## 5.4 Conclusions

In this chapter the use of a Galvano scanner based two photon polymerization system for the structuring of a PLA based photocurable oligomer was reported, with a previously unreported resolution for this polymer of 800 nm. Applications in neural tissue engineering were investigated, and the adhesion and viability of neuronal type cells (NG108-15 and PC12) on the photocurable PLA as well as a photocurable PCL based oligomer were investigated in combination with surface characterisation techniques (water contact angle and X-ray photoelectron spectroscopy).

Cell viability was found to be as good on these materials as on glass controls, indicating no cytotoxic effect due to contamination (for example by remaining uncured oligomers or photoinitiator. Cell adhesion on these materials was found to be good, with cells exhibiting a flattened morphology on these materials, compared with a 'ball like' morphology on (for example) linear PCL controls. The growth rate of cells on these materials also appeared to be higher than on glass controls, indicating a high affinity for the polymer surface. In the case of microstructures fabricated from the photocurable PLA, scanning electron microscopy imaging revealed adherent cells proliferating on the structures.

On linear structures fabricated from the PLA material, adherent cells exhibited a degree of alignment as evidenced by SEM, confocal microscopy and DAB staining/ optical microscopy. In three dimensional scaffolds cells quickly migrated into the pores, completely filling the structures. In summary the potential application of photocurable biomaterials and laser direct write technology to neural tissue engineering, via modular scaffold self-assembly and the creation of microfiber scaffolds was demonstrated.

# Chapter 6: Replication of Two photon Laser Direct Write Produced Structures for Nerve Guidance Conduits with Functional Structure

---

*Aspects of this chapter published in (Koroleva et al. 2012) with significant modification. The author would like to thank A. Koroleva (Laser Zentrum Hannover) for fabrication of the original microstructures for replication and the Comet Assay. The author was responsible for synthesis and characterisation of the resin, and additional cell culture and imaging. Aspects of the cell culture and staining were undertaken with assistance from Í. Ortega (University of Sheffield).*

## **Abstract**

The use of soft lithography (PDMS) stamping enables rapid reproduction of structures created by two photon polymerization (2PP) providing that the structure allows removal of the mould, containing no overhanging features that prevent ‘lifting off’ of the PDMS stamp. In this chapter the production by 2PP of stackable ‘discs’ consisting of an array parallel tubes designed for cell migration, and their assembly into scaffolds by PDMS replication is demonstrated. The use of a photocurable PLA based material for the production of both the initial structures by 2PP and also for curing in the PDMS mould is explored, and the ability of this material to support Schwann cell adhesion and growth was investigated. Schwann cell growth was demonstrated up to 7 days on thin films and structures of the cured material. A Schwann cell purity of 99% was determined by S100 $\beta$  staining, and bipolar and tripolar cell morphology was observed with an ordered arrangement of actin filaments and focal adhesions, indicating that this material supports Schwann cell growth and adhesion. The structures were successfully replicated with a dimensional accuracy of  $\geq 95\%$ .

It was successfully demonstrated that i) multilumen discs may be created with high resolution using 2PP, and replicated accurately using soft lithography resulting in a reduction of production time ii) the photocurable PLA based material supports Schwann proliferation and adhesion and iii) the stackable multi-lumen discs provide a suitable environment for Schwann

cell migration and after 7 days in culture the scaffold contains adherent Schwann cells, which assist in axon regeneration by guiding growth and releasing nerve growth factor (NGF).

## **6.1 Introduction**

As discussed in chapter 3, peripheral nervous system (PNS) injury can lead to a significant reduction in quality of life, due to loss of sensory and/ or motor function. PNS injury is estimated to affect 1 in 1000 individuals annually, making this a very common type of injury. Functional recovery of the nerve is possible due to the regenerative potential of the peripheral nervous system, however for injuries greater than around 2 mm axonal regeneration is not possible (Schmidt and Leach 2003). Large numbers of nerve cells undergo apoptosis following traumatic nerve injury (transection) leading to reduced functional recovery of the nerve, and loss of sensation or motor function (Bell and Haycock 2012; Schmidt and Leach 2003). Individuals receiving this type of injury will suffer lifelong impairment of sensory and motor ability. Surgical options include auto/ allografting and also the use of entubulation devices. Nerve entubulation devices provide a protected environment for axon regeneration, and may contain structural, cellular and chemical clues which guide regrowth (Schmidt and Leach 2003).

The one step fabrication of multi-lumen nerve guidance conduits (NGC's) was described in chapter 3. In chapter 5 the use of two photon polymerization (2PP) for neural applications was discussed, and the potential use of 2PP for the optimization of fibre spacing and diameter for neuronal type cell (NG108-15) alignment was explored. In this section the use of a combination of techniques (2PP and microreplication) to produce stackable discs for incorporation into NGC's is demonstrated. The ability of the photocurable PLA material to support Schwann cell growth and attachment, and furthermore the interaction of Schwann cells with the features of the stackable discs was studied. The process of using 2PP to produce multi-lumen discs, and replication and stacking of these discs by PDMS stamping is outlined in figure 74. Reproduction of structures produced by 2PP using PDMS stamping allows the rapid reproduction of suitably designed structures, overcoming the problem of low production rates associated with 2PP.

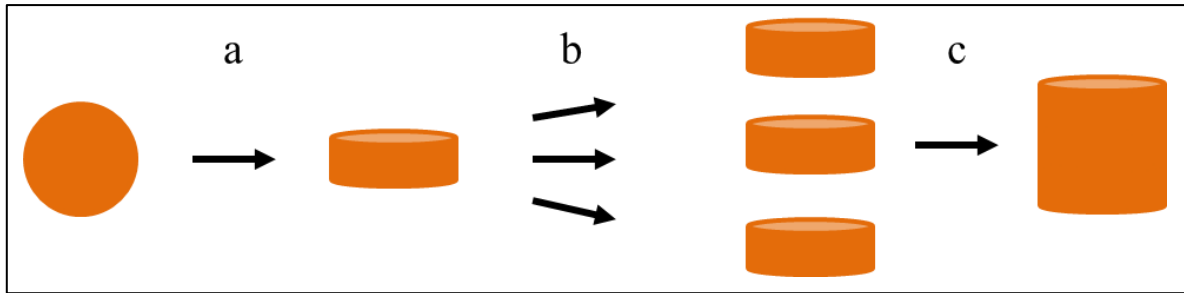


*Figure 74: A multi-lumen disc is produced by 2PP (a), multiple PDMS stamps are made using the original structure and the resulting stamps are used to create many replica structures by UV curing, taking just a few minutes (b) and finally the resulting structures are stacked to form a tube or conduit (c).*

### **6.1.1 Soft Lithography using Poly(dimethylsiloxane)**

One focus in this chapter was the reduction in production time required for the discs by the use of PDMS stamping. The time required to fabricate one structure by 2PP can be as long as several hours. Using PDMS replication, one structure may be used to produce several moulds and the production rate of the discs increases rapidly. Poly(dimethylsiloxane) (PDMS) possesses a unique balance of properties including resistance to degradation by light/radiation and heat, chemical resistance and importantly, high flexibility and low surface energy (Esteves et al. 2009). PDMS replication has been applied to flexible and stretchable electronic devices (Morent et al. 2007), corrosion resistant and anti-fouling coatings (Kim et al. 2012; Sugama, Brothers, and Weber 2003) as well as biomedical devices (Xia and Whitesides 1998; Abbasi, Mirzadeh, and Katbab 2002; Koroleva et al. 2010)

Various strategies for PDMS replication have been developed, as reviewed by Xia and Whitesides (Xia and Whitesides 1998). Four distinct methodologies exist for the reproduction of structures and surface patterns, replica molding (REM), microtransfer molding ( $\mu$ TM), micromolding in capillaries (MIMIC) and solvent assisted micromolding (SAMIM). Whereas  $\mu$ TM, MIMIC and SAMIM are largely layer-by-layer or surface patterning techniques, REM allows the accurate reproduction of whole structures by curing within a mold. UV curable polymers typically undergo shrinkage of less than 3 % upon curing and therefore can accurately replicate structures with high fidelity. The accuracy of replication is determined by the degree of mold filling, van der Waals interactions between the curable substrate and the mold and the wettability of the mold surface. The low surface energy of PDMS makes it ideal for REM, with an achievable resolution of replication of <100 nm (Xia and Whitesides 1998).

In this chapter the use of PDMS replica micromolding using photocurable PLA for both the original structure (by 2PP) and replication (by REM) is demonstrated. In a multi-step process 2PP is first used to create a PLA microstructure, which is then developed (washed with solvent) to remove uncured resin. The structure is then reproduced by covering in PDMS contained within a thin aluminium tube and vacuumed to remove trapped air. The PDMS is then cured using heat to create the negative replica or ‘mold’. The PDMS mold can then be filled with photosensitized PLA and cured by UV exposure multiple times to create several stackable PLA discs. The soft elastomeric nature and low surface energy of PDMS prevents damage to the negative mold allowing multiple (>10) PLA copies to be reproduced without damage to the mold (Xia and Whitesides 1998). The creation of a multi-lumen structure within nerve guidance conduits can enhance nerve regeneration by providing a larger surface area for Schwann cell adhesion and also by contact guidance.

### **6.1.2 Synthetic Materials for Nerve Guidance Conduits**

An important aspect of nerve repair device design is the choice of material. The benefits of autologous transplantation (no rejection, ideal material and structural properties) are balanced with the need for two operation sites and also the loss of function in the donor site. Other autologous transplant options include arteries/veins. Natural materials such as chitosan and collagen have also been explored (Phillips et al. 2005; Yang et al. 2004). As discussed in chapter 2, the biocompatibility and tuneability of synthetic and resorbable materials in terms of stiffness or elasticity, degradation rate and to a degree hydrophobicity make polymers such as polylactic acid (PLA), poly(lactide-*co*-glycolide) (PLGA) and polycaprolactone (PCL) an attractive and readily available alternative to naturally harvested materials (Gill and Claeysens 2011; Bell and Haycock 2012; Hutmacher et al. 2001; Martina and Hutmacher 2007). By producing photocurable analogues of these bioresorbable synthetic polymers, conduits with bespoke geometrical features may be fabricated with unparalleled resolution using microstereolithography.

### **6.1.3 The Role of Schwann Cells in Nerve Regeneration**

Peripheral nerves consist of multiple sensory and motor axons within an organised tissue matrix, which provides protection from external forces experienced during the natural movement of the body. The functional unit of the peripheral nervous system is the nerve fiber, consisting of an axon ensheathed within multiple layers of Schwann cell plasma

membrane known as the myelin sheath. Individual Schwann cells arranged in a parallel fashion encircle sections of the axon several times with their plasma membrane to form this sheath, which helps to maintain action potentials, the electrical impulses which transmit sensory and motor information along the nerve (Topp and Boyd 2012).

Since the work of Ramón y Cajal (Cajal and May 1928) it has been understood that Schwann cells are essential in guiding axonal growth and regeneration. Following transection of a peripheral nerve, a process known as Wallerian degeneration occurs, in which the axons undergo degeneration and Schwann cells degrade their myelin sheath. The remaining debris is then removed by macrophages and Schwann cells (Zhu et al. 2012). Following this process, which is essential for regeneration of the axon, the surrounding Schwann cells dedifferentiate and proliferate to form tubular structures known as the bands of Büngner, which act as cables to guide regrowth of the axon (Schmidt and Leach 2003). By the incorporation of fibres into nerve guidance conduits artificial bands of Büngner are created, which improve neuronal cell alignment and migration (Ribeiro-Resende et al. 2009). In this study the aim was to create microchannels along the axis of the conduit in the form of stackable discs consisting of parallel cylindrical tubes, which would provide a suitable environment for aligned Schwann cell migration improving axonal alignment and reinnervation.

The inclusion of cells, and in particular Schwann cells into nerve guidance conduits is one of the most widely explored strategies for enhancing the distance over which functional recovery can be achieved using nerve entubulation devices (Ruiter et al. 2009). In small gap defects, following entubulation of the nerve endings within a nerve guidance conduit a fibrin matrix builds up upon which Schwann cells migrate. It is unknown whether this fibrin structure builds up in the absence of an entubulation device (Schmidt and Leach 2003). Over larger distances Schwann cells may help bridge the gap, guiding the axons towards the bands of Büngner (Torigoe et al. 1996). Schwann cells also aid in recovery by the secretion of extracellular matrix proteins such as laminin, and furthermore by secretion of signals such as nerve growth factor (NGF) (Assouline et al. 1987), stimulating regeneration.

#### **6.1.4 An Optimized Approach to Nerve Guidance Conduits**

The aim of this study was to optimize every aspect of the production of nerve guidance conduits demonstrating a combined approach of 2PP and soft lithography. Production times

were optimized by the use of soft lithography for reproduction of the multi-lumen discs. The increased surface area of the multi-lumen provides greater area for cell attachment, and the subsequent release of regenerative factors from the adherent Schwann cells. The enhanced microstructure will also help to stabilize the fibrin matrix formed within the nerve tube, and additionally may guide regenerating cells by ‘contact guidance’ (Ruiter et al. 2009).

## **6.2 Materials and Methods**

### **6.2.1 Photocurable Material Synthesis and Preparation**

Photocurable PLA was produced according to the protocol described in chapter 2. In brief a four armed oligomer with a targeted molecular weight of  $\sim 1290 \text{ gmol}^{-1}$  was produced by the reaction of 1 molar equivalent of pentaerythritol to 8 molar equivalents of lactide. As one lactide ring contains two lactic acid monomers this corresponds theoretically to four lactic acid monomers per each of the four arms.

In the synthesis step (3S)-cis-3,6-dimethyl-1,4-dioxane-2,5-dione (98%), pentaerythritol (>99%), stannous octoate (95%), toluene (anhydrous, 99.8%), methacrylic anhydride (94%), triethylamine (>99 %), dichloromethane (95.5%) and isopropanol (>99%) were used as purchased from Sigma-Aldrich, UK without further purification. The photocurable mixture was prepared using Irgacure 369 (Ciba). Glassware was dried at 120 °C overnight prior to use.

### **6.2.2 Four-armed PLA synthesis**

In the ring opening polymerization step, (3S)-cis-3,6-dimethyl-1,4-dioxane-2,5-dione (8.07 g, 0.056 moles, 8 molar equivalents) and pentaerythritol (1.0 g, 0.007 moles, 1 molar equivalent) were stirred in 100 mL of toluene as solvent using a magnetic stirrer bar and brought up to 160 °C under reflux conditions with a nitrogen atmosphere. One drop of stannous octoate catalyst was added and the polymerization was continued at 160 °C for 8 h before cooling, upon which the oligomer precipitated as a lower viscous clear layer. The product was decanted and dried *in vacuo* to yield 8.73 g of the product as a highly viscous clear resin.

### **6.2.3 Methacrylate Functionalization of the Four Armed PLA**

Using a dry reaction vessel purged with nitrogen, the dry four armed PLA (8.73 g, 0.007 moles, 1 molar equivalent) was dissolved in 100 mL of dry dichloromethane and triethylamine (11.34 g, 0.112 moles, 16 molar equivalents) and the solution was cooled to 0 °C using an ice bath. To this solution methacrylic anhydride (8.63 g, 0.056 moles, 8 molar equivalents) in 50 mL of dry dichloromethane was added dropwise using an addition funnel with vigorous stirring using a magnetic stirrer bar. The mixture was raised to room temperature and the solution allowed to react for 24 h. The reaction mixture was then evaporated using vacuum distillation and the photocurable polymer precipitated in ice cold isopropanol at -20 °C overnight. The precipitated polymer was isolated by decanting the isopropanol and drying under vacuum for at least 24 h. The product was a clear highly viscous resin.

### **6.2.4 Photosensitive Solution Preparation**

To prepare a photosensitive solution, the methacrylate functionalized PLA was mixed with 2% w/w of Irgacure 369, a commercially available photoinitiator sensitive to UV radiation.

### **6.2.5 Two Photon Laser Direct Write**

Two photon polymerization of the photocurable PLA based resin was accomplished using a system previously described by Gittard *et al.* (Gittard et al. 2011). The photocurable material was sandwiched between two glass coverslips spaced by a 1 mm thick ring of PDMS, facilitating easy separation of the slides following curing of the material. The direct write system consists of a Chameleon titanium:sapphire laser (Coherent, Santa Clara, CA) emitting at 780 nm delivering 120 fs pulses of radiation at a repetition rate of 80 MHz in this case focussed to within the volume of the sample with a 20× microscope objective (Zeiss, Epiplan). Horizontal (*x,y*) scanning within the resin in the plane of the objective was accomplished using a hurrySCAN Galvano scanner (Scanlabs, Puchheim, Germany). Translation in the Z axis was accomplished using three linear translation stages (model C-843, Physik Instrumente, Karlsruhe, Germany) and stereolithography (STL) files were generated using Solidworks Education Edition 2009 (Dassault Systems SA, Velizy, France), a commercially available software package. Following the laser direct write process the

produced structure is developed by soaking in a mixed (1:1) solvent system of isopropanol and 4-methyl-2-pentanone ( $\geq 98.5\%$ , Sigma-Aldrich).

### **6.2.6 PDMS Replication of Structures**

Using a precision micromolding technique (previously described by Koroleva *et al.* (Koroleva *et al.* 2010)) the discs produced by laser direct write were reproduced by PDMS stamping. The 2PP fabricated structure was placed in an aluminium ring with 1 cm high walls, which was then filled with liquid PDMS (Sylgard 184, Dow Corning). The material was then degassed under vacuum and cross-linked by curing at 100 °C for 1h. The resulting PDMS mold contained within the aluminium ring was then attached to a high precision piezo-electric stage and the structure fixed in place. The mold was then carefully lifted upwards at a speed of 10  $\mu\text{m s}^{-1}$  to detach it from the structure. Following creation of the PDMS mold the structure could be reproduced by filling the mold with the photosensitive PLA material, curing with a UV lamp (EXFO 100W) in contact with a surface for structure adhesion and lifting the mold off of the structure once again. The soft and non adhesive nature of the PDMS mould allows the release of the structures without damage.

### **6.2.7 Materials Characterization**

The photocurable PLA was characterized with FT-IR and NMR as described in chapter 2. IR Spectra were recorded on a Perkin Elmer SPECTRUM 2000 spectrometer. NMR Spectra were recorded at 400 MHz on a Bruker AV1-400 spectrometer. NMR Samples were prepared by dissolving 20 mg of the polymer in deuterated chloroform and filtering into a standard NMR tube.

The 3D structures and films were observed using a FEI Sirion FEG SEM microscope using an accelerating voltage of 10 kV and a spot size of three. Samples were coated with a ~20 nm thick layer of gold prior to imaging using an Emscope SC 500 coating device.

### **6.2.8 Cell Culture and Analysis**

#### **6.2.8.1 Schwann Cell Isolation and Culture**

Cell culture was mainly performed using primary Schwann cells obtained from adult male Wistar rats. An isolation procedure described previously (Kaewkhaw, Scutt, and Haycock

2012) was used with some modification. Connective tissue extracted from 2-3 mm sections of sciatic nerve was teased out and incubated for 60 minutes at 37 °C in in 0.05% w/v collagenase solution (Sigma UK). Macroscopic debris was removed by passing the solution through a Falcon filter (40 µm, Becton Dickinson, USA), and the cells formed into a pellet by centrifugation at 400 g for 5 minutes. The pellet was then rinsed carefully with a solution of Dulbecco's modified Eagle's medium (DMEM, D-valine) containing 10% v/v foetal bovine serum (FBS). The cell pellet was then resuspended in Schwann cell growth medium consisting of DMEM-D valine (PAA, UK), glutamine (2 mM), FBS (10% v/v), N2 supplement (Gibco BRL, UK), bovine pituitary extract (20 µg ml<sup>-1</sup>), forskolin (5 µM, Sigma-Aldrich, UK), penicillin (100 µg mL<sup>-1</sup>), streptomycin (100 µg mL<sup>-1</sup>) and amphotericin B (0.025 µg mL<sup>-1</sup>). The resulting suspension of cells was seeded in a 35 mm Petri dish pre-coated with 0.01% poly-L-lysine (Sigma-Aldrich, UK). The cells were then cultured in an incubator at 37 °C with 5% CO<sub>2</sub>.

For sub culturing of Schwann cells the media solution was removed and the cells washed twice with warmed PBS. The cells were then covered with trypsin for 5 minutes in an incubator and the flask tapped to detach the cells. Cells were then passaged as described in the procedure in chapter 3 and seeded according to the individual experiment.

#### **6.2.8.2 Material Genotoxicity Analysis using Comet Assay**

Comet assay is used to quantify the degree of genetic damage experienced by cells (Kent et al. 1995). The technique was first established in 1984 as a combination of DNA gel electrophoresis and fluorescence imaging for the study the migration of damaged DNA strands from individual cells embedded in an agarose slab (Ostling and Johanson 1984). As DNA is negatively charged, damaged fragments may migrate out during electrophoresis, forming a 'tail' of genetic material which may be labelled with a fluorescent dye. Undamaged strands prove too large to migrate out and remain trapped within the cell. By comparing the tail length (moment), or intensity of the tail of a sample population of cells the degree of genetic damage can be quantified (Olive and Banath 2006). Visual scoring methods can be used (Collins 2004) however automatic software makes the random sampling and scoring of a large number of cells possible.

The genotoxicity of the photocured PLA thin films was assessed using human SH-SY5Y neuroblastoma cells (provided by DSZM-German collection of microorganisms and cells,

Braunschweig, Germany). These neuroblastoma cells are formed by neuronal stem cells, and are derived from a tumor in children consisting of neuroblasts and Schwannian like cells.

The aim of the Comet assay was used to detect any genetic damage caused by the photocurable PLA based material. Genetic damage will lead to cell death or mutations, and must be ruled out if a material is to be considered for use in biomedical devices (Schlie et al. 2007). Using thin films of PLA prepared as described in chapter 2, two sets of samples were tested. In one group, the thin PLA films were washed in distilled water for a week, and in the other the samples were soaked in 70% ethanol for a week before washing for an additional day in distilled water. Both sample sets were then sterilized by UV exposure for 30 minutes and placed in a 24 well plate, along with a glass control. The samples were covered with 2 mL of media per well (DMEM-F12, Sigma-Aldrich, Taufkirchen, Germany) supplemented with 10% FCS and antibiotics). The samples were then seeded with SH-SY5Y neuroblastoma cells and cultured for 24h in an incubator (Heraeus, Hanau, Germany) gassed with 5% CO<sub>2</sub>.

The cells were then trypsinised, collected and reduced to a pellet by centrifugation at 800 g for 10 minutes. The cells were resuspended in PBS to a concentration of  $2 \times 10^6$  cells ml<sup>-1</sup>. 50 µL of the resulting solution was then mixed with 100 µL of low melting agarose (0.6%). 100 µL of this solution was taken up in a pipette and deposited on agarose coated glass slides. A microscope cover slip was then placed on top, and the samples were solidified at 4 °C for ten minutes. The cover slips were removed and a further 100 µL of agarose added. After a further 10 minutes solidifying at 4 °C the slabs were incubated for 90 minutes in a pH10 lysis buffer containing 2.5 M sodium chloride, 100 mM disodium EDTA, 10 mM Tris, 1% lauryl sarcosin, 1% Triton X-100 and 10% DMSO.

Following the lysis step the samples were placed in a chamber for horizontal gel electrophoresis, and covered in electrophoresis buffer for alkaline Comet assay (1 mM disodium EDTA, 300 mM sodium chloride, pH ≥13). After 40 minutes soaking in the buffer, electrophoresis was carried out (25 V, 300 mA, 4 °C, 20 minutes). Following separation, the slabs were neutralized by washing three times by washing with Tris-buffer (pH 7.4, 400 mM) and air dried at room temperature.

The tail moment or 'Comets' were visualized by staining with ethidium bromide (20 µg mL<sup>-1</sup>) and observed using a fluorescence microscope (Zeiss, Oberkochen, Germany) at a magnification of 200 x. Illumination was performed with a Xenon lamp using a filter set for ethidium bromide excitation at 520 nm. Image acquisition was performed using a CCD

camera ('Xaw TV'). Automatic scoring of the collected images was performed using software created for Comet assay (<http://autocomet.com/home.php>). Results were displayed as mean value (Tailmoment)  $\pm$  standard error of the means (n=4, four samples per washing regime). A minimum of 1000 cells per regime were analysed.

#### **6.2.8.3 Schwann Cell Proliferation, Morphology and Purity on PLA Substrates**

To assess primary Schwann cell proliferation on the spin coated PLA films, cell counting and MTT assay was performed. The cell proliferation assay provides a visual quantification of cell number at selected timepoints by manual counting of cells in randomly selected image areas. The MTT assay provides an indication of the number of metabolically active cells by conversion of a substrate to produce a highly chromophoric product which can be quantified by absorbance using a spectrophotometer. This is discussed in more detail in chapter 2.

#### **6.2.8.4 Cell Proliferation Assay**

In the cell counting experiment Schwann cells were seeded on PLA films and a glass coverslip control in 1 mL of media per well in a 24 well plate, at a density of  $5 \times 10^4$  cells per well. Optical microscope images were taken at one, three and seven days using an Olympus CK40 phase contrast microscope, allowing the cell number per unit area to be counted. Using the program ImageJ five discrete areas of  $0.015 \text{ mm}^2$  were randomly selected in each sample and the cells counted manually for quantification.

#### **6.2.8.5 MTT Assay**

MTT assay was used to assess cell viability after 48 h in culture. Primary Schwann were seeded as for the proliferation assay in a 24 well plate at a density of  $5 \times 10^4$  cells per well, in 1 mL of media on PLA and glass controls. The media was then removed and the cells washed carefully with PBS and 1 mL MTT solution added. After 40 minutes the solution was removed and the stain taken up in 300  $\mu\text{L}$  of acidified isopropanol. The eluted MTT in each well was thoroughly mixed and transferred to a 96 well plate. Absorbance was measured at 540 nm and referenced at 630 nm using a BIO-TEK ELx 800 microplate reader.

#### **6.2.8.6 Scanning Electron Microscopy**

Schwann cells cultured on both thin films of the photocurable PLA based material and also the multi-lumen discs were imaged using scanning electron microscopy (SEM). In the thin film experiment Schwann cells were seeded on spin-coated cured PLA films, which had been washed using the ethanol soaking regime to avoid any possible cytotoxic effect influencing cell morphology. The cells were seeded at a density of  $5 \times 10^4$  cells  $\text{ml}^{-1}$  in 1 ml of media and maintained in an incubator for ten days before fixation. In the multilumen disc experiment the same cell number and media quantity was used, however the cells were seeded directly onto the structure before careful addition of the media and maintained for 7 days before fixation for imaging.

Samples were fixed and dehydrated for SEM imaging using an adaptation of the hexamethyldisilazane (HMDS) procedure (Bray, Bagu, and Koegler 1993). The cells were first fixed in glutaraldehyde (2.5 % in PBS buffer) for one hour then washed with PBS and finally distilled water. The samples were then dehydrated using progressively higher concentrations of ethanol (from 35 to 100%) with soaking for 15 minutes at each concentration. The final drying step was completed by soaking in a 1:1 solution of hexamethyldisilazane (HMDS): ethanol for one hour and then 100% HMDS for 5 minutes. Following removal of the HMDS solution the samples were allowed to dry in a fume hood overnight before sputter coating with a thin layer of gold (Emscope SC 500 coater) and imaging using a FEI Sirion FEG SEM with an accelerating voltage of 15 kV and a spot size of three, as determined for the photocurable PLA based structures described in chapter 4.

#### **6.2.8.7 Confocal Imaging of Schwann Cells**

For confocal imaging, films were prepared by ethanol soaking and Schwann cells were seeded at a concentration of  $5 \times 10^4$  cells  $\text{mL}^{-1}$  in 1 mL of media per well. Initial staining for actin filaments (with TRITC-phalloidin) and nuclei (with DAPI) was performed in order to visualize the overall cell morphology as well as the organization of actin filaments within the cell body. This experiment was repeated with additional staining of focal contacts using vinculin monoclonal antibody, in which case an actin cytoskeleton and focal adhesion staining kit (Millipore) was used.

Cells were first fixed in formalin (10% in PBS) for 30 minutes at room temperature. This solution was then removed and phalloidin-TRITC and DAPI were added at a concentration of

1:1000 in PBS and left for 30 minutes. Cells were then washed twice with PBS and mounted on microscopy slides using a fluorescent mounting medium (Cityfluor Glycerol/ PBS solution). Samples were stored in a fridge and observed using a confocal microscope (Carl Zeiss LSM510-META, Germany).

#### **6.2.8.8 Statistical Testing**

Significance was determined between sample and control values using two-tailed Student's *t*-test, and *p*-values are stated where relevant.

#### **6.2.8.9 Quantification of Schwann Cell Purity**

In order to verify the purity of cultured Schwann cells S100 $\beta$  positive immunolabelling was used. Schwann cells were cultured on PLA, glass and laminin coated glass controls. The cells were seeded at a concentration of  $5 \times 10^4$  cells per sample and cultured for 7 days. The samples were then fixed by soaking in paraformaldehyde solution (4% v/v) for 20 minutes and then permeabilized using 0.1% Triton X-100 for a further 20 minutes. The cells were then washed carefully three times for 10 minutes per wash with PBS and blocked with bovine serum albumin (BSA, 7.5% w/v) by soaking for 60 minutes, and incubated with polyclonal rabbit anti-S100 $\beta$  (1:250, Dako, Denmark) in 1% BSA overnight at 4°C. The samples were then washed with PBS three times as before and conjugated with FITC-conjugated secondary anti-rabbit IgG antibody (1:100 in 1% BSA, Vector Laboratories, USA) for 90 minutes and washed again with PBS. Nuclei staining was then performed by the addition of DAPI (1:1000 in PBS). Samples were stored in a refrigerator and observed first using fluorescent microscopy (Carl Zeiss LSM510-META, Germany). DAPI images (nuclei) were taken at  $\lambda_{ex} = 358 \text{ nm}$ / $\lambda_{em} = 461 \text{ nm}$ , and FITC labelled S100 $\beta$  at  $\lambda_{ex} = 495 \text{ nm}$ / $\lambda_{em} = 515 \text{ nm}$ .

### **6.3 Results**

Successful structuring of the photocurable PLA based resin was achieved with both 2PP and micromolding techniques. The biocompatibility of the material as well as its ability to support Schwann cell growth and attachment was assessed *in vitro*. Finally the migration and morphology of Schwann cells was assessed in culture on multi-lumen discs mimicking the native structure of human nerve tissue, in order to investigate potential applications for this technology in the production of improved nerve guidance conduits. A soft lithography

strategy (PDMS stamping) was applied in order to reproduce the original structures produced by 2PP. The use of PDMS replication allows rapid reproduction of the original structure created by 2PP, a time consuming process.

### 6.3.1 Structuring Resolution

The PLA based photocurable resin was again found to give excellent structuring results with the laser system and photoinitiator described in the methods section. Parallel lines with a thickness of approximately 250 nm and a length of 100  $\mu\text{m}$  were fabricated on a silane treated glass surface in order to demonstrate the minimum feature size (see figure 75). The high degree of methacrylate functionality present in the resin due to the low molecular weight and multi-armed nature of the oligomer may facilitates rapid curing and crosslinking, allowing a good resolution. As a comparison, linear PCL based photocurable polymers cured by 2PP with a much higher molecular weight can achieve a resolution of 4  $\mu\text{m}$  (Claeyssens et al. 2009), indicating a 16-fold improvement in terms of resolution.

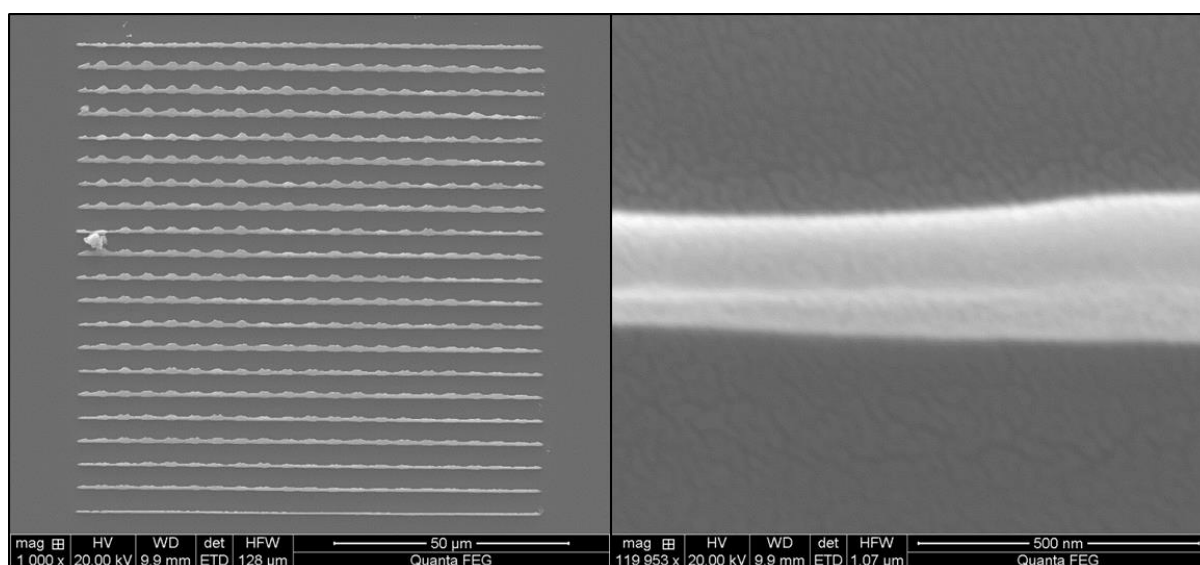


Figure 75: Lines written in photocurable PLA using laser direct write. Close up detail (right) illustrates a line width of around 250 nm.

### 6.3.2 Direct Write of Multi-Lumen Discs

Using laser direct write stackable discs were fabricated as a series of open parallel cylinders, the cylinders possessing a wall thickness of 20  $\mu\text{m}$ , an inner diameter of 100  $\mu\text{m}$  and a height of 300  $\mu\text{m}$ . The open features were incorporated in order to facilitate easy replication by micromoulding technique with polydimethylsiloxane (PDMS). PDMS is a soft elastomeric

material used for micromoulding. The low adhesiveness of the material combined with its softness facilitates easy separation of the produced replicas. By creating multiple negative replicas of the 2PP produced structures in PDMS a large number of stackable discs may be produced in a relatively short time.

In figure 76 a 2PP created disc is shown along with a stacked series of discs replicated by PDMS stamping, it was observed using SEM that the replicated discs reproduced the originals with an overall dimensional accuracy of 99 %, and the wall thickness were within 5 % of the 2PP produced scaffold dimensions. Slight damage is evident on the outer edges of the scaffold however the bulk features and interconnecting pores within remain intact.

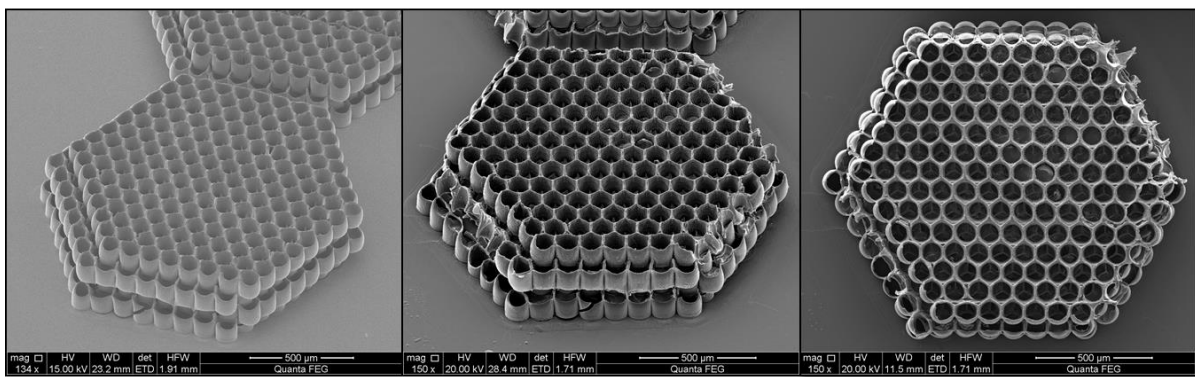


*Figure 76: Stackable photocured PLA structures produced by 2PP (left) and PDMS stamping. (middle and right). Height of individual discs around 100 µm.*

### **6.3.3 Material Genotoxicity Analysis using Comet Assay**

Comet assay examines the degree of genetic damage within cells cultured on a given substrate, giving a clear indication of the genotoxicity of a material. Using electrophoresis damaged genetic material is fluorescently labelled leading to the appearance of a ‘tail’ similar to that of a comet which is examined using a fluorescent microscope.

The comet assay was used to compare two different washing regimes on the spin coated PLA films post cure. Interestingly the material was shown to produce significant genetic damage compared to the glass control when washed in only water ( $p < 0.01$ ) however when soaked in ethanol for 7 days and rinsed for 24 h with water no cytotoxic effect was observed.

Treatment	Comet Tailmoment $\pm$ S.E.M
Control	1.19 $\pm$ 0.07
7 Days soaking in ethanol, 24 h water rinse	1.24 $\pm$ 0.1
7 Days soaking in water	1.75 $\pm$ 0.15

*Table 2: Comet assay comparing ethanol and water treatment of samples and their effect on the degree of genetic damage caused by the photocurable PLA compared to a control. Values repeated as mean of four repeats (n=4)  $\pm$  S.E.M.*

### **6.3.4 Schwann Cell Viability and Adhesion**

In order to verify that Schwann cell viability (and also adhesion) was maintained over extended time periods, the ability of the photocurable PLA to support Schwann cell survival and attachment was therefore examined using a cell counting based proliferation assay, MTT assay and a range of imaging techniques in order to examine cell morphology and focal adhesions.

### **6.3.5 Schwann cell Proliferation Assay**

Schwann cell proliferation was compared on thin films of spin coated PLA (prepared as described in chapter 2) and glass coverslip controls after 1, 3 and 7 days by cell counting and after 2 days using MTT assay. Cell counting was performed using 30 randomly selected areas of 0.015 mm<sup>2</sup> photographed with an optical microscope and the results converted to cell number per mm. At all timepoints in the cell counting experiment the average cell number was higher than on the glass control, however the large error bars typical of cell counting due to the random dispersion of cells prevented statistical significance being determined (in all cases PLA vs Glass  $p > 0.05$ ). Both glass and PLA films supported cell attachment and a similar rate of cell proliferation. The MTT assay at 48 h demonstrated significantly higher Schwann cell numbers on the PLA films compared to the glass control ( $p < 0.01$ ). The results are presented in figure 77. Schwann cells proliferating on and adhering to spin coated films of the photocured PLA are shown in figure 78.

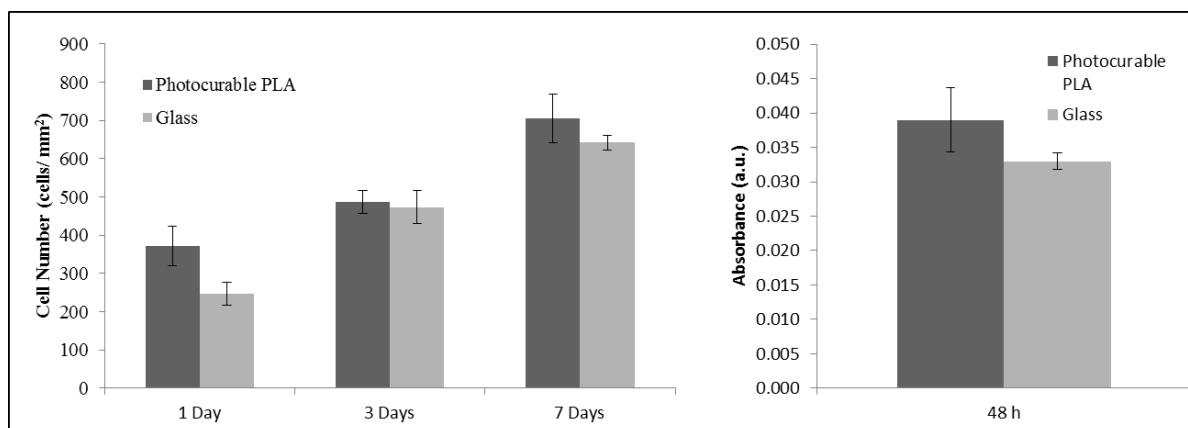


Figure 77: Schwann cell density at 1, 3 and 7 days determined by cell counting using optical microscopy images (left) and MTT assay at 48 h (right) on both photocurable PLA and glass substrates. Similar growth rates are observed on both materials.

Schwann cell adhesion on the photocurable PLA was also compared to linear high molecular weight PLA. Cells were seeded at a density of 50,000 per well in 1 ml of cell culture media and cultured for three days. After 72 h in culture more Schwann cells were clearly visible on the spin coated photocured PLA, as shown in figure 79. Schwann cell proliferation on linear and photocurable PLA was not compared quantitatively, however the visibly higher cell density on the photocurable PLA indicates good cell adhesion on the photocurable polymers,

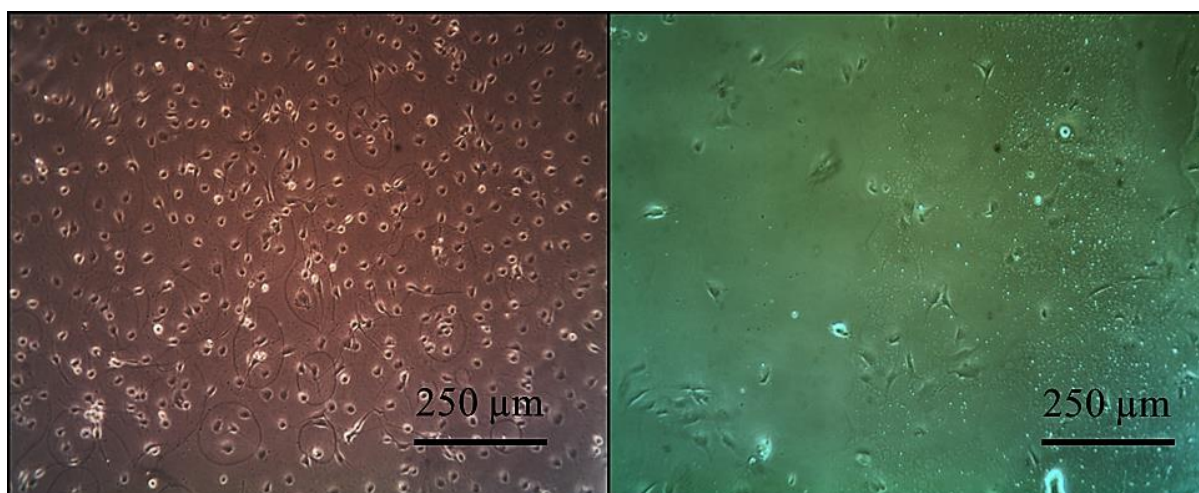


Figure 78: Schwann cells proliferating successfully on spin coated photocurable PLA films at 24, 48 and 72 h. Cells are observed to retain Schwannian morphology indicating the material supports growth and attachment.

in agreement with other results such as figure 13 in chapter 2, where cell adhesion on glass coverslips is compared with adhesion on a glass coverslip control by MTT assay, and figure 65 in chapter 5 where cell adhesion on photocured PLA thin films is compared with a glass control for up to 5 days, by cell counting.

The improved cell adhesion on the cured polymers compared to their linear analogues may be due to the increased swelling of the photocurable polymers due to the high degree of branching in the structure, as examined in chapter 2. The increased water uptake reduces the

hydrophobicity of the photocurable polymers, whereas in the linear polymers the chains are tightly packed and water is unable to penetrate to the same extent. Samples of photocurable PLA were shown to increase to ~9% of their original mass by immersion in water after around three days, whereas the linear PLA reached a maximum value of ~0.5%.



*Figure 79: Phase contrast micrographies of PSC's grown on photocurable (a) and linear PLA (b) for 72h. These typical microscopy images indicate that cells have proliferated more on the photocurable PLA cured film. The morphological appearance of the cells indicates a high affinity for this material compared to the linear polymer, as observed using confocal microscopy below.*

The combination of multiple assays and also optical microscopy imaging supports the hypothesis that the photocurable PLA based resin is capable of supporting Schwann cell adhesion and proliferation over a period of at least 7 days. This suggests that nerve guidance conduits produced from this material would support Schwann cell culture without the need for coating with adhesive proteins or other materials.

### **6.3.6 Analysis of Schwann Cell Morphology**

The suitability of a material for the culture of different cell types may be examined using high resolution confocal microscopy and scanning electron microscopy (SEM). In confocal microscopy specific cellular proteins or regions may be labelled with fluorescent dyes either directly or through a linking molecule such as phalloidin.

Initial confocal microscopy was performed on Schwann cells cultured on the PLA thin films after 7 days in culture. Staining was performed using TRITC-phalloidin (for actin filaments)

and DAPI (for the cell nuclei). Schwann cells were observed to have grown to confluence, and to exhibit a range of different morphologies on the PLA based material. Predominantly cells adopted a more flattened tri-polar morphology which is not commonly encountered with Schwann cells. Irrespective of this the cells displayed organized actin filaments running throughout the cellular body from the nucleus through the plasma membrane (as can be observed in figure 80) indicating a structured cytoskeleton and adhesion on the polymer surface. Cells were also examined exhibiting the more typical elongated bi-polar Schwann cell morphology, indicated by arrow 'b' in figure 80.

Potential contamination of the Schwann cell culture with fibroblasts during the extraction procedure would give a possible explanation for the fibroblast like nature of the cells observed using the confocal microscope (Schmidt and Leach 2003). To quantify their phenotypic purity the Schwann cells were immunolabelled with FITC for S100 $\beta$  glial marker and also stained with DAPI, to allow Schwann and total cell count to be performed.

Using a fluorescent microscope the cells were then imaged and cell counting was carried out on the DAPI and S100 $\beta$  images in order to determine the Schwann cell purity. On the PLA surface Schwann cell purity was  $99.2 \pm 0.4\%$ , on the glass surface  $99.6 \pm 0.2\%$  and on the poly-L-lysine surface  $99.3 \pm 0.9\%$ , indicating that the culture consisted predominantly of Schwann cells, with no significant difference between the three surfaces ( $p > 0.05$ ). The Schwann cells cultured on the poly-L-lysine coated surface exhibit a more commonly

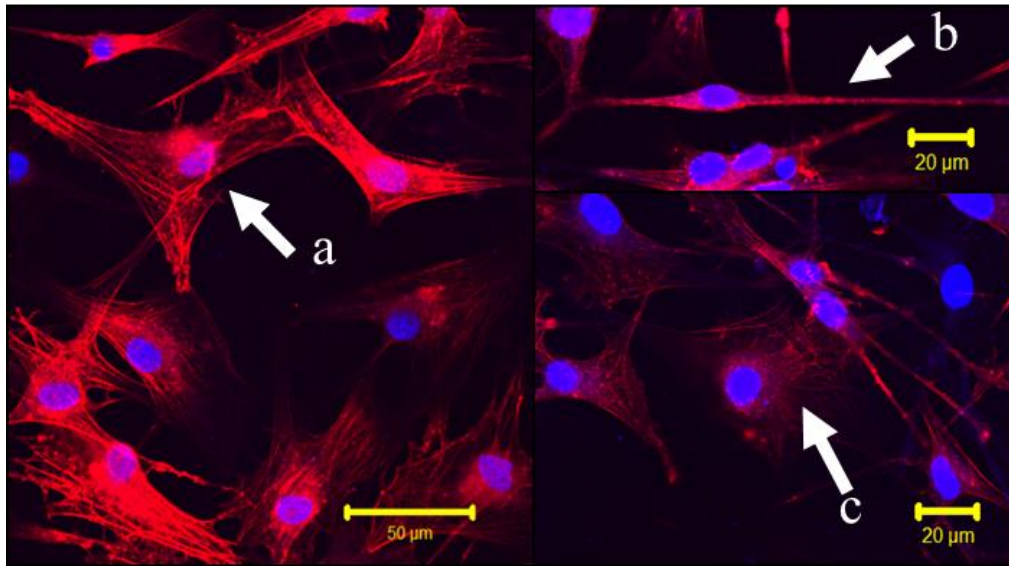


*Figure 80: Primary Schwann cells cultured on photocurable PLA for 7 days stained for actin (red) and nuclei (blue). Arrows indicate Schwann cells with tripolar morphology (a), elongated bi-polar morphology (b) and flattened morphology with actin filaments extending from the PLA surface through the cytoskeleton to the nucleus (c). The cell indicated by arrow 'b' is the only cell exhibiting typical Schwann cell morphology.*

observed spindle like morphology and the cells form a 'swirling' pattern on the substrate, (also described by Kreider et al. (Kreider et al. 1981)). Schwann cells cultured on the PLA and glass surfaces however exhibit the more heterogeneous morphology observed in the confocal experiment. The S100 $\beta$  labelled cells are shown in figure 81.

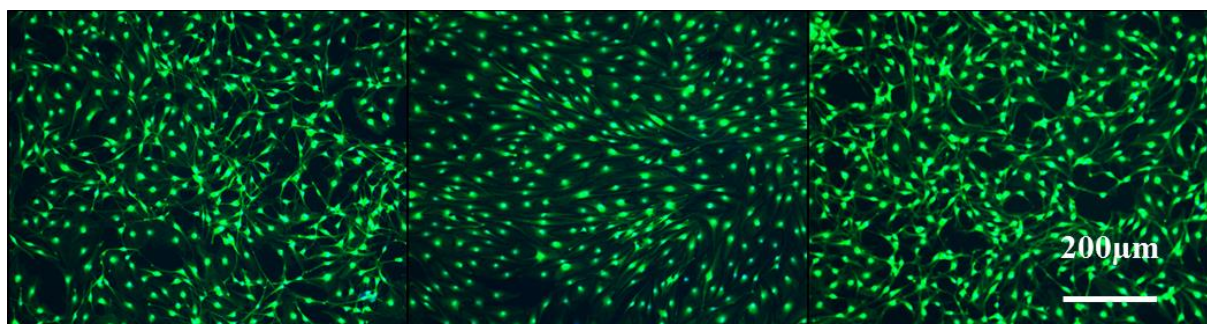


*Figure 81: Primary Schwann cells cultured on glass, poly-L-lysine coated TCP and photocurable PLA for 7 days visualised by S-100 $\beta$  immunostaining.*

Schwann cells were also observed after ten days in culture on PLA thin films after fixing with HDMS solution and gold coating. The cells were observed to be highly confluent, and exhibit

a mixture of both flattened and spindle like morphology. The cells exhibit a high degree of spreading, with a large cytoplasmic area and clear adhesions on the surface and cell to cell contacts, indicating strong adhesion on this material. Extensions present between the Schwann cells (inset figure 82), also observed in figure 84 have been suggested to carry information such as signals for directional alignment between cells (Ahmed and Brown 1999). The presence of aligned neurites extending from NG108 cells was demonstrated by expression of  $\beta$ -tubulin III in chapter 5.

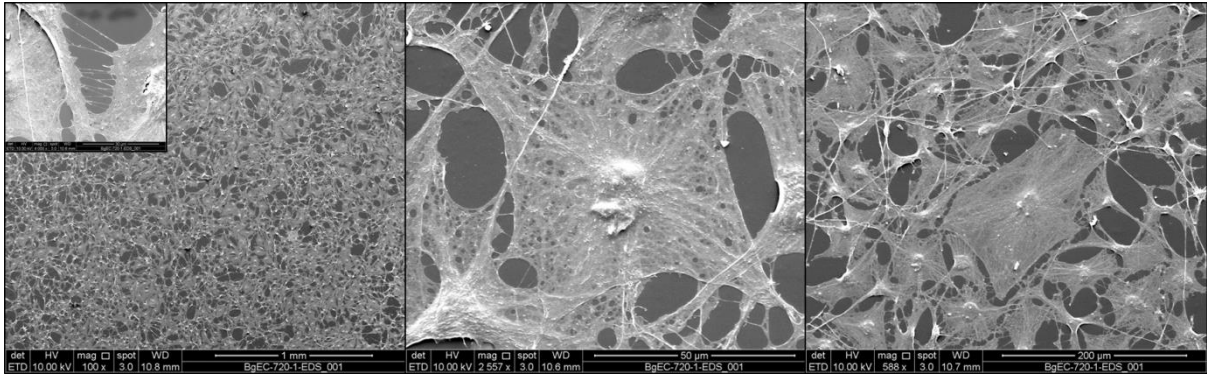


*Figure 82: Primary Schwann cells cultured on photocurable PLA for 10 days imaged by SEM. The cells are highly confluent and the high degree of spreading indicates that the cells are capable of attaching to the photocured PLA surface.*

To further verify adhesion of the Schwann cells co-staining of actin and vinculin was performed. Discreet sub 1  $\mu$ m regions corresponding to focal adhesions were observed in the central body of the cells, with a mainly orthogonal arrangement of actin filaments. Initial imaging was performed using an axon microscope, which allowed the observation of a confluent layer of Schwann cells with focal adhesions localised to the central cell body (see figure 83).

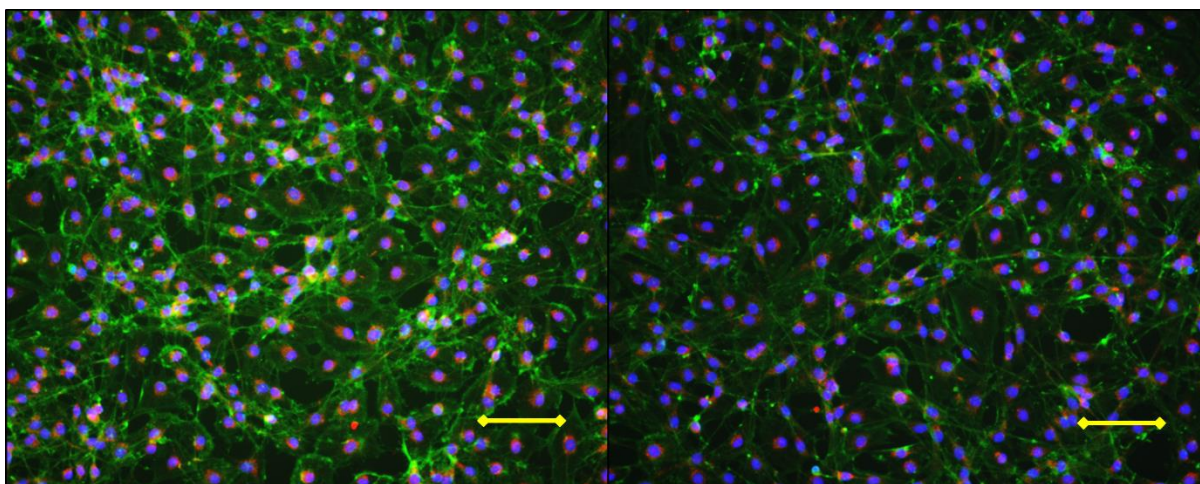


*Figure 83: Confluent Schwann cells proliferating on thin films of photocured PLA. The cells were stained with FITC-phalloidin for actin (green) and vinculin for focal adhesions (red). Nuclei were stained with DAPI (blue). Scale bars 125 μm.*

In order to examine the precise distribution of the focal adhesions a high resolution confocal microscope was used. This allowed direct imaging of the focal adhesions, observed as sub-micron punctate regions in the central cell body, as seen in figure 84 confirming the formation of focal adhesions on the photocured PLA.

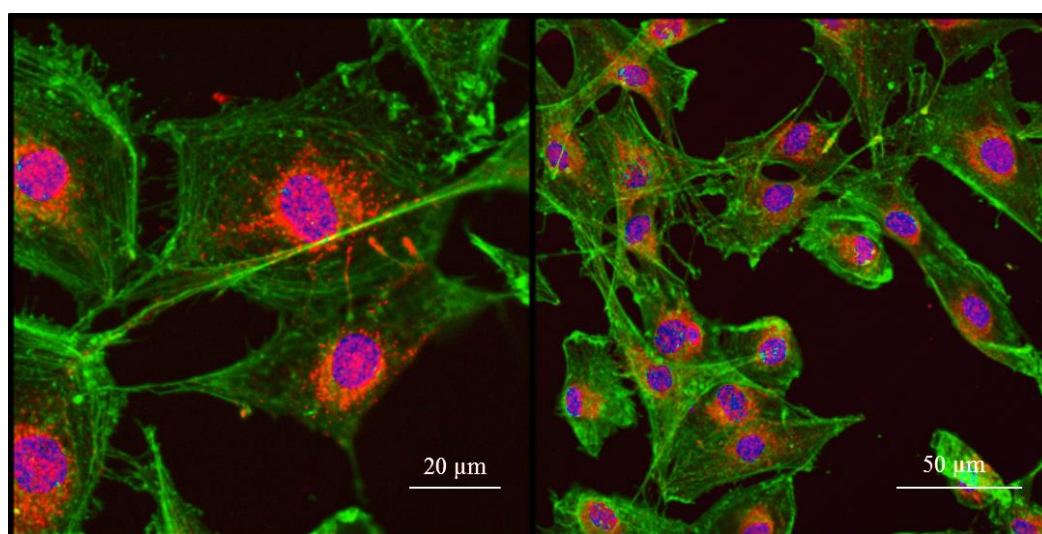


*Figure 84: Schwann cells displaying nuclei (blue), actin filaments (green) and focal adhesions (red).*

### 6.3.7 Schwann Cell Culture on Stackable Multi-Lumen Discs

Loading of Schwann cells into the PLA discs created by PDMS stamping was visualized using SEM. Cells were seeded directly onto the structures before the addition of media, then dehydrated and fixed for SEM imaging. After seven days in culture the majority of lumens

were filled with Schwann cells. The Schwann cells exhibited a mixture of morphologies, with flattened cells migrating along the intraluminal walls and ‘spindle like’ bipolar and tripolar cells aligning with the features of the scaffold and spanning from the top to the bottom of the cavities (see figure 85). It is interesting to note that Schwann cells cultured on flat photocured PLA surfaces appear to exhibit the more flattened fibroblast like morphology described previously, whereas those existing on the three dimensional scaffold features display much more variation in morphology. This extent of this effect was not quantified but would be an interesting point for further investigation. It is possible that the 3D environment forces the Schwann cells to adopt a different morphology in order to attach securely to the surface, or that the structure provides some protection for the bipolar Schwann cells (which are typically less adherent (Kreider et al. 1981)) from flow forces experienced during culture caused by pipetting of media or washing with PBS prior to fixation.

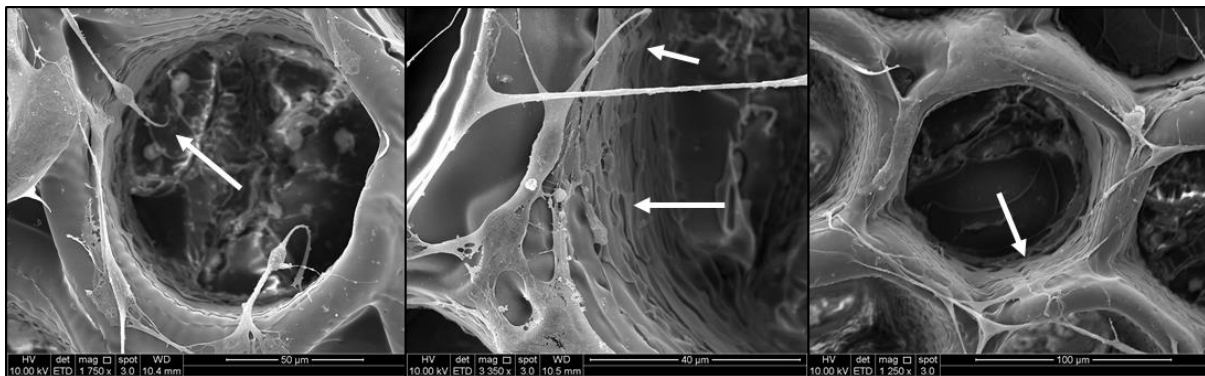


*Figure 85: Individual microchannels in PLA multi-lumen disc loaded with Schwann cells after 7 days in culture.*

One of the most important functions of Schwann cells within nerve conduits is the excretion of NGF. Devices which contain NGF within the polymer matrix, slowly releasing the factor over time have been suggested as a strategy to mimic the action of Schwann cells. This would eliminate the need to harvest Schwann cells from the patient (or a donor, leading to immune rejection issues) for incorporation into the device pre-surgery. The limitations of NGF incorporation in the polymer matrix include loss of activity over time or during the sterilization process (Ruiter et al. 2009). The incorporation of living Schwann cells allows a constant and steady release of these factors providing cell viability is maintained. This observation also indicates that Schwann cell migration into the multi-lumen conduit would readily occur. The SEM images shown in figure 85 indicate that the PLA discs support Schwann cell growth, adhesion and proliferation for at least 7 days.

## 6.4 Discussion

In this chapter a combined approach to scaffold fabrication was demonstrated, using a photocurable PLA based resin for the fabrication of microdevices by 2PP and furthermore for replication of these devices by PDMS stamping and UV curing. Using the same photoinitiator the material was cured (cross-linked) by both ultraviolet light (by one photon processes) and infra-red (IR) radiation (by two photon initiation). A resolution of approximately 250 nm was determined for curing of the resin using the described laser direct write system and initiator (Irgacure 369).

The genotoxicity of the photocurable material was assessed using Comet assay. The importance of proper sample pre-treatment, by soaking in ethanol for seven days and rinsing in distilled water prior to cell culture was clearly demonstrated by this technique. The likely cause of the genotoxicity demonstrated by the Comet assay for the material not soaked in ethanol is remaining photoinitiator. This finding is in agreement with results reported by other authors (Ovsianikov, Malinauskas, Schlie, Chichkov, Gittard, Narayan, Löbner, et al. 2011). Soaking of samples in a suitable solvent prior to cell culture in order to remove trace chemicals remaining from the fabrication process is not unique to microstereolithography, and has been demonstrated to affect cell attachment on scaffolds prepared by electrospinning, a technique widely explored by the tissue engineering community and also used in clinical applications (Murray-Dunning et al. 2011).

The inclusion of Schwann cells into nerve guidance conduits has been shown to improve neural regeneration distance (Tohill et al. 2004). The ability of the photocurable PLA based material to support Schwann cell growth and proliferation was investigated using a range of techniques. Schwann cell purity after 7 days in culture on thin films of the cross-linked material was quantified by staining for a specific Schwann cell marker (S100 $\beta$ ) and compared to both glass and poly-L-lysine controls. Schwann cell purity was determined to be around 99.5% on all surfaces with no significant difference between batches.

A thorough analysis of Schwann cell morphology was also performed using a combination of optical microscopy, SEM and confocal imaging. The cells were observed to adopt a both bipolar and triplicate morphology on the material. The more fibroblast like triplicate cells were shown to adopt a 'wreath-like' organization of actin filaments around the nucleus and central cell body with focal adhesions (visualized by fluorescent labelling of vinculin, a component of focal adhesions) around the central and intermediate regions of the cell. As

discussed in detail by Weiner *et al.* (Weiner *et al.* 2001) this indicates that the Schwann cells exhibit a high affinity for the PLA based material.

The ability of the photocurable PLA material to support Schwann cell attachment indicates that this or similar materials may be suitable for the creation of nerve guidance conduits. The fabrication of stackable discs by 2PP and their replication using PDMS stamping was shown to be an efficient method for the production of devices that may interact with Schwann cells in a way that is beneficial for nerve regeneration. In culture conditions Schwann cells seeded on the stackable discs migrated throughout the structure and filled the majority of the cylindrical voids, expressing both a flattened morphology and adhering to the inner walls of the tubes and also expressing a more Schwann cell like bipolar morphology when spanning the length of the tubes.

From a materials perspective polylactic acid (PLA) possesses an intermediate degradation rate, degrading more slowly than polycaprolactone (PCL) but more rapidly than poly(lactide-co-glycolide) (PLGA) or polyglycolide (PGA). PLGA is in fact a copolymer of lactic and glycolic acid, and the degradation rate increases with increasing glycolic acid content, due to the susceptibility of the glycolic acid monomer to ester hydrolysis (Anderson and Shive 1997). The degradation rate of the photocurable PLA, and other photocurable biomaterials produced using the same strategies requires further investigation, however similar photocurable materials have been shown to undergo degradation by hydrolysis *in vitro* (Mizutani and Matsuda 2002b).

FDA approved nerve guidance conduits in current clinical use have been produced from natural materials (type I collagen, porcine small intestinal sub mucosa (SIS)) and various synthetic polymers (polyvinyl alcohol (PVA), PGA and poly(DL-lactide- $\epsilon$ -caprolactone)/polycaprolactone) (Kehoe, Zhang, and Boyd 2012). Although the synthetic devices overcome the rejection issues and natural variability of natural materials some progress is still to be made. Conduits made from PGA for example suffer from a high degradation rate and build up of acidic breakdown products leading to necrosis (Schlosshauer *et al.* 2006). Despite these limitations however PGA based nerve guidance conduit (Neurotube®) was shown in random clinical trials to be as effective as the gold standard for defects up to 20 mm in length (Kehoe, Zhang, and Boyd 2012). The poly(lactide-co-caprolactone) based conduit Neurolac®, containing in part the same monomeric units as the photocurable PLA in this study have been shown to be as effective as the gold standard in defects up to 20 mm in size in humans, but do suffer limitations due to the high stiffness of the material leading to ruptures at the implant/

nerve surface due to the poor match in mechanical properties (Kehoe, Zhang, and Boyd 2012).

This issue would likely occur in conduits prepared from the photocurable PLA also due to the stiffness of linear PLA and the high degree of cross linking. If the stackable discs of photocured PLA were filled in a flexible tube this may be alleviated to a degree. Photocurable and bioresorbable elastomers such as trimethylene carbonate have also been prepared which would provide a more suitable mechanical match to the properties of nerve tissue (Bat et al. 2011).

## **6.5 Conclusions**

The incorporation of multiple lumens into nerve guidance conduits may improve the distance over which functional recovery of transected peripheral nerves is possible. This is due to increased surface area, over which a) the resulting fibrin matrix that develops within the conduit is protected and b) Schwann cells may attach, guiding axon regeneration. Furthermore, the presence of multiple lumens may guide axon regeneration the by contact guidance. The production of these multilumen devices can be accomplished with unparalleled resolution using 2PP, however the process is time consuming. The use of PDMS for the replication of these structures allows the rapid reproduction of these discs. The accuracy of the PDMS based soft lithography technique was shown to be within 99 % of the original overall dimensions, and the internal walls did not deviate from the original thickness by more than 5 %.

The loading of Schwann cells into nerve guidance conduits has been widely investigated and shown to result in improved recovery. The ability of the photocurable PLA based material to support Schwann cell adhesion and proliferation was demonstrated by a range of different assays and imaging techniques. Furthermore the material was shown to be non-genotoxic by Comet assay, an important feature for biomedical materials. Photocurable PLA based discs loaded with Schwann cells were prepared and imaged using scanning electron microscopy after 7 days.

In summary the photocurable PLA resin has been shown to be a suitable material for the creation of Schwann cell loaded nerve guidance conduits, being non-genotoxic and Schwann cell adhesive. The use of both 2PP and PDMS replication has been shown to be an effective method for the microstructuring of experimental nerve repair devices. Further optimization of both the device geometry and also material mechanical properties, as well as a thorough

analysis of the material degradation rate *in vivo* would be required to take this technology to the clinic.

# Chapter 7: Thesis Summary

---

## **Abstract**

In this short chapter the original rationale behind the research presented is examined in light of the results described in the preceding chapters. Future work based on the techniques established within the studies performed to date is suggested and progress towards taking this technology towards real world clinical applications is discussed.

## **7.1 Microfabrication of Designer Tissue Engineering Devices**

The fabrication of devices with user defined architecture in a CAD-CAM fashion, from materials which can be customised in terms of mechanical and physical properties through the use of selected copolymers allows total control over the three dimensional environment experienced by the cells within (although the influence of mechanical properties was not studied in this thesis). Cells have been demonstrated to be directly influenced by their surrounding environment, completely changing their behaviour depending on both the three-dimensional environment in which they are cultured (Abbott 2003), and also the modulus or ‘elasticity’ of the substrate on which they are cultured (Engler et al. 2006).

In their native tissue cells are supported within the extracellular matrix (ECM), a network of proteins such as laminin, collagen and elastin that acts as a support structure and it is these proteins that control the mechanical properties of the tissue. The activation of receptors for these proteins within cells has a direct influence on cellular behaviour. In one study, matrix elasticity was shown to influence stem cell differentiation (Engler et al. 2006). This is suggested to occur by the contraction of the transmembrane protein actomyosin, acting as a spring through which the cell can ‘pull’ against the substrate in order to determine the elastic response (Even-Ram, Artym, and Yamada 2006).

Key properties such as the degradation rate of tissue scaffolds are also important in order to prevent the support structure resorbing before the growing tissue is fully formed and capable of maintaining structural integrity, or conversely remaining intact too long and inhibiting

tissue growth. Manipulation of polymer degradation by blending or copolymerization is commonly employed in order to manipulate degradation characteristics, so that degradation occurs on a timescale that matches that of tissue growth (Kim et al. 2003).

The creation of scaffolds with user defined structure by projection microstereolithography was demonstrated in chapter 3, and has been successfully explored by other authors in order to demonstrate better cell distribution compared to bulk porous structures (Melchels et al. 2011). In chapter 3 and chapter 6 the preparation of multi-lumen structures for nerve guidance conduits was presented demonstrating how high surface area structures may be used to achieve high loadings of adherent Schwann cells, demonstrated to aid in peripheral nerve recovery (Ruiter et al. 2009). The demonstrated adhesion of Schwann cells on the PLA based material eliminates the need for coating of the internal features with proteins such as laminin, as demonstrated by some authors working with linear PLA (Rangappa et al. 2000). In chapter 5 the preparation of cell delivery devices with user defined structure and high porosity was explored and cell infiltration into the scaffolds was demonstrated, as well as the effect of structural characteristics on cell alignment (Melissinaki et al. 2011). Microfabricated self-assembled scaffolds produced by two photon polymerization presents a novel application of this technology.

## **7.2 Custom Polymers and Designer Biomaterials for Tissue Engineering**

Two photocurable resins based on bioresorbable polymers currently approved for internal medical use were prepared according to a published protocol as a proof of concept for this type of material (Gill and Claeysens 2011). The resins were shown to be curable, biocompatible and capable of supporting cell attachment. Excellent structuring results were achieved with the different microstereolithography systems used, and structuring by two photon polymerization with a resolution of around 250 nm with the polylactic acid (PLA) based resin was achieved.

## **7.3 Device Fabrication using Microstereolithography**

The key feature linking the applications of microstereolithography in this thesis has been the creation of a microenvironment where a defined three-dimensional structure has offered clear advantages over existing technologies which have so far been demonstrated. In the development of improved nerve guidance conduits, the enhanced microstructure has allowed

greater cell loading and alignment when compared with hollow tube based devices (Koroleva et al. 2012). In the development of injectable cell carrier devices the benefit achieved is higher potential cell loading and mechanical protection compared to simple microspherical cell carriers (Melissinaki et al. 2011; Bible et al. 2009b). The microfabricated rings for corneal repair will contain a physically protected space for a self-renewing population of stem cells, the lack of which is often a cause of failure for the current therapy in which a membrane is loaded with cells before degrading and depositing the cells onto the cornea (Deshpande et al. 2010).

Microfabrication has been attracting growing interest in recent years due to the ability to accurately mimic the structure of native tissues within the human body (Berthiaume, Maguire, and Yarmush 2011). The ability to recreate body sections from medical imaging for the purpose of prostheses, surgical planning and potentially tissue scaffolds and other implantable devices is becoming a reality (Rengier et al. 2010). Two photon polymerization possesses clear advantages over competing techniques including the unparalleled resolution and in-volume true three dimensional writing ability which allow unique micro-devices to be created according to a computer model (Narayan et al. 2010; Ovsianikov, Chichkov, Adunka, et al. 2007; Schizas et al. 2010). Progress in the development of suitable materials and initiators (Lemercier et al. 2006), improvements in fabrication time, efficiency and cost (Wang et al. 2002; Hsieh et al. 2010) and efforts to address concerns regarding the biocompatibility of photoinitiators take this technology even closer to the clinic.

#### **7.4 Future Work**

The characterisation of these resins was only taken to a very preliminary level. Further work is required to examine in detail the molecular characteristics of these materials, characterising fully the molecular weight, polydispersity and extent of functionalization of the resins. Potential exists for the preparation of a vast range of copolymers and block copolymers, taking into account polymer miscibility. Varying the functionality of the initiator in order to create multi-armed oligomers and careful control over molecular weight and functionalization with different cross-linkable groups would allow the creation of resins with enhanced curing characteristics and final mechanical properties (Matsuda and Mizutani 2000; Matsuda, Mizutani, and Arnold 2000).

Advanced techniques for the selective spatial patterning of proteins within hydrogels, such as the use of using two photon labile protecting groups which break down upon two photon initiation to anchor growth factors to an agarose substrate allow the direct writing of cell adhesive networks in three dimensions (Luo and Shoichet 2004; Wylie and Shoichet 2011). Another possibility currently being explored is patterned surface function of polymeric devices in order to enhance cell attachment and survival. Functionalization of the ring based micropockets described in chapter 3 with surface-bound proteins is being explored in order to create biochemically enhanced limbal stem cell niches, with the potential of taking this technology to the clinic.

The work presented in this thesis has demonstrated that microfabrication with photocurable polymers based on materials already approved for internal medical use is possible by both one and two photon methods with excellent structuring results. Several potential applications have been investigated and it has been shown how this technology may be used to address real world healthcare problems such as traumatic nerve injury and corneal blindness. Remaining research challenges include i) the optimisation of material characteristics, by the development of copolymers suitable for their selected applications ii) determination of the necessary structural features for each selected application iii) optimisation of the fabrication process in terms of fabrication time and equipment cost (through development of suitable initiators and low cost microlasers) and iv) an understanding of the translational framework in order to bring these products to the clinic.

# References

---

- Abbasi, F., H. Mirzadeh, and A. A. Katbab. 2002. "Bulk and surface modification of silicone rubber for biomedical applications." *Polymer International* no. 51 (10):882-888.
- Abbott, A. 2003. "Cell culture: Biology's new dimension." *Nature* no. 424 (6951):870-872.
- Ahmed, Z., and R. A. Brown. 1999. "Adhesion, alignment, and migration of cultured Schwann cells on ultrathin fibronectin fibres." *Cell Motility and the Cytoskeleton* no. 42 (4):331-343.
- Albu, S., G. Babighian, and F. Trabalzini. 1998. "Prognostic factors in tympanoplasty." *American Journal of Otology* no. 19 (2):136-140.
- Amass, W., A. Amass, and B. Tighe. 1998. "A review of biodegradable polymers: Uses, current developments in the synthesis and characterization of biodegradable polyesters, blends of biodegradable polymers and recent advances in biodegradation studies." *Polymer International* no. 47 (2):89-144.
- Anderson, J. M., and M. S. Shive. 1997. "Biodegradation and biocompatibility of PLA and PLGA microspheres." *Advanced Drug Delivery Reviews* no. 28 (1):5-24.
- Arcaute, K., L. Ochoa, B. K. Mann, and R. B. Wicker. 2005. "Stereolithography of PEG hydrogel multi-lumen nerve regeneration conduits." *Manufacturing Engineering and Materials Handling* no 16 (0):161-167.
- Ashammakhi, N., E. A. Makela, P. Tormala, T. Waris, and P. Rokkanen. 2000. "Effect of self-reinforced polyglycolide membrane on osteogenesis: an experimental study in rats." *European Journal of Plastic Surgery* no. 23 (8):423-428.
- Assouline, J. G., P. Bosch, R. Lim, I. S. Kim, R. Jensen, and N. J. Pantazis. 1987. "Rat Astrocytes and Schwann-Cells in Culture Synthesize Nerve Growth Factor-Like Neurite-Promoting Factors." *Developmental Brain Research* no. 31 (1):103-118.
- Atala, A., S. B. Bauer, S. Soker, J. J. Yoo, and A. B. Retik. 2006. "Tissue-engineered autologous bladders for patients needing cystoplasty." *The Lancet* no. 367 (9518):1241-1246.

- Awwad, H. K., M. El Naggar, N. Mocktar, and M. Barsoum. 1986. "Intercapillary distance measurement as an indicator of hypoxia in carcinoma of the cervix uteri." *International Journal of Radiation Oncology Biology Physics* no. 12 (8):1329-1333.
- Bain, C. D., and G. M. Whitesides. 1988. "Depth sensitivity of wetting - monolayers of omega-mercapto ethers on gold ." *Journal of the American Chemical Society* no. 110 (17):5897-5898.
- Balakrishnan, H., A. Hassan, M. Imran, and M. U. Wahit. 2011. "Aging of Toughened Polylactic Acid Nanocomposites: Water Absorption, Hygrothermal Degradation and Soil Burial Analysis." *Journal of Polymers and the Environment* no. 19 (4):863-875.
- Baldeck, P. L., Olivier Stephan, and C. Andraud. 2010. "Tri-dimensional micro-structuration of materials by two-photon induced photochemistry." *Basics and Applications of Photopolymerization Reactions* no. 3 (1) 199-220.
- Barry, J. J. A., D. Howard, K. M. Shakesheff, S. M. Howdle, and M. R. Alexander. 2006. "Using a core-sheath distribution of surface chemistry through 3D tissue engineering scaffolds to control cell ingress." *Advanced Materials* no. 18 (11):1406-1410
- Bat, E., T. G. van Kooten, F. J. Jan, and D. W. Grijpma. 2011. "Resorbable elastomeric networks prepared by photocrosslinking of high-molecular-weight poly(trimethylene carbonate) with photoinitiators and poly(trimethylene carbonate) macromers as crosslinking aids." *Acta Biomaterialia* no. 7 (5):1939-1948.
- Baudis, S., C. Heller, R. Liska, J. Stampfl, H. Bergmeister, and G. Weigel. 2009. "(Meth)Acrylate-Based Photoelastomers as Tailored Biomaterials for Artificial Vascular Grafts." *Journal of Polymer Science Part a-Polymer Chemistry* no. 47 (10):2664-2676.
- Belfield, K. D., X. B. Ren, E. W. Van Stryland, D. J. Hagan, V. Dubikovsky, and E. J. Miesak. 2000. "Near-IR two-photon photoinitiated polymerization using a fluorone/amine initiating system." *Journal of the American Chemical Society* no. 122 (6):1217-1218.
- Bell, J. H. A., and J. W. Haycock. 2012. "Next Generation Nerve Guides: Materials, Fabrication, Growth Factors, and Cell Delivery." *Tissue Engineering Part B-Reviews* no. 18 (2):116-128.
- Bellucci, D., V. Cannillo, A. Cattini, and A. Sola. 2011. "A new generation of scaffolds for bone tissue engineering." *Industrial Ceramics* no. 31 (1):59-62.

- Berthiaume, F., T. J. Maguire, and M. L. Yarmush. 2011. "Tissue Engineering and Regenerative Medicine: History, Progress, and Challenges." *Annual Review of Chemical and Biomolecular Engineering* no. 2 (1):403-430.
- Bhuiyan, B., R. J. Winfield, S. O'Brien, and G. M. Crean. 2007. "Pattern generation using axicon lens beam shaping in two-photon polymerisation." *Applied Surface Science* no. 254 (4):841-844.
- Bible, E., D. Y. S. Chau, M. R. Alexander, J. Price, K. M. Shakesheff, and M. Modo. 2009a. "Attachment of stem cells to scaffold particles for intra-cerebral transplantation." *Nature Protocols* no. 4 (10):1440-1453.
- . 2009b. "The support of neural stem cells transplanted into stroke-induced brain cavities by PLGA particles." *Biomaterials* no. 30 (16):2985-2994.
- Brauker, J. H., V. E. Carrbrendel, L. A. Martinson, J. Crudele, W. D. Johnston, and R. C. Johnson. 1995. "Neovascularization of synthetic membranes directed by membrane microarchitecture." *Journal of Biomedical Materials Research* no. 29 (12):1517-1524.
- Bray, D. F., J. Bagu, and P. Koegler. 1993. "Comparison of hexamethyldisilazane (HMDS), Peldri II, and critical-point drying methods for scanning electron microscopy of biological specimens." *Microscopy Research and Technique* no. 26 (6):489-495.
- Bunge, R. P. 1994. "The role of the Schwann-cell in trophic support and regeneration." *Journal of Neurology* no. 242 (1):S19-S21.
- Cai, Q., J. A. Yang, J. Z. Bei, and S. G. Wang. 2002. "A novel porous cells scaffold made of polylactide-dextran blend by combining phase-separation and particle-leaching techniques." *Biomaterials* no. 23 (23):4483-4492.
- Cajal, S.R., and R.M. May. 1928. "*Degeneration & Regeneration of the Nervous System.*" *Oxford University Press* no. 2 (1):558-582.
- Chen, C. S., M. Mrksich, S. Huang, G. M. Whitesides, and D. E. Ingber. 1997. "Geometric control of cell life and death." *Science* no. 276 (5317):1425-1428.
- . 1998. "Micropatterned surfaces for control of cell shape, position, and function." *Biotechnology Progress* no. 14 (3):356-363.
- Chen, M. Q., X. Wang, Z. Y. Ye, Y. Zhang, Y. Zhou, and W. S. Tan. 2011. "A modular approach to the engineering of a centimeter-sized bone tissue construct with human amniotic mesenchymal stem cells-laden microcarriers." *Biomaterials* no. 32 (30):7532-7542.

- Chin, V. I., P. Taupin, S. Sanga, J. Scheel, F. H. Gage, and S. N. Bhatia. 2004. "Microfabricated platform for studying stem cell fates." *Biotechnology and Bioengineering* no. 88 (3):399-415.
- Choi, J. W., E. MacDonald, and R. Wicker. "Multi-material microstereolithography." *International Journal of Advanced Manufacturing Technology* no. 49 (5-8):543-551.
- Choi, J. W., R. B. Wicker, S. H. Cho, C. S. Ha, and S. H. Lee. 2009. "Cure depth control for complex 3D microstructure fabrication in dynamic mask projection microstereolithography." *Rapid Prototyping Journal* no. 15 (1):59-70.
- Choi, J. W., R. Wicker, S. H. Lee, K. H. Choi, C. S. Ha, and I. Chung. 2009. "Fabrication of 3D biocompatible/biodegradable micro-scaffolds using dynamic mask projection microstereolithography." *Journal of Materials Processing Technology* no. 209 (15-16):5494-5503.
- Choi, S. H., and T. G. Park. 2002. "Synthesis and characterization of elastic PLGA/PCL/PLGA tri-block copolymers." *Journal of Biomaterials Science-Polymer Edition* no. 13 (10):1163-1173.
- Chua, C. K., K. F. Leong, C. M. Cheah, and S. W. Chua. 2003a. "Development of a tissue engineering scaffold structure library for rapid prototyping. Part 1: Investigation and classification." *International Journal of Advanced Manufacturing Technology* no. 21 (4):291-301.
- . 2003b. "Development of a tissue engineering scaffold structure library for rapid prototyping. Part 2: Parametric library and assembly program." *International Journal of Advanced Manufacturing Technology* no. 21 (4):302-312.
- Claeysens, F., E. A. Hasan, A. Gaidukeviciute, D. S. Achilleos, A. Ranella, C. Reinhardt, A. Ovsianikov, S. Xiao, C. Fotakis, M. Vamvakaki, B. N. Chichkov, and M. Farsari. 2009. "Three-Dimensional Biodegradable Structures Fabricated by Two-Photon Polymerization." *Langmuir* no. 25 (5):3219-3223.
- Cohn, D., and A. F. Salomon. 2005. "Designing biodegradable multiblock PCL/PLA thermoplastic elastomers." *Biomaterials* no. 26 (15):2297-2305.
- Colletti, V., and F. G. Fiorino. 1999. "Malleus-to-footplate prosthetic interposition: Experience with 265 patients." *Otolaryngology-Head and Neck Surgery* no. 120 (3):437-444.
- Collins, A. R. 2004. "The comet assay for DNA damage and repair - Principles, applications, and limitations." *Molecular Biotechnology* no. 26 (3):249-261.

- Colton, C. K. 1995. "Implantable biohybrid artificial organs." *Cell Transplantation* no. 4 (4):415-436.
- Coster, D J, R K Aggarwal, and K A Williams. 1995. "Surgical management of ocular surface disorders using conjunctival and stem cell allografts." *British Journal of Ophthalmology* no. 79 (11):977-982.
- Cotsarelis, G., S. Z. Cheng, G. Dong, T. T. Sun, and R. M. Lavker. 1989. "Existence of  $\mu$ ow-cycling limbal epithelial basal cells that can be preferentially stimulated to proliferate: Implications on epithelial stem cells." *Cell* no. 57 (2):201-209.
- Coutu, D. L., A. M. Yousefi, and J. Galipeau. 2009. "Three-Dimensional Porous Scaffolds at the Crossroads of Tissue Engineering and Cell-Based Gene Therapy." *Journal of Cellular Biochemistry* no. 108 (3):537-546.
- Daud, M. F., K. C. Pawar, F. Claeysens, A. J. Ryan, and J. W. Haycock. 2012. "An aligned 3D neuronal-glia co-culture model for peripheral nerve studies." *Biomaterials* no. 33 (25):5901-13.
- Deshpande, P., R. McKean, K. A. Blackwood, R. A. Senior, A. Ogunbanjo, A. J. Ryan, and S. MacNeil. 2010. "Using poly(lactide-co-glycolide) electrospun scaffolds to deliver cultured epithelial cells to the cornea." *Regenerative Medicine* no. 5 (3):395-401.
- Dike, L. E., C. S. Chen, M. Mrksich, J. Tien, G. M. Whitesides, and D. E. Ingber. 1999. "Geometric control of switching between growth, apoptosis, and differentiation during angiogenesis using micropatterned substrates." *In Vitro Cellular & Developmental Biology-Animal* no. 35 (8):441-448.
- Doraiswamy, A., C. Jin, R. J. Narayan, P. Mageswaran, P. Mente, R. Modi, R. Auyeung, D. B. Chrisey, A. Ovsianikov, and B. Chichkov. 2006. "Two photon induced polymerization of organic-inorganic hybrid biomaterials for microstructured medical devices." *Acta Biomaterialia* no. 2 (3):267-275.
- Doraiswamy, A., T. Patz, R. Narayan, B. Chichkov, A. Ovsianikov, R. Houbertz, R. Modi, R. Auyeung, and D. B. Chrisey. 2005. "Biocompatibility of CAD/CAM ORMOCER polymer scaffold structures." *Nanoscale Materials Science in Biology and Medicine* no. 845 (1):51-56.
- Dravida, S., S. Gaddipati, M. Griffith, K. Merrett, S. L. Madhira, V. S. Sangwan, and G. K. Vemuganti. 2008. "A biomimetic scaffold for culturing limbal stem cells: a promising alternative for clinical transplantation." *Journal of Tissue Engineering and Regenerative Medicine* no. 2 (5):263-271.

- Drieskens, M., R. Peeters, J. Mullens, D. Franco, P. J. Lemstra, and D. G. Hristova-Bogaerds. 2009. "Structure Versus Properties Relationship of Polylactic acid. I. Effect of Crystallinity on Barrier Properties." *Journal of Polymer Science Part B-Polymer Physics* no. 47 (22):2247-2258.
- Du, Y. A., M. Ghodousi, H. Qi, N. Haas, W. Q. Xiao, and A. Khademhosseini. 2011. "Sequential Assembly of Cell-Laden Hydrogel Constructs to Engineer Vascular-Like Microchannels." *Biotechnology and Bioengineering* no. 108 (7):1693-1703.
- Durst, C. A., M. P. Cuchiara, E. G. Mansfield, J. L. West, and K. J. Grande-Allen. 2011. "Flexural characterization of cell encapsulated PEGDA hydrogels with applications for tissue engineered heart valves." *Acta Biomaterialia* no. 7 (6):2467-2476.
- Ealey, P. A., M. E. Yateman, S. J. Holt, and N. J. Marshall. 1988. "ESTA - A bioassay system for the determination of the potencies of hormones and antibodies which mimic their action." *Journal of Molecular Endocrinology* no. 1 (2):R1-R4.
- Ebato, B., J. Friend, and R. A. Thoft. 1987. "Comparison of central and peripheral human corneal epithelium in tissue culture." *Investigative Ophthalmology & Visual Science* no. 28 (9):1450-6.
- Elomaa, L., S. Teixeira, R. Hakala, H. Korhonen, D. W. Grijpma, and J. V. Seppälä. 2011. "Preparation of poly( $\epsilon$ -caprolactone)-based tissue engineering scaffolds by stereolithography." *Acta Biomaterialia* no. 7 (11):3850-3856.
- Engelmayr, G. C., M. Y. Cheng, C. J. Bettinger, J. T. Borenstein, R. Langer, and L. E. Freed. 2008. "Accordion-like honeycombs for tissue engineering of cardiac anisotropy." *Nature Materials* no. 7 (12):1003-1010.
- Engler, Adam J., Shamik Sen, H. Lee Sweeney, and Dennis E. Discher. 2006. "Matrix Elasticity Directs Stem Cell Lineage Specification." *Cell* no. 126 (4):677-689.
- Esteves, A. C. C., J. Brokken-Zijp, J. Laven, H. P. Huinink, N. J. W. Reuvers, M. P. Van, and G. de With. 2009. "Influence of cross-linker concentration on the cross-linking of PDMS and the network structures formed." *Polymer* no. 50 (16):3955-3966.
- Sharona, E. R., V. Artym, and K. M. Yamada. 2006. "Matrix Control of Stem Cell Fate." *Cell* no. 126 (4):645-647.
- Falconnet, D., G. Csucs, H. M. Grandin, and M. Textor. 2006. "Surface engineering approaches to micropattern surfaces for cell-based assays." *Biomaterials* no. 27 (16):3044-3063.
- Farsari, M., and B. N. Chichkov. 2009. "Two-photon fabrication." *Nature Photonics* no. 3 (8):450-452.

- Farsari, M., G. Filippidis, K. Sambani, T. S. Drakakis, and C. Fotakis. 2006. "Two-photon polymerization of an Eosin Y-sensitized acrylate composite." *Journal of Photochemistry and Photobiology a-Chemistry* no. 181 (1):132-135.
- Farsari, M., M. Vamvakaki, and B. N. Chichkov. 2010. "Multiphoton polymerization of hybrid materials." *Journal of Optics* no. 12 (12):1-16
- Fischer, J., and M. Wegener. 2011. "Three-dimensional direct laser writing inspired by stimulated-emission-depletion microscopy Invited." *Optical Materials Express* no. 1 (4):614-624.
- Friedl, P., and K. Wolf. 2003. "Tumour-cell invasion and migration: diversity and escape mechanisms." *Nat Rev Cancer* no. 3 (5):362-374.
- Fuchs, E., T. Tumber, and G. Guasch. 2004. "Socializing with the Neighbors: Stem Cells and Their Niche." *Cell* no. 116 (6):769-778.
- Gan, X. P., H. P. Zhou, P. F. Shi, P. Wang, J. Y. Wu, Y. P. Tian, J. X. Yang, G. B. Xu, Y. F. Zhou, and M. H. Jiang. 2009. "A new series of two-photon polymerization initiators: Synthesis and nonlinear optical properties." *Science in China Series B-Chemistry* no. 52 (12):2180-2185.
- Gandhi, P. S., and S. Deshmukh. 2010. "A 2D optomechanical focused laser spot scanner: analysis and experimental results for microstereolithography." *Journal of Micromechanics and Microengineering* no. 20 (1):015035-015046.
- Gill, Andrew A., and Frederik Claeysens. 2011. "3D Structuring of Biocompatible and Biodegradable Polymers Via Stereolithography." *3D Cell Culture, Methods in Molecular Biology* no. 695 (1):309-321.
- Gittard, S. D., A. Ovsianikov, H. Akar, B. Chichkov, N. A. Monteiro-Riviere, S. Stafslin, B. Chisholm, C. C. Shin, C. M. Shih, S. J. Lin, Y. Y. Su, and R. J. Narayan. 2010. "Two Photon Polymerization-Micromolding of Polyethylene Glycol-Gentamicin Sulfate Microneedles." *Advanced Engineering Materials* no. 12 (4):B77-B82.
- Gittard, Shaun D., Philip R. Miller, Ryan D. Boehm, Aleksandr Ovsianikov, Boris N. Chichkov, Jeremy Heiser, John Gordon, Nancy A. Monteiro-Riviere, and Roger J. Narayan. 2011. "Multiphoton microscopy of transdermal quantum dot delivery using two photon polymerization-fabricated polymer microneedles." *Faraday Discussions* no. 149 (0):171-185.
- Glasscock, Michael E., III, C. Gary Jackson, and Glenn W. Knox. 1988. "Can Acquired Immunodeficiency Syndrome and Creutzfeldt-Jakob Disease Be Transmitted via Otolologic Homografts?" *Arch Otolaryngol Head Neck Surg* no. 114 (11):1252-1255.

- Gogolewski, S., and A. J. Pennings. 1983. "An artificial skin based on biodegradable mixtures of polylactides and polyurethanes for full-thickness skin wound covering." *Makromolekulare Chemie-Rapid Communications* no. 4 (10):675-680.
- Goppert-Mayer, M. 1931. "Elementary file with two quantum fissures." *Annalen Der Physik* no. 9 (3):273-294.
- Goulet, R. W., S. A. Goldstein, M. J. Ciarelli, J. L. Kuhn, M. B. Brown, and L. A. Feldkamp. 1994. "The relationship between the structural and orthogonal compressive properties of trabecular bone." *Journal of Biomechanics* no. 27 (4):375-389.
- Griffith, L. G. 2000. "Polymeric biomaterials." *Acta Materialia* no. 48 (1):263-277.
- Grinnell, F., L. B. Rocha, C. Iucu, S. Rhee, and H. M. Jiang. 2006. "Nested collagen matrices: A new model to study migration of human fibroblast populations in three dimensions." *Experimental Cell Research* no. 312 (1):86-94.
- Ha, Young, Jae Choi, and Seok Lee. 2008. "Mass production of 3-D microstructures using projection microstereolithography." *Journal of Mechanical Science and Technology* no. 22 (3):514-521.
- Hagstrom, S., C. Nordling, and K. Siegbahn. 1964. "Electron spectroscopy for chemical analysis." *Physics Letters* no. 9 (3):235-236.
- Halstenberg, S., A. Panitch, S. Rizzi, H. Hall, and J. A. Hubbell. 2002. "Biologically engineered protein-graft-polyethylene glycol hydrogels: A cell adhesive and plasm in-degradable biosynthetic material for tissue repair." *Biomacromolecules* no. 3 (4):710-723.
- Han, L. H., G. Mapili, S. Chen, and K. Roy. 2008. "Projection microfabrication of three-dimensional scaffolds for tissue engineering." *Journal of Manufacturing Science and Engineering-Transactions of the Asme* no. 130 (2):021005-021008.
- Haske, W., V. W. Chen, J. M. Hales, W. T. Dong, S. Barlow, S. R. Marder, and J. W. Perry. 2007. "65 nm feature sizes using visible wavelength 3-D multiphoton lithography." *Optics Express* no. 15 (6):3426-3436.
- Haycock, J. W. 2011. "3D Cell Culture: A Review of Current Approaches and Techniques." *3D Cell Culture, Methods in Molecular Biology* no. 695 (1): 1-15.
- Henderson, T. R. M., D. J. Coster, and K. A. Williams. 2001. "The long term outcome of limbal allografts: the search for surviving cells." *British Journal of Ophthalmology* no. 85 (5):604-609.
- Hollister, S. J. 2005. "Porous scaffold design for tissue engineering." *Nature Materials* no. 4 (7):518-524.

- Hou, Qingpu, Dirk W. Grijpma, and Jan Feijen. 2009. "Creep-resistant elastomeric networks prepared by photocrosslinking fumaric acid monoethyl ester-functionalized poly(trimethylene carbonate) oligomers." *Acta Biomaterialia* no. 5 (5):1543-1551.
- Hsieh, Tseng Ming, Chien Wei Benjamin Ng, Karthikeyan Narayanan, Andrew C. A. Wan, and Jackie Y. Ying. 2010. "Three-dimensional microstructured tissue scaffolds fabricated by two-photon laser scanning photolithography." *Biomaterials* no. 31 (30):7648-7652.
- Hsu, S. H., and H. C. Ni. 2009. "Fabrication of the Microgrooved/Microporous Polylactide Substrates as Peripheral Nerve Conduits and In Vivo Evaluation." *Tissue Engineering Part A* no. 15 (6):1381-1390.
- Huang, A. J., and S. C. Tseng. 1991. "Corneal epithelial wound healing in the absence of limbal epithelium." *Investigative Ophthalmology & Visual Science* no. 32 (1):96-105.
- Huang, Yi-Cheng, and Yi-You Huang. 2006. "Biomaterials and Strategies for Nerve Regeneration." *Artificial Organs* no. 30 (7):514-522.
- Hutmacher, D. W., T. Schantz, I. Zein, K. W. Ng, S. H. Teoh, and K. C. Tan. 2001. "Mechanical properties and cell cultural response of polycaprolactone scaffolds designed and fabricated via fused deposition modeling." *Journal of Biomedical Materials Research* no. 55 (2):203-216.
- Hutmacher, D. W., M. Sittinger, and M. V. Risbud. 2004. "Scaffold-based tissue engineering: rationale for computer-aided design and solid free-form fabrication systems." *Trends in Biotechnology* no. 22 (7):354-362.
- Jain, R., and A. F. von Recum. 2004. "Fibroblast attachment to smooth and microtextured PET and thin cp-Ti films." *Journal of Biomedical Materials Research Part A* no. 68A (2):296-304.
- Jhaveri, S. J., J. D. McMullen, R. Sijbesma, L. S. Tan, W. Zipfel, and C. K. Ober. 2009. "Direct Three-Dimensional Microfabrication of Hydrogels via Two-Photon Lithography in Aqueous Solution." *Chemistry of Materials* no. 21 (10):2003-2006.
- Jiang, X., S. H. Lim, H. Q. Mao, and S. Y. Chew. 2010. "Current applications and future perspectives of artificial nerve conduits." *Experimental Neurology* no. 223 (1):86-101.
- Kaewkhaw, R., A. M. Scutt, and J. W. Haycock. 2011. "Anatomical Site Influences the Differentiation of Adipose-Derived Stem Cells for Schwann-Cell Phenotype and Function." *Glia* no. 59 (5):734-749.

- Kaewkhaw, R., A. M. Scutt, and J. W. Haycock. 2012. "Integrated culture and purification of rat Schwann cells from freshly isolated adult tissue." *Nature Protocols* no. 7 (11):1996-2004.
- Kaiser, J. P., A. Reinmann, and A. Bruinink. 2006. "The effect of topographic characteristics on cell migration velocity." *Biomaterials* no. 27 (30):5230-5241.
- Kaiser, W., and C. G. B. Garrett. 1961. "2-Photon excitation in  $\text{CaF}_2 - \text{Eu}^{2+}$ ." *Physical Review Letters* no. 7 (6):229-231.
- Kato, J., N. Takeyasu, Y. Adachi, H. B. Sun, and S. Kawata. 2005. "Multiple-spot parallel processing for laser micromanofabrication." *Applied Physics Letters* no. 86 (4):044102-044104
- Kehoe, S., X. F. Zhang, and D. Boyd. 2012. "FDA approved guidance conduits and wraps for peripheral nerve injury: A review of materials and efficacy." *Injury-International Journal of the Care of the Injured* no. 43 (5):553-572.
- Kent, C. R. H., J. J. Eady, G. M. Ross, and G. G. Steel. 1995. "The comet moment as a measure of DNA-damage in the comet assay." *International Journal of Radiation Biology* no. 67 (6):655-660.
- Keselowsky, B. G., D. M. Collard, and A. J. Garcia. 2003. "Surface chemistry modulates fibronectin conformation and directs integrin binding and specificity to control cell adhesion." *Journal of Biomedical Materials Research Part A* no. 66A (2):247-259.
- . 2004. "Surface chemistry modulates focal adhesion composition and signaling through changes in integrin binding." *Biomaterials* no. 25 (28):5947-5954.
- Kim, K., M. Yu, X. H. Zong, J. Chiu, D. F. Fang, Y. S. Seo, B. S. Hsiao, B. Chu, and M. Hadjiargyrou. 2003. "Control of degradation rate and hydrophilicity in electrospun non-woven poly(D,L-lactide) nanofiber scaffolds for biomedical applications." *Biomaterials* no. 24 (27):4977-4985.
- Kim, Y. H., M. G. Jeong, H. O. Seo, S. Y. Park, I. B. Jeong, K. D. Kim, S. M. Cho, D. C. Lim, and Y. D. Kim. 2012. "Preparation of ultrathin polydimethylsiloxane-coating on Cu as oxidation-protection layer." *Applied Surface Science* no. 258 (19):7562-7566.
- Klawitter, J. J., and S. F. Hulbert. 1971. "Application of porous ceramics for the attachment of load bearing internal orthopedic applications." *Journal of Biomedical Materials Research* no. 5 (6):161-229.
- Klein, F., T. Striebel, J. Fischer, Z. X. Jiang, C. M. Franz, G. von Freymann, M. Wegener, and M. Bastmeyer. "Elastic Fully Three-dimensional Microstructure Scaffolds for Cell Force Measurements." *Advanced Materials* no. 22 (8):868-871.

- Koenig, A. L., V. Gambillara, and D. W. Grainger. 2003. "Correlating fibronectin adsorption with endothelial cell adhesion and signaling on polymer substrates." *Journal of Biomedical Materials Research Part A* no. 64A (1):20-37.
- Koo, G. H., and J. Jang. 2008. "Surface modification of polylactic acid by UV/Ozone irradiation." *Fibers and Polymers* no. 9 (6):674-678.
- Koroleva, A., A. A. Gill, I. Ortega, J. W. Haycock, S. Schlie, S. D. Gittard, B. N. Chichkov, and F. Claeysens. 2012. "Two-photon polymerization-generated and micromolding-replicated 3D scaffolds for peripheral neural tissue engineering applications." *Biofabrication* no. 4 (2):1-11.
- Koroleva, A., S. Schlie, E. Fadeeva, S. D. Gittard, P. Miller, A. Ovsianikov, J. Koch, R. J. Narayan, and B. N. Chichkov. 2010. "Microreplication of laser-fabricated surface and three-dimensional structures." *Journal of Optics* no. 12 (12):124009-124015.
- Kreider, B. Q., A. Messing, H. Doan, S. U. Kim, R. P. Lisak, and D. E. Pleasure. 1981. "Enrichment of Schwann-cell cultures from neonatal rat sciatic-nerve by differential adhesion." *Brain Research* no. 207 (2):433-444.
- Kuebler, S. M., M. Rumi, T. Watanabe, K. Braun, A. A. Heikal, B. H. Cumpston, L. L. Erskine, S. Thayumanavan, S. Barlow, J. W. Perry, and S. R. Marder. 2001. "Optimizing Two-Photon Initiators and Exposure Conditions for Three-Dimensional Lithographic Microfabrication." *Journal of Photopolymer Science and Technology* no. 14 (4):657-668.
- Kulkarni, R. K., E. G. Moore, A. F. Hegyeli, and Fred Leonard. 1971. "Biodegradable polylactic acid polymers." *Journal of Biomedical Materials Research* no. 5 (3):169-181.
- Kwon, I. K., and T. Matsuda. 2005. "Photo-polymerized microarchitectural constructs prepared by microstereolithography ( $\mu$ SL) using liquid acrylate-end-capped trimethylene carbonate-based prepolymers." *Biomaterials* no. 26 (14):1675-1684.
- LaFratta, C. N., J. T. Fourkas, T. Baldacchini, and R. A. Farrer. 2007. "Multiphoton fabrication." *Angewandte Chemie-International Edition* no. 46 (33):6238-6258.
- Langer, R., and J. P. Vacanti. 1993. "Tissue Engineering." *Science* no. 260 (5110):920-926.
- Lanza, R., J. Gearhart, B. Hogan, D. Melton, R. Pedersen, E. Donall Thomas, J. Thomson, M. West. 2006. "Essentials of Stem Cell Biology." Elsevier Academic no. 1(1):1-11
- Laschke, M. W., Y. Harder, M. Amon, I. Martin, J. Farhadi, A. Ring, N. Torio-Padron, R. Schramm, M. Rucker, D. Junker, J. M. Haufel, C. Carvalho, M. Heberer, G. Germann, B. Vollmar, and M. D. Menger. 2006. "Angiogenesis in tissue engineering:

- Breathing life into constructed tissue substitutes." *Tissue Engineering* no. 12 (8):2093-2104.
- Lee, K. S., D. Y. Yang, S. H. Park, and R. H. Kim. 2006. "Recent developments in the use of two-photon polymerization in precise 2D and 3D microfabrications." *Polymers for Advanced Technologies* no. 17 (2):72-82.
- Lee, K. Y., and D. J. Mooney. 2001. "Hydrogels for tissue engineering." *Chemical Reviews* no. 101 (7):1869-1879.
- Lee, S. J., J. W. Rhie, and D. W. Cho. 2008. "Development of three-dimensional alginate encapsulated chondrocyte hybrid scaffold using microstereolithography." *Journal of Manufacturing Science and Engineering-Transactions of the Asme* no. 130 (2):021007-021011.
- Lee, S. H., J. J. Moon, and J. L. West. 2008. "Three-dimensional micropatterning of bioactive hydrogels via two-photon laser scanning photolithography for guided 3D cell migration." *Biomaterials* no. 29 (20):2962-2968.
- Lemercier, G., C. Martineau, J. C. Mulatier, I. Wang, O. Stephan, P. Baldeck, and C. Andraud. 2006. "Analogues of Michler's ketone for two-photon absorption initiation of polymerization in the near infrared: synthesis and photophysical properties." *New Journal of Chemistry* no. 30 (11):1606-1613.
- Li, X. F., R. J. Winfield, S. O'Brien, and G. M. Crean. 2009. "Application of Bessel beams to 2D microfabrication." *Applied Surface Science* no. 255 (10):5146-5149.
- Li, X. F., R. Winfield, S. O'Brien, and L. Y. Chen. 2009. "Fabrication of 3D Templates Using a Large Depth of Focus Femtosecond Laser." *Chinese Physics Letters* no. 26 (9):1-3.
- Liao, C. Y., M. Bouriauand, P. L. Baldeck, J. C. Leon, C. Masclet, and T. T. Chung. 2007. "Two-dimensional slicing method to speed up the fabrication of micro-objects based on two-photon polymerization." *Applied Physics Letters* no. 91 (3).
- Lietz, M., L. Dreesmann, M. Hoss, S. Oberhoffner, and B. Schlosshauer. 2006. "Neuro tissue engineering of glial nerve guides and the impact of different cell types." *Biomaterials* no. 27 (8):1425-1436.
- Lim, L. T., R. Auras, and M. Rubino. 2008. "Processing technologies for polylactic acid." *Progress in Polymer Science* no. 33 (8):820-852.
- Liu, V. A., and S. N. Bhatia. 2002. "Three-dimensional photopatterning of hydrogels containing living cells." *Biomedical Microdevices* no. 4 (4):257-266.
- Luo, Y., and M. S. Shoichet. 2004. "A photolabile hydrogel for guided three-dimensional cell growth and migration." *Nature Materials* no. 3 (4):249-253.

- Lutolf, Matthias P., and Helen M. Blau. 2009. "Artificial Stem Cell Niches." *Advanced Materials* no. 21 (32-33):3255-3268.
- Ma, P. X., and J. W. Choi. 2001. "Biodegradable polymer scaffolds with well-defined interconnected spherical pore network." *Tissue Engineering* no. 7 (1):23-33.
- Mackinnon, S. E., V. B. Doolabh, C. B. Novak, and E. P. Trulock. 2001. "Clinical outcome following nerve allograft transplantation." *Plastic and Reconstructive Surgery* no. 107 (6):1419-1429.
- Macneil, S., R. A. Dawson, G. Crocker, W. F. G. Tucker, B. Bittiner, J. G. Singleton, T. Hunter, and D. F. Tierney. 1993. "Antiproliferative effects on keratinocytes of a range of clinically used drugs with calmodulin antagonist activity." *British Journal of Dermatology* no. 128 (2):143-150.
- Mahoney, M. J., R. R. Chen, J. Tan, and W. M. Saltzman. 2005. "The influence of microchannels on neurite growth and architecture." *Biomaterials* no. 26 (7):771-778.
- Marletta, G., G. Ciapetti, C. Satriano, S. Pagani, and N. Baldini. 2005. "The effect of irradiation modification and RGD sequence adsorption on the response of human osteoblasts to polycaprolactone." *Biomaterials* no. 26 (23):4793-4804.
- Martin, D. P., and S. F. Williams. 2003. "Medical applications of poly-4-hydroxybutyrate: a strong flexible absorbable biomaterial." *Biochemical Engineering Journal* no. 16 (2):97-105.
- Martina, M., and D. W. Hutmacher. 2007. "Biodegradable polymers applied in tissue engineering research: a review." *Polymer International* no. 56 (2):145-157.
- Maruo, S., and J. T. Fourkas. 2008. "Recent progress in multiphoton microfabrication." *Laser & Photonics Reviews* no. 2 (1-2):100-111.
- Maruo, S., O. Nakamura, and S. Kawata. 1997. "Three-dimensional microfabrication with two-photon-absorbed photopolymerization." *Optics Letters* no. 22 (2):132-134.
- Matsuda, T., I. K. Kwon, and S. Kidoaki. 2004. "Photocurable biodegradable liquid copolymers: Synthesis of acrylate-end-capped trimethylene carbonate-based prepolymers, photocuring, and hydrolysis." *Biomacromolecules* no. 5 (2):295-305.
- Matsuda, T., and M. Mizutani. 2000. "Molecular design of photocurable liquid biodegradable copolymers. 2. Synthesis of coumarin-derivatized oligo(methacrylate)s and photocuring." *Macromolecules* no. 33 (3):791-794.
- Matsuda, T., M. Mizutani, and S. C. Arnold. 2000. "Molecular design of photocurable liquid biodegradable copolymers. 1. Synthesis and photocuring characteristics." *Macromolecules* no. 33 (3):795-800.

- McArthur, Sally L. 2006. "Applications of XPS in bioengineering." *Surface and Interface Analysis* no. 38 (11):1380-1385.
- Meier, M. A. R., and U. S. Schubert. 2005. "Synthesis and characterization of 4- and 6-arm star-shaped poly(epsilon-caprolactone)s." *E-Polymers* no. 085 (1):1-8.
- Melchels, F. P. W., A. M. C. Barradas, C. A. van Blitterswijk, J. de Boer, J. Feijen, and D. W. Grijpma. 2010. "Effects of the architecture of tissue engineering scaffolds on cell seeding and culturing." *Acta Biomaterialia* no. 6 (11):4208-4217.
- Melchels, F. P. W., K. Bertoldi, R. Gabbriellini, A. H. Velders, J. Feijen, and D. W. Grijpma. 2010. "Mathematically defined tissue engineering scaffold architectures prepared by stereolithography." *Biomaterials* no. 31 (27):6909-6916.
- Melchels, F. P. W., J. Feijen, and D. W. Grijpma. 2009. "A poly(D,L-lactide) resin for the preparation of tissue engineering scaffolds by stereolithography." *Biomaterials* no. 30 (23-24):3801-3809.
- Melchels, Ferry P. W., Beatrice Tonnarelli, Andy L. Olivares, Ivan Martin, Damien Lacroix, Jan Feijen, David J. Wendt, and Dirk W. Grijpma. 2011. "The influence of the scaffold design on the distribution of adhering cells after perfusion cell seeding." *Biomaterials* no. 32 (11):2878-2884.
- Melissinaki, V., A. A. Gill, I. Ortega, M. Vamvakaki, A. Ranella, J. W. Haycock, C. Fotakis, M. Farsari, and F. Claeysens. 2011. "Direct laser writing of 3D scaffolds for neural tissue engineering applications." *Biofabrication* no. 3 (4):045005-045016.
- Millesi, H., and R. Schmidhammer. 2007. "End-to-side coaptation — controversial research issue or important tool in human patients." *How to Improve the Results of Peripheral Nerve Surgery* no. 100 (1):103-106.
- Mironov, V., T. Boland, T. Trusk, G. Forgacs, and R. R. Markwald. 2003. "Organ printing: computer-aided jet-based 3D tissue engineering." *Trends in Biotechnology* no. 21 (4):157-161.
- Mironov, V., V. Kasyanov, C. Drake, and R. R. Markwald. 2008. "Organ printing: promises and challenges." *Regenerative Medicine* no. 3 (1):93-103.
- Mizutani, M., and T. Matsuda. 2002a. "Liquid photocurable biodegradable copolymers: In vivo degradation of photocured poly(epsilon-caprolactone-co-trimethylene carbonate)." *Journal of Biomedical Materials Research* no. 61 (1):53-60.
- . 2002b. "Photocurable liquid biodegradable copolymers: In vitro hydrolytic degradation behaviors of photocured films of coumarin-endcapped poly(epsilon-caprolactone-co-trimethylene carbonate)." *Biomacromolecules* no. 3 (2):249-255.

- Morent, R., N. De Geyter, F. Axisa, N. De Smet, L. Gengembre, E. De Leersnyder, C. Leys, J. Vanfleteren, M. Rymarczyk-Machal, E. Schacht, and E. Payen. 2007. "Adhesion enhancement by a dielectric barrier discharge of PDMS used for flexible and stretchable electronics." *Journal of Physics D-Applied Physics* no. 40 (23):7392-7401.
- Murray-Dunning, C., S. L. McArthur, T. Sun, R. McKean, A. J. Ryan, and J. W. Haycock. 2011. "Three-Dimensional Alignment of Schwann Cells Using Hydrolysable Microfiber Scaffolds: Strategies for Peripheral Nerve Repair." *3D Cell Culture, Methods in Molecular Biology* no. 695 (1):155-166.
- Narayan, R. J., A. Doraiswamy, D. B. Chrisey, and B. N. Chichkov. 2010. "Medical prototyping using two photon polymerization." *Materials Today* no. 13 (12):42-48.
- Nie, J, and C. N. Bowman. 2002. "Synthesis and photopolymerization of N,N'-dimethyl-, N,N'-di(methacryloxy ethyl)-1,6-hexanediamine as a polymerizable amine coinitiator for dental restorations." *Biomaterials* no. 23 (4):1221-1226.
- Olive, P. L., and J. P. Banath. 2006. "The comet assay: a method to measure DNA damage in individual cells." *Nature Protocols* no. 1 (1):23-29.
- Ostendorf, A., and B. N. Chichkov. 2006. "Two-photon polymerization: A new approach to micromachining." *Photonics Spectra* no. 40 (10):72-73.
- Ostling, O., and K. J. Johanson. 1984. "Microelectrophoretic study of radiation-induced DNA damages in individual mammalian-cells." *Biochemical and Biophysical Research Communications* no. 123 (1):291-298.
- Ovsianikov, A., B. Chichkov, O. Adunka, H. Pillsbury, A. Doraiswamy, and R. J. Narayan. 2007. "Rapid prototyping of ossicular replacement prostheses." *Applied Surface Science* no. 253 (15):6603-6607.
- Ovsianikov, A., B. Chichkov, P. Mente, N. A. Monteiro-Riviere, A. Doraiswamy, and R. J. Narayan. 2007. "Two Photon Polymerization of Polymer-Ceramic Hybrid Materials for Transdermal Drug Delivery." *International Journal of Applied Ceramic Technology* no. 4 (1):22-29.
- Ovsianikov, A., M. Malinauskas, S. Schlie, B. Chichkov, S. Gittard, R. Narayan, M. Lobler, K. Sternberg, K. P. Schmitz, and A. Haverich. 2011. "Three-dimensional laser micro- and nano-structuring of acrylated poly(ethylene glycol) materials and evaluation of their cytotoxicity for tissue engineering applications." *Acta Biomaterialia* no. 7 (3):967-974.

- Ovsianikov, A., A. Ostendorf, and B. N. Chichkov. 2007. "Three-dimensional photofabrication with femtosecond lasers for applications in photonics and biomedicine." *Applied Surface Science* no. 253 (15):6599-6602.
- Ovsianikov, A., S. Schlie, A. Ngezahayo, A. Haverich, and B. N. Chichkov. 2007. "Two-photon polymerization technique for microfabrication of CAD-designed 3D scaffolds from commercially available photosensitive materials." *Journal of Tissue Engineering and Regenerative Medicine* no. 1 (6):443-449.
- Ovsianikov, A., A. Deiwick, S. Van Vlierberghe, P. Dubruel, L. Moeller, G. Draeger, and B. Chichkov. 2011. "Laser Fabrication of Three-Dimensional CAD Scaffolds from Photosensitive Gelatin for Applications in Tissue Engineering." *Biomacromolecules* no. 12 (4):851-858.
- Panseri, S., C. Cunha, J. Lowery, U. Del Carro, F. Taraballi, S. Amadio, A. Vescovi, and F. Gelain. 2008. "Electrospun micro- and nanofiber tubes for functional nervous regeneration in sciatic nerve transections." *Bmc Biotechnology* no. 8:39-50.
- Park, S. H., S. H. Lee, D. Y. Yang, H. J. Kong, and K. S. Lee. 2005. "Subregional slicing method to increase three-dimensional nanofabrication efficiency in two-photon polymerization." *Applied Physics Letters* no. 87 (15):154108-154110.
- Pego, A. P., Clam Vleggeert-Lankamp, M. Deenen, Eajf Lakke, D. W. Grijpma, A. A. Poot, E. Marani, and J. Feijen. 2003. "Adhesion and growth of human schwann cells on trimethylene carbonate (co)polymers." *Journal of Biomedical Materials Research Part A* no. 67A (3):876-885.
- Phillips, J. B., S. C. J. Bunting, S. M. Hall, and R. A. Brown. 2005. "Neural tissue engineering: A self-organizing collagen guidance conduit." *Tissue Engineering* no. 11 (9-10):1611-1617.
- Porter, J. R., A. Henson, and K. C. Popat. 2009. "Biodegradable poly(epsilon-caprolactone) nanowires for bone tissue engineering applications." *Biomaterials* no. 30 (5):780-788.
- Ranella, A., M. Barberoglou, S. Bakogianni, C. Fotakis, and E. Stratakis. 2010. "Tuning cell adhesion by controlling the roughness and wettability of 3D micro/nano silicon structures." *Acta Biomaterialia* no. 6 (7):2711-2720.
- Rangappa, N., A. Romero, K. D. Nelson, R. C. Eberhart, and G. M. Smith. 2000. "Laminin-coated poly(L-lactide) filaments induce robust neurite growth while providing directional orientation." *Journal of Biomedical Materials Research* no. 51 (4):625-634.

- Rengier, F., A. Mehndiratta, H. von Tengg-Kobligk, C. M. Zechmann, R. Unterhinninghofen, H. U. Kauczor, and F. L. Giesel. 2010. "3D printing based on imaging data: review of medical applications." *International Journal of Computer Assisted Radiology and Surgery* no. 5 (4):335-341.
- Ribeiro-Resende, V. T., B. Koenig, S. Nichterwitz, S. Oberhoffner, and B. Schlosshauer. 2009. "Strategies for inducing the formation of bands of Bungner in peripheral nerve regeneration." *Biomaterials* no. 30 (29):5251-5259.
- Roach, P., T. Parker, N. Gadegaard, and M. R. Alexander. 2010. "Surface strategies for control of neuronal cell adhesion: A review." *Surface Science Reports* no. 65 (6):145-173.
- Ruiter, G. C. W., M. J. A. Malessy, M. J. Yaszemski, A. J. Windebank, and R. J. Spinner. 2009. "Designing ideal conduits for peripheral nerve repair." *Neurosurgical Focus* no. 26 (2):E5 1-15.
- Scheideler, L., J. Geis-Gerstorfer, D. Kern, F. Pfeiffer, F. Rupp, H. Weber, and H. Wolburg. 2003. "Investigation of cell reactions to microstructured implant surfaces." *Materials Science & Engineering C-Biomimetic and Supramolecular Systems* no. 23 (3):455-459.
- Schermer, A., S. Galvin, and T. T. Sun. 1986. "Differentiation-related expression of a major 64K corneal keratin in vivo and in culture suggests limbal location of corneal epithelial stem cells." *The Journal of Cell Biology* no. 103 (1):49-62.
- Schizas, C., V. Melissinaki, A. Gaidukeviciute, C. Reinhardt, C. Ohrt, V. Dedoussis, B. N. Chichkov, C. Fotakis, M. Farsari, and D. Karalekas. 2010. "On the design and fabrication by two-photon polymerization of a readily assembled micro-valve." *International Journal of Advanced Manufacturing Technology* no. 48 (5-8):435-441.
- Schlie, S., A. Ngezahayo, A. Ovsianikov, T. Fabian, H. A. Kolb, H. Haferkamp, and B. N. Chichkov. 2007. "Three-dimensional cell growth on structures fabricated from ORMOCER (R) by two-photon polymerization technique." *Journal of Biomaterials Applications* no. 22 (3):275-287.
- Schlosshauer, B., L. Dreesmann, H. E. Schaller, and N. Sinis. 2006. "Synthetic nerve guide implants in humans: A comprehensive survey." *Neurosurgery* no. 59 (4):740-747.
- Schmidt, C. E., and J. B. Leach. 2003. "Neural tissue engineering: Strategies for repair and regeneration." *Annual Review of Biomedical Engineering* no. 5:293-347.

- Schneider, T. W., H. M. Schessler, K. M. Shaffer, J. M. Dumm, and L. A. Yonce. 2001. "Surface Patterning and Adhesion of Neuroblastoma X Glioma (NG108-15) Cells." *Biomedical Microdevices* no. 3 (4):315-322.
- Scott, Timothy F., Benjamin A. Kowalski, Amy C. Sullivan, Christopher N. Bowman, and Robert R. McLeod. 2009. "Two-Color Single-Photon Photoinitiation and Photoinhibition for Subdiffraction Photolithography." *Science* no. 324 (5929):913-917.
- Seck, T. M., F. P. W. Melchels, J. Feijen, and D. W. Grijpma. 2010. "Designed biodegradable hydrogel structures prepared by stereolithography using poly(ethylene glycol)/poly(D,L-lactide)-based resins." *Journal of Controlled Release* no. 148 (1):34-41.
- Serbin, J., and B. N. Chichkov. 2003. "Three-dimensional nanostructuring by two-photon polymerization of hybrid materials." *Nanotechnology* no. 1 (1):571-576.
- Serbin, J., A. Egbert, A. Ostendorf, B. N. Chichkov, R. Houbertz, G. Domann, J. Schulz, C. Cronauer, L. Fröhlich, and M. Popall. 2003. "Femtosecond laser-induced two-photon polymerization of inorganic organic hybrid materials for applications in photonics." *Opt. Lett.* no. 28 (5):301-303.
- Sheridan, M. H., L. D. Shea, M. C. Peters, and D. J. Mooney. 2000. "Bioabsorbable polymer scaffolds for tissue engineering capable of sustained growth factor delivery." *Journal of Controlled Release* no. 64 (1-3):91-102.
- Sigal, G. B., M. Mrksich, and G. M. Whitesides. 1998. "Effect of surface wettability on the adsorption of proteins and detergents." *Journal of the American Chemical Society* no. 120 (14):3464-3473.
- Sitalakshmi, G., B. Sudha, H. N. Madhavan, S. Vinay, S. Krishnakumar, Yuichi Mori, Hiroshi Yoshioka, and Samuel Abraham. 2008. "Ex Vivo Cultivation of Corneal Limbal Epithelial Cells in a Thermoreversible Polymer (Mebiol Gel) and Their Transplantation in Rabbits: An Animal Model." *Tissue Engineering Part A* no. 15 (2):407-415.
- Solaro, P., E. Pierangeli, C. Pizzoni, P. Boffi, and G. Scalese. 2008. "From computerized tomography data processing to rapid manufacturing of custom-made prostheses for cranioplasty Case report." *Journal of Neurosurgical Sciences* no. 52 (4):113-116.
- Stampfl, J., S. Baudis, C. Heller, R. Liska, A. Neumeister, R. Kling, A. Ostendorf, and M. Spitzbart. 2008. "Photopolymers with tunable mechanical properties processed by

- laser-based high-resolution stereolithography." *Journal of Micromechanics and Microengineering* no. 18 (12):125014-125125022.
- Smith, L. E., S. Rimmer, and S. Macneil. 2006. "Examination of the effects of poly(N-vinylpyrrolidone) hydrogels in direct and indirect contact with cells." *Biomaterials* no. 27 (14):2806-2812.
- Stoelinga, P. J. W., and J. I. Cawood. 2011. "Fundamentals of bone grafting in implantology." *Preprosthetic and Maxillofacial Surgery: Biomaterials, Bone Grafting and Tissue Engineering* no. 32 (1):25-35.
- Stute, U., J. Serbin, C. Kulik, and B. N. Chichkov. 2004. "Three-dimensional micro- and nanostructuring with two-photon polymerisation." *International Journal of Materials & Product Technology* no. 21 (4):273-284.
- Sugama, T., L. E. Brothers, and L. Weber. 2003. "Acid-resistant polydimethylsiloxane additive for geothermal well cement in 150 degrees C H<sub>2</sub>SO<sub>4</sub> solution." *Advances in Cement Research* no. 15 (1):35-44.
- Sun, H. B., and S. Kawata. 2003. "Two-photon laser precision microfabrication and its applications to micro-nano devices and systems." *Journal of Lightwave Technology* no. 21 (3):624-633.
- Sun, H. B., and S. Kawata. 2004. "Two-Photon Photopolymerization and 3D Lithographic Microfabrication." *Advances in Polymer Science* no. 170 (1):169-273.
- Tack, J. 2011. "Current and future therapies for chronic constipation." *Best Practice & Research Clinical Gastroenterology* no. 25 (1):151-158.
- Takada, K., H. B. Sun, and S. Kawata. 2005. "Improved spatial resolution and surface roughness in photopolymerization-based laser nanowriting." *Applied Physics Letters* no. 86 (7):071122-071124
- Tan, W., and T. A. Desai. 2003. "Microfluidic patterning of cellular biopolymer matrices for biomimetic 3-D structures." *Biomedical Microdevices* no. 5 (3):235-244.
- Tayalia, P., C. R. Mendonca, T. Baldacchini, D. J. Mooney, and E. Mazur. 2008. "3D Cell-Migration Studies using Two-Photon Engineered Polymer Scaffolds." *Advanced Materials* no. 20 (23):4494-4498.
- Tohill, M. P., D. J. Mann, C. M. Mantovani, M. Wiberg, and G. Terenghi. 2004. "Green fluorescent protein is a stable morphological marker for Schwann cell transplants in bioengineered nerve conduits." *Tissue Engineering* no. 10 (9-10):1359-1367.

- Topp, K. S., and B. S. Boyd. 2012. "Peripheral Nerve: From the Microscopic Functional Unit of the Axon to the Biomechanically Loaded Macroscopic Structure." *Journal of Hand Therapy* no. 25 (2):142-152.
- Torigoe, K., H. F. Tanaka, A. Takahashi, A. Awaya, and K. Hashimoto. 1996. "Basic behavior of migratory Schwann cells in peripheral nerve regeneration." *Experimental Neurology* no. 137 (2):301-308.
- Truckenmuller, R., S. Giselbrecht, M. Escalante-Marun, M. Groenendijk, B. Papenburg, N. Rivron, H. Unadkat, V. Saile, V. Subramaniam, A. van den Berg, C. van Blitterswijk, M. Wessling, J. de Boer, and D. Stamatialis. 2012. "Fabrication of cell container arrays with overlaid surface topographies." *Biomedical Microdevices* no. 14 (1):95-107.
- Tseng, S. C. G., P. Prabhasawat, K. Barton, T. Gray, and D. Meller. 1998. "Amniotic Membrane Transplantation With or Without Limbal Allografts for Corneal Surface Reconstruction in Patients With Limbal Stem Cell Deficiency." *Archives of Ophthalmology* no. 116 (4):431-441.
- Tumbar, T., G. Guasch, V. Greco, C. Blanpain, W. E. Lowry, M. Rendl, and E. Fuchs. 2004. "Defining the Epithelial Stem Cell Niche in Skin." *Science* no. 303 (5656):359-363.
- Underhill, G. H., and S. N. Bhatia. 2007. "High-throughput analysis of signals regulating stem cell fate and function." *Current Opinion in Chemical Biology* no. 11 (4):357-366.
- van Dorp, W. F., and C. W. Hagen. 2008. "A critical literature review of focused electron beam induced deposition." *Journal of Applied Physics* no. 104 (8):081301-081342.
- Wang, I., M. Bouriau, P. L. Baldeck, C. Martineau, and C. Andraud. 2002. "Three-dimensional microfabrication by two-photon-initiated polymerization with a low-cost microlaser." *Optics Letters* no. 27 (15):1348-1350.
- Weiner, J. A., N. Fukushima, J. J. A. Contos, S. S. Scherer, and J. Chun. 2001. "Regulation of Schwann cell morphology and adhesion by receptor-mediated lysophosphatidic acid signaling." *Journal of Neuroscience* no. 21 (18):7069-7078.
- Whang, K., K. E. Healy, D. R. Elenz, E. K. Nam, D. C. Tsai, C. H. Thomas, G. W. Nuber, F. H. Glorieux, R. Travers, and S. M. Sprague. 1999. "Engineering bone regeneration with bioabsorbable scaffolds with novel microarchitecture." *Tissue Engineering* no. 5 (1):35-51.

- Winfield, R. J., B. Bhuian, S. O'Brien, and G. M. Crean. 2007a. "Fabrication of grating structures by simultaneous multi-spot fs laser writing." *Applied Surface Science* no. 253 (19):8086-8090.
- . 2007b. "Refractive femtosecond laser beam shaping for two-photon polymerization." *Applied Physics Letters* no. 90 (11):111115-111117.
- Winfield, R. J., and S. O'Brien. 2011. "Two-photon polymerization of an epoxy-acrylate resin material system." *Applied Surface Science* no. 257 (12):5389-5392.
- Wu, E. S., J. H. Strickler, W. R. Harrell, and W. W. Webb. 1992. "2-Photon lithography for microelectronic application." *Optical/Laser Microlithography* no. 1674 (5):776-782.
- Wu, S. H., J. Serbin, and M. Gu. 2006. "Two-photon polymerisation for three-dimensional micro-fabrication." *Journal of Photochemistry and Photobiology a-Chemistry* no. 181 (1):1-11.
- Wylie, R. G., and M. S. Shoichet. 2011. "Three-Dimensional Spatial Patterning of Proteins in Hydrogels." *Biomacromolecules* no. 12 (10):3789-3796.
- Xia, Y. N., and G. M. Whitesides. 1998. "Soft lithography." *Annual review of materials science* no. 28:153-184.
- Yan, X. and P. Gu. 1996. "A review of rapid prototyping technologies and systems." *Computer-Aided Design* no. 28 (4):307-318.
- Yang, Y. M., X. S. Gu, R. X. Tan, W. Hu, X. D. Wang, P. Y. Zhang, and T. Y. Zhang. 2004. "Fabrication and properties of a porous chitin/chitosan conduit for nerve regeneration." *Biotechnology Letters* no. 26 (23):1793-1797.
- Yu, T. Y., and C. K. Ober. 2003. "Methods for the topographical patterning and patterned surface modification of hydrogels based on hydroxyethyl methacrylate." *Biomacromolecules* no. 4 (5):1126-1131.
- Zelzer, M., R. Majani, J. W. Bradley, F. R. A. J. Rose, M. C. Davies, and M. R. Alexander. 2008. "Investigation of cell-surface interactions using chemical gradients formed from plasma polymers." *Biomaterials* no. 29 (2):172-184.
- Zhang, Y., B. Meng, L. Chen, J. Tao, and Z. H. Wu. 2012. "Properties and structures of polylactide filled with poly( $\epsilon$ -caprolactone)-coated calcium carbonate." *Journal of Applied Polymer Science* no. 125 (2):952-958.
- Zhu, L., Y. H. Yan, K. F. Ke, X. M. Wu, Y. L. Gao, A. G. Shen, J. Li, L. H. Kang, G. W. Zhang, Q. Y. Wu, and H. G. Yang. 2012. "Dynamic change of numbl expression after sciatic nerve crush and its role in Schwann cell differentiation." *Journal of Neuroscience Research* no. 90 (8):1557-1565.